Bacterial Cell Wall Synthases Require Outer Membrane Lipoprotein Cofactors

Dissertation Advisor: Dr. Thomas G. Bernhardt **Monica Markovski**

Bacterial cell wall synthases require outer membrane lipoprotein cofactors

Abstract

To fortify their cytoplasmic membrane and protect it from osmotic rupture, most bacteria surround themselves with a peptidoglycan (PG) exoskeleton. The PG synthases that build this structure are called penicillin-binding proteins (PBPs). Since they are the targets of penicillin and related antibiotics, the structures and *in vitro* biochemical functions of the PBPs have been extensively studied. However, the *in vivo* functions of the PBPs and the factors they work with to build the PG meshwork remain poorly understood.

PBPs work in the context of multicomponent complexes organized by cytoskeletal elements. A major outstanding question has been whether or not these complexes contain factors required for PBP function. I addressed this using *Escherichia coli* as a model system by taking advantage of the synthetic lethal phenotype resulting from simultaneous inactivation of the major PG synthases: PBP1a and PBP1b. Using a screen for mutants synthetically lethal with the inactivation of PBP1b, I identified LpoA as a factor required for PBP1a function. A colleague in the lab performed the analogous screen for mutants synthetically lethal with the inactivation of PBP1a and identified LpoB as a factor required for PBP1b function. We showed that the Lpo factors are outer membrane lipoproteins that form specific trans-envelope complexes with their cognate PBPs in the inner membrane and that LpoB can stimulate the activity of PBP1b *in vitro*.

Our results reveal unexpected complexity in the control of PBP activity and indicate that they likely receive regulatory input from the outer membrane in addition to cytoskeletal elements in the cytoplasm.

To investigate the role of LpoB in morphogenesis further, I took a genetic approach that has identified PBP1b* variants capable of functioning *in vivo* in the absence of LpoB. Preliminary characterization of these variants indicates that LpoB has cellular functions in addition to PBP1b activation and that LpoB may be important for coordinating the two different catalytic activities of PBP1b. Future study of these mutants is likely to uncover important insights into PBP function and their control by the Lpo factors. These insights may open new avenues for the development of novel therapeutics that target the PBPs.

Table of Contents

Acknowledgments

I would like to thank my advisor, Tom Bernhardt. He taught me to how to think and act like a geneticist and showed me firsthand how a new lab gets its start. From him, I learned how to think critically and how to communicate my science effectively. His constant support has made me a better scientist. Most importantly, I want to thank him for his willingness to listen. Tom never turned me away when I needed to talk about science or about life in general. His advice, guidance, and support have really shaped me into the scientist and person I am today.

I am grateful to each member of my lab for their scientific and emotional support. Working with my colleagues has been a great joy. I want to particularly thank Tsuyoshi Uehara and Catherine Paradis-Bleau for our fruitful collaboration on the beginnings of the Lpo project, and Tania Lupoli from the Kahne group who collaborates with me to this day. I also wanted to acknowledge both Desirée Yang and Nick Peters. Both Desirée and Nick always provided a listening ear, even though my sentences were filled with “howevers” and corny jokes. Also, thanks to Nick Peters, Mary-Jane Tsang Mui Ching, and Heather McManus for critical reading of this dissertation. I also wanted to acknowledge Hongbaek Cho. He is the type of scientist I strive to be, and I am grateful for his constant support and help. Finally, to the new graduate students in our lab, Ghee Chuan Lai, Mary-Jane Tsang Mui Ching, and Rachel Yunck. Although our overlapping time together has been brief, it has been a pleasure working with you. I wish you continued success in the lab.

A big sincere thanks to my close friends who have gone through this graduate school experience with me -- Heather McManus, Alison Taylor, and Sylvia Vong. Heather taught me how to be confident while simultaneously embracing my geeky side. Alison and Sylvia have always kept me grounded and reminded me that graduate school is hard, but it will make us stronger. Our shared stories and experiences have really solidified a bond between us. I also wanted to thank my friends Ishan Mahapatra, Julia Hoy and Sze-Ling Ng, who have never doubted my capabilities. I will always be grateful for their support.

И многу и благодарам на мојата фамилија за подржката сто ми га дале. I would like to express my gratitude to my brother and sister-in-law, Petar and Cynthia Markovski. They always gave me an outside perspective when the experiments were daunting and always made me laugh when the long lab hours seemed never-ending. I sincerely appreciate their support and love. Also to my Baba Lena for her infectious laughter, warmth, and love. “It doesn’t matter if you are a seamstress or president,” she would say, “just put your heart into it.” Finally, I would like to express my deepest thanks to my parents, Gjorgji and Mirjana Markovski, who had emigrated from the Republic of Macedonia to settle into the United States -- the land of opportunity -- with only a suitcase in hand. As a child, they helped spark my curiosity about every little detail in the world around me and encouraged me to pursue my scientific passion. They have instilled strength, confidence, and perseverance within me. Through their hard work and immense sacrifice, I have become the young woman I am today. For their continuous emotional support and love, I will eternally be grateful. Многу ве сакам.

List of Figures

List of Tables

Chapter 1:

Peptidoglycan Structure and Assembly

Overview

Gram-negative bacteria, like *Escherichia coli*, contain complex cell envelopes that consist of three different layers: an inner membrane (IM) and an outer membrane (OM), with a layer of crosslinked polysaccharide called peptidoglycan (PG) found in the periplasmic space between them (**Figure 1.1**). Because bacteria are encased within this exoskeleton, their growth and morphogenesis are intimately linked to PG synthesis, and the shape of the organism is defined by the PG network (46). This large, polymeric shell is synthesized by PG synthases called the penicillin-binding proteins (PBPs). Because they are the targets of penicillin and related antibiotics, the structure and biochemical function of the PBPs have been extensively studied (59, 77, 88). Despite this, we still know surprisingly little about how these enzymes build the PG layer *in vivo*.

Composition of the PG

PG is an essential component of the bacterial cell envelope whose main function is to preserve cell integrity in spite of internal turgor pressure (31, 89). This exoskeleton is unique to bacteria and is mainly composed of linear glycan strands crosslinked by short peptide chains. The glycan strands are composed of alternating subunits of *N*-acetylglucosamine (GlcNAc) and *N*-acetylmuramic acid (MurNAc) linked by β(1,4)-glycosidic bonds (**Figure 1.2A**) (31, 91). Attached to each MurNAc sugar is a pentapeptide (pep5) chain that is used to form crosslinks between adjacent glycan strands. In Gram-negative bacteria the peptide sequence is most often L-alanine,

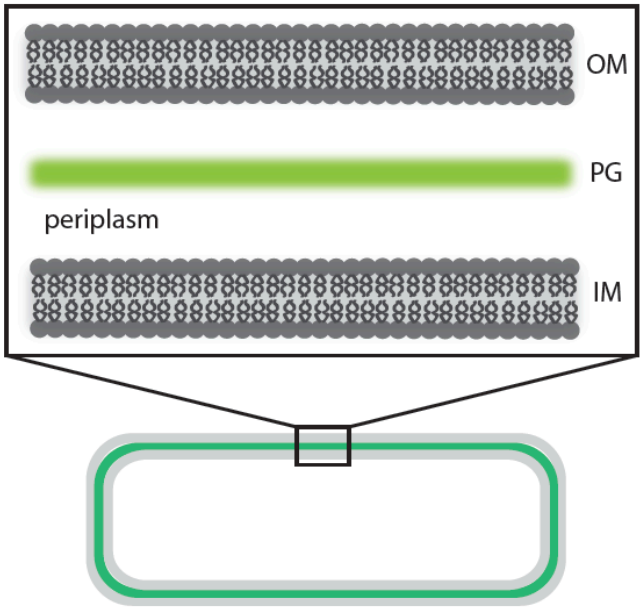

Figure 1.1. The cell envelope of *E. coli*. Gram-negative bacteria like the rod-shaped *E. coli* have a three layered cell envelope consisting of an inner membrane (IM) that protects the cytoplasm, an outer membrane (OM), and a periplasmic layer in between that contains a thin peptidoglycan layer (PG, in green).

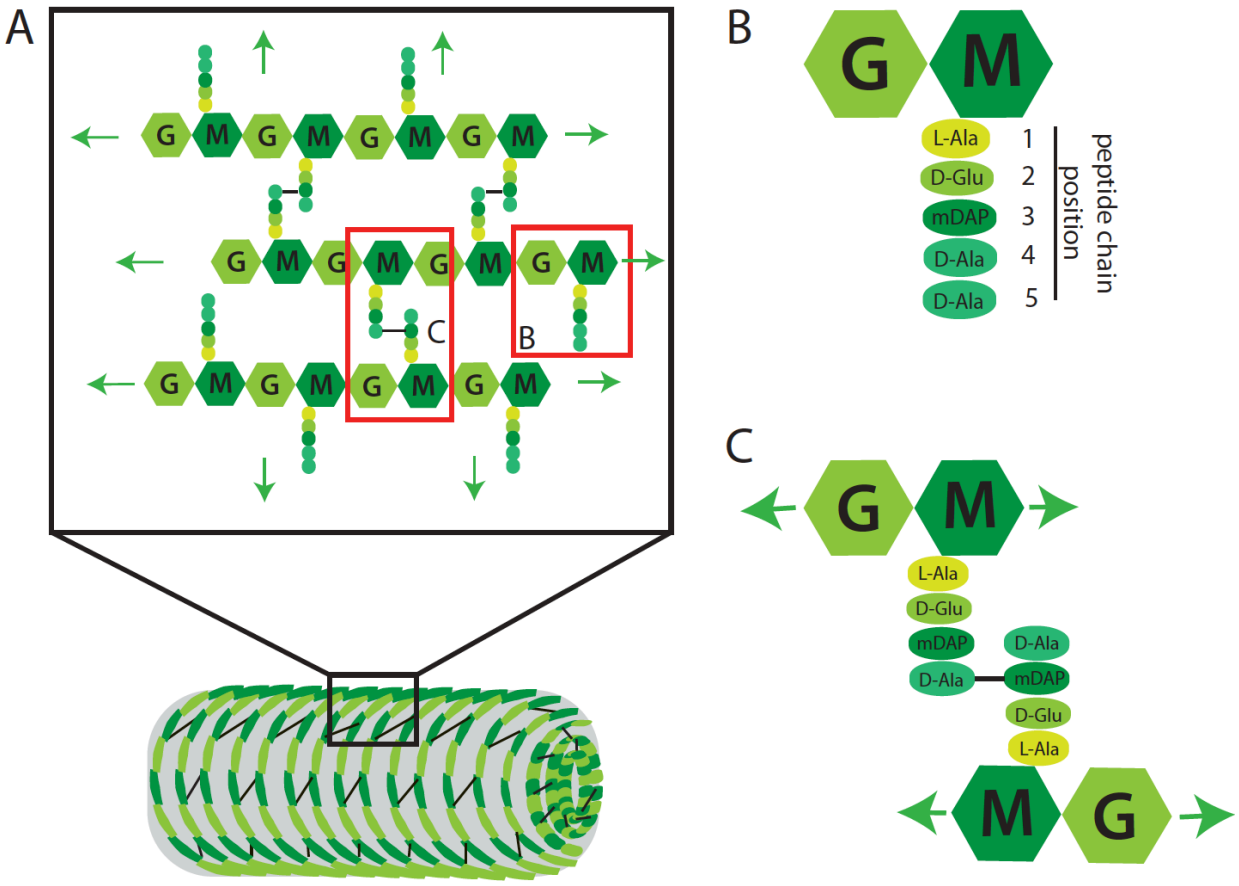

Figure 1.2. The structure of *E. coli* peptidoglycan. A schematic showing of the organization of the PG. **A.** Composed of alternating units of *N*-acetylglucosamine (G) and *N*-acetylmuramic acid (M), bacterial PG forms a large continuous meshwork (green arrows). Green dots represent attached peptides. Below the structure is an architectural representation of the PG surrounding the entire cell. Glycan strands (green hoops) are thought to be oriented perpendicular to the long axis of the rod-shaped bacterium while the peptide crosslinks (black lines) are parallel to that axis. The degree of crosslinking varies by organism. **(Legend continued on next page.)**

Figure 1.2 (Continued) Red boxes are insets that are shown in **B** and **C**. **B.** A schematic illustrating the disaccharide building block of PG with the five peptides attached to *N*-acetylmuramic acid. L-Ala, L-alanine; D-Glu, D-glutamate; mDAP, *meso*-diaminopimelic acid; D-Ala, D-alanine. **C.** A representation of the 3-4 crosslink found between the D-Ala of one disaccharide unit and the mDAP of another. The terminal D-Ala residues are released because of crosslinking and carboxypeptidation reactions (see text for details).

D-glutamic acid, *meso*-diaminopimelic acid (mDAP) and D-alanyl-D-alanine (D-Ala-D-Ala) in nascent PG, where the final D-Ala is lost upon PG maturation (88, 89) (**Figure 1.2B and C**). However, in most Gram-positive bacteria, which lack an outer membrane and have a thicker PG layer, the peptide stem contains an L-Lysine in position 3 instead of mDAP (89).

Most variation in the PG structure occurs in the crosslinks. The 3-4 crosslink is the most common. It forms when the side chain of the amino group at position 3 links to the carboxyl group of the D-Ala at position 4 (**Figure 1.2C**). This linkage is either direct or occurs through an interpeptide bridge (as in many Gram-positive bacteria) (89). The size of the interpeptide bridge, however, can range from one to seven residues. For example, *Staphylococcus aureus* contains a penta-glycine interpeptide bridge that links L-Lys (position 3) to D-Ala (position 4) (56).

As in most Gram-negative species, the crosslinks found in *E. coli* are formed between the penultimate D-Ala on one glycan strand to the mDAP on an adjacent peptide chain (**Figure 1.2C**). This 3-4 crosslink is the result of D,D-transpeptidation reactions responsible for incorporating new PG precursors into the existing cell wall (31, 62). In addition to 3-4 crosslinks, *E. coli* and many other bacteria also form 3-3 crosslinks between two adjacent mDAP residues. These crosslinks are synthesized by L,D-transpeptidases (28, 29) that were recently identified in both Gram-positive and Gram-negative bacteria (44, 45). The functional significance of 3-3 crosslinks is not known. However, several groups have proposed that this type of crosslink may be important in cases where the bacterium is being assaulted by penicillins or their derivatives because penicillin does not inhibit the transpeptidase activity of L,D-

transpeptidases (31, 45). These crosslinks may also be important under conditions where little to no pentapeptides are present in the cell (31, 45).

The PG assembly pathway

The pathway for PG biogenesis occurs in three main stages and spans multiple cellular compartments. The initial steps of assembly occur in the cytoplasm where the monomeric unit of PG, MurNAc(pep5)-GlcNAc, is made. First, the activated sugar UDP-GlcNAc is converted to UDP-MurNAc by the enzymes MurA and MurB (**Figure 1.3A**) (82, 83). This is then followed by the sequential addition of the amino acids comprising the stem peptide attached to the D-lactoyl group of MurNAc. These reactions are catalyzed by the extensively studied Mur ligases (MurC, MurD, MurE and MurF) to add L-Ala, D-Glu, mDAP, and D-Ala-D-Ala, respectively (82).

The essential enzyme, MraY, transfers phospho-MurNAc-pep5 from UDP-MurNAc-pep5 to undecaprenyl-phosphate (a C_{55} isoprenyl-phosphate lipid carrier) to form Lipid I at the cytoplasmic surface of the IM (**Figure 1.3B**) (82, 83). Lipid I formation is likely to be a rate-limiting step due to the limited availability of undecaprenyl-phosphate (82, 83). Lipid II is formed by the attachment of GlcNAc to Lipid I by MurG, a glycosyltransferase using UDP-GlcNAc as a substrate.

In the next phase of PG assembly, Lipid II is translocated from the cytoplasmic side of the IM to the periplasmic side. In recent years, two candidates have been proposed to be the elusive “flippase” that catalyzes this translocation. Work by Ruiz implicates the essential *E. coli* protein MviN (recently renamed MurJ) in this role because when depleted, PG synthesis is reduced and an increase in

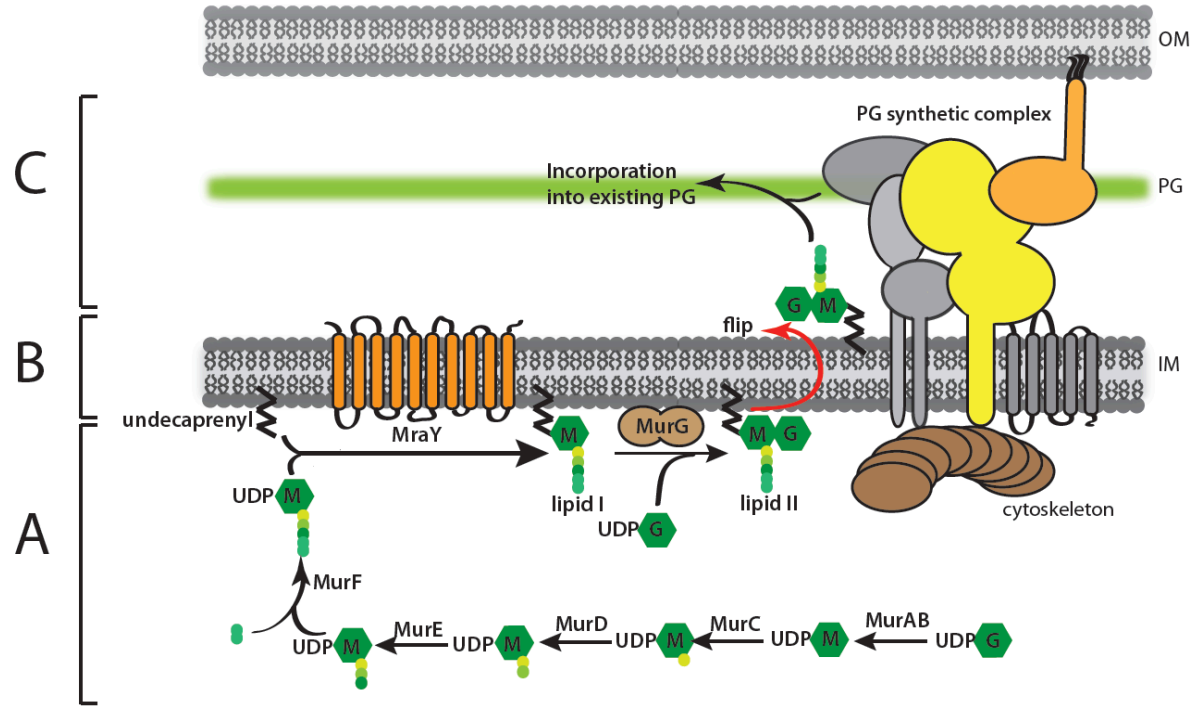

Figure 1.3. Peptidoglycan biogenesis occurs in different cellular compartments.

An overview of the three stages of PG assembly is provided. In the first stage (**A**) UDP-*N*-acetylglucosamine is first converted to UDP-*N*-acetylmuramic acid (M) in the bacterial cytoplasm. Then the five peptide residues are subsequently addition (green dots colored as in **Figure 2B**). See text for enzyme activities. The next stage (**B**) occurs at the cytoplasmic face of the inner membrane where the M-pentapeptide unit is linked to a C_{55}-lipid carrier, undecaprenyl, by the enzyme MraY to form Lipid I. MurG then adds UDP-G to Lipid I to make Lipid II. This PG precursor is then flipped to the periplasmic side of the inner membrane (IM) by a flippase (see text for details) (48, 58).

(Legend continued on next page.)

Figure 1.3 (Continued) (**C**) In the periplasm, Lipid II is polymerized into glycan strands that are crosslinked into the existing PG layer (green). A multi-enzyme PG synthetic complex is thought to perform these activities (see text for details). OM, outer membrane.

cytoplasmic PG precursors is observed (58). This is also supported by work from Kato and coworkers who reported similar results (32). However, MviN homologs in *Bacillus subtilis* were not found to be essential (22). Contradicting these results, a recent report by Mohammadi *et al*. presented biochemical evidence that the Lipid II is flipped to the periplasmic side of the IM by the essential divisome component FtsW rather than MviN (48). They showed that, when purified, the transmembrane protein, FtsW, translocated Lipid II across proteoliposome membranes *in vitro*. No such activity was observed when purified MviN was tested in their assay (48). *In vivo* evidence linking FtsW with flippase activity is lacking, however. Thus, a definitive identification of the Lipid-II flippase awaits further experimentation.

The final stage of PG assembly occurs in the periplasmic compartment of the cell (**Figure 1.3C**). Once exposed to the periplasmic face of the IM, the disaccharide moiety of Lipid II is polymerized and crosslinked into the existing PG layer by the penicillin-binding proteins (PBPs). Undecaprenyl-diphosphate is released and then subsequently recycled for additional rounds of PG synthesis.

The penicillin-binding proteins

Penicillin, an antibiotic targeting the bacterial cell wall, was key in the identification of the PBPs. It forms a covalent complex with these enzymes and inhibits their transpeptidase (TP) activity. Thus, radiolabelled penicillin was used as a probe to identify the PBPs (9). *E. coli,* like many other bacteria, encodes a number of PBPs classified into two main groups: the high-molecular weight (HMW) PBPs and the low-molecular weight (LMW) PBPs (30, 59) (**Table 1.1**). The HMW-PBPs are all integral

membrane proteins with large domains facing the periplasm (**Figure 1.4**). Class A HMW-PBPs (PBP1a, PBP1b, and PBP1c) have both peptidoglycan glycosyltransferase (PGT) and TP activities for polymerizing the glycan strands and crosslinking them, respectively. Class B HMW-PBPs (PBP2 and PBP3) only have TP domains.

In contrast, the LMW-PBPs are all secreted periplasmic proteins and have hydrolytic activity for breaking bonds in PG (**Table 1.1**). They are either D-Ala-D-Ala carboxypeptidases (DD-CPs) that hydrolyze the D-Ala-D-Ala bonds of pentapeptides (PBP4, 5, 6, and 6b), or they are D,D-endopeptidases (DD-EPs) that cleave D-Ala-mDAP crosslinks (PBP4 and 7) (59). Because of their activities, the LMW-PBPs are thought to be regulatory factors that help control where and when PG is made by limiting the supply of donors available to make crosslinks, and by opening up spaces in the existing PG structure to allow the insertion of new material as the cell grows (52).

Reactions catalyzed by the HMW PBPs

Glycosyltransferase reaction. Sequence alignments amongst the PGTs reveal five conserved motifs in the catalytic cleft. Motif 1 (EDxxFxxHXG) (where x indicates a random amino acid) and motif 3 (RKxxE) contain conserved glutamic acids proposed to be involved in catalysis (59). Motif 2 (GxSTxxQQxxK) divides the cleft into two pockets and may play a role in substrate recognition. Both motif 4 (KxxYxxxYxN) and motif 5 (RxxxxL) are thought to maintain the overall fold of the PGT domain (41, 59).

To gain better insight into the PGT reaction mechanism, the crystal structures of three PGT enzymes were recently solved: *S. aureus* PBP2 (41), PBP1a from the thermostable *Aquifex aeolicus* (97), and *E. coli* PBP1b (68). All three structures show

Table 1.1. The penicillin binding proteins of *E. coli*[a].

Class	Protein	Gene	Activity[b]	Essential?	Localization
HMW					
Class A	PBP1a	*ponA (mrcA)*	PGT/TP	No	IM
	PBP1b	*ponB (mrcB)*	PGT/TP	No	IM
	PBP1c	*pbpC*	PGT/TP	No	IM
Class B	PBP2	*pbpA*	TP	Yes	IM
	PBP3	*ftsI*	TP	Yes	IM
LMW					
Class C	PBP4	*dacB*	D,D-EP	No	Periplasm
	PBP4b	*yefW*	D,D-CP	No	Periplasm
	PBP5	*dacA*	D,D-CP	No	Periplasm
	PBP6	*dacC*	D,D-CP	No	Periplasm
	PBP6b	*dacD*	D,D-CP	No	Periplasm
	PBP7	*pbpG*	D,D-EP	No	Periplasm
	AmpH	*ampH*	D,D-Peptidase	No	Periplasm

[a]References: (30, 59, 88, 90)

[b]HMW, high molecular weight; LMW, low molecular weight; PGT, peptidoglycan glycosyltransferase; TP, transpeptidase; EP, endopeptidase; CP, carboxypeptidase

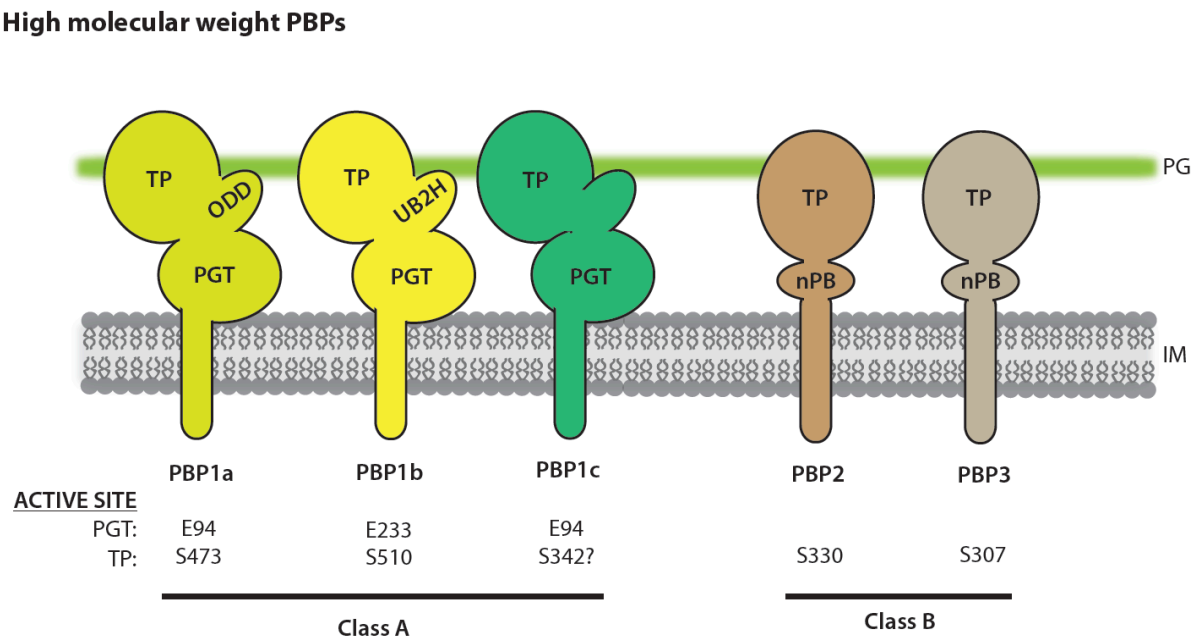

Figure 1.4. The high molecular weight PBPs of *E. coli.* The five *E. coli* proteins are subdivided into two classes based on their activities. The bifunctional class A enzymes PBP1a, PBP1b, and PBP1c contain modular domains exhibiting either peptidoglycan glycosyltransferase (PGT) or transpeptidase (TP) activities. PBP1a and PBP1b both contain an additional domain thought to interact with their cognate Lpo factors (see text for details). The class B proteins PBP2 and PBP3 are essential monofunctional enzymes only exhibiting TP activity. These enzymes also contain a non-penicillin binding domain (nPB) that is thought to mediate protein-protein interactions. The active sites for the specified domains are listed below the enzymes. While PBP1c has no observable TP activity, the putative catalytic serine based upon sequence alignments is listed. ODD, outer membrane PBP1a docking domain (78); UB2H, UvrB domain 2 homolog (68).

hydrophobic surface sites in the portion of the protein closest to the IM, suggesting that the PGT is partially embedded within the membrane (68). In this way, the PGT may easily access the membrane-bound substrate Lipid II for the reaction. The crystal structures also show that the PGT domain consists mostly of α-helices with a fold similar to that of λ-lysozyme, a bacteriophage hydrolase that cleaves the β(1,4)-glycosidic bond.

In addition to the structures, the development of chemical and biochemical synthetic routes to Lipid II production (11, 63, 95) has promoted significant progress in our understanding of the PGT reaction. Several lines of evidence indicate that glycan polymer elongation proceeds by successive attacks of the growing glycan chain (donor) on the reducing end of Lipid-II (acceptor) (63, 75, 93). This is catalyzed by the deprotonation of the 4-OH nucleophile of GlcNAc by the catalytic glutamate of motif 1 (**Figure 1.5**). Concurrently, glutamate of motif 3 stabilizes the leaving diphospho-undecaprenyl group, potentially via a divalent metal (63).

Transpeptidation reaction. The crystal structure of *S. aureus* PBP2a solved by Lim and Strynadka shows that the TP domain consists of two subdomains: a five stranded β-sheet covered by three α-helices and an all-helical domain (40). The active site lies at their interface and contains nine residues broadly conserved in the PBPs (underlined in the motifs below). The active site serine is positioned at the beginning of helix α2 and is followed by a lysine to form a S*xxK (where S* denotes the active site serine). This motif defines a superfamily of serine acyltransferases in bacteria (30). In the formation of crosslinks by the HMW PBPs, the conserved lysine residue is thought

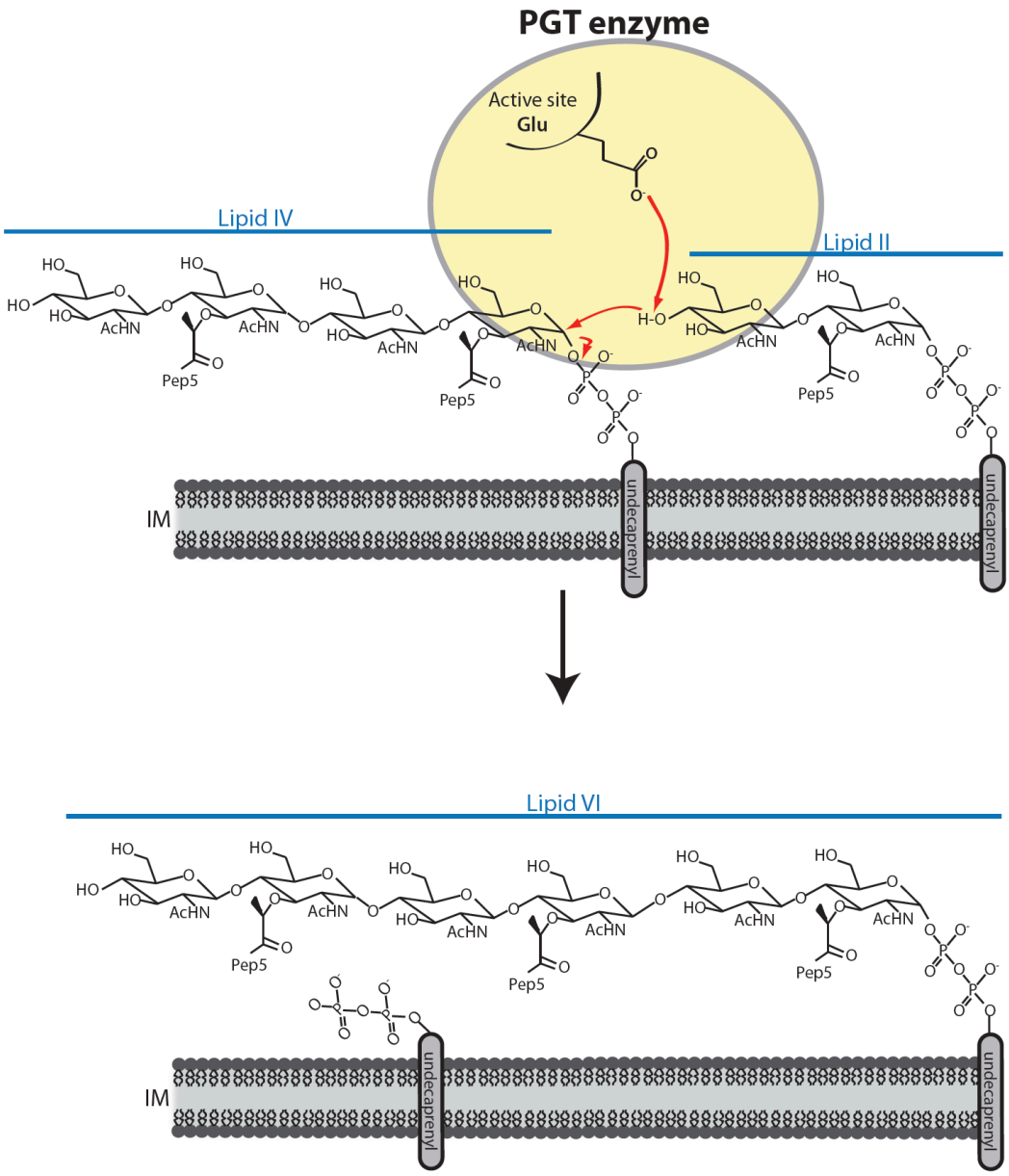

Figure 1.5. The peptidoglycan glycosyltransferase (PGT) reaction. The chemical reaction catalyzed by the PGT synthases predicted to proceed via acid-base chemistry is shown. The attachment of the Lipid II to the non-reducing end of the growing glycan polymer (illustrated as Lipid IV) is mediated by a catalytic glutamate residue in the active site of the PGT enzyme. See text for detailed mechanism.

to deprotonate the active site serine. This deprotonated serine then attacks the penultimate D-Ala of the substrate strand (donor) to form an acylenzyme intermediate with the simultaneous release of the terminal D-Ala (26, 75). This intermediate is thought to be deacylated by a second motif (SxN) situated in a loop between helices α4 and α5 (59). In *E. coli,* a crosslink is then formed between the mDAP residue of a second peptide chain (acceptor) to the penultimate D-Ala on the donor strand strand (**Figure 1.6**) (26, 59).

While the third conserved motif (KTG(T/S)) is not directly involved in catalysis, it is thought to recognize the incoming substrate (59). In the TP domains of the HMW PBPs, the residue following motif 3 is either a serine or threonine for class A PBPs or an alanine for class B PBPs. While the functional significance of this residue is unknown, it is likely playing a class-specific role (59). Further work by Ghosh and Young showed that residues following motif 3 in PBP5 are involved in shape maintenance (25). Finally, the ninth conserved residue in the catalytic cleft is a glycine located at the rear of the active site (59). It is thought to impart binding specificity of the PBPs to the penultimate D-Ala of pep5 (1, 59).

The class A HMW PBPs of *E. coli*

Penicillin-binding protein 1a (PBP1a). Like all class A HMW PBPs (**Figure 1.4**), *E. coli* PBP1a is a bifunctional PG synthase containing a PGT domain and a TP domain. Using Lipid II as a substrate *in vitro*, PBP1a is able to polymerize and crosslink glycan strands. The average glycan strand length produced by PBP1a is 20 disaccharide units with 20% of the pentapeptides involved in crosslinking (10) while a

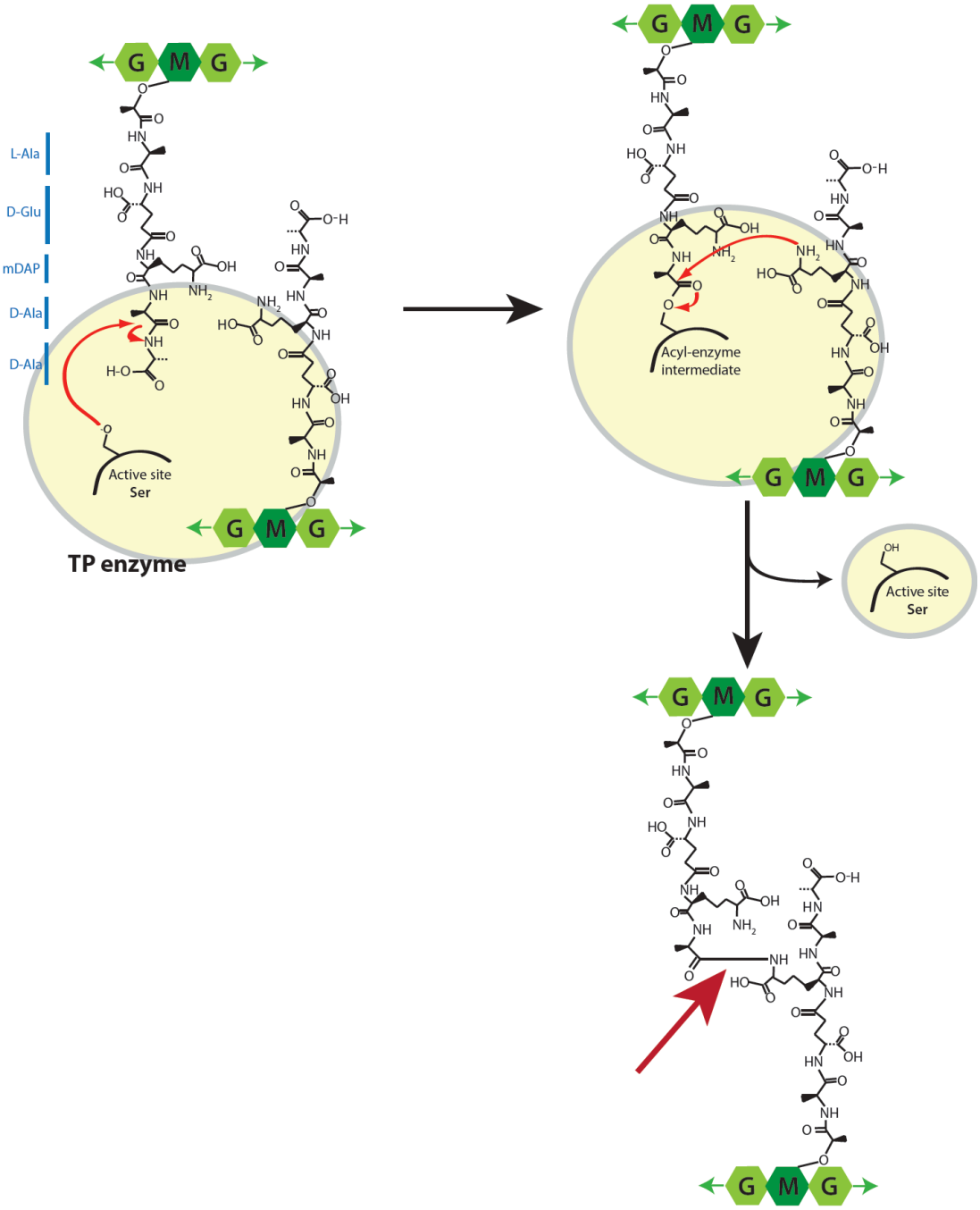

Figure 1.6. The mechanism of transpeptidation (TP). In the first step, the deprotonated active site serine attacks the penultimate D-Ala residue of a donor strand to form an acyl-enzyme intermediate between the TP enzyme and the peptide chain.

(Legend continued on next page.)

Figure 1.6 (Continued) The final D-Ala is released concomitantly. In the second step, the nucleophilic amine of the acceptor strand then attacks the acyl-enzyme intermediate to produce crosslinked peptide side chains. The crosslink is highlighted by the red arrow in the final step. This overall mechanism is conserved among bacteria. Note that the TP enzyme is not drawn to scale.

report by Wang *et al.* found that the limiting length for the PGT domain of PBP1a was 30 disaccharide units (92). Poor TP activity was observed after Lipid II had been exhausted, suggesting that ongoing glycan strand polymerization is needed for TP function (10). Also, no TP activity was observed when a PGT mutant of PBP1a was mixed with a PBP1a TP mutant (10). This has also been observed for other class A PBPs and likely points to an interaction between the two domains of PBP1a leading to TP activation (3, 10, 51, 74).

Even though the biochemical activities of PBP1a have been extensively characterized (2, 10, 42, 88, 92), the physiological role of PBP1a remains unclear. Cells lacking PBP1a do not exhibit any significant growth defect, change in cell shape, or sensitivity towards β-lactam antibiotics (54, 96). However, cells without PBP1b (see below) are more sensitive to these same antibiotics, consistent with the idea that PBP1a has a higher affinity to most β-lactams as compared to PBP1b (70, 88). Also, experiments by Vollmer and coworkers highlighted unique differences between cells lacking PBP1a, PBP1b, or both. Only cells without PBP1b lose cell integrity when the essential PBP2, PBP3, or the cell division protein FtsQ are inactivated (10, 23, 88). Also, PBP1a is only able to dimerize with itself and not with PBP1b (19, 98). These results, along with the genetic evidence above, suggest that both proteins have distinct cellular functions. However, PBP1a and PBP1b are partially redundant because neither is essential, and only inactivation of both PBP1a and PBP1b leads to a synthetic lethal phenotype (70, 73).

Even though the structures of other class A HMW PBPs have been solved (41, 97), *E. coli* PBP1a contains an additional domain not present in these crystal

structures. Recently, bioinformatics work by Typas *et al*. discovered this domain named ODD, for outer-membrane PBP1a docking domain, in PBP1a that may be required for interactions with its binding partners (78).

Penicillin-binding protein 1b (PBP1b). PBP1b is thought to play a prominent role in PG synthesis (39, 71). Even though PBP1b is not essential, cells lacking it show little to no PG synthetic activity (36, 37, 54) and are more sensitive to β-lactam antibiotics (96). PBP1b exists in three different isoforms: α, β, and γ. PBP1b-α is the full-length protein, while PBP1b-β is considered an artifact that results from proteolytic processing of the first 24 residues due to *in vitro* preparation (69). The γ isoform arises from a translational start site beginning 46 residues downstream from the full-length PBP1b start site (69). While the functional significance of the α and γ isoforms is unclear, it has been proposed that PBP1b-α may be involved in cell division while PBP1b-γ may play a role during elongation of the PG at the lateral wall (17, 88). While analyzing the three PBP1b isoforms, Chalut *et al*. found only full-length PBP1b is able to suppress cell lysis when cells were treated with cephaloridine (a cephalosporin that preferentially binds PBP1a) and aztreonam (that preferentially binds PBP3) (17), thus suggesting a specific role for PBP1b-α in cell division.

Similar to PBP1a, PBP1b also forms dimers *in vivo* (19, 98). This is not dependent on disulfide bond formation (18), and the N-terminal cytoplasmic tail is not involved in the dimerization process (17). Studies performed by truncating the protein show that dimerization is mediated by an interaction in the N-terminal region of the protein before residue G405 (98). Also, two dimensional gel analysis indicates that only

homodimers of PBP1b isoforms (α-α, β-β, and γ-γ) are formed (98). Recent work by Vollmer and coworkers has shown that PBP1b dimer formation is likely required for robust synthetic activity (3, 10, 88).

Recently, the crystal structure of *E. coli* PBP1b was solved with the PGT inhibitor, moenomycin, in the presumed Lipid II binding cleft (68). This structure had an additional small domain located between the PGT and TP domains. This UB2H (UvrB domain 2 homolog) domain is not present in other class A HMW PBP crystal structures (41). It is only present in γ-proteobacteria (78). Originally, this domain was thought to play a proofreading and editing role based upon its homology to UvrB in the nucleotide excision repair system for DNA damage (68). Sung *et al*. showed that PBP1b variants lacking this domain are partially functional and filament at high temperatures. However, Typas *et al*. were not able to confirm these results. Rather, they proposed that UB2H is a domain that interacts with other factors, similar to the ODD domain of PBP1a (78).

Penicillin-binding protein 1c (PBP1c). Even though the domain structure of PBP1c is similar to both PBP1a and PBP1b (**Figure 1.4**), two major differences exist between these proteins. First, the PGT domain of PBP1c lacks three highly conserved residues thought to be required for glycan strand polymerization (R136 and E140 of motif 3 and R218 in motif 5) (59), however, it still exhibits PGT activity in ether-permeabilized cells and in crude membrane vesicle extracts (61). Additionally, it is still inhibited by the moenomycin, similar to PBP1a and PBP1b (61). These results suggest that residues other than those described enable PBP1c to polymerize glycan strands. Second, while PBP1c has a TP domain similar to the other class A HMW PBPs, it is

unaffected by most β-lactam antibiotics and exhibits significantly different binding affinities for them as compared to other PBPs (38, 61, 88). Combined with the observed lack of TP activity (61), these results are consistent with the idea that PBP1c acts as a monofunctional PGT *in vivo*. The TP domain instead may act as a scaffold to interact with other proteins like PBP1b, PBP3 and MltA (57, 61, 87). While the physiological importance of PBP1c is unclear, it is likely that PBP1c has a specific function that differs from PBP1a or PBP1b, especially since it cannot support cell growth in their absence (59, 61, 88).

Two modes of PG synthesis in rod-shaped cells

To determine if different PBPs played specific roles in cell growth and morphogenesis, Spratt treated cells with an array of different penicillin derivatives to determine if any had specific effects on cell shape or cell division. He found that treating cells with either mecillinam or cephalexin led to drastic morphological changes where rod-shaped *E. coli* turned into spheres or filamentous cells, respectively (66, 67). Competitive binding experiments revealed that mecillinam specifically bound PBP2, highlighting a role for it in maintaining the rod-shape of the cell. Cephalexin, on the other hand, was shown to have a high affinity for PBP3, suggesting a primary role for it in cell division (66, 67). This work combined with experiments monitoring the incorporation of new material into the PG led to the hypothesis that for rod-shaped bacteria like *E. coli*, two distinct complexes are associated with two different phases of PG growth: an elongation phase and a division phase (14, 15). During elongation, new material is inserted along the cylindrical portion of the PG. Following elongation, the

mode of PG growth switches to a concentrated zone of synthesis at the site of cell division (14, 15).

The PBPs are part of multi-enzyme complexes *in vivo*

A growing body of evidence suggests that the different modes of PG biogenesis are carried our by multi-enzyme complexes controlled by an underlying cytoskeletal structure. MreB, an actin-like cytoskeletal protein (21, 53), appears to work with PBP1a, PBP2, RodA, MreC, and MreD to control PG synthesis along the cylindrical portion of *E. coli* (14, 15, 77). When MreB is either depleted or inhibited by the drug A22, rod-shaped cells become spheres (27, 33, 72), similar to PBP2 inhibition by mecillinam. This is consistent with the idea that MreB is required for rod shape (27, 33, 72). Also MreB localizes in a helical pattern similar to the pattern observed when new PG material is inserted into the lateral wall (16, 65, 76). This result further implicated MreB in lateral PG synthesis. To investigate this, Garner *et al.* recently compared the localization dynamics of MreB and the elongation machinery in *Bacillus subtilis* (24). They observed that the dynamic movement of MreB is blocked when PG synthesis is inhibited by drugs or when essential components of the elongation complex were depleted (24). This suggests that MreB acts to guide the lateral wall PG synthetic complex but not to drive PG synthesis. This idea is also supported by evidence from Carballido-López and coworkers (20).

During the division phase, the essential FtsZ, a tubulin-like protein, coordinates the formation of the divisome (or Z-ring) at the site of cell division and is required for the recruitment of all downstream divisome factors (5, 6, 15, 50). Inhibition or depletion

of FtsZ blocked cell division and caused rod-shaped cells to filament thus implicating FtsZ in shape determination (5, 7, 43, 60). In *E. coli*, the divisome starts to assemble when FtsZ and its associated proteins FtsA and ZipA localize to future sites of cell division. The latter two components are required to help stabilize the forming Z-ring at the IM. Other Fts proteins are then recruited in a hierarchical manner (**Figure 1.7**) along with factors needed for PG synthesis and PG splitting at the septum (12, 43, 85, 86). PBP1b is thought to primarily work during cell division based on observed interactions with the division proteins PBP3 (FtsI) and FtsN (4, 49).

While it is clear that these cytoskeletal structures are playing major roles in PG biogenesis, we currently know very little about the organization of these cytoskeletal assemblies and exactly how they are controlling the PG construction process.

Hydrolytic enzymes involved in PG synthesis

In order for the PG layer to grow, bonds in the existing PG structure need to be broken to insert new material. Components of the multi-enzyme PG synthetic complexes with PG hydrolase activity are thought to perform this function (31, 34, 35, 78, 84, 87). In addition to PG growth, hydrolases are also required for PG turnover, PG recycling, and cell division (31). During division the septal PG shared by two daughter cells needs to be split for cytokinesis to occur. This septal PG then forms the poles of these daughter cells (8, 79).

PG hydrolases need to be properly controlled to prevent breaches in the PG layer from forming. This is especially important for Gram-negative bacteria that have a thin PG layer. Thus these factors are tightly regulated both spatially and temporally,

especially the enzymes involved in cell separation (55, 64, 80, 81, 94). Work from our lab has shown that the activity of the *E. coli* cell separation amidases (AmiA, AmiB and AmiC) is controlled by a group LytM-domain containing proteins (80). Genetic experiments and biochemical studies using labelled PG revealed that these amidases, which cleave the peptide chain from glycan strands, are only active in the presence of their cognate LytM domain-containing factor (80). Additionally, our lab recently showed that the regulator of AmiA and AmiB activity, EnvC, is itself regulated by a transmembrane component of the divisome, FtsEX (94). Although FtsEX is an ABC transporter-like complex that is recruited to the divisome (**Figure 1.7)**, its role has remained unclear. However, we showed that EnvC needs to directly interact with FtsX to localize to the divisome (94). Additionally, mutations in the nucleotide binding component of the complex, FtsE predicted to abolish ATPase activity, do not affect the localization of EnvC or the FtsEX complex. However, these ATPase-defective complexes failed to promote daughter cell separation, suggesting that ATP-driven conformational changes in the complex might regulate the ability of EnvC to activate the amidases (see **Appendix 1**) (94). Such a role for FtsEX appears to be widely conserved as Sham and co-workers have connected the complex to the major cell separation protein PcsB of *S. pneumoniae* (64).

While a clearer picture is emerging for how hydrolases are controlled during septal PG splitting, little is known about the PG hydrolases involved in lateral wall growth or how they are regulated. It is widely believed that PG synthesis and PG hydrolysis are coordinated by the multi-enzyme PG biogenesis complexes. The overall idea is that the PG hydrolases may work only when they join an active complex

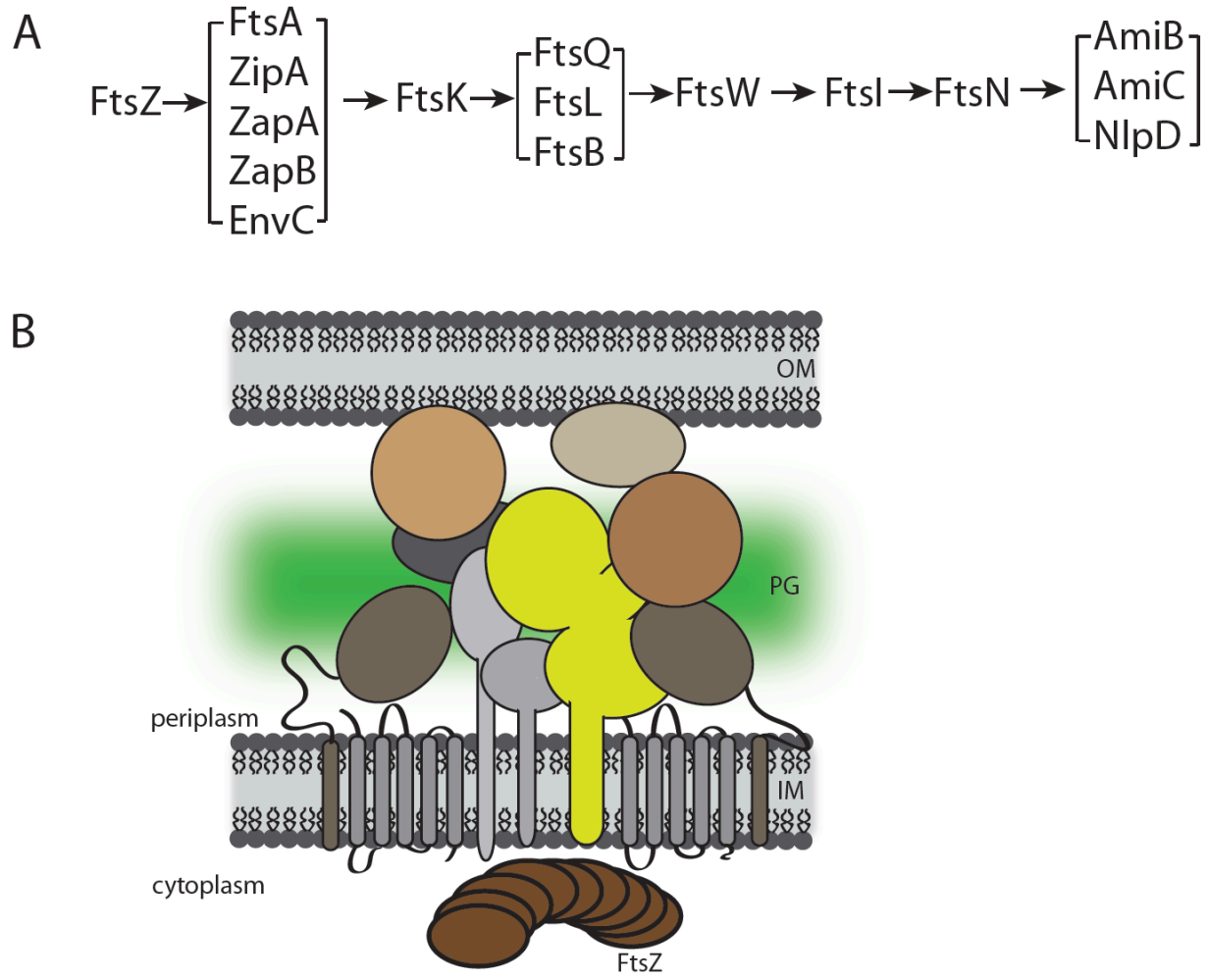

Figure 1.7. Recruitment of proteins to the division site. Once FtsZ is localized to the midcell, proteins are recruited to the division complex (divisome) in a hierarchical manner. The recruitment order of these proteins is illustrated in (**A**). Localization of each protein to the divisome is dependent on the protein preceding it. A schematic of the trans-envelope division complex that spans multiple cellular compartments is shown in (**B**) (13, 55).

containing PBPs. Indeed, several studies have identified interactions connecting PBPs with PG hydrolases (47, 78, 87). However, the functional significance of these complexes has not been established.

Research statement

Although we know a great deal about PBP structure and biochemical activity, surprisingly little is understood about how the multi-enzyme complexes containing PBPs function to build the PG matrix. Just as the PG hydrolase must be regulated, it is likely that the PBPs themselves are controlled by components of the synthetic complexes. Such regulators have been difficult to identify because functional redundancy has hampered genetic analysis of PBP function. The work described in this thesis began by developing a strategy to turn the redundancy of the E. coli PBPs into an advantage. Based on the essentiality of the PBP1a/PBP1b combination, we reasoned that factors required to promote PBP1a activity could be identified by screening for mutants synthetically lethal with the loss of PBP1b (*slb* mutants) and vice versa. Using this technique, we identified the *E. coli* outer membrane lipoproteins LpoA (YraM) and LpoB (YcfM) as essential PBP cofactors. We showed that they form specific trans-envelope complexes with their cognate PBP1 and are critical for PBP1 function *in vivo*. Overall, our results showed that these PBP accessory factors play a crucial role in PG biogenesis (see **Chapter 2**) (54).

However, while we had shown that one of these cofactors, LpoB is critical for PBP1b activity *in vivo* and activates the PGT activity of PBP1b *in vitro*, the role of LpoB still in PG assembly remained unclear. To investigate the role of LpoB further, we

sought to identify variants of PBP1b that bypass the need for LpoB function *in vivo*. To isolate these *ponB** alleles, we took advantage of the cefsulodin hypersensitive phenotype shared by *ponB* and *lpoB* mutants. We reasoned that the cefsulodin hypersensitivity of *lpoB* mutants results from a defect in PBP1b activity. Therefore, *ponB** alleles with partially restored PBP1b function might be isolated by selecting for *lpoB* mutants with increased cefsulodin resistance. Using this strategy, several PBP1b* variants were isolated. The characterization of these PBP1b* variants is detailed in **Chapter 3**.

The final chapter (**Chapter 4**) of this thesis focuses on our current understanding of how PG synthesis fits into the overall process of cellular growth. Although much progress has been made in our understanding of the bacterial cell envelope and PG biogenesis over the years, many unanswered questions still remain. For example, we still do not know how the switch between the elongation and division modes of PG synthesis is controlled or how cytoskeletal structures organize PG biogenesis. Moreover, the precise roles of PG hydrolases in the PG assembly process are not known or how their potentially lethal activity is regulated, especially during lateral PG growth. While much remains to be understood, the work described in this thesis represents a significant advance in the area of PBP regulation and it paves the way for future studies aimed at determining the detailed mechanism of PG biogenesis *in vivo*.

References

1. **Adediran, S. A.**, **Z. Zhang**, **M. Nukaga**, **T. Palzkill**, **and R. F. Pratt**. 2005. The D-methyl group in beta-lactamase evolution: evidence from the Y221G and GC1 mutants of the class C beta-lactamase of Enterobacter cloacae P99. Biochemistry **44**:7543–7552.

2. **Barrett, D.**, **T.-S. A. Wang**, **Y. Yuan**, **Y. Zhang**, **D. Kahne**, **and S. Walker**. 2007. Analysis of glycan polymers produced by peptidoglycan glycosyltransferases. J Biol Chem **282**:31964–31971.

3. **Bertsche, U.**, **E. Breukink**, **T. Kast**, **and W. Vollmer**. 2005. In vitro murein peptidoglycan synthesis by dimers of the bifunctional transglycosylase-transpeptidase PBP1B from Escherichia coli. J Biol Chem **280**:38096–38101.

4. **Bertsche, U.**, **T. Kast**, **B. Wolf**, **C. Fraipont**, **M. E. G. Aarsman**, **K. Kannenberg**, **M. von Rechenberg**, **M. Nguyen-Distèche**, **T. den Blaauwen**, **J.-V. Höltje**, **and W. Vollmer**. 2006. Interaction between two murein (peptidoglycan) synthases, PBP3 and PBP1B, in Escherichia coli. Mol Microbiol **61**:675–690.

5. **Bi, E. F.**, **and J. Lutkenhaus**. 1991. FtsZ ring structure associated with division in Escherichia coli. Nature **354**:161–164.

6. **Bi, E.**, **K. Dai**, **S. Subbarao**, **B. Beall**, **and J. Lutkenhaus**. 1991. FtsZ and cell division. Research in Microbiology **142**:249–252.

7. **Bi, E.**, **and J. Lutkenhaus**. 1992. Isolation and characterization of ftsZ alleles that affect septal morphology. J Bacteriol **174**:5414–5423.

8. **Blaauwen, den, T.**, **M. A. de Pedro**, **M. Nguyen-DistÃ che**, **and J. A. Ayala**. 2008. Morphogenesis of rod-shaped sacculi. FEMS Microbiol Rev **32**:321–344.

9. **Blumberg, P. M.**, **and J. L. Strominger**. 1972. Five penicillin-binding components occur in Bacillus subtilis membranes. J Biol Chem **247**:8107–8113.

10. **Born, P.**, **E. Breukink**, **and W. Vollmer**. 2006. In vitro synthesis of cross-linked murein and its attachment to sacculi by PBP1A from Escherichia coli. J Biol Chem **281**:26985–26993.

11. **Breukink, E.** 2003. Lipid II Is an Intrinsic Component of the Pore Induced by Nisin in Bacterial Membranes. Journal of Biological Chemistry **278**:19898–19903.

12. **Buddelmeijer, N.**, **and J. Beckwith**. 2004. A complex of the Escherichia coli cell division proteins FtsL, FtsB and FtsQ forms independently of its localization to the septal region. Mol Microbiol **52**:1315–1327.

13. **Buddelmeijer, N.**, **and J. Beckwith**. 2002. Assembly of cell division proteins at the E. coli cell center. Curr Opin Microbiol **5**:553–557.

14. **Cabeen, M.**, **and C. Jacobs-Wagner**. 2007. Skin and bones: the bacterial cytoskeleton, cell wall, and cell morphogenesis. The Journal of Cell Biology **175**:381-387.

15. **Cabeen, M. T.**, **and C. Jacobs-Wagner**. 2005. Bacterial cell shape. Nat Rev Micro **3**:601–610.

16. **Carballido-López, R.**, **and J. Errington**. 2003. The bacterial cytoskeleton: in vivo dynamics of the actin-like protein Mbl of Bacillus subtilis. Developmental Cell **4**:19–28.

17. **Chalut, C.**, **X. Charpentier**, **M. H. Rémy**, **and J. M. Masson**. 2001. Differential responses of Escherichia coli cells expressing cytoplasmic domain mutants of penicillin-binding protein 1b after impairment of penicillin-binding proteins 1a and 3. J Bacteriol **183**:200–206.

18. **Chalut, C.**, **M. H. Rémy**, **and J. M. Masson**. 1999. Disulfide bridges are not involved in penicillin-binding protein 1b dimerization in Escherichia coli. J Bacteriol **181**:2970–2972.

19. **Charpentier, X.**, **C. Chalut**, **M.-H. Rémy**, **and J.-M. Masson**. 2002. Penicillin-binding proteins 1a and 1b form independent dimers in Escherichia coli. J Bacteriol **184**:3749–3752.

20. **Domínguez-Escobar, J.**, **A. Chastanet**, **A. H. Crevenna**, **V. Fromion**, **R. Wedlich-Söldner**, **and R. Carballido-López**. 2011. Processive movement of MreB-associated cell wall biosynthetic complexes in bacteria. Science **333**:225–228.

21. **Erickson, H. P.** 2001. Cytoskeleton. Evolution in bacteria. Nature **413**:30.

22. **Fay, A.**, **and J. Dworkin**. 2009. Bacillus subtilis Homologs of MviN (MurJ), the Putative Escherichia coli Lipid II Flippase, Are Not Essential for Growth. J Bacteriol **191**:6020–6028.

23. **García del Portillo, F.**, **and M. A. de Pedro**. 1990. Differential effect of mutational impairment of penicillin-binding proteins 1A and 1B on Escherichia coli strains harboring thermosensitive mutations in the cell division genes ftsA, ftsQ, ftsZ, and pbpB. J Bacteriol **172**:5863–5870.

24. **Garner, E. C.**, **R. Bernard**, **W. Wang**, **X. Zhuang**, **D. Z. Rudner**, **and T. Mitchison**. 2011. Coupled, circumferential motions of the cell wall synthesis machinery and MreB filaments in B. subtilis. Science **333**:222–225.

25. **Ghosh, A. S.**, **and K. D. Young**. 2003. Sequences near the active site in chimeric penicillin binding proteins 5 and 6 affect uniform morphology of Escherichia coli. J Bacteriol **185**:2178–2186.

26. **Ghuysen, J. M.** 1991. Serine beta-lactamases and penicillin-binding proteins. Annu Rev Microbiol **45**:37–67.

27. **Gitai, Z.**, **N. A. Dye**, **A. Reisenauer**, **M. Wachi**, **and L. Shapiro**. 2005. MreB Actin-Mediated Segregation of a Specific Region of a Bacterial Chromosome. Cell **120**:329–341.

28. **Glauner, B.**, **and J. V. Höltje**. 1990. Growth pattern of the murein sacculus of Escherichia coli. J Biol Chem **265**:18988–18996.

29. **Glauner, B.**, **J. V. Höltje**, **and U. Schwarz**. 1988. The composition of the murein of Escherichia coli. J Biol Chem **263**:10088–10095.

30. **Goffin, C.**, **and J. M. Ghuysen**. 1998. Multimodular penicillin-binding proteins: an enigmatic family of orthologs and paralogs. Microbiol Mol Biol Rev **62**:1079–1093.

31. **Höltje, J. V.** 1998. Growth of the stress-bearing and shape-maintaining murein sacculus of Escherichia coli. Microbiol Mol Biol Rev **62**:181–203.

32. **Inoue, A.**, **Y. Murata**, **H. Takahashi**, **N. Tsuji**, **S. Fujisaki**, **and J. I. Kato**. 2008. Involvement of an Essential Gene, mviN, in Murein Synthesis in Escherichia coli. J Bacteriol **190**:7298–7301.

33. **Karczmarek, A.**, **R. M.-A. Baselga**, **S. Alexeeva**, **F. G. Hansen**, **M. Vicente**, **N. Nanninga**, **and T. den Blaauwen**. 2007. DNA and origin region segregation are not affected by the transition from rod to sphere after inhibition of Escherichia coliMreB by A22. Mol Microbiol **65**:51–63.

34. **Koch, A. L.** 1990. Additional arguments for the key role of “smart” autolysins in the enlargement of the wall of gram-negative bacteria. Research in Microbiology **141**:529–541.

35. **Koch, A. L.** 1982. On the growth and form of Escherichia coli. J Gen Microbiol **128**:2527–2539.

36. **Kraus, W.**, **B. Glauner**, **and J. V. Höltje**. 1985. UDP-N-acetylmuramylpentapeptide as acceptor in murein biosynthesis in Escherichia coli membranes and ether-permeabilized cells. J Bacteriol **162**:1000–1004.

37. **Kraus, W.**, **and J. V. Höltje**. 1987. Two distinct transpeptidation reactions during murein synthesis in Escherichia coli. J Bacteriol **169**:3099–3103.

38. **Labia, R.**, **P. Baron**, **and J. M. Masson**. 1985. Binding of latamoxef (moxalactam) and its decarboxylated derivative to Escherichia coli and Pseudomonas aeruginosa penicillin-binding proteins. J Antimicrob Chemother **15**:9–15.

39. **Lefèvre, F.**, **M. H. Rémy**, **and J. M. Masson**. 1997. Topographical and functional investigation of Escherichia coli penicillin-binding protein 1b by alanine stretch scanning mutagenesis. J Bacteriol **179**:4761–4767.

40. **Lim, D.**, **and N. C. J. Strynadka**. 2002. Structural basis for the beta lactam resistance of PBP2a from methicillin-resistant Staphylococcus aureus. Nat. Struct. Biol. **9**:870–876.

41. **Lovering, A. L.**, **L. H. de Castro**, **D. Lim**, **and N. C. J. Strynadka**. 2007. Structural insight into the transglycosylation step of bacterial cell-wall biosynthesis. Science **315**:1402–1405.

42. **Lupoli, T. J.**, **H. Tsukamoto**, **E. H. Doud**, **T.-S. A. Wang**, **S. Walker**, **and D. Kahne**. 2011. Transpeptidase-Mediated Incorporation of d-Amino Acids into Bacterial Peptidoglycan. J Am Chem Soc **133**:10748–10751.

43. **Lutkenhaus, J.**, **and S. G. Addinall**. 1997. Bacterial cell division and the Z ring. Annu Rev Biochem **66**:93–116.

44. **Magnet, S.**, **L. Dubost**, **A. Marie**, **M. Arthur**, **and L. Gutmann**. 2008. Identification of the L,D-Transpeptidases for Peptidoglycan Cross-Linking in Escherichia coli. J Bacteriol **190**:4782–4785.

45. **Mainardi, J.-L.**, **M. Fourgeaud**, **J.-E. Hugonnet**, **L. Dubost**, **J.-P. Brouard**, **J. Ouazzani**, **L. B. Rice**, **L. Gutmann**, **and M. Arthur**. 2005. A novel

peptidoglycan cross-linking enzyme for a beta-lactam-resistant transpeptidation pathway. J Biol Chem **280**:38146–38152.

46. **Margolin, W.** 2009. Sculpting the Bacterial Cell. Current Biology **19**:R812–R822.

47. **Meisel, U.**, **J.-V. Höltje**, **and W. Vollmer**. 2003. Overproduction of inactive variants of the murein synthase PBP1B causes lysis in Escherichia coli. J Bacteriol **185**:5342–5348.

48. **Mohammadi, T.**, **V. van Dam**, **R. Sijbrandi**, **T. Vernet**, **A. Zapun**, **A. Bouhss**, **M. Diepeveen-de Bruin**, **M. Nguyen-Distèche**, **B. de Kruijff**, **and E. Breukink**. 2011. Identification of FtsW as a transporter of lipid-linked cell wall precursors across the membrane. EMBO J **30**:1425–1432.

49. **Müller, P.**, **C. Ewers**, **U. Bertsche**, **M. Anstett**, **T. Kallis**, **E. Breukink**, **C. Fraipont**, **M. Terrak**, **M. Nguyen-Distèche**, **and W. Vollmer**. 2007. The essential cell division protein FtsN interacts with the murein (peptidoglycan) synthase PBP1B in Escherichia coli. J Biol Chem **282**:36394–36402.

50. **Møller-Jensen, J.**, **and J. Löwe**. 2005. Increasing complexity of the bacterial cytoskeleton. Current Opinion in Cell Biology **17**:75–81.

51. **Nakagawa, J.**, **S. Tamaki**, **S. Tomioka**, **and M. Matsuhashi**. 1984. Functional biosynthesis of cell wall peptidoglycan by polymorphic bifunctional polypeptides. Penicillin-binding protein 1Bs of Escherichia coli with activities of transglycosylase and transpeptidase. J Biol Chem **259**:13937–13946.

52. **Nelson, D. E.**, **and K. D. Young**. 2001. Contributions of PBP 5 and DD-carboxypeptidase penicillin binding proteins to maintenance of cell shape in Escherichia coli. J Bacteriol **183**:3055–3064.

53. **Normark, S.** 1969. Mutation in Escherichia coli K-12 mediating spherelike envelopes and changes tolerance to ultraviolet irradiation and some antibiotics. J Bacteriol **98**:1274–1277.

54. **Paradis-Bleau, C.**, **M. Markovski**, **T. Uehara**, **T. J. Lupoli**, **S. Walker**, **D. E. Kahne**, **and T. G. Bernhardt**. 2010. Lipoprotein cofactors located in the outer membrane activate bacterial cell wall polymerases. Cell **143**:1110–1120.

55. **Peters, N. T.**, **T. Dinh**, **and T. G. Bernhardt**. 2011. A fail-safe mechanism in the septal ring assembly pathway generated by the sequential recruitment of cell separation amidases and their activators. J Bacteriol **193:**4973-4983.

56. **Plata, K.**, **A. E. Rosato**, **and G. Wegrzyn**. 2009. Staphylococcus aureus as an infectious agent: overview of biochemistry and molecular genetics of its pathogenicity. Acta Biochim Pol **56**:597–612.

57. **Rechenberg, von, M.**, **A. Ursinus**, **and J. V. Höltje**. 1996. Affinity chromatography as a means to study multienzyme complexes involved in murein synthesis. Microb. Drug Resist. **2**:155–157.

58. **Ruiz, N.** 2008. Bioinformatics identification of MurJ (MviN) as the peptidoglycan lipid II flippase in Escherichia coli. Proc Natl Acad Sci USA **105:**15553-15557.

59. **Sauvage, E.**, **F. D. R. Kerff**, **M. Terrak**, **J. A. Ayala**, **and P. Charlier**. 2008. The penicillin-binding proteins: structure and role in peptidoglycan biosynthesis. FEMS Microbiol Rev **32**:234–258.

60. **Scheffers, D.-J.** 2007. Cell wall growth during elongation and division: one ring to bind them? Mol Microbiol **64**:877–880.

61. **Schiffer, G.**, **and J. V. Höltje**. 1999. Cloning and characterization of PBP 1C, a third member of the multimodular class A penicillin-binding proteins of Escherichia coli. J Biol Chem **274**:32031–32039.

62. **Schleifer, K. H.**, **and O. Kandler**. 1972. Peptidoglycan types of bacterial cell walls and their taxonomic implications. Bacteriological reviews **36**:407–477.

63. **Schwartz, B.**, **J. A. Markwalder**, **S. P. Seitz**, **Y. Wang**, **and R. L. Stein**. 2002. A kinetic characterization of the glycosyltransferase activity of Eschericia coli PBP1b and development of a continuous fluorescence assay. Biochemistry **41**:12552–12561.

64. **Sham, L.-T.**, **S. M. Barendt**, **K. E. Kopecky**, **and M. E. Winkler**. 2011. Essential PcsB putative peptidoglycan hydrolase interacts with the essential FtsXSpn cell division protein in Streptococcus pneumoniae D39. Proc Natl Acad Sci USA **108**:E1061–9.

65. **Soufo, H. J. D.**, **and P. L. Graumann**. 2003. Actin-like proteins MreB and Mbl from Bacillus subtilis are required for bipolar positioning of replication origins. Curr. Biol. **13**:1916–1920.

66. **Spratt, B. G.** 1975. Distinct penicillin binding proteins involved in the division, elongation, and shape of Escherichia coli K12. Proc Natl Acad Sci USA **72**:2999–3003.

67. **Spratt, B. G.**, **and A. B. Pardee**. 1975. Penicillin-binding proteins and cell shape in E. coli. Nature **254**:516–517.

68. **Sung, M.-T.**, **Y.-T. Lai**, **C.-Y. Huang**, **L.-Y. Chou**, **H.-W. Shih**, **W.-C. Cheng**, **C.-H. Wong**, **and C. Ma**. 2009. Crystal structure of the membrane-bound bifunctional transglycosylase PBP1b from Escherichia coli. Proc Natl Acad Sci USA **106**:8824–8829.

69. **Suzuki, H.**, **J. Kato**, **Y. Sakagami**, **M. Mori**, **A. Suzuki**, **and Y. Hirota**. 1987. Conversion of the alpha component of penicillin-binding protein 1b to the beta component in Escherichia coli. J Bacteriol **169**:891–893.

70. **Suzuki, H.**, **Y. Nishimura**, **and Y. Hirota**. 1978. On the process of cellular division in Escherichia coli: a series of mutants of E. coli altered in the penicillin-binding proteins. Proc Natl Acad Sci USA **75**:664–668.

71. **Suzuki, H.**, **Y. van Heijenoort**, **T. Tamura**, **J. Mizoguchi**, **Y. Hirota**, **and J. van Heijenoort**. 1980. In vitro peptidoglycan polymerization catalysed by penicillin binding protein 1b of Escherichia coli K-12. FEBS Letters **110**:245–249.

72. **Takacs, C. N.**, **S. Poggio**, **G. Charbon**, **M. Pucheault**, **W. Vollmer**, **and C. Jacobs-Wagner**. 2010. MreB Drives De Novo Rod Morphogenesis in Caulobacter crescentus via Remodeling of the Cell Wall. J Bacteriol **192**:1671–1684.

73. **Tamaki, S.**, **S. Nakajima**, **and M. Matsuhashi**. 1977. Thermosensitive mutation in Escherichia coli simultaneously causing defects in penicillin-binding protein-1Bs and in enzyme activity for peptidoglycan synthesis in vitro. Proc Natl Acad Sci USA **74**:5472–5476.

74. **Terrak, M.**, **T. K. Ghosh**, **J. van Heijenoort**, **J. Van Beeumen**, **M. Lampilas**, **J. Aszodi**, **J. A. Ayala**, **J. M. Ghuysen**, **and M. Nguyen-Distèche**. 1999. The catalytic, glycosyl transferase and acyl transferase modules of the cell wall peptidoglycan-polymerizing penicillin-binding protein 1b of Escherichia coli. Mol Microbiol **34**:350–364.

75. **Terrak, M.**, **E. Sauvage**, **A. Derouaux**, **D. Dehareng**, **A. Bouhss**, **E. Breukink**, **S. Jeanjean**, **and M. Nguyen-Distèche**. 2008. Importance of the conserved residues in the peptidoglycan glycosyltransferase module of the class A penicillin-binding protein 1b of Escherichia coli. J Biol Chem **283**:28464–28470.

76. **Tiyanont, K.**, **T. Doan**, **M. B. Lazarus**, **X. Fang**, **D. Z. Rudner**, **and S. Walker**. 2006. Imaging peptidoglycan biosynthesis in Bacillus subtilis with fluorescent antibiotics. Proc Natl Acad Sci USA **103**:11033–11038.

77. **Typas, A.**, **M. Banzhaf**, **C. A. Gross**, **and W. Vollmer**. 2011. From the regulation of peptidoglycan synthesis to bacterial growth and morphology. Nat Rev Micro **10:**123-136.

78. **Typas, A.**, **M. Banzhaf**, **B. van den Berg van Saparoea**, **J. Verheul**, **J. Biboy**, **R. J. Nichols**, **M. Zietek**, **K. Beilharz**, **K. Kannenberg**, **M. von Rechenberg**, **E. Breukink**, **T. den Blaauwen**, **C. A. Gross**, **and W. Vollmer**. 2010. Regulation of peptidoglycan synthesis by outer-membrane proteins. Cell **143**:1097–1109.

79. **Uehara, T.**, **and T. G. Bernhardt**. 2011. More than just lysins: peptidoglycan hydrolases tailor the cell wall. Curr Opin Microbiol **14**:698–703.

80. **Uehara, T.**, **T. Dinh**, **and T. G. Bernhardt**. 2009. LytM-domain factors are required for daughter cell separation and rapid ampicillin-induced lysis in Escherichia coli. J Bacteriol **191**:5094–5107.

81. **Uehara, T.**, **K. R. Parzych**, **T. Dinh**, **and T. G. Bernhardt**. 2010. Daughter cell separation is controlled by cytokinetic ring-activated cell wall hydrolysis. EMBO J **29**:1412–1422.

82. **van Heijenoort, J.** 1998. Assembly of the monomer unit of bacterial peptidoglycan. Cell Mol Life Sci **54**:300–304.

83. **van Heijenoort, J.** 2007. Lipid Intermediates in the Biosynthesis of Bacterial Peptidoglycan. Microbiol Mol Biol Rev **71**:620–635.

84. **van Heijenoort, J.** 2011. Peptidoglycan hydrolases of *Escherichia coli*. Microbiol Mol Biol Rev 1–29.

85. **Varma, A.**, **and K. D. Young**. 2009. In Escherichia coli, MreB and FtsZ Direct the Synthesis of Lateral Cell Wall via Independent Pathways That Require PBP 2. J Bacteriol **191**:3526–3533.

86. **Varma, A.**, **and K. D. Young**. 2004. FtsZ collaborates with penicillin binding proteins to generate bacterial cell shape in Escherichia coli. J Bacteriol **186**:6768–6774.

87. **Vollmer, W.**, **M. von Rechenberg**, **and J. V. Höltje**. 1999. Demonstration of molecular interactions between the murein polymerase PBP1B, the lytic

transglycosylase MltA, and the scaffolding protein MipA of Escherichia coli. J Biol Chem **274**:6726–6734.

88. **Vollmer, W.**, **and U. Bertsche**. 2008. Murein (peptidoglycan) structure, architecture and biosynthesis in Escherichia coli. Biochim Biophys Acta **1778**:1714–1734.

89. **Vollmer, W.**, **D. Blanot**, **and M. A. de Pedro**. 2008. Peptidoglycan structure and architecture. FEMS Microbiol Rev **32**:149–167.

90. **Vollmer, W.**, **B. Joris**, **P. Charlier**, **and S. Foster**. 2008. Bacterial peptidoglycan (murein) hydrolases. FEMS Microbiol Rev **32**:259–286.

91. **Vollmer, W.**, **and S. J. Seligman**. 2010. Architecture of peptidoglycan: more data and more models. Trends Microbiol **18**:59–66.

92. **Wang, T.-S. A.**, **S. A. Manning**, **S. Walker**, **and D. Kahne**. 2008. Isolated peptidoglycan glycosyltransferases from different organisms produce different glycan chain lengths. J Am Chem Soc **130**:14068–14069.

93. **Welzel, P.** 2005. Syntheses around the transglycosylation step in peptidoglycan biosynthesis. Chem Rev **105**:4610–4660.

94. **Yang, D. C.**, **N. T. Peters**, **K. R. Parzych**, **T. Uehara**, **M. Markovski**, **and T. G. Bernhardt**. 2011. An ATP-binding cassette transporter-like complex governs cell-wall hydrolysis at the bacterial cytokinetic ring. Proceedings of the National Academy of Sciences **108**:E1052–60.

95. **Ye, X.-Y.**, **M.-C. Lo**, **L. Brunner**, **D. Walker**, **D. Kahne**, **and S. Walker**. 2001. Better Substrates for Bacterial Transglycosylases. J Am Chem Soc **123**:3155–3156.

96. **Yousif, S. Y.**, **J. K. Broome-Smith**, **and B. G. Spratt**. 1985. Lysis of Escherichia coli by beta-lactam antibiotics: deletion analysis of the role of penicillin-binding proteins 1A and 1B. J Gen Microbiol **131**:2839–2845.

97. **Yuan, Y.**, **D. Barrett**, **Y. Zhang**, **D. Kahne**, **P. Sliz**, **and S. Walker**. 2007. Crystal structure of a peptidoglycan glycosyltransferase suggests a model for processive glycan chain synthesis. Proc Natl Acad Sci USA **104**:5348–5353.

98. **Zijderveld, C. A.**, **M. E. Aarsman**, **T. den Blaauwen**, **and N. Nanninga**. 1991. Penicillin-binding protein 1B of Escherichia coli exists in dimeric forms. J Bacteriol **173**:5740–5746.

Chapter 2:

Lipoprotein cofactors located in the outer membrane activate bacterial cell wall polymerases

Reprinted with permission from Elsevier Publishing and the journal *Cell*

Author contributions:

The work presented in this Chapter was largely a collaborative effort. All authors had a role in conceptualizing experiments, and interpreting data. Thomas Bernhardt wrote the manuscript. The bulk of the experiments were performed by Catherine Paradis-Bleau, Tsuyoshi Uehara, and myself. In particular, I identified LpoA as a factor required for PBP1a function using the *slb* synthetic lethal screen. I also performed experiments to show: (i) the terminal phenotype of *lpo* mutants when their non-partner PBP1 was depleted (including growth curves and microscopy), (ii) the terminal phenotype of a *lpoB* mutant when LpoA was depleted (including growth curves and microscopy), (iii) that the *lpo* mutants were able to be complemented in trans *in vivo*, (iv) PBP levels in the *lpo* mutants, and (v) that the Lpo proteins are outer membrane attached using a cytological assay to observe the localization of fluorescently tagged proteins in plasmolyzed cells. Catherine Paradis-Bleau performed the reciprocal *sla* screen and identified LpoB as a factor required for PBP1b function, performed minimal inhibitory concentration experiments to show that the *lpoB* mutant phenocopies cells lacking PBP1b, and showed a specific interaction between the PBP1 proteins and their cognate Lpo factor. Tsuyoshi Uehara conceptualized the synthetic lethal screen for PBP effectors and performed preliminary experiments to set up the screen for *slb* mutants. He also showed that the Lpo factors are outer membrane proteins using membrane fractionation and that PBP1b needs LpoB to achieve its biochemical activity using ether-permeabilized cells. Additionally, Tania Lupoli from the Kahne/Walker groups performed the biochemistry to show that purified LpoB increases the rate of glycan strand polymerization performed by PBP1b and helps to produce shorter glycan strands.

Lipoprotein cofactors located in the outer membrane activate bacterial cell wall polymerases

Catherine Paradis-Bleau[1†], Monica Markovski[1†], Tsuyoshi Uehara[1†], Tania J. Lupoli[3], Suzanne Walker[1,3], Daniel E. Kahne[2,3], and Thomas G. Bernhardt[1*]

[1]Department of Microbiology and Molecular Genetics

and [2]Department of Biological Chemistry and Molecular Pharmacology

Harvard Medical School

Boston, MA 02115

[3]Department of Chemistry and Chemical Biology

Harvard University

Cambridge, MA 02138

[†]These authors contributed equally to this work.

Graphical Abstract

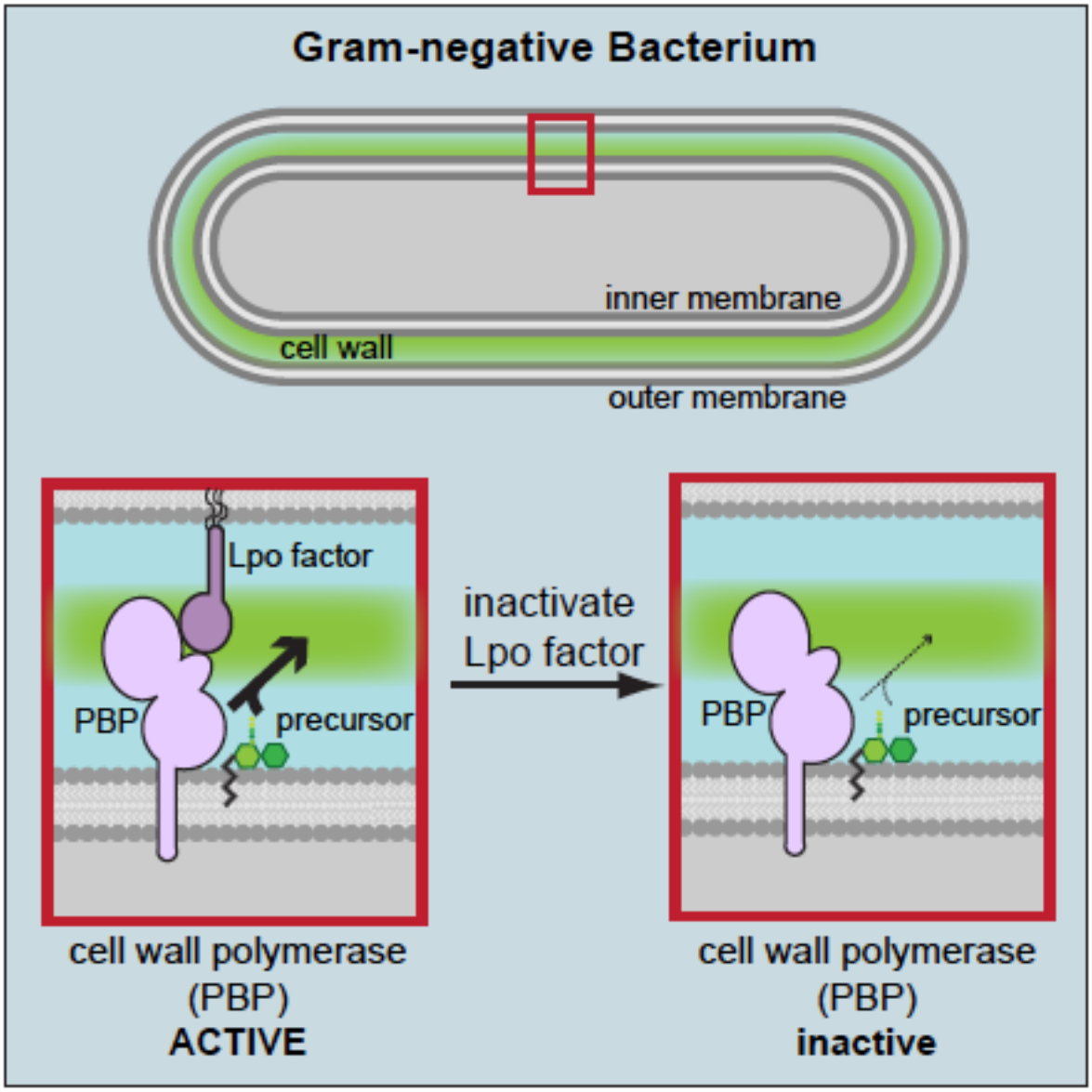

Figure 2.0. Graphical abstract. The figure above represents a graphical abstract of the content of this chapter.

Summary

Most bacteria surround themselves with a peptidoglycan (PG) exoskeleton synthesized by polymerases called penicillin-binding proteins (PBPs). Because they are the targets of penicillin and related antibiotics, the structure and biochemical functions of the PBPs have been extensively studied. Despite this, we still know surprisingly little about how these enzymes build PG *in vivo*. Here, we identify the *Escherichia coli* lipoproteins LpoA and LpoB as essential PBP cofactors. We show that LpoA and LpoB form specific trans-envelope complexes with their cognate PBP and are critical for PBP function *in vivo*. We further show that LpoB promotes PG synthesis by its partner PBP *in vitro* and that it does so by stimulating glycan chain polymerization. Overall, our results indicate that PBP accessory proteins play a central role in PG biogenesis and, like the PBPs they work with, these factors are attractive targets for antibiotic development.

Introduction

To fortify their cytoplasmic membrane and protect it from osmotic rupture, most bacteria surround themselves with a peptidoglycan (PG) exoskeleton. This tough polysaccharide layer is constructed from long glycan chains crosslinked to one another via attached peptides to form a continuous matrix that envelops the cell (**Figure 2.1A**). Because bacteria are encased within this polymeric shell, their growth and morphogenesis is intimately linked to PG synthesis and remodeling; PG expansion is essential for growth, and the shape of the organism is defined by the PG network (31).

The PG synthesis pathway is of tremendous practical importance as it is the target of many of our most effective antibiotics, notably penicillin and related β-lactams. Since its discovery over eighty years ago, penicillin has served as a key probe of the PG assembly process as well as a widely used therapeutic. It covalently modifies and inhibits PG synthases called high molecular weight penicillin-binding proteins (HMW-PBPs) (37), which henceforth will be referred to simply as PBPs. Bacteria typically encode two varieties of PBPs: class A and class B (37). Both types are integral membrane proteins with relatively large domains facing the cell exterior. Class A PBPs are thought to be the primary cellular PG synthases since they are bifunctional and have both peptidoglycan glycosyl transferase (PGT) and transpeptidase (TP) domains capable of polymerizing the glycan strands of PG and crosslinking them, respectively (**Figure 2.1A and 2.1B**). Class B PBPs are mono-functional and only have TP activity.

Although purified bifunctional PBPs can polymerize and crosslink PG *in vitro* from lipid-II substrate (**Figure 2.1B**) (4, 10), the PBPs alone are insufficient for the proper assembly of the cell-shaped PG network *in vivo*. To build a dynamic, uniformly-shaped PG

mesh that grows in step with the rest of the cell, PBP activity must be spatially and temporally controlled (31). Adding to the complexity, rod-shaped bacteria like *Escherichia coli* and *Bacillus subtilis* must properly switch between different modes of PG growth: elongation of the cylindrical portion of the rod and synthesis of the hemispherical polar caps during division. It is therefore not surprising that, besides the PBPs, an array of additional proteins have been implicated in PG assembly (13, 31). Recent work indicates that many of these factors are organized into multi-enzyme PG synthesizing complexes by cytoskeletal polymers of FtsZ (tubulin-like) and MreB (actin-like), which are thought to direct their activity to appropriate subcellular locations (**Figure 2.1B**). Studies from a number of laboratories have identified likely components of these complexes, including: (i) many, if not all, of the enzymes required for lipid-II synthesis (MurA-MurG), (ii) both classes of synthetic PBPs, (iii) various PG hydrolases, and (iv) several essential integral membrane proteins of unknown function, such as SEDS-domain proteins like RodA or FtsW and the elongation specific factors MreC and MreD (13, 31, 51). Many questions regarding the function and composition of these PBP-containing, multi-enzyme complexes remain to be addressed. One of the most fundamental, however, is whether such complexes promote PG synthesis simply by providing the PBPs with access to substrate via lipid-II synthesis and flipping (**Figure 2.1B**), or whether they also contain critical accessory factors that facilitate and/or regulate PBP activity by affecting lipid-II utilization or the incorporation of nascent PG into the existing network.

Here, we report the discovery of protein cofactors essential for the *in vivo* function of the bifunctional PBPs. They were identified using directed genetic screens in the model Gram-negative bacterium, *E. coli*. We have designated them LpoA (YraM) and LpoB (YcfM)

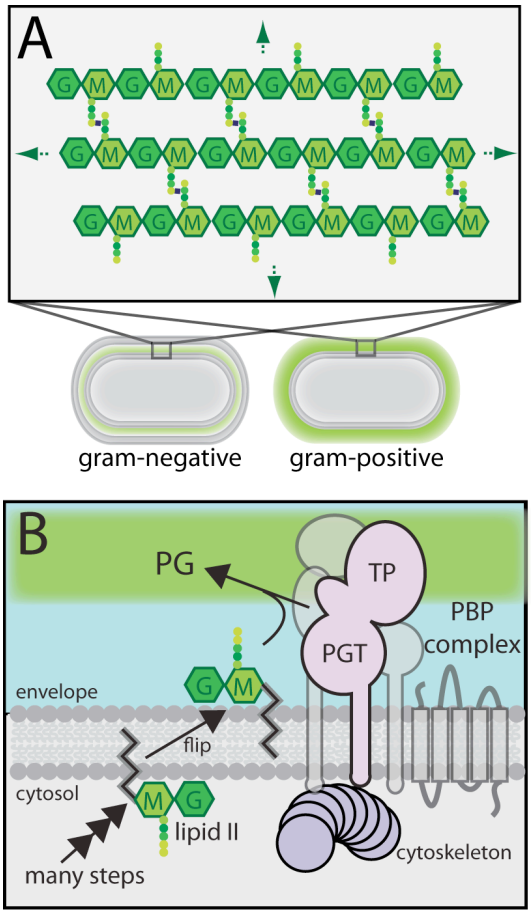

Figure 2.1. Cell wall structure and assembly. A. Schematic of bacterial cells with the cell wall (PG layer) in green. Gram-negative cells have a relatively thin PG layer surrounded by an additional (outer) membrane. Above the cells is a schematic detailing the structure of PG, which continues in all directions to envelop the cell (green arrows). M, *N*-acetylmuramic acid; G, *N*-acetylglucosamine. Dots represent the attached peptides. **B.** Overview of PG assembly. A generic multi-protein complex (grey) containing a class A PBP (purple) is shown. For simplicity, the other PG assembly factors thought to participate in the final stages of PG construction are not specifically labeled. See text for details. PGT, peptidoglycan glycosyltransferase domain; TP, transpeptidase domain.

for lipoprotein activators of bifunctional PBP activity from the outer membrane. We demonstrate that they directly affect PBP activity through the formation of specific trans-envelope Lpo-PBP complexes. In addition, we show that LpoB promotes PG synthesis by its partner PBP *in vitro* and that it does so by stimulating glycan chain polymerization. Overall, our results indicate that PBP accessory proteins play a central role in PG biogenesis and, like the PBPs they work with, these factors are attractive targets for antibiotic development. An accompanying report from Typas *et al*. (44) describes the independent discovery of the Lpo factors using large-scale phenotyping and proteomic approaches.

Results

Rationale for the synthetic lethal screens. *E. coli*, like many bacteria, encodes multiple class A PBPs: PBP1a, PBP1b, and PBP1c (37). Prior genetic studies indicated that cells remain viable if either PBP1a or PBP1b is inactivated, but not if they both are (28, 54). This suggests that there are at least two major PG synthesizing complexes in the cell, one containing PBP1a and the other PBP1b, an idea supported by crosslinking studies in *Haemophilus influenzae* and immunoprecipitation studies in *E. coli* (2, 14). Based on this, we reasoned that we could identify critical components of these multi-enzyme PBP complexes by performing a screen for mutations synthetically lethal with the loss of either PBP1a or PBP1b. For example, if factor X is an important component of a PBP1a synthetic complex, one might expect mutations that inactivate factor X to be just as lethal when PBP1b is depleted as the inactivation of PBP1a is. Therefore, a screen for mutants synthetically lethal with the loss of PBP1b should yield factor X mutants as well as *ponA*

(PBP1a) mutants. The converse is also true. Important components of the PBP1b synthetic complex should be identified by a screen for mutants synthetically lethal with the loss of PBP1a.

Screening for mutants synthetically lethal with the loss of PBP1a or PBP1b. Our synthetic lethal screen employed methodology we used previously to identify new cell division factors and regulators of division site placement (7, 8). To apply the screen to the PBPs, we initially searched for mutants synthetically lethal with the loss of PBP1b function (*slb* mutants). Our parental strain for the screen had chromosomal deletions removing both *lacZ* and *ponB* (PBP1b). The strain also harbored an unstable plasmid containing both the *ponB* and *lacZ* genes under control of the inducible lactose promoter (P_{lac}). Since PBP1b is not essential, cells frequently lost the plasmid when they were grown on non-selective media containing the P_{lac} inducer, IPTG, and the LacZ indicator, X-gal. They formed either white ($LacZ^-$) colonies or blue-sectored colonies resulting from plasmid loss before or during colony formation, respectively (**Figure 2.2A and 2.2B**). To find *slb* mutants, we mutagenized the parental strain with a transposon and plated the resulting library on indicator medium to look for rare solid-blue colonies (**Figure 2.2A and 2.2B**). Mutants forming such colonies presumably could not lose the plasmid because the transposon insertion rendered PBP1b essential. To confirm this, we tested the *slb* candidates for growth with or without IPTG. Mutants truly dependent on PBP1b for growth should require the presence of IPTG to induce *ponB* expression from the plasmid.

We screened a total of 30,000 colonies and isolated 16 *slb* mutants. Less than half of these (5/16) were completely dependent on IPTG for growth. Three of the IPTG-

dependent mutants had transposon insertions that mapped to the gene for PBP1a (*ponA*), indicating that the screen worked as expected (**Figure 2.2D**). Two of the remaining IPTG-dependent mutants had transposons that mapped within *lpoA* (*yraM*) (**Figure 2.2C and 2.2D**). The *lpoA* reading frame codes for a 678 amino acid protein with an LppC domain that is well conserved among the γ-proteobacteria but has an unknown function (1, 21). LpoA is also predicted to have a lipoprotein signal sequence for targeting it to the outer membrane (see below). Besides the *ponA* and *lpoA* alleles, most of the remaining *slb* isolates showed a synthetically sick phenotype in combination with a PBP1b defect. They all had transposon insertions that mapped to genes encoding factors previously implicated in cell division and will be described as part of a separate report.

We also performed the converse screen for mutants synthetically lethal with the loss of PBP1a function (*sla* mutants). The screen design was identical to the one described above except that the parental strain was deleted for the *ponA* (PBP1a) gene and *gfp-ponA* was encoded on the unstable plasmid. A total of 41 *sla* mutants displaying IPTG-dependent growth were isolated. The majority (34/41) were found to have transposon insertions disrupting the gene coding for PBP1b (**Figure 2.2D**), and 7/41 *sla* mutants had transposon insertions disrupting the gene coding for LpoB (YcfM) (**Figure 2.2C and 2.2D**). LpoB is a 213 amino acid protein of previously unknown function that, like LpoA, is predicted to have a lipoprotein signal sequence for targeting it to the outer membrane (see below). Since the bias in the isolation of *ponB* mutants might have prevented us from identifying additional *sla* loci, we repeated the *sla* screen in a strain containing a second copy of *ponB*. In this case, only one mutant was isolated and it contained a transposon

insertion in *lpoB*. We therefore conclude that *ponB* and *lpoB* are likely to be the only *sla* loci in the genome.

Specificity of the synthetically lethal combinations and their terminal phenotypes. To test the specificity of the synthetic lethal combinations, we constructed strains TU121(*att*λTB309) [Δ*ponA*(P_{ara}::*ponA*)] and MM11 [P_{ara}::*ponB*] in which the production of either PBP1a or PBP1b was controlled by the arabinose promoter, respectively. In the case of TU121(*att*λTB309), the native *ponA* locus was deleted and a second copy of *ponA* under arabinose promoter control was integrated at the λ *att* site. For MM11, the native *ponB* promoter was replaced with the arabinose promoter. Growth of TU121(*att*λTB309) [Δ*ponA*(P_{ara}::*ponA*)] derivatives lacking PBP1b or LpoB was severely inhibited on media without arabinose (**Figure 2.2E**). Growth of the corresponding $LpoA^-$ strain was unaffected (**Figure 2.2E**). Similarly, MM11 [P_{ara}::*ponB*] derivatives defective for PBP1a or LpoA failed to grow without arabinose supplementation, while the corresponding $LpoB^-$ strain showed robust growth (**Figure 2.2E**). Thus, LpoA is specifically required in the absence of PBP1b and LpoB is specifically required in the absence of PBP1a.

The terminal phenotype of PBP1a depletion in the absence of PBP1b is cell lysis, and vice versa (**Figure 2.2F and 2.2G**) (54). To determine if cells lacking specific Lpo-PBP1 combinations also lyse, we followed the growth and morphology of strains lacking Lpo factors after initiating PBP1 depletion. When PBP1a was depleted, cells lacking PBP1b or LpoB displayed a dramatic lysis phenotype. About three generations following the initiation of PBP1a depletion, the optical density of the mutant cultures began to decline rapidly (**Figure 2.2F**). This coincided with the appearance of cell ghosts and lysing cells

with membrane blebs in the cultures (**Figure 2.3**). The only difference between the PBP1b$^-$ and LpoB$^-$ cells upon PBP1a depletion was that the LpoB$^-$ cells consistently began lysing about 10 minutes later than PBP1b$^-$ cells (**Figure 2.2F**). Similar results were obtained when we compared the effect of PBP1b depletion on cells defective for PBP1a or LpoA. In both cases, the terminal phenotype was lysis (**Figure 2.2G**). As on plates, growth of PBP1a$^-$ LpoA$^-$ or PBP1b$^-$ LpoB$^-$ cells in liquid was normal (data not shown). Importantly, the synthetic lethal phenotypes resulting from the *lpoA* or *lpoB* deletions were corrected by their expression in *trans*, indicating that the phenotypes observed were not due to an adverse effect of the deletions on the expression of nearby genes (**Figure 2.4**). In addition, Bocillin labeling and immunoblotting indicated that the defects observed for the LpoA/B$^-$ mutants were not due to a decrease in PBP1 protein levels (**Figure 2.5**).

Although PBP1a and PBP1b appear to be largely redundant, the phenotypes of cells lacking individual PBP1s are not identical. Loss of PBP1b leads to a hypersensitivity to β-lactam antibiotics that is not observed for PBP1a$^-$ mutants (38, 54). In addition, inhibition of the class B PBPs, PBP2 with mecillinam or PBP3 with cephalexin, normally leads to the formation of spherical or filamentous cells, respectively, that are slow to lyse (40). Similar treatments of mutants lacking PBP1b, however, rapidly induce cell lysis (23, 38). Although the reasons for the aberrant β-lactam phenotypes of PBP1b mutants are not known, we used these observations to further investigate the equivalence of LpoB and PBP1b defects. We found that LpoB defective mutants indeed shared a β-lactam hypersensitivity phenotype with PBP1b$^-$ mutants (**Figure 2.6**). Moreover, LpoB$^-$ cells also lysed rapidly when treated with mecillinam or cephalexin (**Figure 2.6B-D**). Thus, a LpoB$^-$ mutant has all of the hallmarks of a PBP1b$^-$ defect.

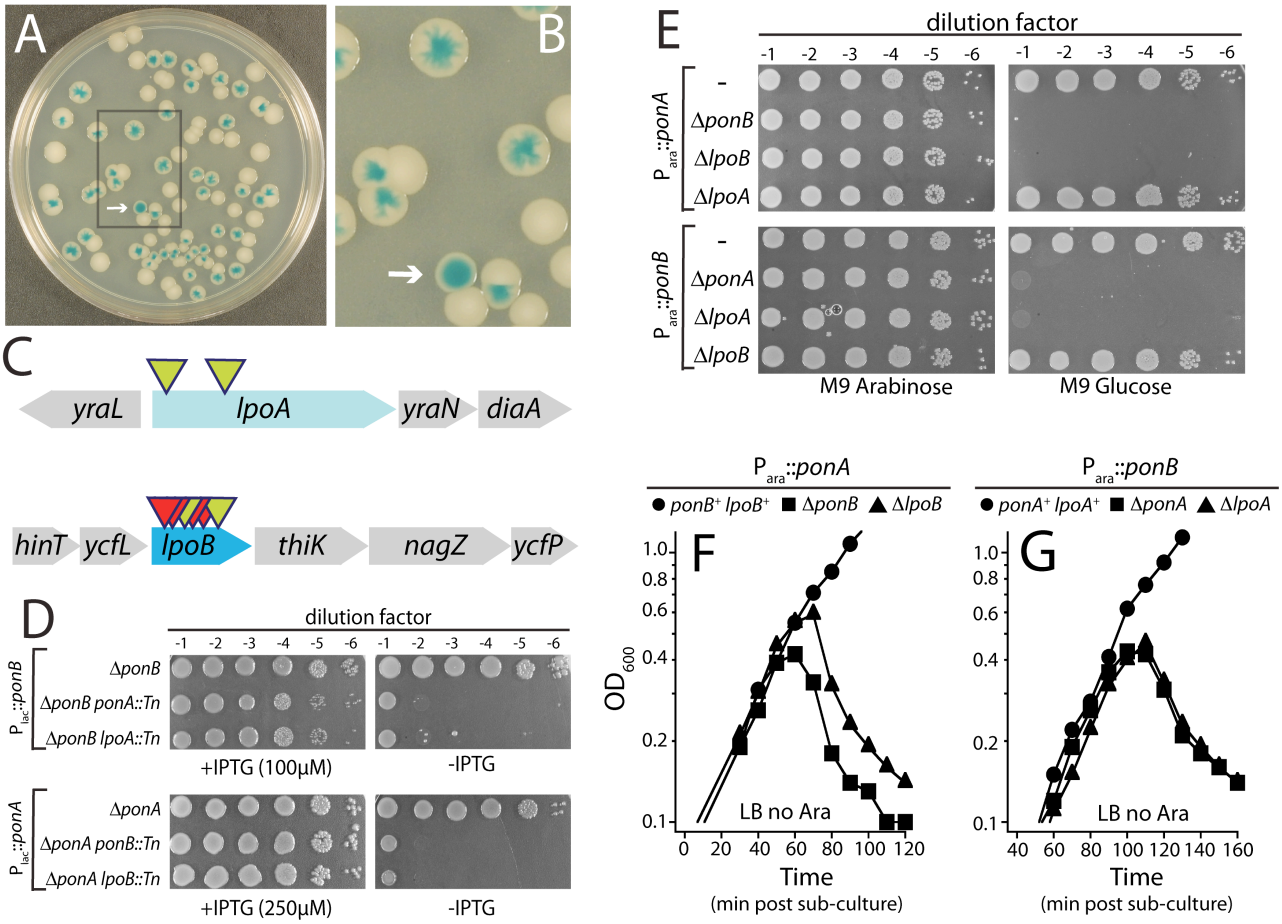

Figure 2.2. Synthetic lethal screens and terminal phenotypes. A-B. Colonies of transposon mutants used for the *slb* mutant screen grown on an indicator plate (LB-IPTG-Xgal) for 2 days at 30°C. The arrow points to a rare solid-blue colony that retained the unstable plasmid. The boxed region in (**A**) is enlarged in (**B**). **C.** Schematics indicating the approximate locations of the transposon insertions in the *lpo* genes. Triangles represent transposon insertion points (green: transcription of the KanR cassette is in the same direction as the target gene; red: transcription is in the opposite direction). **D.** Plating defects of representative *slb* and *sla* mutants isolated in the screens. **(Legend continued on next page.)**

Figure 2.2 (continued). Cells of TU122/pTU110 [Δ*ponB*/P_{lac}::*ponB lacZ*] (top) or TU121/ pCB1 [Δ*ponA*/P_{lac}::*gfp-ponA lacZ*] (bottom) and their derivatives with the indicated transposon insertions were grown overnight at 30°C. Culture densities were normalized, 10-fold serial dilutions were prepared for each, and 5 µl of each dilution was spotted onto LB with or without IPTG as indicated. **E.** Cells of TU121(*att*λTB309) [Δ*ponA*(P_{ara}::*ponA*)] (top) or MM11 [P_{ara}::*ponB*] (bottom) and their derivatives were grown overnight at 37°C. Serial dilutions were prepared as in (**D**) and dilutions were spotted onto the indicated media. **F-G.** Strains used in (**E**) were grown in LB-arabinose at 37°C to an OD_{600} = 0.6-1.1. They were then pelleted, washed three times with LB, and resuspended in LB-glucose at an OD_{600} = 0.08 or 0.02 for TU121(*att*λTB309) (**F**) or MM11 derivatives (**G**), respectively. Cell growth following subculture (t = 0) was then monitored by regular OD_{600} measurements.

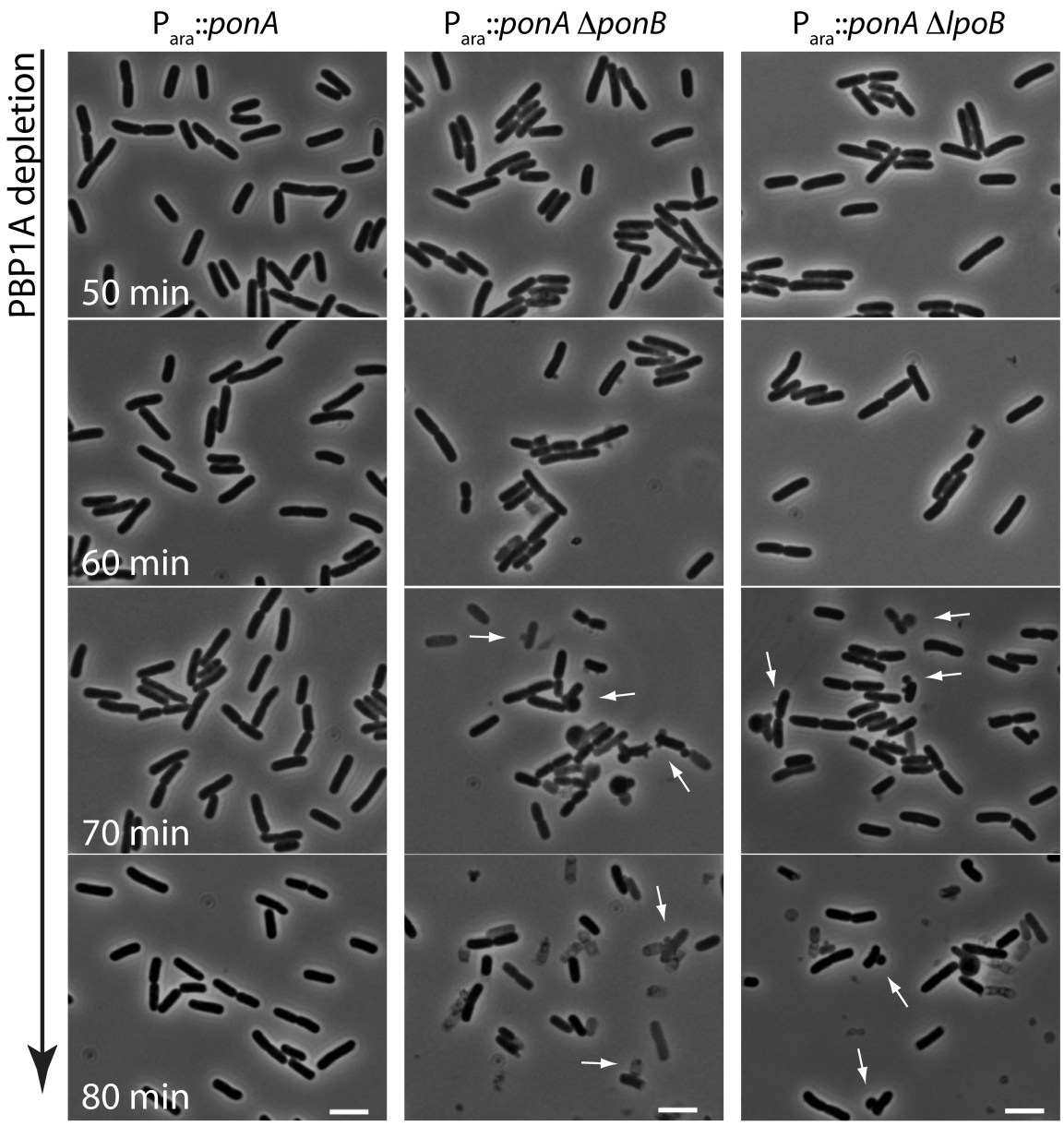

Figure 2.3. Terminal phenotype of PBP1a$^-$ PBP1b$^-$ and PBP1a$^-$ LpoB$^-$ cells. At t = 50, 60, 70, and 80 minutes an aliquot of cells from the cultures in **Figure 2.2F** were fixed. Following completion of the growth measurements, fixed cells were visualized by phase contrast microscopy. Representative images are shown. Arrows highlight lysed cell ghost and lysing cells with membrane blebs. Bars equal 3 microns.

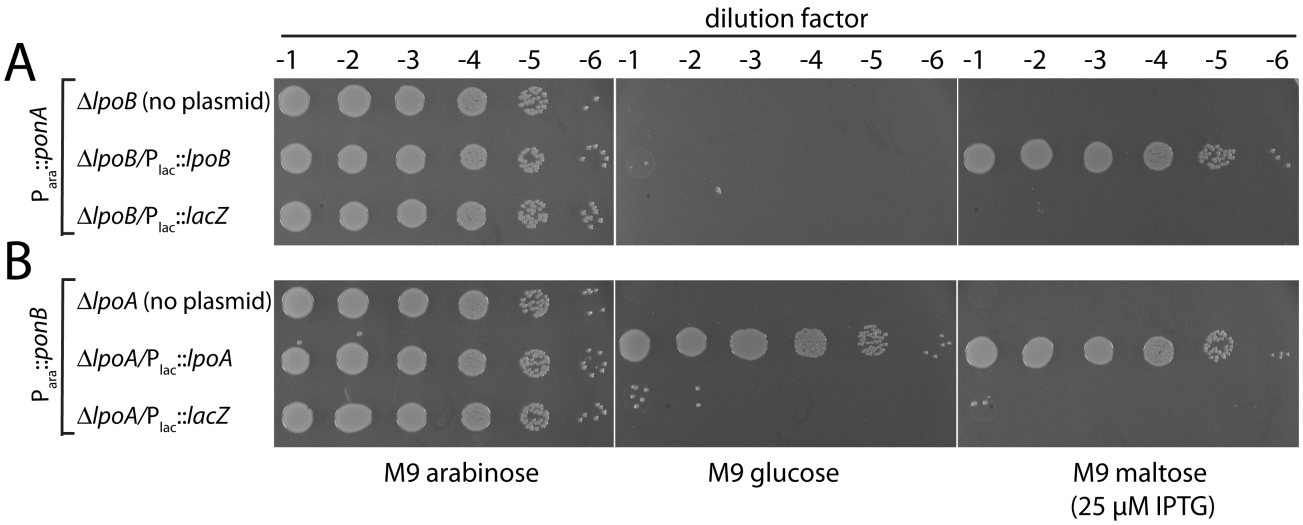

Figure 2.4. Complementation of *lpo* deletions by expression of *lpo* genes in *trans*.

Cells of CB4(*att*λTB309) [Δ*ponA* Δ*lpoB*(P_{ara}::*ponA*)] (**A**) or MM13 [P_{ara}::*ponB* Δ*lpoA*] (**B**) with or without the indicated plasmids were grown over night in M9-arabinose at 37°C. Culture densities were normalized, 10-fold serial dilutions were prepared for each, and 5 μl of each dilution was spotted onto the indicated solid media. Plates were incubated overnight at 37°C and photographed. Plasmids used were: pCB25 [P_{lac}::*lpoB*], pMM12 [P_{lac}::*lpoA*], and pMLB1113 [P_{lac}::*lacZ*]. Plasmids pCB25 [P_{lac}::*lpoB*] and pMM12 [P_{lac}::*lpoA*] possess native ribosome binding sites and 5'UTRs for *lpoB* and *lpoA*, respectively. pMM12 presumably has a higher basal level of expression than pCB25 since it can correct the PBP1B$^-$ LpoA$^-$ phenotype of MM13 without IPTG induction whereas pCB25 requires IPTG to correct the PBP1A$^-$ LpoB$^-$ phenotype of CB4(*att*λTB309). Alternatively, relative to LpoB, lower levels of LpoA are required to support growth.

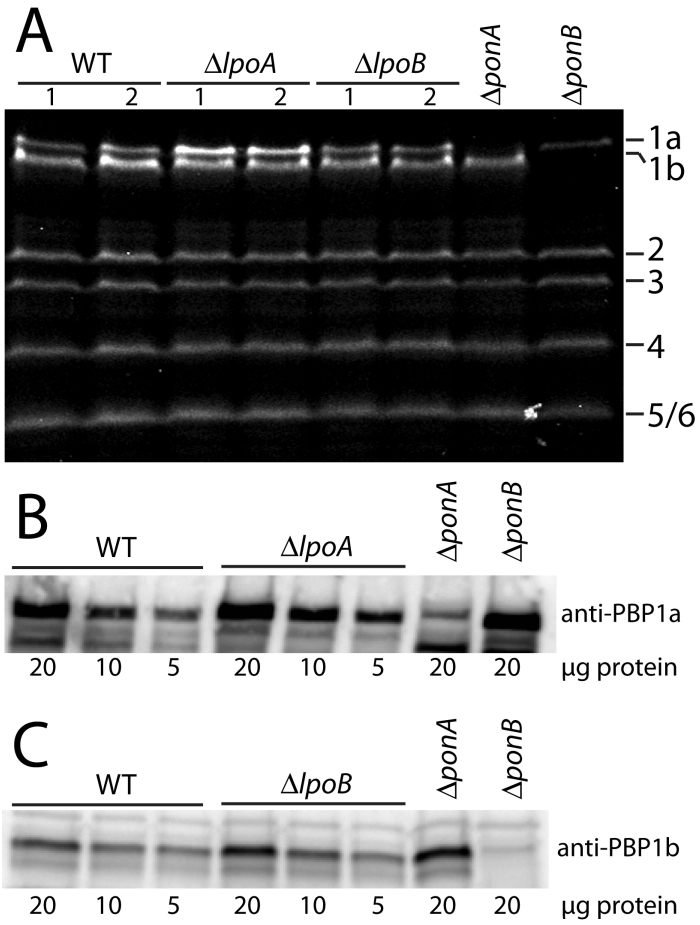

Figure 2.5. PBP levels in the *lpo* mutants. A. Cells of TB28 [WT], MM8 [Δ*lpoA*], CB6 [Δ*lpoB*], TU121 [Δ*ponA*], and TU122 [Δ*ponB*] were labeled with Bocillin. Proteins in whole-cell extracts were separated on a 10% SDS polyacrylamide gel, and fluorescently labeled PBPs were visualized using a fluorescence scanner (Typhoon). Duplicate samples are shown for TB28 [WT], MM8 [Δ*lpoA*], and CB6 [Δ*lpoB*]. **B-C.** Whole cell extracts of the strains used in A were prepared and PBP1a or PBP1b levels determined by immunoblotting with antisera generated against purified proteins.

A

Strain	MIC (μg/ml)				
	Chloramphenicol	Ampicillin	Mecillinam	Cephalexin	Cefsulodin
WT	3	3	0.1	6	25
Δ*ponA*	3	3	0.1	6	25
Δ*lpoA*	3	1.5-3	0.1	6	25
Δ*ponB*	3	0.75	0.025-0.05	1.5	0.039-0.078
Δ*lpoB*	3	0.75	0.05	3	0.039-0.078

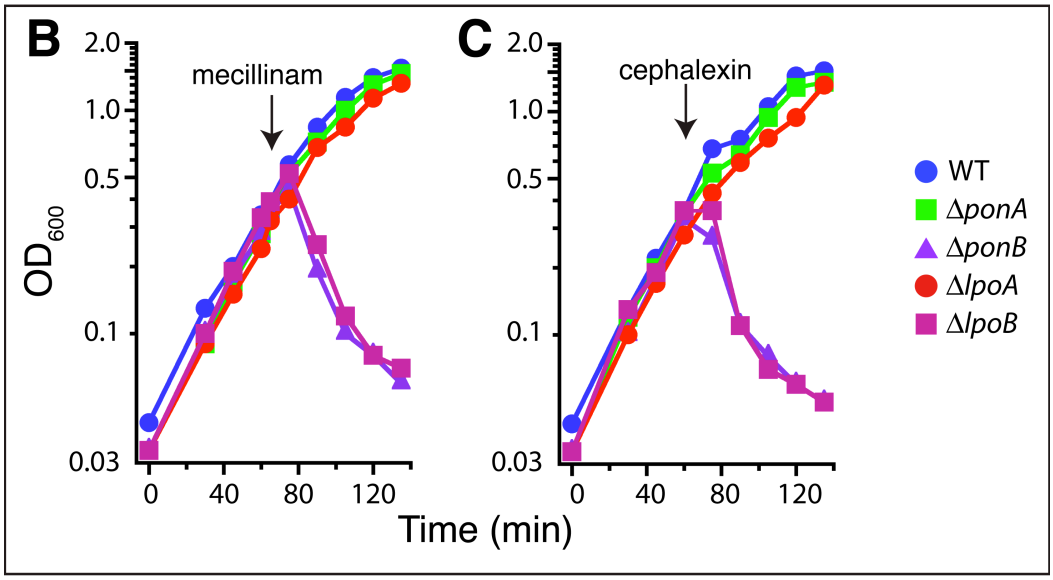

Figure 2.6. LpoB defective cells are hypersensitive to β-lactams. A. Minimal inhibitory concentrations (MIC) for the indicated β-lactams are tabulated for the strains with the indicated deletion mutations. Similar results were obtained for three independent measurements. **B-C.** Cells of TB28 [WT], TU121 [Δ*ponA*], TU122 [Δ*ponB*], MM22 [Δ*lpoA*] and CB26 [Δ*lpoB*] were grown to mid log in LB at 37°C and treated with either mecillinam (**B**) (10 μg/ml) or cephalexin (**C**) (10 μg/ml) at the indicated time points (arrows). Cell growth was then followed by regular OD_{600} measurements.

At least one Lpo factor is required for growth. Our results thus far suggest that LpoA is important for PBP1a function and that LpoB is important for PBP1b function. If this is true, then the combined loss of LpoA and LpoB should phenocopy the lysis and lethality observed when PBP1a and PBP1b are simultaneously inactivated. Accordingly, when LpoA was depleted in the absence of LpoB, cells lysed and failed to grow on media lacking inducer for *lpoA* expression (**Figure 2.7A and 2.7B**).

The Lpo factors are essential for PBP1 function. To determine whether or not the Lpo proteins are essential for PBP1 function, we tested the ability of PBP1a/b overproduction to suppress the synthetic lethal phenotypes associated with a LpoA/B$^-$ defect. Overproduction of PBP1a by approximately 4 fold from plasmid pCB62 [$P_{lac\text{-}con}$::*ponA*] was not sufficient to suppress the Slb phenotype of MM13 [P_{ara}::*ponB* Δ*lpoA*] cells upon PBP1b depletion in liquid or solid medium (**Figure 2.7C, 2.7E, and 2.7G**). Only a minor delay in the timing of lysis was observed for MM13 cells harboring pCB62 relative to pTB284 [$P_{lac\text{-}con}$::*gfp*] (**Figure 2.7C**). Similarly, an approximately 8 fold overproduction of PBP1b from pCB72 [$P_{lac\text{-}con}$::*ponB*] failed to rescue the lytic phenotype and plating defects of CB4(*att*λTB309) [Δ*ponA* Δ*lpoB*(P_{ara}::*ponA*)] cells depleted of PBP1a (**Figure 2.7D, 2.7F, and 2.7G**). We conclude that the Lpo proteins are essential for the *in vivo* function of their cognate PBP as opposed to factors that simply stimulate PBP activity but are not critical for their function.

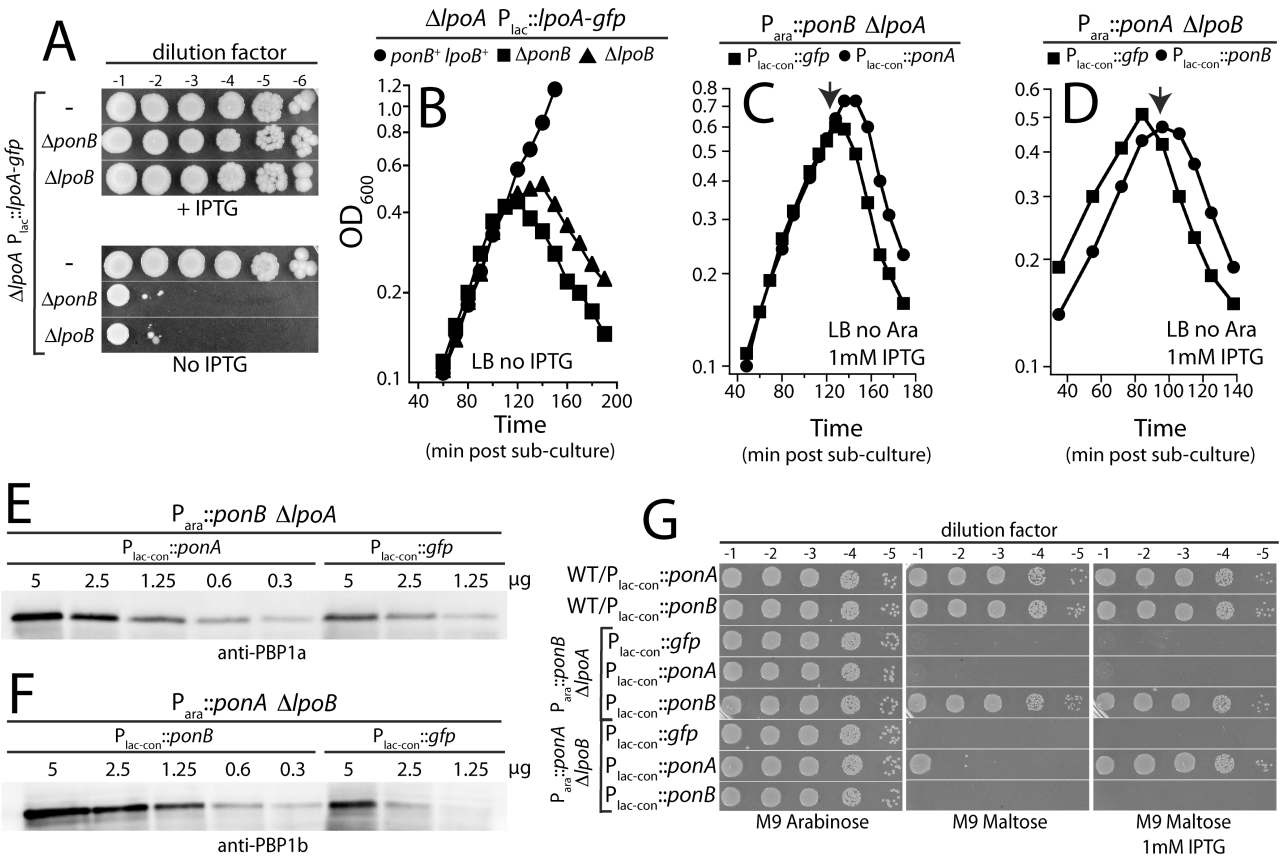

Figure 2.7. Lpo factors are essential for growth and PBP1 function. A. Cells of MM22(*att*HKMM10) [Δ*lpoA*(P_{lac}::*lpoA-gfp*)] and its derivatives were grown overnight in LB-IPTG (50μM) at 37°C. Serial dilutions were prepared as in Figure 2, and spotted onto the indicated solid media. Identical results were obtained when LpoB was depleted in the absence of LpoA (data not shown). **B.** Cultures of cells from (**A**) were grown to an OD_{600} of 0.3-0.4 in LB-IPTG (50μM) at 37°C. The cells were then pelleted, washed three times with LB, and resuspended in LB-glucose at an OD_{600} = 0.02. Cell growth following subculture (t = 0) was then monitored by regular OD_{600} measurements. **C-D.** Cells of MM13 [P_{ara}::*ponB* Δ*lpoA*] (**C**) or CB4(*att*λTB309) [Δ*ponA* Δ*lpoB*(P_{ara}::*ponA*)] **(Legend continued on next page.)**

Figure 2.7. (continued). (**D**) containing the low-copy plasmids pTB284 [$P_{lac\text{-}con}$::*gfp*], pCB62 [$P_{lac\text{-}con}$::*ponA*], or pCB72 [$P_{lac\text{-}con}$::*ponB*] were grown to an OD_{600} of 0.5-0.7 in LB-Ara-Spc (**C**) or M9-Ara-Spc (**D**) at 37°C. They were then washed, diluted into LB-IPTG (1mM), and growth at 37°C was followed as in (**B**). **E-F**. To determine the extent of PBP1a or PBP1b overproduction in the cultures from (**C**) and (**D**), respectively, extracts were prepared from cells harvested at times indicated by the arrows above the growth curves (**C-D**). Immunoblot analysis was then performed to determine the levels of PBP1a (**E**) or PBP1b (**F**) in strains MM13/pCB62 or CB4(*att*λTB309)/pCB72, respectively, relative to corresponding control strains harboring pTB284. Numbers above lanes indicate the amount of total protein loaded. **G**. Cultures of TB28 [WT], MM13, or CB4(*att*λTB309) containing the aforementioned plasmids were diluted, plated on the indicated media containing Spc, and incubated overnight at 37°C. Plasmids pCB62 [$P_{lac\text{-}con}$::*ponA*] and pCB72 [$P_{lac\text{-}con}$::*ponB*] possess native ribosome binding sites and 5'UTRs for *ponA* and *ponB*, respectively. pCB72 likely has a higher basal level of expression than pCB62 since it can correct the $PBP1B^-$ $LpoA^-$ phenotype of MM13 without IPTG induction. $P_{lac\text{-}con}$ is a synthetic *lac* promoter with consensus -35 and -10 elements.

Lpo factors localize throughout the outer membrane. Based on the sequence of their signal peptides, LpoA and LpoB are both predicted to be outer membrane lipoproteins (**Figure 2.8A**). To test this, we used a cytological assay for lipoprotein transport developed by Pugsley and co-workers (29). In this assay, cells expressing a fluorescent protein fused to a lipoprotein or lipobox-containing signal sequence are visualized following osmotic shock. This treatment induces the formation of plasmolysis bays where the inner membrane retracts from the rest of the cell envelope. Thus, a fluorescently labeled lipoprotein that is retained in the inner membrane will localize to the invaginations of the plasmolysis bays whereas an outer membrane lipoprotein will retain a peripheral localization pattern.

Before osmotic shock, GFP fusions to LpoA and LpoB displayed a patchy, non-uniform peripheral localization pattern (**Figure S2.9E and S2.9G**), indicating that they are broadly distributed throughout the envelope. In unconstricted cells, GFP-LpoA and GFP-LpoB retained their peripheral distribution following osmotic shock, suggesting that they are indeed outer membrane proteins (**Figure 2.10A and 2.10D**). This was confirmed using membrane fractionation experiments (**Figure S2.8B-E**). In dividing cells, the GFP-LpoA and GFP-LpoB signals became enriched at the septum following osmotic shock (**Figure S2.9F and S2.9H**). This was also observed for GFP-PBP1b, but not GFP-PBP1a (**Figure S2.9A-D)**. It is not clear why plasmolysis leads to the enrichment of these fusion proteins at the septum, but this may reflect some propensity of the native proteins to be recruited to the division apparatus (11, 44).

To determine the importance of outer membrane localization and/or lipidation for Lpo factor function, we generated LpoA-GFP and LpoB-GFP variants with D^{+2} D/E^{+3}

substitutions in their signal sequences to cause their retention in the inner membrane (**Figure 2.8A**), as well as variants in which the entire lipoprotein signal sequence was replaced with that of DsbA, a secreted periplasmic protein. All variants displayed the expected localization pattern following osmotic shock (**Figure 2.10A-F**). Fusions with the DsbA signal sequence appeared to fill the periplasm of the plasmolysis bays (**Figure 2.10B and 2.10E**), and those with the D^{+2} D/E^{+3} substitutions appeared to co-localize with invaginations of the inner membrane where it retracted from the envelope (**Figure 2.10C and 2.10F**). We tested the ability of these variants to support the function of their cognate PBP1 by assaying whether or not they could correct the synthetic lethal phenotypes of Lpo/PBP1 mutant combinations. As shown in **Figure 2.10G**, LpoA variants with a DsbA signal peptide or the D^{+2} D^{+3} double substitution were not active, suggesting that LpoA must be targeted to the outer membrane to promote PBP1a function. Immunoblot analysis showed that all of the LpoA variants were produced at levels similar to the wild-type protein (data not shown), indicating that the observed defects were not due to reduced protein accumulation. In contrast to the results with LpoA, all of the LpoB variants were functional (**Figure 2.10H**), suggesting that LpoB does not need to be lipidated or transported to the outer membrane to support PBP1b function.

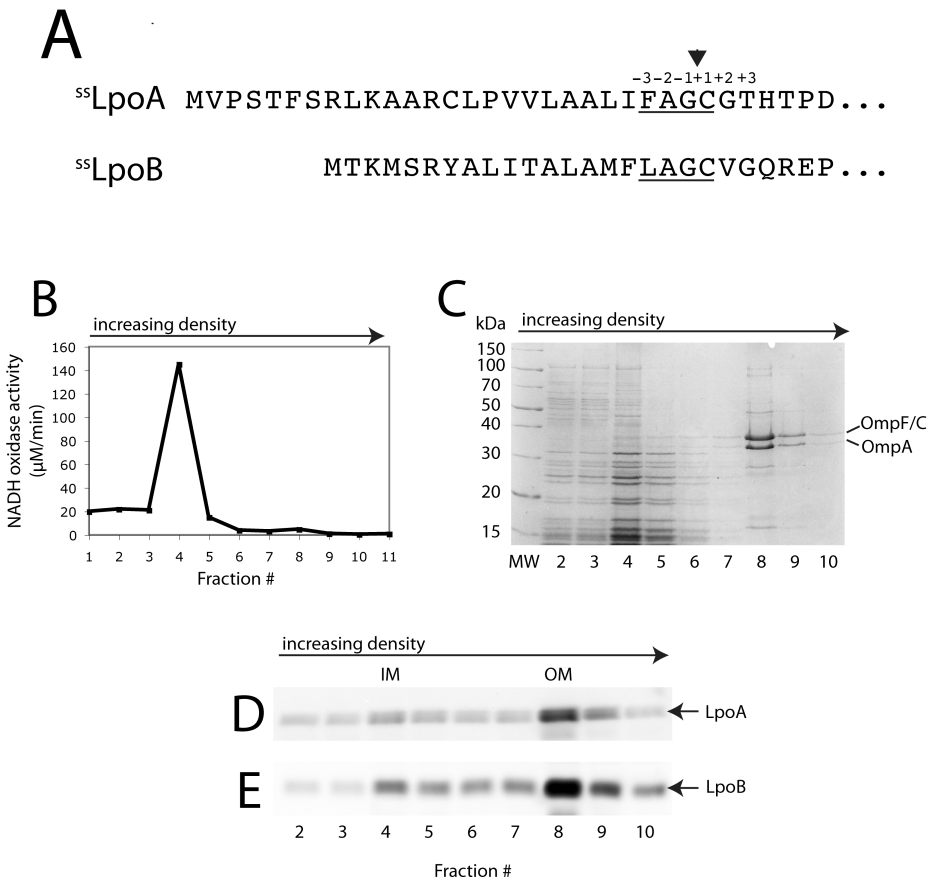

Figure 2.8. Lpo protein signal sequences and membrane fractionation. A. Shown are the signal sequences of LpoA and LpoB. Lipo-box signatures are underlined, and predicted cleavage and lipidation site is indicated by the arrowhead. *Background:* In Gram-negative bacteria, lipoproteins are synthesized with specialized N-terminal signal sequences containing a lipobox motif with a consensus sequence of L^{-3}-A/S^{-2}-G/A^{-1}-C^{+1} (43). Following translocation through the Sec machinery, prolipoproteins are lipidated at C^{+1} and cleaved between residues -1 and +1 (43). Once fully processed, a mature lipoprotein is typically either retained in the outer leaflet of the inner membrane or transported to the inner leaflet of the outer membrane by the Lol system (43). **(Legend continued on next page.)**

Figure 2.8. (continued). While most lipoproteins are transported to the outer membrane, those with an aspartic acid (D) in the +2 position are typically retained in the inner membrane (43). Retention is also influenced by the residue in the +3 position with D, E, or Q at +3 providing an exceptionally strong retention signal in combination with D at the +2 position (43). **B-E.** Results from membrane fractionations. Total membranes were isolated from TB28 [WT] cells were layered onto a sucrose step gradient (2.2, 1.44, and 0.77 M sucrose) and centrifuged at 100,000xg for 17 hours. Fractions (1ml) were then collected from the top of the gradient and analyzed for NADH oxidase activity, an inner membrane marker (**B**). Activity peaked in fraction 4. Total protein in each fraction was visualized by SDS-PAGE and coomassie staining (**C**). Bands corresponding to the major outer membrane porins were significantly enriched in fraction 8. Fractions were also analyzed for LpoA (**D**) or LpoB (**E**) by immunoblotting. Both proteins were also significantly enriched in the outer membrane fraction (#8).

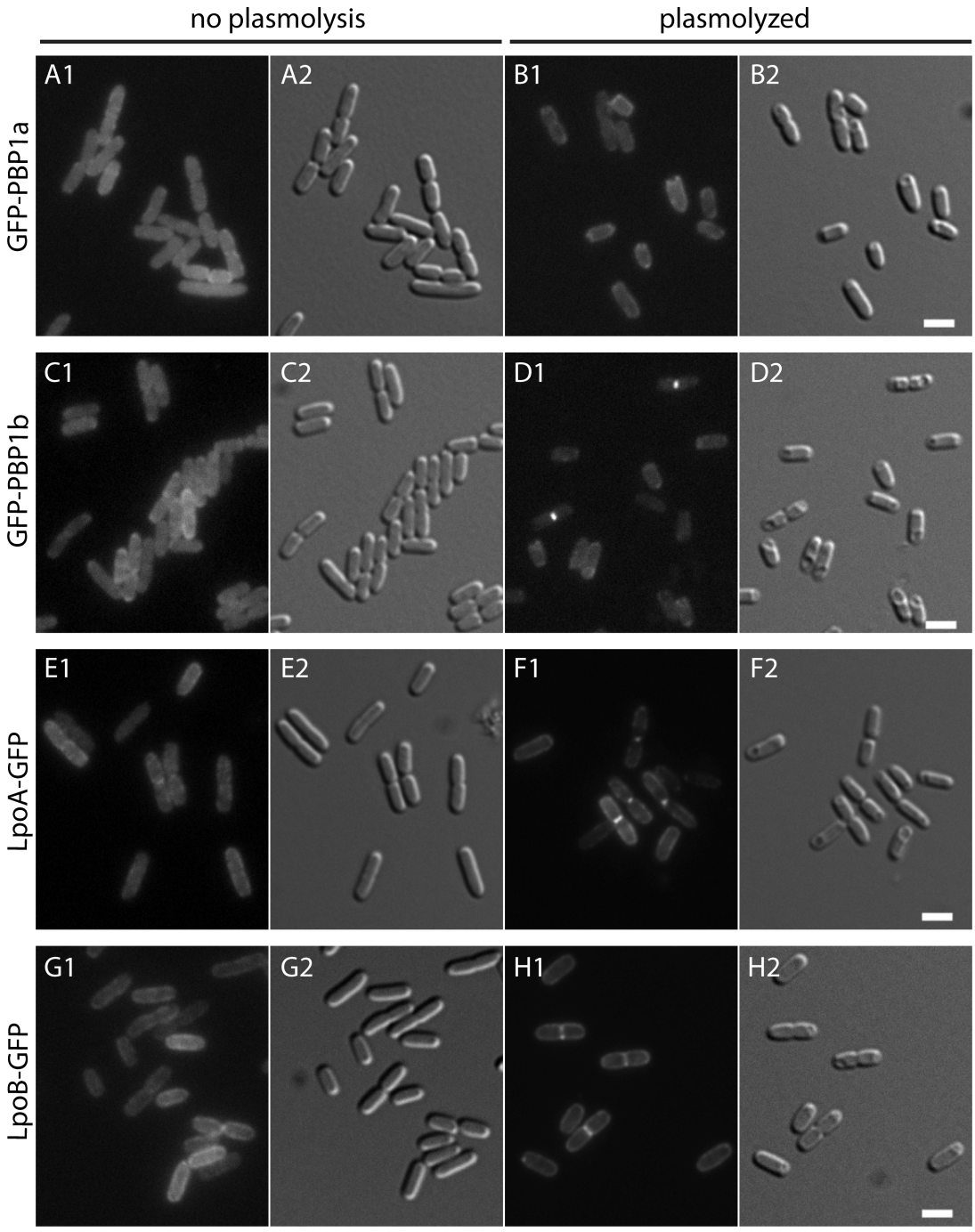

Figure 2.9. Subcellular localization of PBP1s and Lpo factors before and after plasmolysis. Cells of TU121(attHKTB307) [Δ*ponA*(P_{lac}::*gfp-ponA*)] (**A-B**), TU122(attHKMM6) [Δ*ponB*(P_{lac}::*gfp-ponB*γ)] (**C-D**), **(Legend continued on next page.)**

Figure 2.9. (continued). MM22(attHKMM10) [Δ*lpoA*(P_{lac}::*lpoA-gfp*)] (**E-F**), and CB26(attHKCB28) [Δ*lpoB*(P_{lac}::*lpoB-gfp*)] (**G-H**) were grown in M9 Maltose supplemented with 50, 25, 50, or 100 μM IPTG, respectively, to an OD_{600} of 0.5-0.6. They were then either visualized without (**A**, **C**, **E**, and **G**) or with plasmolysis (**B**, **D**, **F**, and **H**) using GFP (panel 1) or DIC (Panel 2) optics. Plasmolysis was performed as in **Figure 2.10**. Plasmolysis bays appear as depressions in DIC as opposed to phase light areas using phase contrast. LpoA-GFP, LpoB-GFP, GFP-PBP1a and GFP-PBP1b were found to be broadly distributed throughout the cell periphery in a patchy, non-uniform pattern in live cells (**A**, **C**, **E**, and **G**). Similar results for PBP1b localization were reported previously when this was investigated by immunofluorescence microscopy (11), except that a modest enrichment of PBP1b at the septum was reported. We did not observe such an enrichment of GFP-PBP1b at the septum. Curiously, however, we observed strong enrichment of LpoA-GFP, LpoB-GFP, and PBP1b-GFP at division sites when cells were plasmolyzed (**D**, **F**, and **H**). GFP-PBP1a, on the other hand, displayed a largely peripheral distribution whether or not cells were plasmolyzed (**B**). The biological significance of this plasmolysis-induced septal localization is not clear, but may be the reason for the discrepancies between live-cell and immunofluorescence microscopy with respect to PBP1b localization. Plasmolyzed cells are “flattened” relative to live cells, similar to cells processed for immunofluorescence. This flattening likely leads to a more apparent peripheral signal for fluorescently labeled membrane proteins (compare cells with and without plasmolysis). Thus, what appears to be enriched protein localization at the septa may in fact be due to the presence of two closely opposed membranes at these sites with the potential for the effect being magnified due to cell flattening. **(Legend continued on next page.)**

Figure 2.9. (continued). Alternatively, our GFP fusions could be partially defective for septal localization even though they corrected phenotypes associated with mutants lacking the corresponding native protein and appear to be largely intact in immunoblots (data not shown).

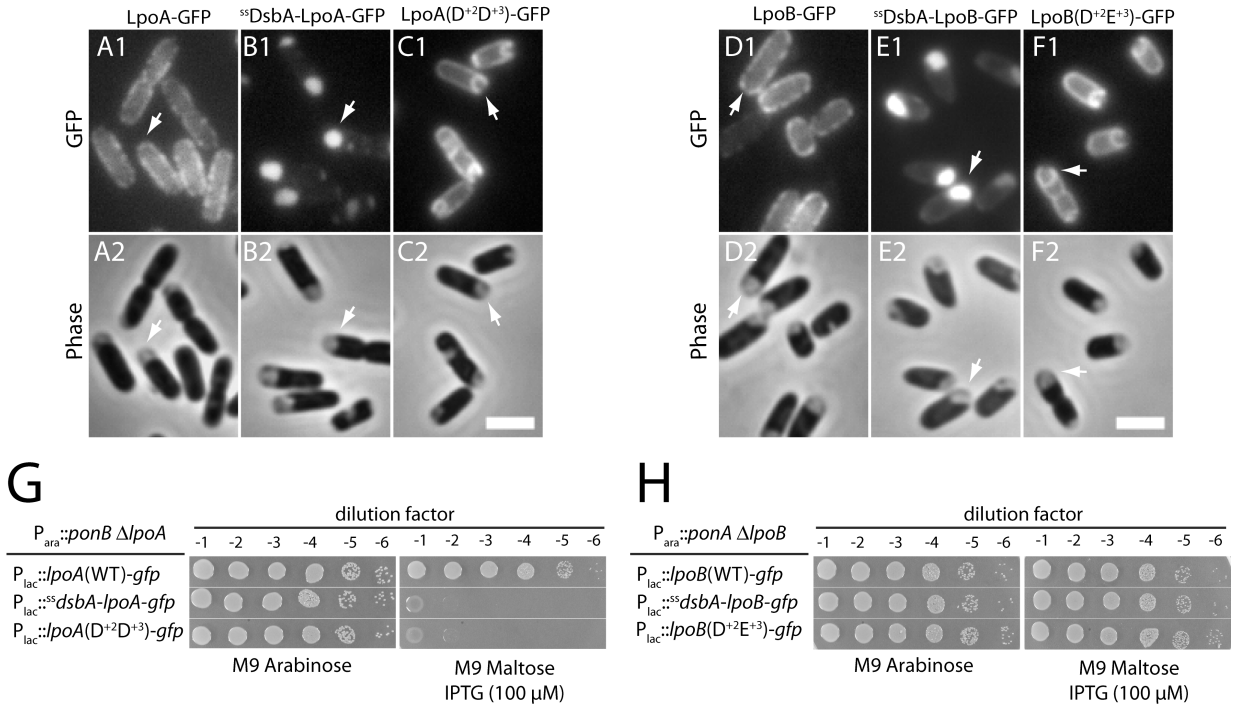

Figure 2.10. LpoA and LpoB are outer membrane lipoproteins. A-F. Cytological assay of membrane localization. Cells of MM13 [P_{ara}::*ponB ΔlpoA*] (**A-C**) or CB4(*att*λTB309) [Δ*ponA ΔlpoB*(P_{ara}::*ponA*)] (**D-F**) harboring the integrated expression constructs (**A**) *att*HKMM10 [P_{lac}::*lpoA-gfp*], (**B**) *att*HKCB42 [P_{lac}::^{ss}*dsbA-lpoA-gfp*], (**C**) *att*HKMM50 [P_{lac}::*lpoA(*$D^{+2}D^{+3}$*)-gfp*],(**D**) *att*HKCB28 [P_{lac}::*lpoB-gfp*], (**E**) *att*HKCB41 [P_{lac}::^{ss}*dsbA-lpoB-gfp*], or (**F**) *att*HKMM51 [P_{lac}::*lpoB(*$D^{+2}E^{+3}$*)-gfp*] were grown at 30ºC to mid-log in M9-arabinose supplemented with 100 μM IPTG. The cells were then plasmolyzed and visualized using GFP (panels 1) and phase contrast (panels 2) optics. Arrows highlight clear examples of protein localization (outer membrane, **A** and **D**; periplasm **B** and **E**; inner membrane, **C** and **F**). Bar equals 2 microns. **G-H.** Functionality of signal sequence mutants. Cultures of cells from (**A-F**) were diluted and plated on the indicated media as described in Figure 2. Please also see data in **Figure 2.8** and **Figure 2.9**.

Specific interaction of the Lpo factors with their cognate PBP. Overall, our results suggest that the Lpo factors are promoting the *in vivo* activity of the PBP1s. To test whether they do so directly, we purified untagged versions of PBP1a and PBP1b, and 6xHis tagged versions of LpoA (H-LpoA) and LpoB (H-LpoB) lacking their signal sequences and lipid modification signals. We then used a pull-down assay to investigate potential PBP1-Lpo interactions. When PBP1a (4μM) was incubated with H-LpoA (4μM), it was found in the eluate from Ni-NTA beads following two wash steps (**Figure 2.11A**). Purified FtsZ (4μM) was included in the binding reactions as a negative control. It was not retained on the beads, indicating that the washes were effective. In contrast to the results with PBP1a, only a very small amount of PBP1b co-purified with H-LpoA (**Figure 2.11B**). Conversely, when PBP1a (4μM) or PBP1b (4μM) were incubated with H-LpoB (4μM), PBP1b was specifically retained on NiNTA beads (**Figure 2.11C and 2.11D**). Thus, as implied by the genetic results, LpoA specifically associates with PBP1a, while LpoB specifically associates with PBP1b.

Similar amounts of Lpo and PBP1 proteins appeared to elute from the Ni-NTA resin, suggesting that the PBP1-Lpo stoichiometries in the isolated complexes were close to 1:1. Accordingly, the cellular copy numbers of the Lpo factors measured using semi-quantitative immunoblotting mirrored those determined for their cognate PBPs. About 500 molecules per cell each of LpoA and PBP1a were detected while PBP1b and LpoB were found to have copy numbers of about 1000 and 2300 molecules per cell, respectively. The *in vivo* PBP1:Lpo stoichiometry is therefore in the range of 1:1 to 1:2. The measured PBP1a/b levels were 2-4 times higher than those determined previously using radiolabeled penicillin as a probe (20), but were consistent with past measurements of PBP1b levels by

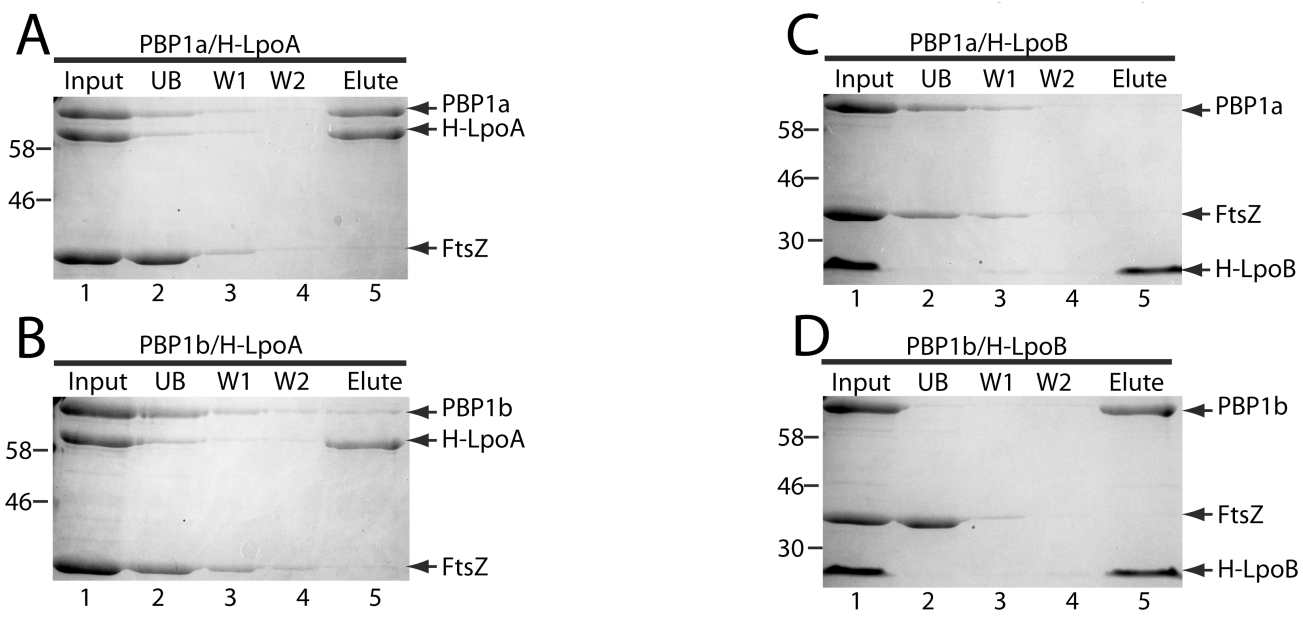

Figure 2.11. LpoA and LpoB specifically interact with their cognate PBP. A-D. H-LpoA (**A-B**) or H-LpoB (**C-D**) was incubated with PBP1a (**A and C**) or PBP1b (**B and D**) for 60 min at room temperature in binding buffer [20mM Tris (pH 7.4), 0.1% Triton-X-100, and either 300mM or 150mM NaCl for **A-B** or **C-D**, respectively]. Ni-NTA resin (Qiagen) was then added to each reaction and they were further incubated for 2 hr at 4°C with rotation. The resin was pelleted by centrifugation, washed twice with binding buffer containing 20mM imadazole, and the proteins retained on the resin were eluted with sample buffer containing EDTA (100 mM). Proteins in the initial reaction (input), initial supernatant (UB), wash supernatants (W1 and W2), and eluate were separated on a 12% SDS polyacrylamide gel and stained with Coomassie Brilliant Blue. FtsZ was included in each reaction as a non-specific control. All proteins were present in the initial binding reaction at a concentration of 4 μM. Positions of molecular weight markers (numbers in kDa) are given to the left of each gel.

immunoblotting (12). Radiolabeled penicillin thus appears to underestimate PBP levels when used for copy number determinations.

Lpo factors promote PBP activity *in vivo* and *in vitro*. To assess the effect of the Lpo proteins on PG assembly, we compared the chemical composition of wild-type PG with PG isolated from PBP1a$^-$ PBP1b$^-$ or LpoA$^-$ LpoB$^-$ cells just before they lysed (**Table 2.1**). For the analysis, purified PG was digested with a muramidase (mutanolysin) that cleaves the β-1,4 linkages between the *N*-acetylmuramic acid (M) and *N*-acetylglucosamine (G) sugars of PG (**Figure 2.1A**). The resulting mixtures of muropeptides, primarily consisting of monomeric G-M disaccharides with attached peptides or dimeric G-M disaccharides connected by crosslinked peptides, were separated by HPLC and the component muropeptides quantitated. The absence of either the PBP1s or the Lpo proteins caused a strikingly similar alteration in relative PG composition. PG from the mutants showed a decrease in peptide crosslinking, from 22% in the wild-type control down to 18-19% (**Table 2.1**). In addition, a dramatic increase (4-7 fold) in pentapeptide-containing muropeptides was observed in the PG isolated from the mutants (**Table 2.1**). Since the terminal D-Ala is cleaved from pentapeptides as part the PBP crosslinking reaction, the observed increase in pentapeptides in the mutant PG preparations coupled with the reduction in crosslinking is consistent with a failure in the efficient incorporation of new PG material into the existing cell wall network.

Next, we examined the effect of LpoB on PG synthesis *in vitro* using ether-permeabilized (EP) cells. In the latter stages of the PG synthesis pathway, lipid-II (**Figure 2.1B**) is made from the activated sugar precursors UDP-M-pentapeptide (UDP-M-pep$_5$)

Table 2.1. PG composition in cells depleted of PBP1s or Lpo factors.

	Strain		
	WT (n=3)	Para::ponB ΔponA (n=2)	Plac::lpoA ΔlpoB (n=3)
Muropeptides		% total	
G-M Monomer (total)	52.4 ± 2.0	60.2 ± 1.0	58.6 ± 0.9
pentapeptide	0.2 ± 0.1	0.9 ± 0.1	1.4 ± 0.7
tetrapeptide	38.6 ± 3.1	42.6 ± 0.5	40.7 ± 1.0
tripeptide	6.7 ± 0.6	11.4 ± 0.9	4.5 ± 2.9
GM-Dimer (total)	39.3 ± 3.2	34.0 ± 2.6	36.1 ± 0.7
GM-Trimer (total)	3.1 ± 0.6	2.4 ± 1.3	1.4 ± 0.1
anhydro-GM (total)	1.4 ± 0.0	0.9 ± 0.0	1.4 ± 0.3
%crosslinkage	21.7 ± 1.2	18.6 ± 0.5	19.0 ± 0.4

and UDP-G. PG synthesis can be reconstituted and measured in ether-permeabilized (EP) cells by supplying them with purified UDP-M-pep_5 and UDP-[^{14}C]G and monitoring the incorporation of label into the detergent-insoluble PG fraction (Mirelman et al., 1976). PBP1b appears to be the major PBP responsible for PG synthesis in this system because EP cells from PBP1b$^-$ mutants are almost completely defective in label incorporation whereas the absence of PBP1a has little to no effect (**Figure 2.12A**) (41). EP cells thus provide a convenient system for following PBP1b activity in a cellular context. To determine if LpoB is required for PBP1b activity in this system, we prepared EP cells from a LpoB$^-$ mutant and tested their ability to synthesize PG. LpoB$^-$ EP cells behaved identically to those prepared from a PBP1b$^-$ mutant and were dramatically reduced in their ability to incorporate UDP-[^{14}C]G into the detergent-insoluble PG fraction (**Figure 2.12A**). Remarkably, the addition of purified untagged LpoB completely restored the ability of LpoB$^-$ EP cells to synthesize PG (**Figure 2.12A**), indicating that the PG synthesis defect was due solely to the absence of LpoB. As expected based on prior results with PBP1a$^-$ mutants, a LpoA defect did not affect PG synthesis in EP cells (**Figure 2.12A**).

To further investigate LpoB function, we monitored its effect on the PGT activity of PBP1b in a purified system using radiolabled lipid-II substrate. LpoB specifically enhanced the initial rate of PBP1b transglycosylation by an average of 1.5x (**Figure 2.12B**). However, it did not affect the activity of PBP1a, nor did LpoA affect the PGT activity of either PBP (**Figure 2.12B-C**). Although the effect of LpoB on the rate of PBP1b PGT activity was relatively modest, it specifically affected the length of glycan chains produced by PBP1b. Much shorter polymers were produced in the presence of LpoB than those formed in its absence (**Figure 2.12D)**. We propose that this indicates that LpoB stimulates the initiation

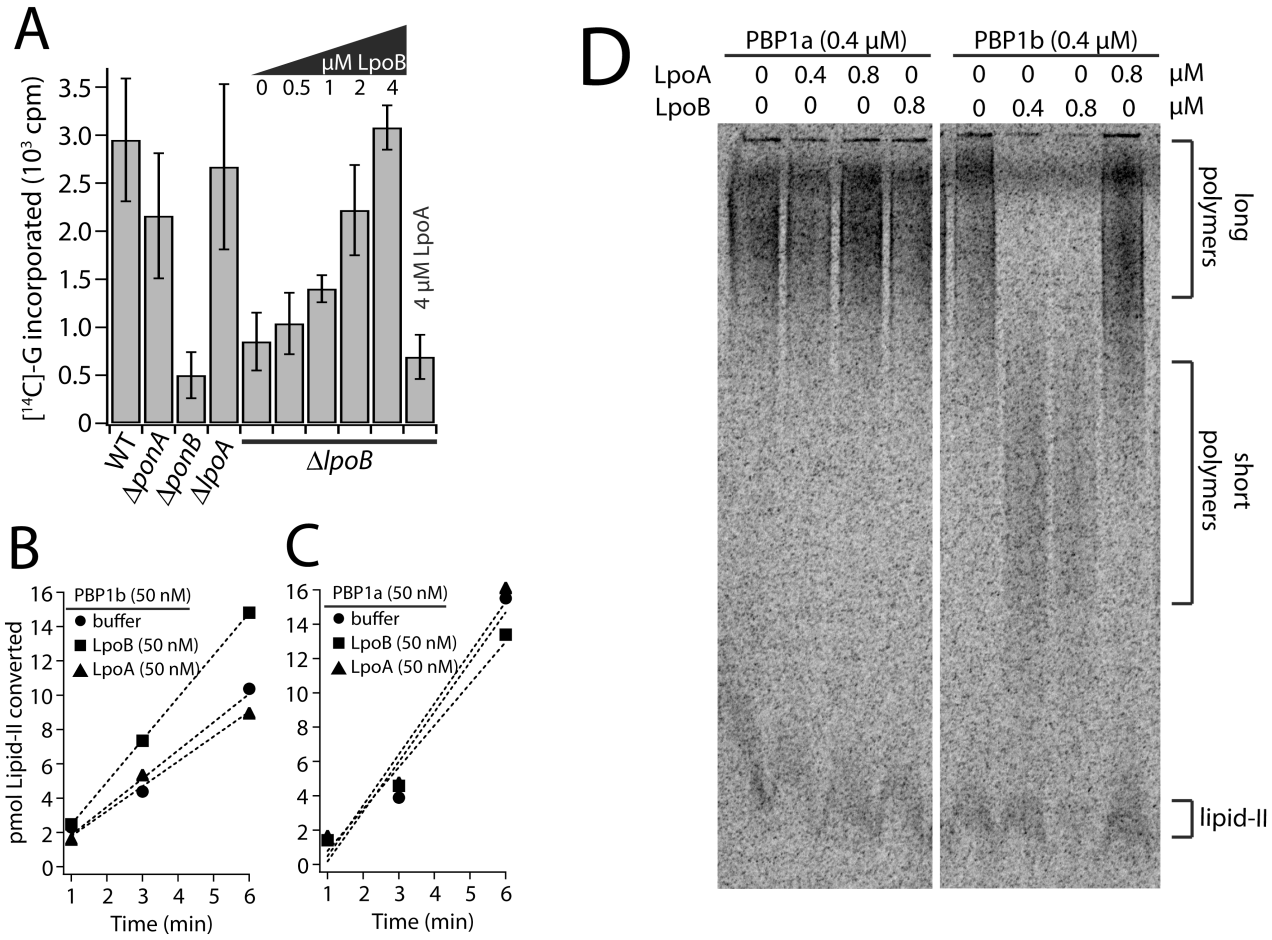

Figure 2.12. LpoB activates PBP1b PGT activity and affects polymer length. A. PG synthesis in EP cells. EP cells from the indicated strains were incubated with or without LpoB (0.5-4 μM, as indicated). Reactions were initiated with the addition of UDP-M-pentapeptide (4 nmol) and UDP-[^{14}C]G. After 60 min they were boiled in 4% SDS and filtered. Labeled PG retained on the filter was quantified by liquid scintillation counting. **B-C.** PBP PGT activity was measured by the incorporation of lipid-II into peptidoglycan in the presence of penicillin G. [^{14}C]G-labeled lipid-II (4-8 μM) was incubated with or without LpoA or LpoB (50 nM) prior to the addition of PBP1a or PBP1b (50 nM), which initiated the reaction. **(Legend continued on next page.)**

Figure 2.12 (continued). At the indicated time points, reactions were quenched and analyzed for remaining substrate and PG product by paper chromatography. Results of single experiments are shown. They are representative of multiple trials (see Supplementary Information). **D.** Glycan chains generated in reactions similar to those in (**B-C**) were separated on an acrylamide gel (9%) and visualized using a phosphorimager. Lipid-II substrate was present at 4 μM in each reaction and protein amounts are indicated above the gel lanes.

of glycan strand formation (see Discussion). Overall, we conclude that LpoB is absolutely required for PBP1b function in a cellular context and is capable of directly and specifically modulating PBP1b PGT activity in a purified system.

Discussion

Despite the fundamental role of PG assembly in bacterial growth and its long history as an effective antibiotic target, we are only just beginning to uncover the molecular mechanisms underlying this complex process. Over the years, a great deal of effort has focused on the structural and biochemical characterization of the PBPs, the major PG synthases. This has led to important insights into the mechanisms by which these enzymes catalyze PG polymerization and crosslinking, how they are inhibited by antibiotic molecules, and why certain variants confer antibiotic resistance (37). While much still remains to be learned about the biochemical function of the PBPs, progress in this area has significantly outpaced our knowledge of the *in vivo* function of the PBPs and how they cooperate with other cellular factors to build the cell-shaped PG mesh. One of the principal reasons for this is that functional redundancy among PG assembly factors has limited the effectiveness of genetic analysis. Here, we turned this redundancy into an advantage by employing synthetic lethal screens to uncover the *E. coli* lipoproteins LpoA and LpoB as the first set of essential PBP cofactors (**Figure 2.13**). Our results suggest that, like other polymerases, the PBPs may generally require accessory factors to augment or regulate their activity. Moving forward, these factors will surely play a significant role in advancing both our understanding of PBP function *in vivo* and PBP enzymology *in vitro*.

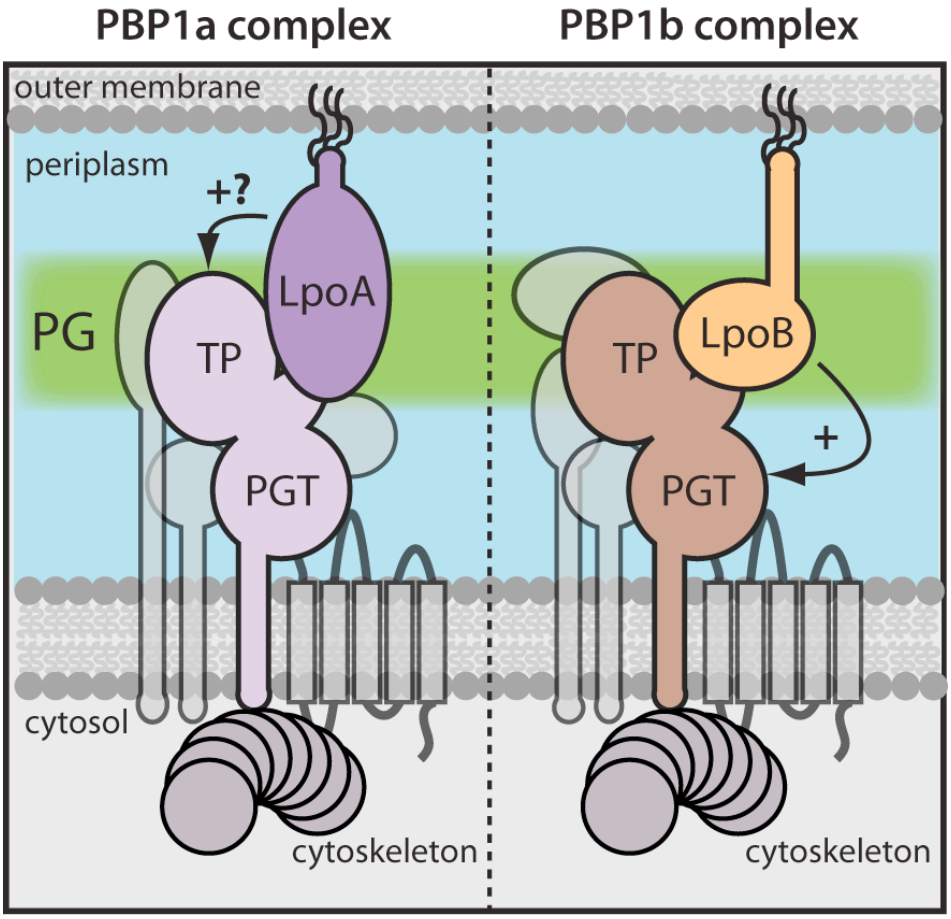

Figure 2.13. Model for Lpo protein function. Shown are schematic diagrams of putative PBP-containing complexes in *E. coli* drawn as in **Figure 2.1**. The partial redundancy of PBP1a (lavender) and PBP1b (brown) suggest that they form part of independent PG synthesizing (sub)complexes that can substitute for one another. LpoA is an essential component of the PBP1a complex (left) that potentially stimulates the transpeptidase activity of this PBP (see text for details). LpoB is an essential component of the PBP1b complex and activates its PGT activity.

The outer membrane and PG biogenesis. Although PG precursor biosynthesis occurs inside the cell, the final stages of PG assembly take place at the cell surface (Figure 2.1B). This presents an interesting challenge for bacteria, which must somehow coordinate PG assembly outside the cytoplasmic membrane with processes that control growth and division on the inside. Recent results indicate that this coordination is, at least in part, mediated by the MreB and FtsZ cytoskeletons (31).

Because they surround their PG layer with a second (outer) membrane, Gram-negative bacteria face the additional challenge of coordinating PG synthesis with outer membrane assembly. The discovery of LpoA and LpoB as outer membrane activators of the PBPs suggests that they may play an important role in coupling outer membrane biogenesis and PG synthesis. While further work is required to test this possibility, it highlights the potential for the PG synthetic machinery receiving regulatory input from the outer membrane as well as cytoskeletal elements in the cytoplasm. An equally attractive possibility is that the outer membrane localization of the Lpo factors might facilitate a "template" function for the existing PG matrix. The glycan strands of PG are thought to be oriented perpendicular to the long-axis of the cell (22) (**Figure 2.14**). Adjacent "tracks" of glycan strands are therefore likely to restrict the lateral diffusion of trans-envelope complexes formed between the Lpo proteins in the outer membrane and the PBPs in the inner membrane. We envision that this arrangement would force the insertion of new PG material along a consistent path directed by the "tracks" in the existing structure (**Figure 2.14**). Thus, as implied by earlier work (24, 39), the PG layer itself may collaborate with cytoskeletal elements to provide a robust mechanism for shape-maintenance and the regular expansion of the PG network. Importantly, the Lpo factors may represent just one

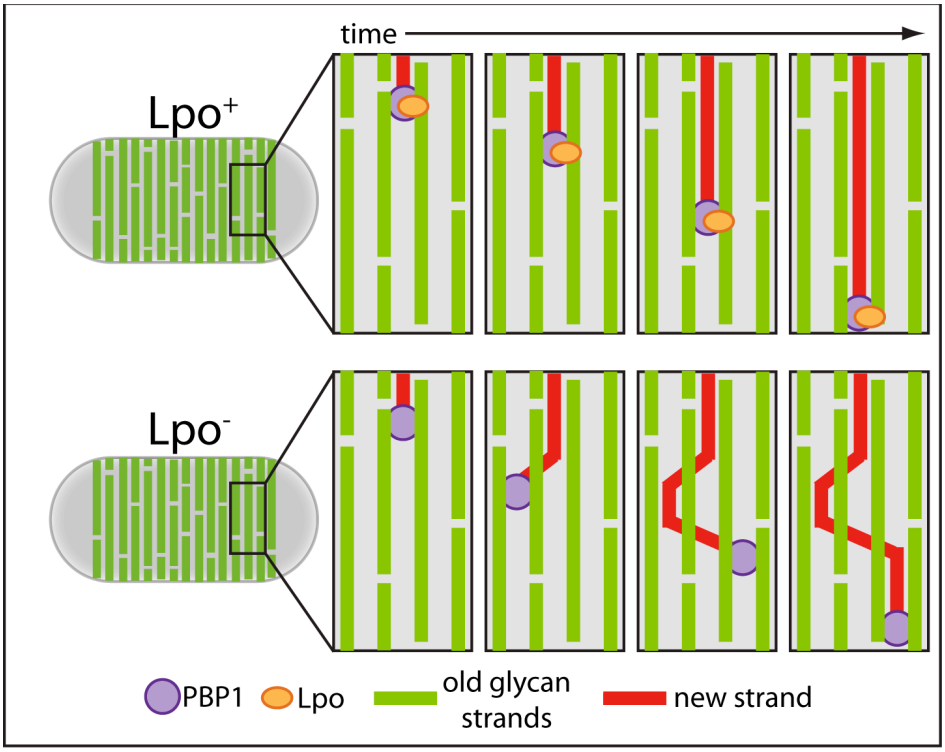

Figure 2.14. Model for the control of glycan strand insertion by trans-envelope Lpo factor-PBP complexes. Shown is a schematic detailing a model in which adjacent glycan strands in the existing PG structure (green) restrict the lateral diffusion of trans-envelope Lpo factor-PBP complexes in the membrane to promote the insertion of new PG material (red) along a regular path (upper panels). Such a model is consistent with the observed insertion of single-stands of new PG between two old strands (16, 19), and previous studies suggesting a templating function for the existing matrix (24, 39). In the absence of the Lpo factors and/or additional components of the PG synthetic machinery that link the PBPs to the outer membrane (e.g. MltA and MipA for PBP1b) (49), PBP complexes may stray from their original path of synthesis resulting in the less orderly insertion of new material (lower panels). **(Legend continued on next page.)**

Figure 2.14 (continued). By directing the path of PG synthesis by envelope-spanning PBP complexes, we envision that the existing PG matrix collaborates with cytoskeletal elements to provide a robust mechanism for cell shape maintenance and the ordered duplication of the PG layer with each cell cycle.

set of potential connections between the PBPs and the outer membrane. Indeed, it was shown previously that PBP1b is connected to the outer membrane through its interactions with the bridging protein MipA that, in turn, associates with the outer membrane PG hydrolase MltA (49). In contrast to LpoB, neither MipA or MltA are required for PBP1b activity. However, the ability of these and potentially other proteins to connect PBP1b to the outer membrane may be one reason why an outer membrane localization is not absolutely required for LpoB to support PBP1b function.

Biochemical activities of LpoA and LpoB. In addition to promoting PBP1b activity in EP cells and stimulating PBP1b PGT activity *in vitro*, LpoB also caused PBP1b to produce dramatically shorter glycan chains. A wide range of glycan strand lengths has been detected in purified cellular PG, but essentially nothing is known about how strand length is determined *in vivo* and whether or not it is regulated. The observation that LpoB affects the length distribution of glycan chains produced by PBP1b suggests the attractive possibility that it regulates PBP1b product length by stimulating the termination of glycan synthesis. However, such a role is difficult to reconcile with the observation that LpoB is essential for PG synthesis by PBP1b in EP cells. We therefore favor a model in which LpoB stimulates the initiation of glycan chain synthesis to explain its effect on product length distribution in PBP1b PGT assays. This model is based on the previous observation that the length distribution of polymers produced by a variety of purified PBPs was unaffected by the PBP:substrate ratio (50). Surprisingly, even in reactions with a 1:1 PBP:substrate ratio, where at most only a few turnovers would be expected, long glycan strands with a size distribution typical of the PBP being assayed were produced. This suggests that the

initiation step of glycan chain synthesis is rate-limiting and that the subsequent elongation process is rapid and processive (50). Thus, consistent with our observations, activation of glycan strand initiation by LpoB would be predicted to result in a greater number of elongating PBP1b polymerases in PGT reactions such that lipid-II is exhausted before longer polymer lengths can be achieved. Because LpoB is not absolutely required for PBP1b activity in a purified system, a subset of PBP1b molecules in PGT reactions lacking LpoB must be capable of initiating glycan strand formation. Initiation may be tightly controlled in the context of multi-protein complexes formed *in vivo*, however, leading to a strict LpoB dependence for PBP1b PGT activity in the cell. Further work will be required to investigate the potential role of LpoB in glycan chain initiation, and whether, in such a capacity, it serves as critical PBP1b regulator that helps coordinate its PGT activity with the activity of other components of the PG or outer membrane assembly machinery.

While our results clearly show that LpoA is essential for PBP1a function *in vivo*, we have yet to detect a biochemical activity that sheds light on the specific role of LpoA in the reactions catalyzed by PBP1a. One potential reason for this is that lipidation and outer membrane localization of LpoA was shown to be essential for its activity *in vivo* and the protein we purified was not lipidated. Interestingly, the structure of the C-terminal domain of *H. influenzae* LpoA was recently solved and was found to share similarities with periplasmic solute binding proteins like maltose binding protein (1). The closest structural relative to LpoA is *E. coli* LivJ (PBD ID# 1z15), a branched-chain amino acid binding protein (1). This suggests that LpoA may associate with the peptide moieties of PG to facilitate crosslinking of nascent material into the PG matrix by PBP1a. Consistent with

this idea, in the accompanying report from Typas et al. (44), the authors present evidence that LpoA greatly enhances the formation of crosslinked PG by purified PBP1a.

A specific role for PBP1b-LpoB complexes in cell division? At least two distinct multi-enzyme complexes are thought to be necessary for proper PG biogenesis in rod shaped cells: one organized by MreB for cell elongation and the other organized by the division protein FtsZ (13). Although they are individually dispensable for growth, at least one type of PBP1 protein is thought to be required for the activity of each of these complexes. It therefore seems likely that PBP1a and PBP1b, along with their associated Lpo activators, are both capable of productively interfacing with the MreB- and FtsZ-directed PG synthesizing machineries. Consistent with this possibility, in normal, unplasmolyzed cells, GFP fusions to the PBP1s and the Lpo factors were found to localize in patches and foci that were broadly distributed around the cell periphery (**Figures 2.9 and 2.10**). In addition, immunofluorescence localization of PBP1b performed previously also found it to be present in many foci throughout the cell cylinder, although a modest enrichment at the division sites of constricting cells was also reported (11).

While PBP1a and PBP1b appear to be largely interchangeable in their capacities to support growth, it is likely that they display some level of functional specialization in wild-type cells. Accordingly, PBP1b has been shown to interact with the division-specific, class B PBP, PBP3, and the division factor FtsN (11, 35). This suggests that PBP1b, along with LpoB, may play a specific role in the division process that PBP1a-LpoA sub-complexes are unable to perform. Interestingly, a number of mutants with lesions in genes coding for factors involved in septal PG biogenesis were isolated using our screen for cells with a Slb

phenotype. Rather than identifying additional co-factors needed for PBP1a activity like LpoA, we favor the interpretation that these division mutants have a Slb phenotype because PBP1b$^-$ cells are partially defective for cell division and are thus sensitized to further insults to the division machinery. A similar class of division mutants was not recovered in the corresponding screen for *sla* mutants, nor did the alleles identified in the Slb screen display synthetic phenotypes with the absence of PBP1a when this was tested directly (data not shown). The phenotype of the PBP1b$^-$/division mutant combinations in each case was a high frequency of cell lysis, suggesting that the absence of PBP1b combined with a defect in one of these division factors often results in catastrophic failures in septal PG assembly. Further analysis of these mutants and their connection to PBP1b function should allow us to elucidate how PBP1b participates in the construction of the polar PG caps, and whether or not this role is unique to PBP1b-LpoB containing complexes.

Lpo factor conservation and the prospect for additional PBP accessory proteins. LpoA is broadly conserved among the γ-proteobacteria while LpoB is primarily restricted to the enterobacteriaceae family within this class (21). We therefore suspect that organisms belonging to bacterial classes other than the γ-proteobacteria are likely to possess PBP accessory proteins distinct from LpoA and LpoB that also promote the function of their PBPs. Some of these factors may play critical roles in the PG assembly process itself, while others may help coordinate PG synthesis with additional envelope components like the outer membranes of other proteobacteria or the teichoic acids of Gram-positive organisms.

We anticipate that several of the many PBP-interacting proteins identified previously will also prove to be PBP accessory proteins that directly assist the PBPs in PG assembly. Prime candidates are the PG hydrolases. These enzymes break bonds in the PG meshwork and have long been thought necessary for providing space in the existing matrix for the insertion of new material. Although this possibility remains attractive on a theoretical basis, experimental support for it is still lacking. Addressing the role of these and other PBP-interacting factors in PBP function represents an important challenge for future work.

PBP accessory factors and antibiotic development. The discovery of penicillin and its ability to inhibit the PBPs to induce bacteriolysis ushered in the antibiotic age of clinical medicine. Since then, the PBPs have proven to be one of the most important drug targets ever identified. Sadly, antibiotic resistance continues to erode the effectiveness of our current cache of antibacterial therapies, including penicillin derivatives and other β-lactams (42). Regardless of their precise biochemical function, the discovery of accessory factors essential for the *in vivo* function of the PBPs suggests new avenues for antibiotic development to help combat drug-resistant bacteria. The observation that LpoA is essential in *H. influenzae* (52) suggests that direct targeting of PBP accessory proteins might be effective in some circumstances. Additionally, further study of the mechanisms by which these accessory factors influence PBP activity is likely to reveal novel ways to block PBP function for therapeutic purposes.

Materials and Methods

Media, bacterial strains, and plasmids

Cells were grown in LB (1% tryptone, 0.5% yeast extract, 0.5% NaCl) or minimal M9 medium supplemented with 0.2% casamino acids and 0.2% sugar (arabinose; Ara, glucose; Glu, or maltose; Malt). The bacterial strains and plasmids used in this study are listed in Tables S2 and S3, respectively, and a detailed description of their construction is given below.

The bacterial strains and plasmids used in this study are listed in Tables S2 and S3, respectively. A detailed description of plasmid construction is given below. All strains used for *in vivo* experiments are derivatives of MG1655 (25), and all deletion alleles were sourced from the Keio knockout collection (3). All expression constructs used for *in vivo* experiments except those used in **Figures 2.4** and **2.7** are derivatives of the CRIM plasmids developed by Wanner and co-workers (26). They were integrated into phage attachment sites (HK022 or λ) as described previously (8, 26). Single copy integrants were identified using diagnostic PCR (26). Integrated vectors were transferred between strains by P1-mediated transduction (32). The plasmids used in **Figure 2.7** were low-copy pSC101 derivatives and those used in **Figure 2.4** were medium-copy pBR derivatives. Plasmids used in this study are described below. In all cases PCR was performed using KOD polymerase (Novagen) according to the instructions. Unless otherwise indicated, MG1655 chromosomal DNA was used as the template. Restriction sites for use in plasmid constructions are italicized and underlined in the primer sequences given below. Plasmid DNA and PCR fragments were purified using the Qiaprep spin miniprep kit (Qiagen) or the Qiaquick PCR purification kit (Qiagen), respectively.

Table 2.2. Bacterial strains used in this study.

Strain	Genotype[a]	Source/Reference[b]
DH5α	F– *hsdR*17 *deoR recA*1 *endA*1 *phoA supE*44 *thi*-1 *gyrA*96 *relA*1 Δ(*lacZYA-argF*)U169 ϕ80d*lacZ*ΔM15	Gibco BRL
BL21(λDE3)	*ompT* rB– mB– (P_{lac}UV5::T7*gene1*)	Novagen
Rosetta(λDE3)	*ompT* rB- mB- *gal dcm* (P_{lac}UV5::T7*gene1*)	Novagen
MG1655	*rph*1 *ilvG rfb*-50	(25)
TB10	*rph*1 *ilvG rfb*-50 λΔ*cro-bio nad*::Tn10	(27)
TB28	MG1655 Δ*lacIZYA*::*frt*	'(7)
BW25113	Δ(*araD-araB*)567 Δ*lacZ*4787(::*rrnB*-3) *rph*-1 Δ(*rhaD-rhaB*)568 *hsdR*514	(3)
JW3359-1	BW25113 Δ*ponA(mrcA)*::Kan^R	(3)
JW0145-1	BW25113 Δ*ponB(mrcB)*::Kan^R	(3)
JW3116-1	BW25113 Δ*lpoA*(*yraM)*::Kan^R	(3)
JW5157-1b	BW25113 Δ*lpoB(ycfM)*::Kan^R	(3)
TU115	TB28 Δ*ponA(mrcA)*::Kan^R	P1(JW3359-1) x TB28
TU116	TB28 Δ*ponB(mrcB)*::Kan^R	P1(JW0145-1) x TB28
TU121	TB28 Δ*ponA(mrcA)*::*frt*	TU115/pCP20
TU122	TB28 Δ*ponB(mrcB)*::*frt*	TU116/pCP20
MM5	TB10 (Kan^R *araC* P_{ara})::*ponB*	recombineering
MM8	TB28 Δ*lpoA*(*yraM)*::Kan^R	P1(JW3116-1) x TB28
MM9	TB28 (Kan^R *araC* P_{ara})::*ponB*	P1(MM5) x TB28
MM10	Δ*ponA(mrcA)*::*frt* (Kan^R *araC* P_{ara})::*ponB*	P1(MM5) x TU121
MM11	TB28 (*frt araC* P_{ara})::*ponB*	MM9/pCP20
MM13	ΔlpoA(*yraM)*::Kan^R (*frt araC* P_{ara})::*ponB*	P1(JW3116-1) x MM11
MM22	TB28 Δ*lpoA*(*yraM)*::*frt*	MM8/pCP20
MM25	TB28 Δ*lpoA*(*yraM)*::*frt* Δ*ponB(mrcB)*::Kan^R	P1(JW0145-1) x MM22(*att*MM10)
MM26	TB28 Δ*lpoA*(*yraM)*::*frt* Δ*lpoB(ycfM)*::Kan^R	P1(JW5157-1b) x MM22(*att*MM10)

Table 2.2. Bacterial strains used in this study. (Continued)

Strain	Genotype[a]	Source/Reference[b]
MM30	TB28 Δ*ponA(mrcA)*::*frt* Δ*lpoA*(*yraM)*::Kan^R	P1(JW3116-1) x TU121(*att*TB309)
CB3	TB28 Δ*ponA(mrcA)*::*frt* Δ*ponB(mrcB)*::Kan^R	P1(JW0145-1) x TU121(*att*TB309)
CB4	TB28 Δ*ponA(mrcA)*::*frt* Δ*lpoB*(*ycfM)*::Kan^R	P1(JW5157-1b) x TU121(*att*TB309)
CB5	TB28 (*frt araC* P_{ara})::*ponB* Δ*lpoB*(*ycfM)*::Kan^R	P1(JW5157-1b) x MM11
CB6	TB28 Δ*lpoB(ycfM)*::Kan^R	P1(JW5157-1b) x TB28
CB26	TB28 Δ*lpoB(ycfM)*::*frt*	CB6/pCP20

[a] The Kan^R cassette is flanked by *frt* sites for removal by FLP recombinase. An *frt* scar remains following removal of the cassette using FLP expressed from pCP20.

[b] Strain constructions by P1 transduction are described using the shorthand: P1(donor) x recipient. In all cases transductants were selected on LB Kan plates. Strains resulting from the removal of a Kan^R cassette using pCP20 are indicated as: Parental strain/pCP20.

Table 2.3. Plasmids used in this study.

Plasmid	Genotype[a]	Origin	Reference/source
plysSRARE	cat lysT7 proL leuW metT argW thrT glyT tyrU thrU argU ileX	p15A	Novagen
pCP20	bla cat cI857 repA(ts) PR::flp	pSC101	(17)
pTB102	cat cI857 repA(ts) PR::intHK022	pSC101	(8)
pInt-ts	bla cI857 repA(ts) PR::intλ	pSC101	(26)
pTB145	bla lacIq PT7::h-ulp1(403-621)	pBR/colE1	(6)
pTB146	bla lacIq PT7::h-sumo	pBR/colE1	(6)
pTB284	aadA Plac-con::gfp	pSC101	This study
pTB307	attHK022 bla lacIq Plac::gfp-ponA	R6K	This study
pTB309	attλ cat Para::ponA	R6K	This study
pTU110	cat lacIq Plac::ponB	mini-F	This study
pCB1	cat lacIq Plac::gfp-ponA	mini-F	This study
pCB7	bla lacIq PT7::h-sumo-lpoB(21-213)	pBR/colE1	This study
pCB21	bla lacIq PT7::h-sumo-ponA	pBR/colE1	This study
pCB22	bla lacIq PT7::h-sumo-ponB	pBR/colE1	This study
pCB25	bla lacIq Plac::lpoB	pBR/colE1	This study
pCB28	attHK022 bla lacIq Plac::lpoB-sfgfp	R6K	This study
pCB39	bla lacIq PT7::h-lpoB(21-213)	pBR/colE1	This study
pCB40	bla lacIq PT7::h-lpoA(28-678)	pBR/colE1	This study
pCB41	attHK022 bla lacIq Plac::ssdsbA-lpoB-sfgfp	R6K	This study
pCB42	attHK022 bla lacIq Plac::ssdsbA-lpoA-sfgfp	R6K	This study
pCB62	aadA Plac-con::ponA	pSC101	This study
pCB72	aadA Plac-con::ponB	pSC101	This study
pMM6	attHK022 bla lacIq Plac::gfp-ponB(γ)	R6K	This study
pMM10	attHK022 bla lacIq Plac::lpoA-sfgfp	R6K	This study

Table 2.3. Plasmids used in this study. (Continued)

Plasmid	Genotype[a]	Origin	Reference/source
pMM12	bla lacIq Plac::lpoA	pBR/colE1	This study
pMM18	bla lacIq PT7::h-sumo-lpoA(28-678)	pBR/colE1	This study
pMM44	attHK022 bla lacIq Plac::sslpoA-mcherry	R6K	This study
pMM45	attHK022 bla lacIq Plac::sslpoB-mcherry	R6K	This study
pMM46	attHK022 bla lacIq Plac::sspal(D+2)-mcherry	R6K	This study
pMM47	attHK022 bla lacIq Plac::sspal-mcherry	R6K	This study
pMM50	attHK022 bla lacIq Plac::lpoA(D+2D+3)-sfgfp	R6K	This study
pMM51	attHK022 bla lacIq Plac::lpoB(D+2E+3)-sfgfp	R6K	This study

[a] A 6xHis tag for purification is indicated by the letter *h*. P_{T7}, P_R, P_{lac}, and P_{ara} indicate the phage T7, λR, lactose, and arabinose promoters, respectively. $P_{lac\text{-}con}$ is a synthetic *lac* promoter with consensus -10 and -35 elements. Numbers in parenthesis indicate the codons included in the relevant clones.

pTU110:

pTU110 [*cat* Plac::*ponB lacZ*] was constructed from pRC7 [*bla lacZ*] (18) in four steps. First, *slmA* was amplified with the primers 5'-GTCC*GAATTC*ACATTTCGTT TGCGGTCATAGCG-3' and 5'-GCCT*AAGCTT*TTACTGCAACTGTGCCGCAATTAGC-3'. The resulting fragment was digested with EcoRI and HindIII and ligated with appropriately digested pRC7 to generate pTB68 [*bla* Plac::*slmA lacZ*]. Second, the *bla* gene was replaced with the *cat* gene amplified from pKD3 (17) with the primers 5'-TTGAAGACGAAAGGG CCTCGTGATACGCCTATTTTTATAGATGAATATCCTCCTT AGTTCC-3' and 5'-TCTAAAGTATATATGAGTAAACTTGGTCTGACAGTTACCAAGTG TAGGCTGGAGCTGCTTCG-3' by recombination in *E. coli* TB10 strain (MG1655 *nadA*::*Tn*10 λ*cI*857 Δ(*cro-bioA*)) (27), generating pTB236 [*cat* Plac::*slmA lacZ*]. Thirdly, the EcoRI-HindIII fragment of pTB236 containing *slmA* was replaced with the EcoRI-HindIII fragment of pTB25 (7) containing *envC* to generate pTB238 [*cat* Plac::*envC lacZ*]. Lastly, *ponB* was amplified with the primers 5'-GTCA*GAATTC*GGGCTTTTGCGCCTGAATATTG-3' and 5'-GTCA*CTCGAG*ATGGGATGTTATTTTACCGGATGGC-3'. The resulting fragment was digested with EcoRI and XhoI and replaced the EcoRI-SalI fragment of pTB238 to generate pTU110 [*cat* Plac::*ponB lacZ*].

pMM6:

The *ponB* gene from pTU110 [*cat lacI*^{q} P_{lac}::*ponB*] was amplified using the primers 5'-GTAC*GGATCC*CCGCGCAAAGGTAAGGG-3' and 5'-GTCA*CTCGAG*ATGGGATGTTATTT TACCGGATGGC-3'. This PCR fragment was then digested with BamHI and XhoI and

ligated with BamHI and SalI digested pTB183 (5) to create pMM6 [*attHK022 bla lacI*^{q} P_{lac}::*gfp-ponB(Y)*].

pMM10:

To generate pMM10 [*attHK022 bla lacI*^{q} P_{lac}::*lpoA-sfgfp*], the *lpoA* gene was amplified using the primers 5'-GTAC*CATATG*GTACCCTCAACATTTTCTCGTTTG-3' and 5'-GTAC*CTCGAG*ACTGACGGGGACTACCTGAC-3'. The PCR product was digested with NdeI and XhoI and ligated with appropriately digested pTB225 (45).

pMM12:

pMM12 was constructed through the intermediate pMM7 [*att*HK022 *bla* P_{lac}::*lpoA*]. pMM7 was created by amplifying the *lpoA* gene using the primers 5'-GTAC*TCTAGA*CG TATTGCCGATTTAATATTGAGCATTGC-3' and 5'-GTAC*AAGCTT*CGCTTGTGCTTCCCAC GCATC-3'. The resulting PCR product was digested with XbaI and HindIII and ligated with appropriately digested pTB183 (5). Subsequently, pMM7 was digested with XbaI and HindIII and the resulting *lpoA* containing fragment was ligated into the appropriately digested pTB28 [*bla lacI*^{q} P_{lac}::*amiC-gfp*] (9) to create pMM12 [*bla lacI*^{q} P_{lac}::*lpoA*].

pMM18:

To construct pMM18, the primers 5'-GTAC*GAGCTC*GGCACCCATACTCCCGA TCAG-3' and 5'-GTAC*CTCGAG*TTAACTGACGGGGACTACCTGAC-3' were used to amplify the part of the *lpoA* gene which code for LpoA residues 28 to 678. The resulting PCR

product was then digested with the restriction enzymes SacI and XhoI and ligated with appropriately digested pTB146 (6) to generate the *h-sumo* fusion.

pMM44-pMM47:

For pMM44, pMM45, pMM46 and pMM47, an important intermediate construct was pMM43 [*attHK022 bla lacI*^{q} P_{lac}::*lpoA-mCherry*]. To make pMM43, an *mCherry* containing XhoI-HindIII fragment from pTU136 (45) was used to replace the corresponding gfp fragment of pMM10. The synthetic nucleotides described below were annealed and ligated into NdeI and XhoI digested pMM43 to create pMM44, pMM45, pMM46 and pMM47.

For pMM44 [*attHK022 bla lacI*^{q} P_{lac}::^{ss}*lpoA-mCherry*], the synthetic oligonucleotides encoding the *lpoA* signal sequence were 5'-TATGGTACCCTCAACATTTTCTCGTTTGAAA GCCGCGCGTTGTCTGCCTGTTGTTCTGGCAGCCCTGATTTTCGCCGGTTGTGGCACCCA TACTCCCGATC-3' and 5'-TCGAGATCGGGAGTATGGGTGCCACAACCGGCGAA AATCAGG GCTGCCAGAACAACAGGCAGACAACGCGCGGCTTTCAAACGAGA AAATGTTGAGGGTACCA-3'.

pMM45 [*attHK022 bla lacI*^{q} P_{lac}::^{ss}*lpoB-mCherry*] was constructed using synthetic oligonucleotides encoding the *lpoB* signal sequence: 5'-TATGACAAAAATGAGTCGCT ACGCCTTGATTACCGCGCTGGCGATGTTTCTCGCCGGGTGTGTGGGGCAACGTGAACCT C-3' and 5'-TCGAGAGGTTCACGTTGCCCCACACACCCGGCGAGAAACATCGCCA GCGCGG TAATCAAGGCG TAGCGACTCATTTTTGTCA-3'.

The synthetic oligonucleotides encoding for a mutated *pal* signal sequence 5'-TATGCAACTGAACAAAGTGCTGAAAGGGCTGATGATTGCTCTGCCTGTTATGGCAATTGCG

GCATGTGATTCCAACAAGAACGCCC-3’ and 5’-TCGAGGGCGTTCTTGTTGGAATCACA TGCCGCAATTGCCATAACAGGCAGAGCAATCATCAGCCCTTTCAGCACTTTGTTCAGTTG CA-3’ were used to create pMM46 [*attHK022 bla lacI*^{q} P_{lac}::^{ss}*pal(D*$^{+2}$*)-mCherry*].

Finally, the synthetic oligonucleotides 5’-TATGCAACTGAACAAAGTGCTGAAAGGG CTGATGATTGCTCTGCCTGTTATGGCAATTGCGGCATGTTCTTCCAACAAGAACGCCC-3’ and 5’-TCGAGGGCGTTCTTGTTGGAAGAACATGCCGCAATTGCCATAACAGGC AGAGCAATCATCAGCCCTTTCAGCACTTTGTTCAGTTGCA-3’ encoding the wild-type *pal* signal sequence were used to make pMM47 [*attHK022 bla lacI*^{q} P_{lac}::^{ss}*pal-mCherry*].

pMM50:

pMM50 [*attHK022 bla lacI*^{q} P_{lac}::*lpoA (D*$^{+2}$*D*$^{+2}$*)-sfgfp*] is identical to pMM10 except that the Gly and Thr codons following the *lpoA* lipobox Cys codon were changed to Asp codons using site-directed mutagenesis. The primers used for this mutagenesis were 5’-GATTTTCGCCGGTTGTGACGACCATACTCCCGATCAG-3’ and its reverse complement.

pMM51:

The Val and Gly codons following the *lpoB* lipobox Cys codon in pCB28 were changed to Asp and Glu codons, respectively, using site-directed mutagenesis to create pMM51 [*attHK022 bla lacI*^{q} P_{lac}::*lpoB (D*$^{+2}$*E*$^{+2}$*)-sfgfp*]. The primers used were 5’-GTTTCTCGCCGGGTGTGATGAGCAACGTGAACCTGCAC-3’ and its reverse complement.

pTB279:

pTB279 [$P_{lac\text{-}con}$::*gfp*] was constructed in three steps. To generate the pTD16 intermediate, the backbone of pTB183 (Bendezú et al., 2009) including *bla*, the replication origin, attHK022 site, and λtL3 terminator was amplified with the primers 5'-ATGA*GTCGAC*AAGCTTATCGATCTCAC-3' and 5'-GTCA*AGATCT*CCGCGGTTGAAGACG AAAGGGCCTCG-3'. The *lacI*^{q} gene and promoter from pMLB1113 (18) were amplified using the primers 5'-GTCA*GTCGAC*CCGGATCCGGTCTAGAGGCTCGAGG GGAATTCCACCATCGAATGGTGCAAAACCTTTCGCG-3' and 5'-GTCA*AGATCT*GCCGG AAGCATAAAGTGTAAAGCC-3'. The two PCR products were digested with BglII and SalI and ligated. To generate pTD17, *gfpmut2* was amplified from pTB183 using the primers 5'-TTAGGCACCCCAGGCTTTACAC-3' and 5'-GTCA*GTCGAC*TTATTTGTATAGTTCATCC ATGCCATGTGTAATC-3'. The resulting fragment was digested with XbaI and SalI and ligated with appropriately digested pTD16. To generate pTB279, the synthetic primers 5'-AATTCAATTGTGAGCGCTCACAATTCAAGCACCCCAGGCTTGACACTTTATGCTTCCGGCT CGTATAATGTGTGGAATTGTGAGCGGATAACAATTTCAT-3' and 5'-CTAGATGAAATT GTTATCCGCTCACAATTCCACACATTATACGAGCCGGAAGCATAAAGTGTCAAGCCTGGGG TGCTTGAATTGTGAGCGCTCACAATTG-3' containing the $P_{lac\text{-}con}$ promoter sequence were annealed and ligated with pTD17 digested with EcoRI and XbaI.

pTB307:

To construct pTB307 [P_{lac}::*gfp-ponA*], the *ponA* gene was amplified with the primers 5'-GTCA*GGATCC*AAGTTCGTAAAGTATTTTTTGATCCTTGCAGTC-3' an 5'-

GTCA*AAGCTT*TGTCAGCAAACTGAAAAGGCGC-3'. The resulting fragment was digested with BamHI and HindIII and ligated with appropriately digested pTB183 (6).

pTB309:

pTB309 [P_{ara}::*ponA*] was constructed in 2 steps. First, the *malF-mCherry* containing the XbaI-SalI fragment of pTB275 (Uehara et al., 2009) was ligated with similarly digested pTB277 (45) to generate pTB283 [*cat* P_{lac}::*envC lacZ*]. The *ponA* gene was amplified using the primers 5'-GTCA*TCTAGA*CCGCGCGTTTGTTTATAAACTGCC-3' and 5'-GTCA*AAGCTT*TGTCAGCAAACTGAAAAGGCGC-3' and the resulting fragment was digested with XbaI and HindIII and ligated with XbaI-HindIII digested pTB283.

pCB1:

The *gfp-ponA* containing EcoRI-HindIII fragment of pTB307 (this study) was ligated with similarly digested pTB238 [*cat* P_{lac}::*envC lacZ*] to generate pCB1 [*cat* P_{lac}::*gfp-ponA*].

pCB6:

pCB6 [*attHK022 bla lacI*^{q} P_{ara}::*gfp-ponB*] was generated in 2 steps. First, the *ponB* gene was amplified using the primers 5'-GTAC*GGATCC*GCCGGGAATGACCGCGAG-3' and 5'-GTCA*CTCGAG*ATGGGATGTTATTTTACCGGATGGC-3'. This PCR fragment was digested with BamHI and XhoI, and ligated into BamHI-SalI-digested pTB183 (Bendezú and de Boer, 2008) to create pMM5 [*attHK022 bla lacI*^{q} P_{lac}::*gfp-ponB*].

pCB6 was then made by digesting pMM5 with NotI and XbaI, and ligating the resulting fragment into appropriately digested pTB265 ((45).

pCB7:

To construct pCB7 [*bla lacI*^{q} P_{T7}::*h-sumo-lpoB(21-213)*], the primers 5'-GGTGGTT*GCTCTTCC*GGTGTGGGGCAACGTGAACCTG-3' and 5'-GTCA*CTCGAG* TTATTGCTGCGAAACGGCACCTTT-3' were used to amplify the part of the *lpoB* gene coding for LpoB residues 21 to 213. This PCR product was then digested with the restriction enzymes SapI and XhoI, and ligated with appropriately digested pTB146 (6)) to generate the *h-sumo* fusion.

pCB21:

pCB21 [*kan*^{R} *lacI*^{q} P_{T7}::*h-sumo-ponA*] was constructed in 2 steps.

The *ponA* gene was amplified with the primers 5'-GGTGGTT*GCTCTTCC*GGTGTGAAGTTCG TAAAGTATTTTTTGATCCTTGCAGTCTG-3' an 5'-GTCA*GAGCTC*CAGCAAACTGAAAAGGC GCCGAAG-3'. The resulting fragment was digested with SapI and SacI, and ligated with appropriately digested pTB146 (6) to generate pCB2 [*bla lacI*^{q} P_{T7}::*h-sumo-ponA*]. In order to change the antibiotic resistance from Amp to Kan, pCB2 was digested with XbaI and NotI, and the resulting fragment was ligated with appropriately digested pET-28a-amiD (46), creating pCB21.

pCB22:

pCB22 [*kan*^{R} *lacI*^{q} P_{T7}::*h-sumo-ponB*] was constructed in 2 steps. The *ponB* gene was amplified with the primers 5'-GTCA*GAGCTC*ATGGCCG GGAATGACCG-3' and 5'-GTCA*CTCGAG*TTAATTACTACCAAACATATCCTTGA TCCAACC-3'. The resulting fragment was digested with SacI and XhoI, and ligated with appropriately digested pTB146 (6) to create pCB17 [*bla lacI*^{q} P_{T7}::*h-sumo-ponA*]. To change the antibiotic resistance from Amp to Kan, pCB17 was digested with XbaI and XhoI, and the resulting fragment was ligated with appropriately digested pET-28a-amiD (46), yielding pCB22.

pCB25:

To generate pCB25 [*bla lacI*^{q} P_{lac}::*lpoB*], the *lpoB* gene was amplified with his native RBS using the primers 5'-GTCA*TCTAGA*TTGTAAGGGGTGAATCTTGATGACAAA AATGAG-3' an 5'-GTCA*AAGCTT*TTATTGCTGCGAAACGGCACCTTT-3'. The resulting fragment was digested with XbaI and HindIII, and ligated with appropriately digested pTB28 [*bla lacI*^{q} P_{lac}::*amiC-gfp*] (9).

pCB28:

pCB28 [*attHK022 bla lacI*^{q} P_{lac}::*lpoB-sfgfp*] was constructed in 4 steps. pTB282 [*attHK022 bla lacI*^{q} P_{lac}::*ssdsbA-linker-sfgfp*] was generated with the synthetic oligomers 5'-TATGAAAAAGATTTGGCTGGCGCTGGCTGGTTTAG TTTTAGCGTTTAGCGCATCGGCGGCGCAGTATGAAGGATCCCAGCAG CTCGAGCCTTATGCGTCTGCGCAGCCTAGGCAA-3' and 5'-GATCTTGC

CTAGGCTGCGCAGACGCATA AGGCTCGAGCTGCTGGGATCCTTCATAC TGCGCCGCCGATGCGCTAAACGCTAAAACTAAACCAGCCAGCGCCAGCCAAATCT TTTTCA-3'. These oligomers were annealed; resulting in the formation of dsDNA with overhangs complementary to the NdeI and BamHI restriction sites. pTB225 [*attHK022 bla lacI*^{q} P_{lac}::*zipA-sfgfp*] (45) was digested with NdeI and BamHI, and the resulting plasmid backbone was ligated with the complementary synthetic dsDNA.

pTU137 [*attHK022 bla lacI*^{q} P_{lac}::*cTAP*] was generated by amplifying *cTAP* from pP30D -YTAP (48) using the primers 5'-GTCA*CCTAGG*TCCATGGAAAAG AGAAGATGGAAAAAG-3' and 5'-GTCA*AAGCTT*GTCGACTCAGGTTGACTT CCCCGCGG-3'. The resulting PCR fragment was digested with AvrII and HindIII, and ligated with appropriately digested pTB282.

To create pCB24 [*attHK022 bla lacI*^{q} P_{lac}::*lpoB-cTAPtag*], the *lpoB* gene was amplified with the primers 5'-CGTAC*CATATG*ACAAAAATGAGTCGCTACGCCTT-3' an 5'-GTCA*CTCGAG*TTGCTGCGAAACGGCACC-3'. The resulting PCR fragment was digested with NdeI and XhoI, and ligated with appropriately digested pTU137.

Finally, pCB24 was digested with NdeI and XhoI, and the resulting fragment was ligated with appropriately digested pTB282, creating pCB28.

pCB39:

The construction of pCB39 [*bla lacI*^{q} P_{T7}::*h-lpoB(21-213)*] involved many intermediates that will be described in 7 distinct steps.

pTB285 was made by site-directed mutagenesis of pTB277 [*att*λ *cat* P_{ara}] (45) in order to remove the BamHI restriction site present in the P_{ara} promotor region.

pTB286 [*attλ cat* P_{bad}::*ssdsbA-linker-sfgfp*] was generated by digesting pTB282 [*attHK022 bla lacI*^{q}] with the restriction enzymes XbaI and HindIII, and ligating the resulting fragment into similarly digested pTB285.

pTB288 [*attλ cat* P_{ara}::*ssdsbA-blaN*] was created by amplifying the *blaN* gene with the primers 5'-GTCA*CCTAGG*CAAGATCCGGCTGGTCACCCAGAAACGCTGGTGAAAG-3' and 5'-GTCA*AAGCTT*GTCGACTTAGCCAGTTAATAGTTTGCGCAACG-3'. This PCR product was digested with the restriction enzymes AvrII and HindIII, and ligated with appropriately digested pTB286.

pTB292 [*attλ cat* P_{ara}::*ssdsbA-cJUNCC-blaN*] was generated using the synthetic oligonucleotides 5'-GATCCGCGAGCATTGCACGCCTGGAAGAGAAAGTTAAGA CCCTGAAAGCGCAGAATTATGAACTGGCGTCTACCGCGAACATGCTCCGTGAACAGGTTG CGCAACTGGGTGCGCCGC-3' and 5'-TCGAGCGGCGCACCCAGTTGCGCAACCTGTTC ACGGAGCATGTTCGCGGTAGACGCCAGTTCATAATTCTGCGCTTTCAGGGTCTTAACTTT CTCTTCCAGGCGTGCAATGCTCGCG-3'. These oligonucleotides were annealed, and the resulting dsDNA with overhangs for BamHI and XhoI was ligated with appropriately digested pTB288.

To create pTB260 [*bla lacI*^{q} P_{T7}::*h-sumo-sfgfp*], the *sfgfp* gene was amplified from pTB225 with the primers 5'-GTCA*CTCGAG*GGTCCGGCTGGTCTGTCTAAAGGTGAAG-3' and 5'-CTAG*AAGCTT*ATTTGTAGAGCTCATCCATGCCGTG-3'. The resulting PCR product was digested with the restriction enzymes XhoI and HindIII and ligated with appropriately digested pTB146 (6).

pCB13 [*bla lacI*^{q} P_{T7}::*h-sumo-sfgfp-lpoB(21-213)*] was generated by amplifying the part of the *lpoB* gene coding for LpoB residues 21 to 213 using the primers 5'-

GTCAT*GGATCC*GTGGGGCAACGTGAACCTG-3' and 5'-GTCA*AAGCTT*TT ATTGCTGCGAAACGGCACCTTT-3'. The resulting PCR product was digested with the restriction enzymes BamHI and HindIII, and ligated with appropriately digested pTB260.

Finally, pCB39 [*bla lacI*^{q} P_{T7}::*h-lpoB(21-213)*] was generated by digesting pCB13 with BamHI and HindIII, and ligating the resulting fragment with appropriately digested pTB292 [*att*λ *cat* P_{ara}::*ssdsbA-cJUNCC-blaN*].

pCB40:

pCB40 [*bla lacI*^{q} P_{T7}::*h-lpoA(28-678)*] was constructed by amplifying the part of the *lpoA* gene coding for LpoA residues 28 to 678 using the primers 5'-GTCAT*GGATCC*GGCACCCATACTCC-3' and 5'-GTAC*AAGCTT*TGGTGGTTAACT GACGGGG-3'. This PCR product was digested with the restriction enzymes BamHI and HindIII, and ligated with appropriately digested pTB292 [*att*λ *cat* P_{ara}::*ssdsbA-cJUNCC-blaN*].

pCB41:

pCB41 [*bla lacI*^{q} P_{lac}::*ssdsbA-lpoB(21-213)-sfgfp*] was constructed by amplifying the part of the *lpoB* gene coding for LpoB residues 21 to 213 using the primers 5'-GTCAT*GGATCC*GTGGGGCAACGTGAACCTG-3' and 5'-GTCA*CTCGAG*TTGCTGC GAAACGGCACC-3'. The resulting PCR product was digested with the restriction enzymes BamHI and XhoI, and ligated with appropriately digested pTB282 [*attHK022 bla lacI*^{q} P_{lac}::*ssdsbA-linker-sfgfp*].

pCB42:

pCB42 [*bla lacI*^{q} P_{lac}:: *ssdsbA-lpoA(28-678)-sfgfp*] was constructed by amplifying the *lpoA* gene coding for LpoA residues 28 to 678 using the primers 5'-GTCAT*GGATCC*GGCACCCATACTCC-3' and 5'-GTAC*CTCGAG*ACTGACGGG GACTACCTGAC-3'. The resulting PCR product was digested with the restriction enzymes BamHI and XhoI, and ligated with appropriately digested pTB282 [*attHK022 bla lacI*^{q} P_{lac}::*ssdsbA-linker-sfgfp*].

pCB62:

The construction of pCB62 [*aadA* P_{lac}::*ponA*] involved many intermediates and will be described in 6 distinct steps.

First, pTB287 [*aadA* $P_{lac\text{-}con}$::*ssdsbA-linker-SF-GFP*] was generated by digesting pTB282 [*attHK022 bla lacI*^{q} P_{lac}::*ssdsbA-linker-sfgfp*] with XbaI and HindIII, and ligating the resulting fragment with appropriately digested pTB284.

pTB289 [*aadA* $P_{lac\text{-}con}$::*ssdsbA-blaC*] was made by amplifying the *blaC* gene with primers 5'-GTCA*CCTAGG*CAAGATCCGGCTGGTCTACTTACTCTAGCTTCCCGGCAAC-3' and 5'-GTCA*AAGCTT*GTCGACAACTTGGTCTGACAGTTACCAATGC-3'. This PCR product was digested with the restriction enzymes AvrII and HindIII, and ligated with appropriately digested pTB287.

pTD33 [*aadA* $P_{lac\text{-}con}$::*tolB-blaC*] was created by amplifying the *tolB* gene with primers 5'-GTCA*TCTAGA*GTGGGCCATCGGTCCAGATAAG-3' and 5'-GTCA *CTCGAG*CAGATACGGCGACCAGGCAG-3'. This PCR product was digested with the restriction enzymes XbaI and XhoI, and ligated with appropriately digested pTB289.

pCB56 [*bla lacI*^{q} P_{lac}::*lpoA*] was constructed by digesting pMM10 (this study) with XbaI and XhoI, and ligating this fragment with appropriately digested pFB120 [P_{lac}::*mreC-LE*] (5)**.**

pCB59 [*aadA* P_{lac}::*lpoA*] was generated by digesting pCB56 with XbaI and HindIII, and ligating the resulting fragment with appropriately digested TD33.

Finally, pCB62 [*aadA* P_{lac}::*ponA*] was made by digesting pCB59 with XbaI and HindIII, and ligating the resulting fragment with appropriately digested TB309.

pCB72:

pCB72 [*aadA* P_{lac}::*ponB*] was constructed in 3 steps. First, pTD34 was made by amplifying the *ponB* gene using primers 5'-GTCA*TCTAGA*GAAAATCGGGCTT TTGCGCCTG-3' and 5'-GTCA*CTCGAG*ATTACTACC AAACATATCCTTGATCCAACCGG-3'**.** This PCR product was then digested with the restriction enzymes XbaI and XhoI, and ligated with appropriately digested pTB289 [*aadA* $P_{lac\text{-}con}$::*ssdsbA-blaC*]. pCB20 [*att*λ *cat* P_{ara}::*ponB-BlaN*] was then generated by digesting pTD34 with the restriction enzymes XbaI and XhoI, and ligating the resulting fragment with appropriately digested pTB288 [*att*λ *cat* P_{ara}::*ssdsbA-blaN*].

Finally, pCB72 was made by digesting pCB20 with the restriction enzymes XbaI and XhoI, and ligating the resulting fragment with appropriately digested pCB59 [*aadA* P_{lac}::*lpoA*].

Synthetic lethal screens

Screens for mutants with a Sla or Slb phenotype were performed as described previously (7). For the Sla or Slb screens, TU121/pCB1 [Δ*lacIZYA* Δ*ponA*/P_{lac}::*gfp-ponA lacZ*] or TU122/pTU110 [Δ*lacIZYA* Δ*ponB*/P_{lac}::*ponB lacZ*], respectively were mutagenized with the EzTn-Kan transposome (Epicentre) as described previously (7) yielding libraries of 40,000 or 75,000 independent mutants, respectively. Mutant libraries were then plated on LB plates supplemented with IPTG and X-gal (40 μg/ml) as described (7) to identify mutants causing a synthetic lethal defect. IPTG was used at 50 or 250 μM, respectively for the Slb and Sla screens. For the Slb screen, 30,000 colonies were screened yielding 16 solid-blue isolates that displayed varying degrees of IPTG-dependent growth. For the Sla screen, 50,000 colonies were screened yielding 41 solid-blue isolates dependent on IPTG for growth. Transposon insertions were mapped using arbitrarily-primed PCR as described (7). Details of the mapping results for the Slb screen are presented in the Results section. For the Sla screen, 34/41 isolates had insertions mapping within *ponB*, while the remaining 7 isolates had insertions mapping within *lpoB*.

Due to the high percentage *ponB* mutants isolated in the Sla screen, the screen was repeated with strain TU121(attCB6)/pCB1 [Δ*lacIZYA* Δ*ponA* (P_{ara}::*ponB*)/P_{lac}::*gfp-ponA lacZ*], which contains an extra copy of *ponB* under control of the arabinose promoter. In this case, the screening plates also contained 0.1% arabinose. TU121(attCB6)/pCB1 was mutagenized with EzTn-Kan transposome (Epicentre) as above, yielding a library of approximately 100,000 independent mutants. We screened 35,000 colonies and only isolated one *sla* mutant. It had a transposon insertion that mapped

within *lpoB*. The positions of insertions that mapped to *lpoA* and *lpoB* are presented in **Table 2.4**.

Protein purification

The PBP1 proteins were overexpressed and purified with a 6xHis-SUMO (H-SUMO) tag fused to their N-termini (6, 30, 34). The sequence of the affinity tag in all cases was MRGSHHHHHHMASG. PBP1a and PBP1b were purified from Rosetta™ 2(DE3)/pCB21 and Rosetta™ 2(DE3)/pCB22; respectively. Overnight cultures were grown in LB supplemented with kanamycin (20 µg/ml), chloramphenicol (34 µg/ml) and glucose (0.2%). The cultures were diluted 1:100 into 4 L of LB supplemented with kanamycin (20 µg/ml) and chloramphenicol (34 µg/ml), and cells were grown at 37°C to an OD_{600} of 0.6. The cultures were cooled for 15 min at 4 °C before addition of IPTG to 1 mM and kanamycin at 15 µg/ml. Cultures were then grown overnight at room temperature and the cells were harvested by centrifugation. Cell pellets were resuspended in 40 ml buffer A (20 mM Tris-HCl 7.4, 150 mM NaCl, 1% CHAPS, 1 mM PMSF, 1 mM EDTA) and stored at -80°C. Cells were thawed and disrupted by passing them through a french pressure cell three times at 10,000 psi. Cell debris and membranes were pelleted by centrifugation at 40,000 x g for 30 mins at 4°C.

PBP1a was efficiently solubilized with 1% CHAPS and was thus found in the soluble fraction whereas PBP1b remained in the insoluble fraction. For the PBP1a preparation, the supernatant was filter sterilized and kept at 4 °C prior to purification. To solubilize PBP1b, the pellet was resuspended in 10 ml of Buffer B (20 mM Tris-HCl pH 7.4, 1M NaCl, 2 % reduced Triton-X100), and incubated overnight at 4 °C with stirring. After a centrifugation

Table 2.4. Transposon mapping results.

Tn allele	gene	positiona	orientationb
sla33	lpoB(ycfM)	after nt 512; second bp of codon 171	minus
sla44	lpoB(ycfM)	after nt 140; second bp of codon 47	minus
sla96	lpoB(ycfM)	after nt 466; first bp of codon 156	minus
sla98	lpoB(ycfM)	after nt 124; first bp of codon 42	minus
sla99	lpoB(ycfM)	after nt 324; third bp of codon 108	plus
sla104	lpoB(ycfM)	after nt 324; third bp of codon 108	plus
sla148	lpoB(ycfM)	after nt 140; second bp of codon 47	minus
sla8c	lpoB(ycfM)	after nt 565; first bp of codon 189	plus
slb30	lpoA(yraM)	after nt 632; second bp of codon 211	plus
slb51	lpoA(yraM)	after nt 131; second bp of codon 44	plus

[a]position relative to first nt of target gene ATG codon.
[b]orientation of KanR cassette transcription relative to target gene transcription.
[c]allele isolated in screen with extra copy of ponB.

at 40,000 x g for 30 mins at 4ºC, the supernatant was filter sterilized and the pellet was resuspended in 7 ml of Buffer B for another round of solubilization. After centrifugation, the supernatant was filter sterilized and pooled with the supernatant from the first solubilization.

H-SUMO-PBP1 proteins were purified by metal-affinity purification using ProPur™ IMAC midi spin columns (Nunc) according to the instructions. Columns were equilibrated in buffer C (20mM Tris, pH7.4, 500mM NaCl, 0.1% reduced Triton) with 10 mM imidazole, washed with buffer C containing 50 mM imidazole, and fusion proteins were eluted with buffer C containing 300 mM imidazole. The purified PBP1a and PBP1b proteins were dialyzed against buffer C and buffer D (20 mM Tris, pH7.4, 1 M NaCl, 0.1% reduced Triton), respectively. The H-SUMO tag was cleaved with 6xHis-tagged SUMO protease (H-SP) as described (47), and protein preparations were concentrated using Amicon Centrifugal Filter Units (MWCO 10 KDa). Cleavage reactions were passed through Ni-NTA resin (ProPur™ IMAC midi spin column) to remove free H-SUMO and H-SP, yielding pure preparations of untagged PBP1 proteins. The columns were washed with buffer C containing 20 mM imidazole to completely recover the PBP1 proteins. The final PBP1a and PBP1b preparations were dialyzed against buffer C or D with 10% glycerol, respectively. Proteins were concentrated using Amicon Centrifugal Filter Units and stored at -80ºC.

Similar to the PBP1s, untagged versions of LpoA(28-678) and LpoB(21-213) were prepared using H-SUMO fusions. LpoA was purified from Rosetta™/pLysRARE/pMM18 cells. An overnight culture was grown in LB supplemented with ampicillin (50 µg/ml), glucose (0.2%) and chloramphenicol (10 µg/ml). The culture was diluted 1:100 into 1L LB

and grown to an OD_{600} of 0.56 at 37°C. IPTG was added to 1mM, and the culture was grown for 6 h at 30°C. Cells were harvested by centrifugation, pellets were resuspended in 35 ml buffer E (50mM Tris-HCl pH 8.0, 300mM NaCl, 25mM imidazole, 10% glycerol), and stored at -80°C. Cells were thawed and disrupted by passing them through a french pressure cell two times at 15,000 psi. This was followed by centrifugation at 100,000 x g for 1 h at 4°C to pellet cell debris and membranes. The cell extracts were then loaded onto a 1 ml NiNTA FF column (GE Healthcare) pre-equilibrated with buffer E using an AKTA purifier 10 system. The column was washed with 39 ml buffer E, and the H-SUMO-LpoA fusion protein was eluted with a linear step gradient of 25mM imidazole to 1M imidazole in buffer E over 18 column volumes. The peak fractions containing the eluted protein were collected and dialyzed against buffer F (50mM Tris-HCl pH 8.0, 300mM NaCl, 10% glycerol). The H-SUMO tag was cleaved using H-SP and protein preparations were passed over 2 ml NiNTA agarose (Qiagen) equilibrated with buffer F. Purified LpoA was then dialyzed against buffer G (50mM Tris-HCl pH 8.0, 25mM NaCl, 10% glycerol). The isolated LpoA protein was then loaded onto a 6 ml Resource Q column (GE Healthcare) equilibrated with buffer G for anion exchange chromatography. LpoA was then eluted off the column using a linear gradient of 25mM NaCl to 1M NaCl in buffer G over 32 column volumes. Peak fractions of purified LpoA were collected and dialyzed against buffer H (50mM Tris-HCl pH 8.0, 150mM NaCl, 10% glycerol). This sample was then aliquoted and stored at -80°C.

LpoB(21-213) was purified from BL21(DE3)/pCB7. An overnight culture of this strain was grown in LB supplemented with ampicillin (50 μg/ml) and glucose (0.2%). The culture was diluted 1:100 into 1 L of LB supplemented with ampicillin (50 μg/ml), and cells were

grown at 37°C to an OD_{600} of 0.6. IPTG was added to 1 mM and the culture was grown for 6 h at 30°C. Cells were harvested by centrifugation, the pellet was resuspended in 30 ml buffer I (50 mM Tris-HCl 7.4, 500 mM NaCl, 20 mM imidazole) and stored at -80°C. Cells were thawed and disrupted by passing them through a french pressure cell two times at 15,000 psi. Cell debris and membranes were pelleted by centrifugation at 100,000 x g for 1 h at 4°C. The resulting extract was loaded onto a 1 ml NiNTA FF column (GE Healthcare) pre-equilibrated with buffer I using an AKTA purifier 10. The column was washed with 10 ml buffer I and the H-SUMO protein fusion was eluted with a linear 20-250 mM gradient of imidazole in buffer I over 25 column volumes. Peak fractions containing the eluted proteins were pooled and dialyzed against buffer J (20 mM Tris-HCl pH 7.4, 150 mM NaCl). The H-SUMO tag was cleaved with H-SP and the protein preparation was passed over 1ml NiNTA resin (Qiagen) equilibrated with buffer J. The isolated LpoB in the flow through was concentrated using Amicon Centrifugal Filter Units (MWCO 10 KDa) and stored at -80°C in buffer J containing 10 % glycerol.

6xHis-tagged versions of LpoA [H-LpoA(28-678)] and LpoB [H-LpoB(21-213)] were purified from BL21(DE3)/pCB39 and pCB40, respectively. Overnight cultures were grown in LB supplemented with ampicillin (50 µg/ml) and glucose (0.2%). The cultures were diluted 1:100 into 0.5 L of LB supplemented with ampicillin (50 µg/ml), and cells were grown at 37°C to an OD_{600} of 0.6. IPTG was added to 1 mM and cultures were grown for 3 h 30 mins at 30°C. Cells were harvested by centrifugation, pellets were resuspended in 15 ml of buffer I and stored at -80°C. Cells were thawed and disrupted by sonication after addition of Bacterial Protease Arrest™ (G Biosciences) according to the instructions. Cell debris and membranes were pelleted by centrifugation at 100,000 x g for 1 h at 4°C.

Proteins were purified using ProPur™ IMAC mini spin columns (Nunc) according to the instructions. Columns were equilibrated in buffer I with 10 mM imidazole, washed with buffer E containing 50 mM imidazole, and eluted with buffer I containing 300 mM imidazole. The purified H-LpoA(28-678) and H-LpoB(21-213) proteins were concentrated using Amicon Centrifugal Filter Units and stored at -80°C in buffer J containing 10 % glycerol.

Antibody preparation

Polyclonal antibodies against PBP1a, PBP1b, LpoA, and LpoB were prepared by Covance Custom Immunology. Untagged proteins prepared as described above were used in their standard antibody production service.

Biochemical Assays

In vitro PG synthesis was measured in ether-permeabilized (EP) cells as described previously with modifications (33). Ether-treated cells (0.18 mg protein) prepared from cultures grown to an OD_{600} of 0.4-0.5 were first incubated with or without 4 μM LpoB on ice for 1 h in 100 μl of reaction buffer (50 mM Tris-HCl pH 8.3, 50 mM NH_4Cl, 20 mM $MgCl_2$, and 1 mM DTT). The reaction was initiated by addition of 4 nmol of UDP-M-pentapeptide (gift from Kyoko Suefuji and James T. Park) and 0.33 nmol of UDP-[^{14}C]G (300 mCi/mmol; American Radiolabeled Chemicals), followed by incubation at 30°C for 1 h. The reaction was terminated by addition of 0.4 ml of heated 5% SDS and the samples were incubated at 100°C for 30 min. The SDS insoluble material was collected on filters (Durapore 0.22 μm membrane filter, Millipore), washed with water, and dried. The dry filters

were then immersed in 3 ml of Ecolite(+)^{TM} (MP biomedicals) and the radioactivity was quantified by scintillation counting.

For transglycosylase assays, [^{14}C]GlcNAc-labeled lipid II (4-8 μM), prepared as described previously (53), was incubated in buffer containing 50 mM Hepes at pH 7.5, 10 mM $CaCl_2$, 1,000 units/ml penicillin-G and 20% DMSO. LpoB (50 nM), LpoA (50 nM) or an equal volume of storage buffer was added prior to addition of PBP1a or PBP1b (50 nM), which initiated the reaction. Reactions were quenched with an equal volume of ice-cold 10% Triton X-100 at indicated time points (1 – 6 min). Conversion into PG was measured as described previously (15). Briefly, reactions were spotted on cellulose chromatography paper (3MM Whatman). Substrates and products were separated with isobutyric acid/1 M NH_4OH (5:3) and quantified by liquid scintillation counting (Beckman LS 6000). The enhancement of PBP1b PGT activity by LpoB was repeated eight times resulting in an average activation of 1.5x. The activation observed in panel B of **Figure 2.12** was 1.5x.

To analyze glycan strand lengths, PBP reactions with or without added lipoprotein were carried out as described above, except for differing preincubation procedures and higher protein concentrations. PBPs (0.4 μM) were preincubated with or without lipoproteins (0.4-0.8 μM as indicated in **Figure 2.12**) at 4°C for 15 min. Reactions were initiated upon addition of protein(s) to lipid-II (4 μM) and incubated at RT for 5 min prior to heat inactivation (90°C, 5 min). Gel electrophoresis analysis was carried out as described previously (4). Briefly, samples were dried and resuspended in sample buffer (125 mM Tris-HCl (pH = 6.8), 40% glycerol, 9% SDS (sodium dodecyl sulfate), 0.004% bromophenol blue) before being loaded onto a 20 × 20 cm gel (9% acrylamide, 1 mm thick) and separated at 30 mA until the dye front was 1.5 cm from the bottom. Gels were

dried overnight, and exposed to a phosphorimager screen for >1 week. Imaging was performed with a Typhoon phosphorimager (GE Healthcare).

Bocillin labeling

Cultures of TB28, TU121, TU122, MM8 and CB6 were grown overnight in LB at 37ºC. The cultures were diluted 1:200 into 50 ml LB and were grown to an OD_{600} between 0.48 to 0.61 at 37°C. TB28, MM8 and CB6 cultures were grown in duplicate. Cell cultures were normalized to an OD_{600} of 0.48, the cells harvested by centrifugation at 4ºC, and then resuspended in 1080 µl cold phosphate-buffered saline (PBS). Phenylmethylsulfonyl fluoride (G Biosciences) was added to a final concentration of 1 mM, and Bocillin-FL (Invitrogen) was added to a final concentration of 10 µM. Cell suspensions were mixed by vortexing, and polymixin B (Amresco) was then added to a final concentration of 500 µg/ml. Suspensions were again mixed by vortexing and then incubated 1.5 hours at 37ºC with rotation. Suspensions were then washed three times with cold PBS and resuspended in 250 µl of PBS. Cell extracts were prepared by adding 250 µl 2X Laemmli sample buffer and incubating at 95ºC for ten minutes. Whole cell extracts were separated on a 10% SDS polyacrylamide gel in the dark. The protein gels were rinsed with water immediately following electrophoresis and the labeled PBPs were visualized using a fluorescence imager (Typhoon 9400™, GE Healthcare) (excitation at 488 nm and emission at 526 nm).

Immunoblotting

For **Figure 2.5**, cultures of TB28, TU121, TU122, MM8 and CB6 were grown overnight in LB media at 37°C. The cultures were diluted 1:100 in 8 ml of LB (with

duplicates of TB28, MM8 and CB6) and grown at 37°C to an OD_{600} between 0.4 to 0.6. Cells were harvested by centrifugation at 4°C and resuspended in PBS and 2X Laemmli sample buffer. Samples were incubated at 95°C for 10 min. For **Figure 2.7**, cells of MM13 [P_{ara}::*ponB* Δ*lpoA*] (**C**) or CB4(*att*λTB309) [Δ*ponA* Δ*lpoB*(P_{ara}::*ponA*)] (**D**) containing the low-copy plasmids pTB284 [$P_{lac\text{-}con}$::*gfp*], pCB62 [$P_{lac\text{-}con}$::*ponA*], or pCB72 [$P_{lac\text{-}con}$::*ponB*] were grown to an OD_{600} of 0.5-0.7 in LB-Ara-Spc (**C**) or M9-Ara-Spc (**D**) at 37°C. They were then washed, diluted into LB-IPTG(1 mM), and growth at 37°C was followed as in (**B**). At time points indicated by the arrows in (**C**) and (**D**), whole cell extracts were prepared from the growing cultures. For both experiments, the total protein concentration of the cell extracts was measured using the Non-Interfering™ Protein Assay (G Biosciences). As indicated in the figures, various quantities of total protein from each extract were separated on a 10% acrylamide gel and transferred to Protran® nitrocellulose membranes (Whatman, 0.22μm). Processing of the immunoblots was performed essentially as described previously (9). PBP1a and PBP1b antisera were used at a dilution of 1:10,000.

PBP and Lpo protein copy number determination

To determine the copy numbers of PBP1a, PBP1b, LpoA and LpoB per cell, four independent cell extract preparations of TB28 [WT] were analyzed by immunoblotting with specific antibodies raised against the purified proteins.

Cells of TB28 [WT] were grown overnight in LB at 37°C and diluted 1:100 into 50 ml of LB. Four independent cultures were grown at 37°C to an OD_{600} of 0.5 and the colony forming units (cfu) of each culture were determined by plating serial dilutions on LB plates in duplicate. Cells of TU121 [Δ*ponA*], TU122 [Δ*ponB*], MM22 [Δ*lpoA*] and CB26 [Δ*lpoB*]

were also grown under the same conditions. Cells were harvested by centrifugation, resuspended in 0.625 ml of PBS and mixed 1:1 with 2x Laemmli sample buffer. Cells were disrupted by sonication after the addition of PMSF and EDTA to 1 mM, and extracts were heated at 100°C for 10 min. Total protein concentrations were determined using the Non-interfering™ Protein Assay (G Biosciences) according to the instructions. Cell extracts were diluted to 1 mg/ml using a 1:1 PBS:Laemmli sample buffer solution and stored at -80°C.

To determine the amount of PBP1a, PBP1b, LpoA and LpoB in each of the four TB28 [WT] extracts, 5, 10 and 20 µg of total protein were loaded on 12 % SDS-polyacrylamide gels along with increasing amounts of purified (untagged) PBP1a, PBP1b, LpoA or LpoB mixed with 10 µg of total protein from extracts of TU121 [ΔponA], TU122 [ΔponB], MM22 [ΔlpoA] or CB26 [ΔlpoB], respectively. Proteins were transfered to PVDF membranes (Westran S, 0.22µm) and PBP1a, PBP1b, LpoA or LpoB were detected with rabbit antisera prepared against the purified proteins essentially as described previously (9). Membranes were blocked with Rapid Block (Amresco) according to the instructions, and incubated with the specific antisera diluted 1:10,000 for 30 minutes at room temperature. After washing, blots were incubated with with goat anti-rabbit IgG conjugated with horseradish peroxidase (Sigma) diluted 1:35,000. Following incubation at room temperature for 30 minutes, blots were washed again and developed using the Super Signal West Pico (Pierce) chemiluminescent detection system. Bands were visualized with a BioRad Chemidoc XRS, and intensities were quantified using Adobe Photoshop. A standard curve plotting signal intensity versus protein concentration was generated for the purified protein samples and was used to determine the concentration of

protein in the TB28 extracts. The cell titers determined for each culture were then used to calculate the number of molecules per cell.

Preparation of sacculi and muropeptide analysis

Overnight cultures of TB28, MM10 and MM26 were grown in 2 mL LB, LB-arabinose or LB-50μM IPTG, respectively. The cultures were then diluted 1:100 into 50 mL of LB (with inducer, as needed). Cultures were grown to an OD_{600} between 0.32 to 0.57 (from all sets) at 37°C. Cells were harvested and washed three times with LB to remove inducer. The cells were then used to inoculate 500mL of LB + 0.2% glucose to achieve a final OD_{600} of 0.02. MM10 and MM26 cells were harvested by centrifugation just before the onset of lysis (OD_{600} of 0.31 and 0.29, respectively). TB28 [WT] control cells were similarly harvested at an OD_{600} of 0.30. Cell pellets were resuspended in 10 mL ice-cold 1X PBS. Sacculi were then prepared essentially as described by Uehara *et al.* (2009) with the following modifications. The PG preparations were treated with α-chymotrypsin (300 μg/ml, final concentration) and incubated for at least 8 h at 37°C. The preparations were then treated again with α-chymotrypsin and incubated overnight at 37°C. After this incubation, 5% SDS was added to a final concentration of 1%, followed by incubation at 65°C for at least 8 h. Following several washes with water, sacculi were then resuspended in water containing 0.02% sodium azide to a final concentration of about 10^9 sacculi/ml. Two or three independent sacculi preparations were analyzed for each strain (see **Table 2.1**). Muropeptide analysis was performed as described by (45).

Cytological assay for membrane localization

Cultures of the cells in **Figure 2.10** were grown to mid-log in M9-Arabinose supplemented with 100 μM IPTG. Cells were harvested by centrifugation, washed in M9-Arabinose, resuspended in plasmolysis buffer [15% sucrose, 25mM HEPES (pH 7.4), 20mM sodium azide], and immediately imaged using phase contrast and GFP optics.

Membrane Fractionation

An overnight culture of TB28 [WT] was diluted 1:100 into 750 ml of LB and grown at 37^{o}C to an OD_{600} of 0.6. Cells were harvested by centrifugation at 5,000 xg for 10 minutes at 4^{o}C. They were then resupended in 20 mM Tris-HCl pH 8.0 with 0.1 mg/ml DNaseI and passed through a french pressure cell twice at 16,000 psi. The resulting lysate was centrifuged at 10,000 xg for 10 minutes at 4^{o}C to remove cell debris. The supernatant was then centrifuged at 100,000 xg for 60 minutes to pellet membranes. Membrane pellets were resuspended in 20 mM Tris-HCl 10% glycerol and then immediately loaded onto a sucrose step gradient (from bottom: 3.3 ml 2.2 M, 4 ml 1.44 M, 4 ml 0.77 M sucrose) and centrifuged at 100,000 xg for 17 hours at 4^{o}C. Fractions (1 ml) were removed from the top of the gradient (#1-11; top to bottom). NADH oxidase activity was measured in each fraction as described previously (36). The proteins in each fraction were separated on an SDS-polyacrylamide gel. Total protein was detected by coomassie staining, and LpoA or LpoB were detected by immunoblotting as described above.

Acknowledgments

The authors would like to thank D. Rudner, M. Waldor, and members of our laboratories for critical reading of the manuscript. We would also like to thank A. Typas, C. Gross, W. Vollmer and co-workers for communicating their results in advance of publication. Special thanks to K. Suefuji and J. T. Park for generously providing the UDP-M-pep$_5$. This work was supported by the Massachusetts Life Science Center (T.G.B), the Burroughs Wellcome Fund (T.G.B), and the National Institutes of Health (R01 AI083365-01A1 for T.G.B, GM066174 for D.E.K., and GM076710 for D.E.K and S.W.). T.G.B. holds a Career Award in the Biomedical Sciences from the Burroughs Wellcome Fund. C.P.B. was supported in part by a fellowship from FRSQ.

References

1. **Vijayalakshmi, J.**, **B. J. Akerley**, **and M. A. Saper**. 2008. Structure of YraM, a protein essential for growth of *Haemophilus influenzae*. **73**:204–217.

2. **Alaedini, A.**, **and R. A. Day**. 1999. Identification of two penicillin-binding multienzyme complexes in Haemophilus influenzae. Biochem. Biophys. Res. Commun. **264**:191–195.

3. **Baba, T.**, **T. Ara**, **M. Hasegawa**, **Y. Takai**, **Y. Okumura**, **M. Baba**, **K. A. Datsenko**, **M. Tomita**, **B. L. Wanner**, **and H. Mori**. 2006. Construction of Escherichia coli K-12 in-frame, single-gene knockout mutants: the Keio collection. Molecular Systems Biology **2**:1-11.

4. **Barrett, D.**, **T.-S. A. Wang**, **Y. Yuan**, **Y. Zhang**, **D. Kahne**, **and S. Walker**. 2007. Analysis of glycan polymers produced by peptidoglycan glycosyltransferases. J Biol Chem **282**:31964–31971.

5. **Bendezú, F. O.**, **and P. A. J. de Boer**. 2008. Conditional lethality, division defects, membrane involution, and endocytosis in mre and mrd shape mutants of Escherichia coli. J Bacteriol **190**:1792–1811.

6. **Bendezú, F. O.**, **C. A. Hale**, **T. G. Bernhardt**, **and P. A. J. de Boer**. 2009. RodZ (YfgA) is required for proper assembly of the MreB actin cytoskeleton and cell shape in E. coli. EMBO J **28**:193–204.

7. **Bernhardt, T. G.**, **and P. A. J. de Boer**. 2004. Screening for synthetic lethal mutants in Escherichia coli and identification of EnvC (YibP) as a periplasmic septal ring factor with murein hydrolase activity. Mol Microbiol **52**:1255–1269.

8. **Bernhardt, T. G.**, **and P. A. J. de Boer**. 2005. SlmA, a nucleoid-associated, FtsZ binding protein required for blocking septal ring assembly over Chromosomes in E. coli. Molecular Cell **18**:555–564.

9. **Bernhardt, T. G.**, **and P. A. J. de Boer**. 2003. The Escherichia coli amidase AmiC is a periplasmic septal ring component exported via the twin-arginine transport pathway. Mol Microbiol **48**:1171–1182.

10. **Bertsche, U.**, **E. Breukink**, **T. Kast**, **and W. Vollmer**. 2005. In vitro murein peptidoglycan synthesis by dimers of the bifunctional transglycosylase-transpeptidase PBP1B from Escherichia coli. J Biol Chem **280**:38096–38101.

11. **Bertsche, U.**, **T. Kast**, **B. Wolf**, **C. Fraipont**, **M. E. G. Aarsman**, **K. Kannenberg**, **M. von Rechenberg**, **M. Nguyen-Distèche**, **T. den Blaauwen**, **J.-V. Höltje**, **and W. Vollmer**. 2006. Interaction between two murein (peptidoglycan) synthases, PBP3 and PBP1B, in Escherichia coli. Mol Microbiol **61**:675–690.

12. **Blaauwen, den, T.**, **and N. Nanninga**. 1990. Topology of penicillin-binding protein 1b of Escherichia coli and topography of four antigenic determinants studied by immunocolabeling electron microscopy. J Bacteriol **172**:71–79.

13. **Blaauwen, den, T.**, **M. A. de Pedro**, **M. Nguyen-DistÃ che**, **and J. A. Ayala**. 2008. Morphogenesis of rod-shaped sacculi. FEMS Microbiol Rev **32**:321–344.

14. **Charpentier, X.**, **C. Chalut**, **M.-H. Rémy**, **and J.-M. Masson**. 2002. Penicillin-binding proteins 1a and 1b form independent dimers in Escherichia coli. J Bacteriol **184**:3749–3752.

15. **Chen, L.**, **D. Walker**, **B. Sun**, **Y. Hu**, **S. Walker**, **and D. Kahne**. 2003. Vancomycin analogues active against vanA-resistant strains inhibit bacterial transglycosylase without binding substrate. Proc Natl Acad Sci USA **100**:5658–5663.

16. **Cooper, S.**, **M. L. Hsieh**, **and B. Guenther**. 1988. Mode of peptidoglycan synthesis in Salmonella typhimurium: single-strand insertion. J Bacteriol **170**:3509–3512.

17. **Datsenko, K. A.**, **and B. L. Wanner**. 2000. One-step inactivation of chromosomal genes in Escherichia coli K-12 using PCR products. Proc Natl Acad Sci USA **97**:6640–6645.

18. **de Boer, P. A.**, **R. E. Crossley**, **and L. I. Rothfield**. 1989. A division inhibitor and a topological specificity factor coded for by the minicell locus determine proper placement of the division septum in E. coli. Cell **56**:641–649.

19. **de Jonge, B. L.**, **F. B. Wientjes**, **I. Jurida**, **F. Driehuis**, **J. T. Wouters**, **and N. Nanninga**. 1989. Peptidoglycan synthesis during the cell cycle of Escherichia coli: composition and mode of insertion. J Bacteriol **171**:5783–5794.

20. **Dougherty, T. J.**, **K. Kennedy**, **R. E. Kessler**, **and M. J. Pucci**. 1996. Direct quantitation of the number of individual penicillin-binding proteins per cell in Escherichia coli. J Bacteriol **178**:6110–6115.

21. **Finn, R. D.**, **J. Tate**, **J. Mistry**, **P. C. Coggill**, **S. J. Sammut**, **H. R. Hotz**, **G. Ceric**, **K. Forslund**, **S. R. Eddy**, **E. L. L. Sonnhammer**, **and A. Bateman**. 2007. The Pfam protein families database. Nucleic Acids Research **36**:D281–D288.

22. **Gan, L.**, **S. Chen**, **and G. J. Jensen**. 2008. Molecular organization of Gram-negative peptidoglycan. Proceedings of the National Academy of Sciences **105**:18953–18957.

23. **García del Portillo, F.**, **and M. A. de Pedro**. 1990. Differential effect of mutational impairment of penicillin-binding proteins 1A and 1B on Escherichia coli strains harboring thermosensitive mutations in the cell division genes ftsA, ftsQ, ftsZ, and pbpB. J Bacteriol **172**:5863–5870.

24. **Goodell, E. W.**, **and U. Schwarz**. 1975. Sphere-rod morphogenesis of Escherichia coli. J Gen Microbiol **86**:201–209.

25. **Guyer, M. S.**, **R. R. Reed**, **J. A. Steitz**, **and K. B. Low**. 1981. Identification of a sex-factor-affinity site in E. coli as gamma delta. Cold Spring Harb. Symp. Quant. Biol. **45 Pt 1**:135–140.

26. **Haldimann, A.**, **and B. L. Wanner**. 2001. Conditional-replication, integration, excision, and retrieval plasmid-host systems for gene structure-function studies of bacteria. J Bacteriol **183**:6384–6393.

27. **Johnson, J. E.**, **L. L. Lackner**, **C. A. Hale**, **and P. A. J. de Boer**. 2004. ZipA is required for targeting of DMinC/DicB, but not DMinC/MinD, complexes to septal ring assemblies in Escherichia coli. J Bacteriol **186**:2418–2429.

28. **Kato, J.**, **H. Suzuki**, **and Y. Hirota**. 1985. Dispensability of either penicillin-binding protein-1a or -1b involved in the essential process for cell elongation in Escherichia coli. Mol. Gen. Genet. **200**:272–277.

29. **Lewenza, S.**, **D. Vidal-Ingigliardi**, **and A. P. Pugsley**. 2006. Direct visualization of red fluorescent lipoproteins indicates conservation of the membrane sorting rules in the family Enterobacteriaceae. J Bacteriol **188**:3516–3524.

30. **Marblestone, J. G.**, **S. C. Edavettal**, **Y. Lim**, **P. Lim**, **X. Zuo**, **and T. R. Butt**. 2006. Comparison of SUMO fusion technology with traditional gene fusion systems: enhanced expression and solubility with SUMO. Protein Sci. **15**:182–189.

31. **Margolin, W.** 2009. Sculpting the Bacterial Cell. Current Biology. Elsevier Ltd **19**:R812–R822.

32. **Miller, J. H.** 1972. Experiments in Molecular Genetics. Cold Spring Harbor Laboratory Pr.

33. **Mirelman, D.**, **Y. Yashouv-Gan**, **and U. Schwarz**. 1976. Peptidoglycan biosynthesis in a thermosensitive division mutant of Escherichia coli. Biochemistry **15**:1781–1790.

34. **Mossessova, E.**, **and C. D. Lima**. 2000. Ulp1-SUMO crystal structure and genetic analysis reveal conserved interactions and a regulatory element essential for cell growth in yeast. Molecular Cell **5**:865–876.

35. **Müller, P.**, **C. Ewers**, **U. Bertsche**, **M. Anstett**, **T. Kallis**, **E. Breukink**, **C. Fraipont**, **M. Terrak**, **M. Nguyen-Distèche**, **and W. Vollmer**. 2007. The essential cell division protein FtsN interacts with the murein (peptidoglycan) synthase PBP1B in Escherichia coli. J Biol Chem **282**:36394–36402.

36. **Osborn, M. J.**, **J. E. Gander**, **E. Parisi**, **and J. Carson**. 1972. Mechanism of assembly of the outer membrane of Salmonella typhimurium. Isolation and characterization of cytoplasmic and outer membrane. J Biol Chem **247**:3962–3972.

37. **Sauvage, E.**, **F. D. R. Kerff**, **M. Terrak**, **J. A. Ayala**, **and P. Charlier**. 2008. The penicillin-binding proteins: structure and role in peptidoglycan biosynthesis. FEMS Microbiol Rev **32**:234–258.

38. **Schmidt, L. S.**, **G. Botta**, **and J. T. Park**. 1981. Effects of furazlocillin, a beta-lactam antibiotic which binds selectively to penicillin-binding protein 3, on Escherichia coli mutants deficient in other penicillin-binding proteins. J Bacteriol **145**:632–637.

39. **Schwarz, U.**, **and W. Leutgeb**. 1971. Morphogenetic aspects of murein structure and biosynthesis. J Bacteriol **106**:588–595.

40. **Spratt, B. G.**, **and A. B. Pardee**. 1975. Penicillin-binding proteins and cell shape in E. coli. Nature **254**:516–517.

41. **Tamaki, S.**, **S. Nakajima**, **and M. Matsuhashi**. 1977. Thermosensitive mutation in Escherichia coli simultaneously causing defects in penicillin-binding protein-1Bs and in enzyme activity for peptidoglycan synthesis in vitro. Proc Natl Acad Sci USA **74**:5472–5476.

42. **Taubes, G.** 2008. The bacteria fight back. Science **321:**356-361.

43. **Tokuda, H.** 2004. Sorting of lipoproteins to the outer membrane in E. coli. Biochimica et Biophysica Acta (BBA) - Molecular Cell Research **1693**:5–13.

44. **Typas, A.**, **M. Banzhaf**, **B. van den Berg van Saparoea**, **J. Verheul**, **J. Biboy**, **R. J. Nichols**, **M. Zietek**, **K. Beilharz**, **K. Kannenberg**, **M. von Rechenberg**, **E. Breukink**, **T. den Blaauwen**, **C. A. Gross**, **and W. Vollmer**. 2010. Regulation of peptidoglycan synthesis by outer-membrane proteins. Cell **143**:1097–1109.

45. **Uehara, T.**, **T. Dinh**, **and T. G. Bernhardt**. 2009. LytM-domain factors are required for daughter cell separation and rapid ampicillin-induced lysis in Escherichia coli. J Bacteriol **191**:5094–5107.

46. **Uehara, T.**, **and J. T. Park**. 2007. An anhydro-N-acetylmuramyl-L-alanine amidase with broad specificity tethered to the outer membrane of Escherichia coli. J Bacteriol **189**:5634–5641.

47. **Uehara, T.**, **K. R. Parzych**, **T. Dinh**, **and T. G. Bernhardt**. 2010. Daughter cell separation is controlled by cytokinetic ring-activated cell wall hydrolysis. EMBO J **29**:1412–1422.

48. **Vallet-Gely, I.**, **K. E. Donovan**, **R. Fang**, **J. K. Joung**, **and S. L. Dove**. 2005. Repression of phase-variable cup gene expression by H-NS-like proteins in Pseudomonas aeruginosa. Proc Natl Acad Sci USA **102**:11082–11087.

49. **Vollmer, W.**, **M. von Rechenberg**, **and J. V. Höltje**. 1999. Demonstration of molecular interactions between the murein polymerase PBP1B, the lytic transglycosylase MltA, and the scaffolding protein MipA of Escherichia coli. J Biol Chem **274**:6726–6734.

50. **Wang, T.-S. A.**, **S. A. Manning**, **S. Walker**, **and D. Kahne**. 2008. Isolated peptidoglycan glycosyltransferases from different organisms produce different glycan chain lengths. J Am Chem Soc **130**:14068–14069.

51. **White, C. L.**, **A. Kitich**, **and J. W. Gober**. 2010. Positioning cell wall synthetic complexes by the bacterial morphogenetic proteins MreB and MreD. Mol Microbiol **76**:616–633.

52. **Wong, S. M.**, **and B. J. Akerley**. 2003. Inducible expression system and marker-linked mutagenesis approach for functional genomics of Haemophilus influenzae. Gene **316**:177–186.

53. **Ye, X.-Y.**, **M.-C. Lo**, **L. Brunner**, **D. Walker**, **D. Kahne**, **and S. Walker**. 2001. Better Substrates for Bacterial Transglycosylases. J Am Chem Soc **123**:3155–3156.

54. **Yousif, S. Y.**, **J. K. Broome-Smith**, **and B. G. Spratt**. 1985. Lysis of Escherichia coli by beta-lactam antibiotics: deletion analysis of the role of penicillin-binding proteins 1A and 1B. J Gen Microbiol **131**:2839–2845.

Chapter 3:

Identification of a PBP1b* variant that bypasses the LpoB requirement

Author contributions:

I performed all the experiments described in this chapter and wrote the text with editorial assistance from Thomas Bernhardt. Tsuyoshi Uehara conceptualized the strategy for isolating variants of PBP1b lacking a LpoB requirement for function.

A PBP1b* variant that bypasses the need for LpoB *in vivo*

Monica Markovski, Tsuyoshi Uehara[1], and Thomas G. Bernhardt

Department of Microbiology and Immunobiology

Harvard Medical School

Boston, MA 02115

[1]Current Address:

Novartis Institutes for Biomedical Research

Emeryville, CA 94608

Summary

To fortify their cytoplasmic membrane and protect it from osmotic rupture, most bacteria surround themselves with a peptidoglycan (PG) exoskeleton synthesized by the penicillin-binding proteins (PBPs). We recently identified the *Escherichia coli* outer membrane lipoprotein, LpoB, as a PBP cofactor that forms a specific trans-envelope complex with PBP1b and is critical for LpoB function *in vivo*. To investigate the role of LpoB further, we sought to identify PBP1b* variants that would no longer require LpoB for their function. To isolate *ponB** alleles encoding PBP1b* variants, we took advantage of the cefsulodin hypersensitive phenotype shared by *ponB* and *lpoB* mutants. We reasoned that the cefsulodin hypersensitivity of *lpoB* mutants results from a defect in PBP1b activity. Therefore, *ponB** alleles with partially restored PBP1b function might be isolated by selecting for *lpoB* mutants with increased cefsulodin resistance. Using this strategy, several PBP1b* variants were isolated. Characterization of these mutants suggests that LpoB possesses a cellular function in addition to its role in promoting PBP1b activity.

Introduction

The peptidoglycan (PG) layer is a large, tough polysaccharide matrix that fortifies the cell membrane against internal osmotic pressure (13). This complex macromolecule is composed of glycan strands crosslinked by attached peptide chains to form a dense meshwork that provides structural integrity and shape to the bacterium (13, 24). The glycan strands are composed of alternating sugar subunits *N*-acetylglucosamine (GlcNAc) and *N*-acetylmuramic acid (MurNAc) that are linked by β(1,4)-glycosidic bonds (13, 27). Attached to each MurNAc sugar is a pentapeptide (pep5) chain (13).

The pathway for PG biogenesis occurs in three main stages and spans multiple cellular compartments. To build the basic monomeric unit of PG, MurNAc(pep5)-GlcNAc, the activated sugar UDP-GlcNAc is first converted to UDP-MurNAc. After sequential addition of the pep5 by a series of cytoplasmic steps the essential enzyme, MraY, transfers phosho-MurNAc(pep5) from UMP to undecaprenyl-phosphate to form Lipid I at the cytoplasmic surface of the inner membrane (IM). GlcNAc is then added to Lipid I by MurG to form Lipid II, which is then flipped to the periplasmic face of the IM (26). Once exposed to the periplasm, this monomeric unit is polymerized and crosslinked into the existing PG layer by the cellular PG synthases called the high molecular weight penicillin-binding proteins (PBPs), the targets of β-lactam antibiotics like penicillin (20).

One class of PBPs are bifunctional enzymes that polymerize glycan strands and crosslink them using their peptidoglycan glycosyl transferase (PGT) and transpeptidase (TP) domains, respectively (10, 20). Because these enzymes have both activities, they are thought to be the primary PG synthetic enzymes in the cell (10, 20). These purified

PBPs retain low PG synthetic activity *in vitro* in the absence of additional components (2, 6). However, *in vivo* they are part of large multi-enzyme complexes organized by cytoskeletal elements that build the PG mesh that surrounds the cell (**Figure 3.1**).

Two distinct complexes are associated with the different phases of PG construction in rod-shaped bacteria: elongation and division (7, 8). During elongation, a complex organized by the actin-like MreB protein inserts along the cylindrical portion of the PG layer (7, 8). The mode of PG growth then switches to a concentrated zone of synthesis at the site of cell division (7, 8, 16). Here, the tubulin-like protein FtsZ directs an array of proteins to facilitate cell division and PG synthesis (7). While it is known that these cytoskeletal elements and their associated complexes play major roles in PG biogenesis, we currently know very little about how they promote PG assembly.

A major outstanding question has been whether or not the PG synthetic complexes contain factors that directly modulate PBP activity. Genetic analysis of PBP activity and regulation has been hindered by functional redundancy. One example of this is the overlapping functions shared by the three *E. coli* bifunctional PBPs: PBP1a, PBP1b, and PBP1c. Loss of any of these proteins is not lethal. However, simultaneous loss of PBP1a and PBP1b results in rapid cell lysis and death (28). Based on this, we reasoned that we could identify critical factors required for PBP function by performing a screen for mutants synthetically lethal with the loss of either PBP1a or PBP1b. For example, factors required to promote PBP1a activity could be identified by screening for mutants synthetically lethal with the loss of PBP1b. The converse is also true. Using this genetic strategy, we recently identified two outer membrane lipoproteins, LpoA and LpoB, as essential PBP cofactors in *E. coli* (19). These factors were found to directly

interact with their cognate PBP to form specific trans-envelope complexes that are critical for PBP function *in vivo* (19). Importantly, biochemical studies demonstrated that LpoB enhances both the PGT and TP activities of its cognate PBP (PBP1b) *in vitro* (19, 25). Our results thus suggest that PBP activity is indeed modulated in the multi-enzyme PG synthetic complexes and that the PBPs in Gram-negative bacteria are likely receiving regulatory input from both membranes: cytoskeletal proteins in the IM and the Lpo factors in the outer membrane (OM).

To further investigate the *in vivo* function of LpoB and the physiological significance of the observed effects of LpoB on PBP1b activity *in vitro*, we developed a genetic selection and screening strategy to identify PBP1b variants that bypass the functional requirement for LpoB. Characterization of these mutants suggests that LpoB possesses a cellular function in addition to its role in promoting PBP1b activity. Also, the activity of one of the variants suggests a possible mechanism by which LpoB might modulate the PGT activity of PBP1b.

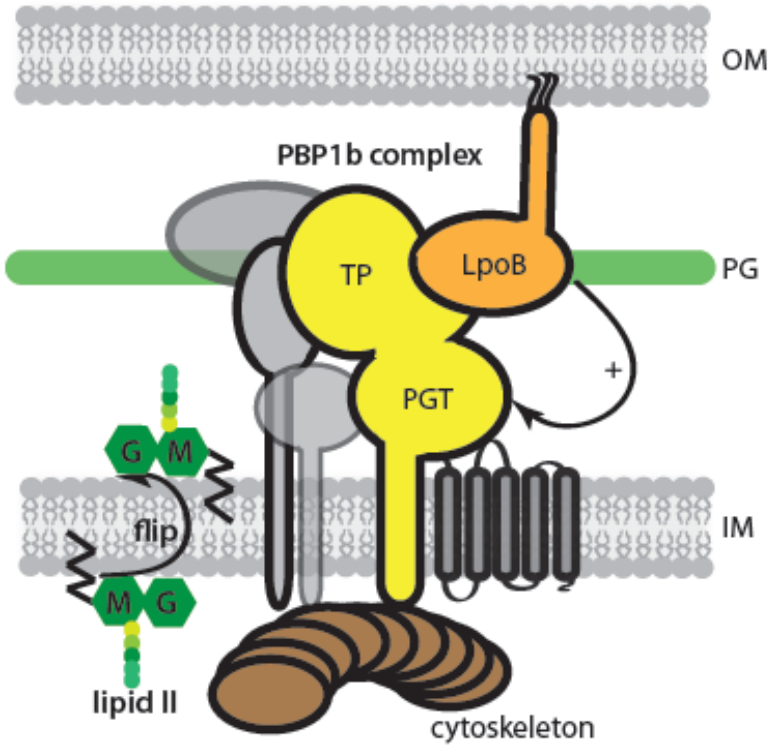

Figure 3.1. Multi-enzyme PG synthetic complex. The schematic above shows one of the multi-enzyme complexes involved in the final stages of PG assembly. This complex contains PBP1b (a class A PBP) and LpoB. The other PG assembly factors thought to participate at this step are not specifically labeled. Also previously we have shown that LpoB activates the PGT activity of PBP1b (as illustrated by the arrow). PG, peptidoglycan; OM, outer membrane; IM, inner membrane; M, *N*-acetylmuramic acid; G, *N*-acetylglucosamine; PGT, peptidoglycan glycosyltransferase domain; TP, transpeptidase domain. Dots represent the peptides attached to M.

Results

Identification of PBP1b* variants that bypass the LpoB requirement for activity. To identify variants of PBP1b (designated PBP1b*) that no longer require LpoB for activity, we took advantage of a cefsulodin-hypersensitivity phenotype shared amongst *ponB* (the gene encoding PBP1b) and *lpoB* mutants. In these strains, the MIC for cefsulodin (a β-lactam that preferentially binds PBP1a/b) is approximately 1000-fold lower than that for wild-type (19). We reasoned that the cefsulodin hypersensitivity of *lpoB* mutants likely results from a defect in PBP1b activity and that *ponB** alleles encoding PBP1b* variants might be identified by a selection for increased cefsulodin resistance in a LpoB$^-$ strain background. Therefore, cells of MM33(attλTB309) [Δ*lpoB* Δ*ponA* (P_{ara}::*ponA*)] were plated at 30˚C on M9-arabinose agar supplemented with 0.01 μg/ml cefsulodin for the isolation of spontaneous drug resistant mutants (**Figure 3.2A**). Survivors plated with an efficiency of 10^{-8} relative to growth on agar lacking cefsulodin. Even though survivors were isolated at a low frequency, we suspected that a high background of uninteresting mutants might be isolated along with mutants with *ponB** alleles, including those possessing PBP1a* variants with a reduced affinity for cefsulodin and/or mutants that overexpress drug efflux pumps. We specifically used MM33(attλTB309) to distinguish between these possibilities. This strain lacks LpoB and its only copy of *ponA* is under arabinose promoter control. Thus, growth of the parental strain is arabinose-dependent because the loss of both LpoB and PBP1a activity results in a synthetic lethal phenotype. We used this phenotype to our advantage and screened the cefsulodin resistant survivors for growth in the absence of PBP1a. Survivors that produce cefsulodin-resistant PBP1a variants or overproduce efflux

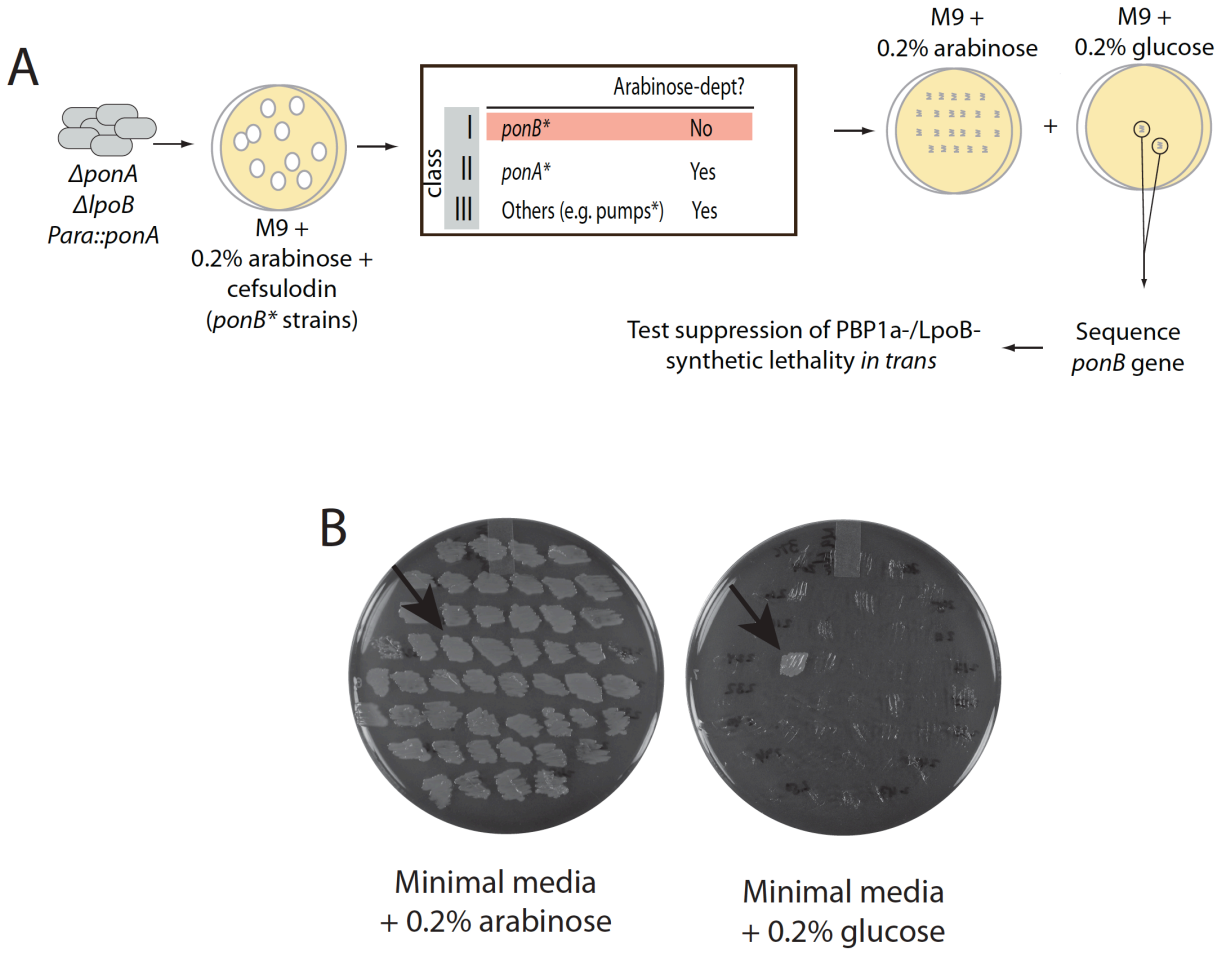

Figure 3.2. Cefsulodin selection and arabinose-independency screen. The strategy for the selection and subsequent screen is diagrammed in (**A**). See text for details. Survivors that grew in the presence of 0.01 μg/ml of cefsulodin were patched onto M9 media containing either 0.2% arabinose or 0.2% glucose. An example plate incubated at 37˚C of this step is shown in (**B**).

pumps will be arabinose-dependent for growth because PBP1a activity will remain required for growth in the absence of LpoB-stimulated PBP1b activity. Mutants producing PBP1b* variants, on the other hand, should grow without arabinose because the PBP1b synthetic pathway will be functional without LpoB, eliminating the synthetic lethality of the PBP1a^{-}/LpoB^{-} combination.

We isolated approximately 600 mutants resistant to 0.01 μg/ml cefsulodin, and patched them on M9 agar supplemented with either 0.2% glucose or 0.2% arabinose (example shown in **Figure 3.2B**). Sixteen arabinose-independent mutants were identified, bringing the overall frequency of mutant isolation to approximately 10^{-10} suggesting that only specific missense mutations confer the LpoB-bypass phenotype. We sequenced the *ponB* gene from all of the arabinose-independent isolates and found that they all possessed missense mutations such that they encoded PBP1b* variants with one of five substitutions (E313D, I202F, Q411R, Q411K and Q447K) (**Table 3.1)**. The *ponB** mutants producing PBP1b^{I202F} and PBP1b^{Q447K} were temperature-sensitive, displaying the LpoB-bypass phenotype at 30°C, but not 37°C or 42°C. To determine if the expression of these variants is sufficient for suppression of the LpoB^{-}/PBP1a^{-} synthetic lethality, we generated *gfp-ponB* or *gfp-ponB** expression constructs in which the fusion was under control of the lactose promoter (P_{lac}). The constructs were integrated into the chromosome of strain MM33(attλTB309) [Δ*lpoB* Δ*ponA* (P_{ara}::*ponA*)] at the HK022 *att* site. The production of all GFP-PBP1b* variants allowed growth of MM33(attλTB309) on media lacking arabinose (LpoB^{-}/PBP1a^{-} conditions) whereas the production of GFP-PBP1b(wild-type) did not (**Figure 3.3**).

Table 3.1. Mapping results of arabinose-independent isolates.

ponB* allele	Gene	Mutation	Amino acid substitution[a]	Temperature isolated
ponB*39	*ponB*	CAG → CGG	Q411R	37˚C
ponB*65[b]	*ponB*	ATC → TTC	I202F	30˚C
ponB*222[b]	*ponB*	GAG → GAT	E313D	37˚C
ponB*414[b]	*ponB*	ATC → TTC	I202F	30˚C
ponB*425	*ponB*	CAG → AAG	Q447K	30˚C
ponB*426	*ponB*	CAG → AAG	Q447K	30˚C
ponB*440	*ponB*	CAG → AAG	Q411K	37˚C
ponB*496[b]	*ponB*	ATC → TTC	I202F	30˚C
ponB*498	*ponB*	CAG → AAG	Q447K	30˚C
ponB*519[b]	*ponB*	GAG → GAT	E313D	37˚C
ponB*528	*ponB*	CAG → AAG	Q447K	30˚C
ponB*536	*ponB*	CAG → AAG	Q447K	30˚C
ponB*567	*ponB*	CAG → AAG	Q447K	30˚C
ponB*583	*ponB*	CAG → AAG	Q447K	30˚C
ponB*698	*ponB*	CAG → AAG	Q447K	30˚C
ponB*699	*ponB*	CAG → AAG	Q447K	30˚C

[a]Position relative to first codon of target gene ATG codon
[b]Alleles isolated independently.

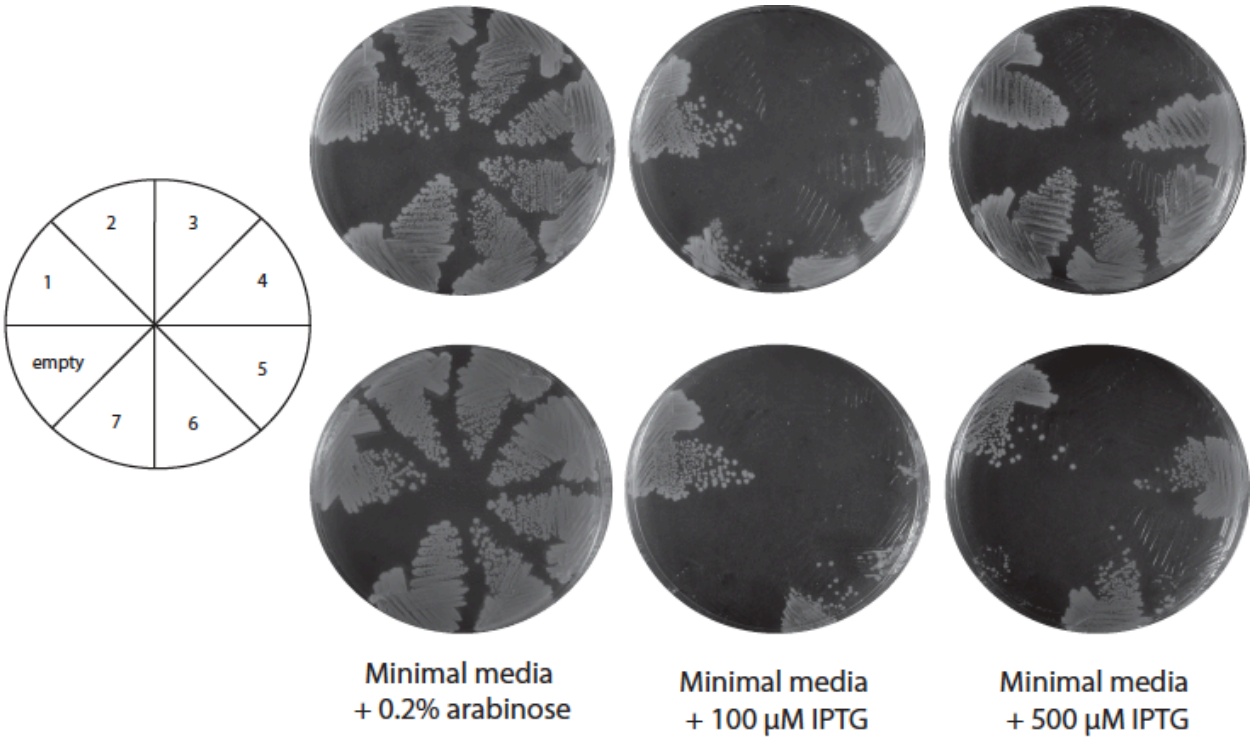

Figure 3.3. The PBP1b* variants isolated suppress the PBP1a^{-}/LpoB^{-} synthetic lethal defect *in trans*. The parent strain from the selection and its derivatives were struck out on the minimal media plates indicated above. Plates in the top row were incubated at 30˚C while those in the bottom row were incubated at 37˚C. TU121(attλTB309) [Δ*ponA* (P_{ara}::*ponA*)] in section **1** grows in all cases, as expected. MM33(attλTB309) [Δ*ponA* Δ*lpoB* (P_{ara}::*ponA*)] in section **2** exhibits a synthetic lethal phenotype when grown under nonpermissive conditions. All other strains are derivatives of MM33(attλTB309) [Δ*ponA* Δ*lpoB* (P_{ara}::*ponA*) (P_{lac}::*ponB*γ*)] (**3**). The versions of PBP1b expressed in each section are: PBP1b$^{wild\text{-}type}$ (**3**); PBP1b^{Q411R} (**4**); PBP1b^{I202F} (**5**); PBP1b^{E313D} (**6**); PBP1b^{Q447K} (**7**). The suppression of the PBP1a-/LpoB- synthetic lethal phenotype is suppressed only when the PBP1b* variants are expressed with 500 µM IPTG.

We therefore conclude that the production of any of the PBP1b* variants identified in the above selection-screen is sufficient for the LpoB-bypass phenotype.

Two classes of PBP1b* variants were identified. The *ponB** alleles encode PBP1b* variants with amino acid substitutions that map to two different regions of the *E. coli* PBP1b crystal structure (22) (PDB: 3FWL, **Figure 3.4**). One substitution, E313D, changes a residue in the PGT domain that is present at the end of the presumed channel for growing glycan strands (**Figure 3.4A and B**). The other substitutions, however, clustered near the UB2H (UvrB domain 2 homolog) domain (**Figure 3.4A and B**), a newly evolved domain in the *Enterobacteriaceae* that folds between the PGT and TP domains of PBP1b (22, 25). Previous work by Typas *et al.* showed that LpoB binds to PBP1b through this domain (25). Thus, it is the LpoB-UB2H interaction that is likely responsible for PBP1b activation by LpoB. An attractive possibility is that the PBP1b* variants with substitutions near UB2H adopt an "activated" conformation that mimics that achieved upon association with LpoB (see **Discussion**).

To determine if the different PBP1b* variants could support the growth of LpoB$^-$ cells in the complete absence of PBP1a activity, as opposed to PBP1a depletion, we attempted to transduce a Δ*ponA*::Kan^R allele into cells of CB7 [*ponB*^{WT} Δ*lpoB*], MM47 [*ponB*^{Q411R} Δ*lpoB*], MM48 [*ponB*^{I202F} Δ*lpoB*] and MM49 [*ponB*^{E313D} Δ*lpoB*)]. Only transductions with MM49 [*ponB*^{E313D} Δ*lpoB*)] yielded kanamycin resistant transductants. Because we could not obtain transductants in MM47 or MM48, we

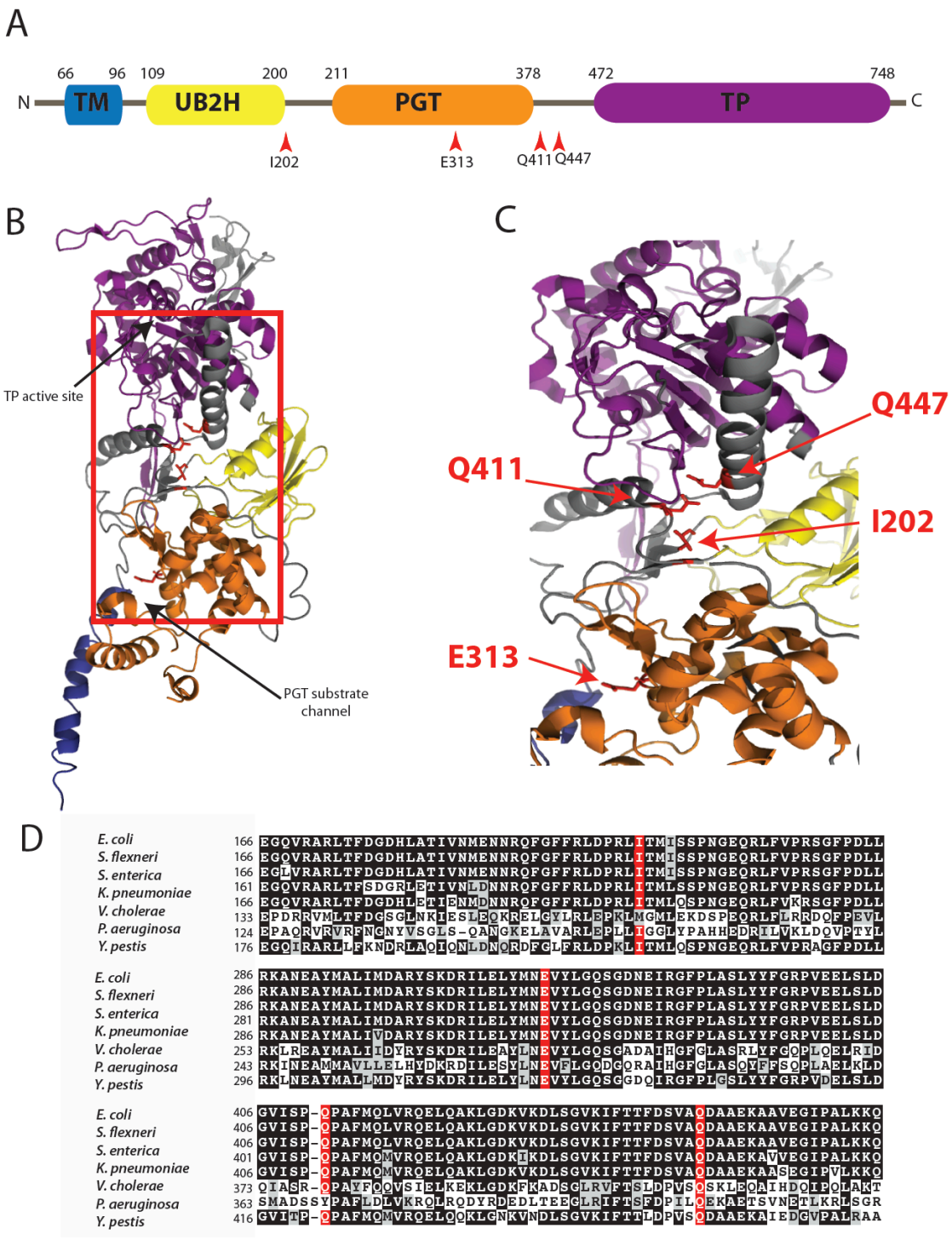

Figure 3.4. Location of substitutions in PBP1b* variants. (**A**) Domain structure of PBP1b. Designation of domain boundaries are based on the crystal structure of *E. coli* PBP1b (PDB: 3FWM) and literature review. **(Legend continued on next page.)**

Figure 3.4 (Continued). (**B**) Crystal structure of *E. coli* PBP1b with the location of the mutated residues highlight in red (PDB: 3FWM). The domains of PBP1b are colored as in (**A**). The PGT lipid II substrate channel and the TP active site are indicated. (**C**) Inset of the red box in (**B**). The mutated residues are highlighted in red with the residues listed above. (**D**) Sequence alignment of PBP1b homologs in organisms with LpoB homologs. Residues mutated (red) in the cefsulodin selection/arabinose-independency screen are well conserved amongst these species.

thought PBP1b* expression could potentially be reduced in these strain backgrounds. However, western blot analysis confirmed that all PBP1b* variants were present at approximately wild-type (WT) levels (**Figure 3.5**). Similar results were obtained for transductions with a Δ*lpoA*::Kan^{R} allele, indicating that in the absence of LpoB, PBP1b^{E313D} can support growth without PBP1a activity. The PBP1b^{I202F} and PBP1b^{Q411R} variants, on the other hand, appear to require basal level production of PBP1a from P$_{ara}$::*ponA* to support growth. Thus, two classes of PBP1b* variants were identified with different levels of LpoB-bypass activity *in vivo*. A substitution in the PGT domain results in full suppression of the LpoB^{-}/PBP1a^{-} phenotype, while substitutions near the UB2H domain only partially suppress this phenotype.

PG synthetic activity of the PBP1b* variants *in vitro*. Lipid II, the PBP1 substrate, is made from the activated sugar precursors UDP-*N*-acetylmuramic acid-pentapeptide (UDP-MurNac-pep5) and UDP-GlcNAc in the cytoplasm of the bacterial cell. This substrate is then flipped to the periplasm where it can be used by the PG synthetic machinery to make PG (see **Introduction** and **Figure 3.1**). PG synthesis can be monitored in ether-permeabilized cells (EPCs) by supplying them with purified UDP-MurNAc-pep5 and radiolabelled UDP-[^{14}C]GlcNAc and monitoring the incorporation of label into the SDS-insoluble PG fraction (18). EPCs made from PBP1b^{-} mutants are defective in label incorporation, thus suggesting a major role for PBP1b during PG synthesis in the cell (14, 15, 23). We previously showed that Δ*lpoB* EPCs phenocopy PBP1b^{-} cells and have dramatically

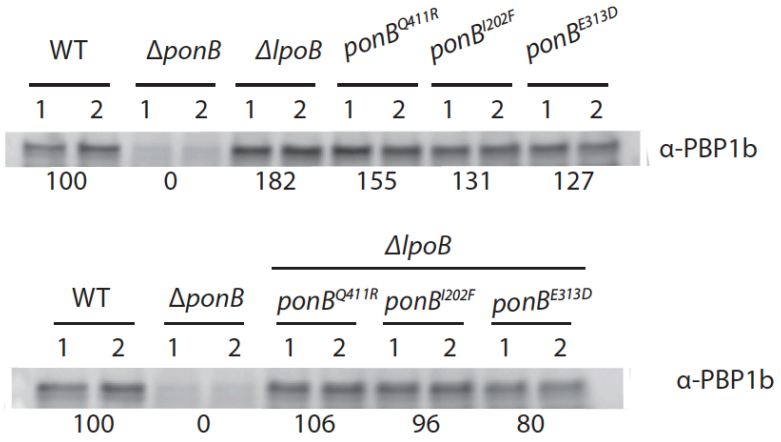

Figure 3.5. PBP1b* variants are expressed at wild-type PBP1b levels *in vivo*. To determine the extent of overproduction of PBP1b (wild-type and variant) in strains used for *in vivo* studies, cell extracts were prepared from MG1655 [wild-type], CB2 [Δ*ponB*], CB7 [Δ*lpoB*], MM41 [*ponB(Q411R)*], MM42 [*ponB(I202F)*], MM43 [*ponB(E313D)*], MM47 [*ponB(Q411R)* Δ*lpoB*], MM48 [*ponB(I202F)* Δ*lpoB*], and MM49 [*ponB(E313D)* Δ*lpoB*]. Cells were grown in LB at 30˚C in duplicate (as indicated by the number above lanes) to an OD600 = 0.33 to 0.71. Immunoblot analysis was then performed to determine the levels of PBP1b variant relative to the corresponding wild-type control. 15 µg of total protein was loaded in each lane. Numbers below each set of replicates indicate percent of PBP1b* variant levels present relative to WT control (at 100%).

reduced PG synthetic activity, indicating that LpoB is required for PBP1b synthetic activity in EPCs (19).

If the PBP1b* variants are LpoB-independent, they should exhibit WT levels of PG synthetic activity in the absence of LpoB. To determine if the PBP1b* LpoB-bypass variants exhibit WT levels of activity, we prepared EPCs from cells expressing PBP1b(WT) or PBP1b* (the same strains used above) with or without LpoB. PBP1b^{E313D} EPCs lacking LpoB exhibited similar levels of PG synthetic activity to EPCs prepared from WT cells, where both PBP1b(WT) and LpoB are expressed (**Figure 3.6A**). However, EPCs prepared from LpoB^{-} cells producing PBP1b^{Q411R} or PBP1b^{I202F} showed low-level PG synthetic activity comparable to LpoB^{-} cells producing PBP1b(WT) (**Figure 3.6A and B**). Thus, the biochemical results parallel the genetic studies. The relatively strong bypass allele, PBP1b^{E313D} retains PG synthetic activity in the absence of LpoB whereas the weaker alleles do not.

The PBP1b* variants are not fully LpoB-independent. Using the EPC assay, we showed that PBP1b^{E313D} retained PG synthetic activity in the absence of LpoB *in vitro*. We therefore wondered if it was fully LpoB-independent *in vivo*. To investigate this, we determined whether production of the PBP1b^{E313D} variant suppressed phenotypes associated with a LpoB^{-} defect other than the synthetic lethality with the loss of PBP1a function. One such phenotype is an increased frequency of lysed cells observed in colonies of PBP1b^{-} or LpoB^{-} mutants (**Figure 3.7B and C**). When cells from these colonies are suspended in saline solution and visualized by phase contrast microscopy, phase-light “cell ghosts” indicative of cell lysis are observed at a low but reproducible

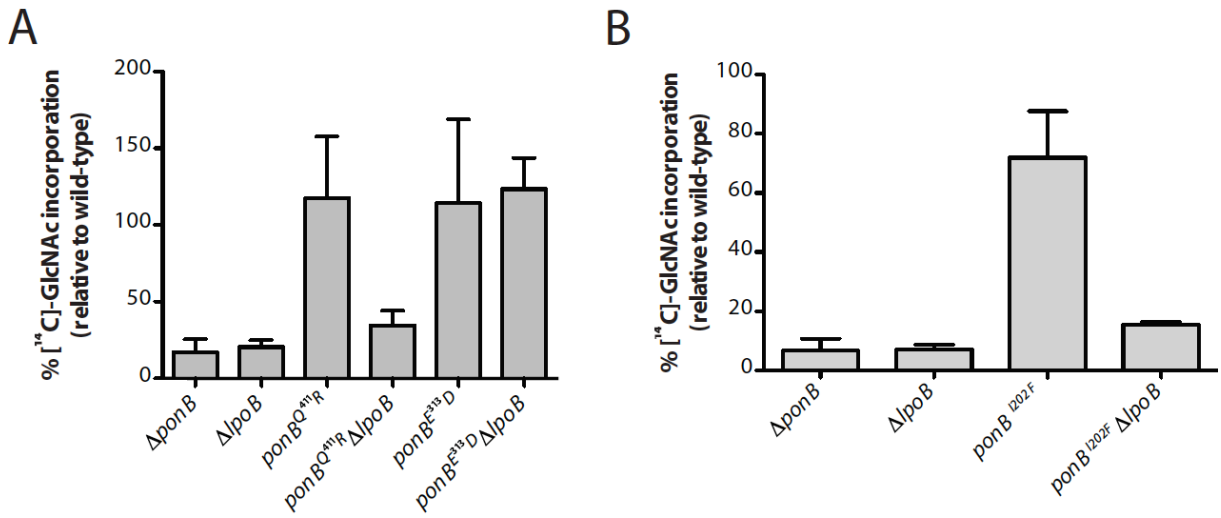

Figure 3.6. PG synthesis in ether-permeabilized (EP) cells. EP cells were prepared from MG1655 [wild-type], CB2 [Δ*ponB*], CB7 [Δ*lpoB*], MM41 [*ponB(Q411R)*], MM42 [*ponB(I202F)*], MM43 [*ponB(E313D)*], MM47 [*ponB(Q411R)* Δ*lpoB*], MM48 [*ponB(I202F)* Δ*lpoB*], and MM49 [*ponB(E313D)* Δ*lpoB*] at either 37˚C (A) or 30˚C (B). Reactions were initiated with the addition of UDP-MurNAc-pentapeptide (40 μM) and UDP-[^{14}C]-GlcNAc (American Radiolabeled Chemicals). After 60 min reactions were boiled in 4% SDS and filtered. Labeled PG retained on the filter was quantified by liquid scintillation counting (Packard Tri-Carb). Cultures were normalized by total protein content: 0.18 mg total protein (**A**) or 0.14 mg total protein (**B**). Error bars indicate the standard deviation of three independent experiments. Statistical significance was calculated using a student's paired t-test comparing each indicated strain to wild-type. The p-values are as follows: *ponB(Q411R)* Δ*lpoB*, p = 0.08; *ponB(E313D)* Δ*lpoB*, p = 0.38; *ponB(I202F)*, p = 0.24; *ponB(I202F)* Δ*lpoB*, p = 0.001.

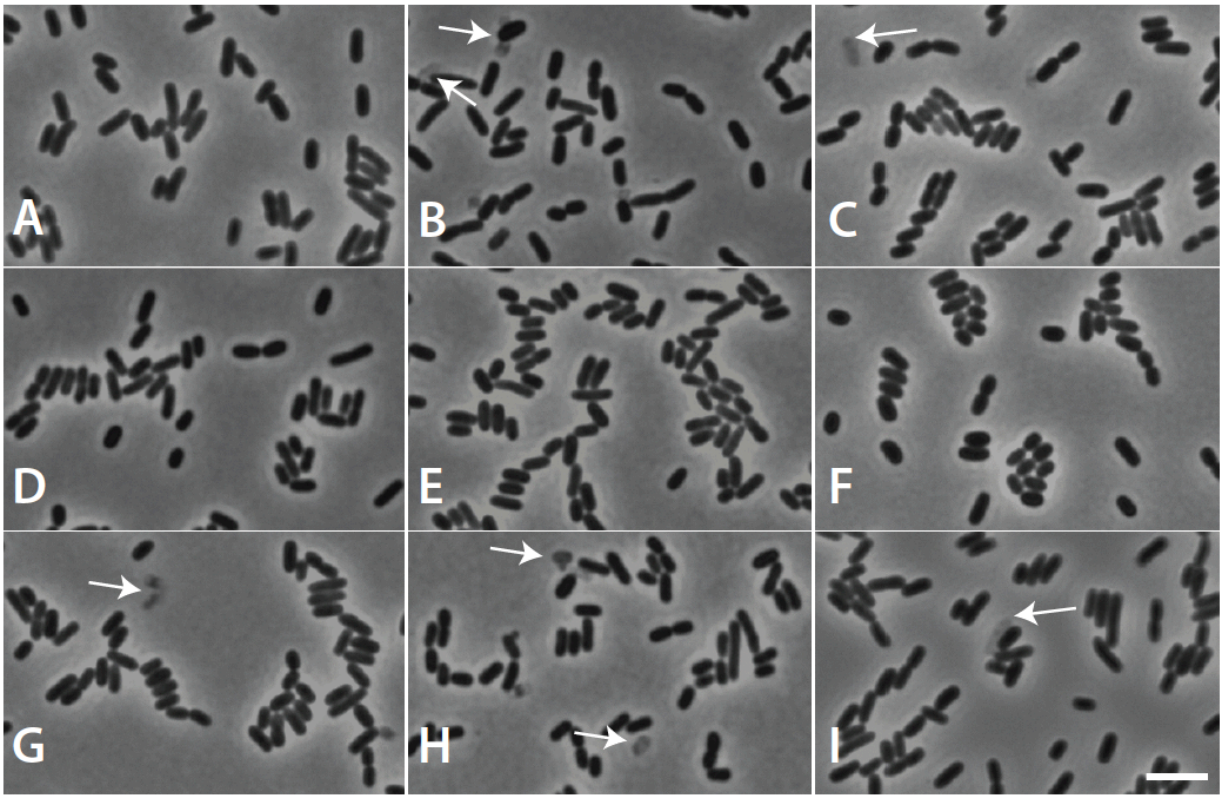

Figure 3.7. PBP1b* variants need LpoB to prevent low frequency of lysis. Cells of MG1655 [wild-type] (**A**), CB2 [Δ*ponB*] (**B**), CB7 [Δ*lpoB*] (**C**), MM41 [*ponB(Q411R)*] (**D**), MM42 [*ponB(I202F)*] (**E**), MM43 [*ponB(E313D)*] (**F**), MM47 [*ponB(Q411R) ΔlpoB*] (**G**), MM48 [*ponB(I202F) ΔlpoB*] (**H**), and MM49 [*ponB(E313D) ΔlpoB*] (**I**) were grown overnight at room temperature on solid rich medium containing 50uM IPTG and 20 μg/ml CPRG. Single colonies were resuspended in 1X PBS and 5 μL were spotted onto agarose pads containing 1.2% agarose and 0.5% NaCl for microscopy. Cells were visualized using phase-contrast microscopy. Arrows show cell bulging or single cells that have lysed. Scale bar is equivalent to 4 microns.

frequency that is well above that for cells from wild-type colonies (**Figure 3.7A**). As expected, no cell ghosts were observed in cells from PBP1b^{E313D} LpoB^{+} colonies (**Figure 3.7F**). However, the frequency of lysis observed for cells from PBP1b^{E313D} LpoB^{-} colonies was indistinguishable from a PBP1b(WT) LpoB^{-} colony (**Figure 3.7I**). Thus, PBP1b^{E313D} fails to correct the lysis phenotype observed for LpoB^{-} cells.

To confirm the results above, we used a colorimetric assay that detects an increased frequency of lysis. This assay utilizes a membrane-impermeable LacZ substrate, chlorophenyl red-β-D-galactopyranoside (CPRG). On this medium, wild-type cells form white colonies because CPRG cannot enter cells and is not hydrolyzed by LacZ (**Figure 3.8A**). However, if a sub-population of cells in a colony are lysing, LacZ will be released into the surrounding medium and hydrolyze CPRG to produce a red color. Cells lacking PBP1b or LpoB form red colonies consistent with the increased frequency of lysed cells observed microscopically (**Figure 3.8B and C**). When cells of MM43 [*ponB^{E313D}*] were plated on CPRG-agar, the resulting cell patch was white, indicating that production of PBP1b^{E313D} does not result in elevated cell lysis in the presence of functional LpoB (**Figure 3.8H**). Cells of MM49 [*ponB^{E313D}* Δ*lpoB*], on the other hand, formed patches that were pink in color (**Figure 3.8I**). This is an intermediate phenotype between the intense red colored patch of CB7 [Δ*lpoB*] cells and the lack of color development for MG1655 [WT] cells. Thus, the *ponB(E313D)* allele only partially suppresses the elevated lysis phenotype of Δ*lpoB* cells. This result suggests that either PBP1b^{E313D} is not fully functional in the absence of LpoB or that LpoB has a cellular

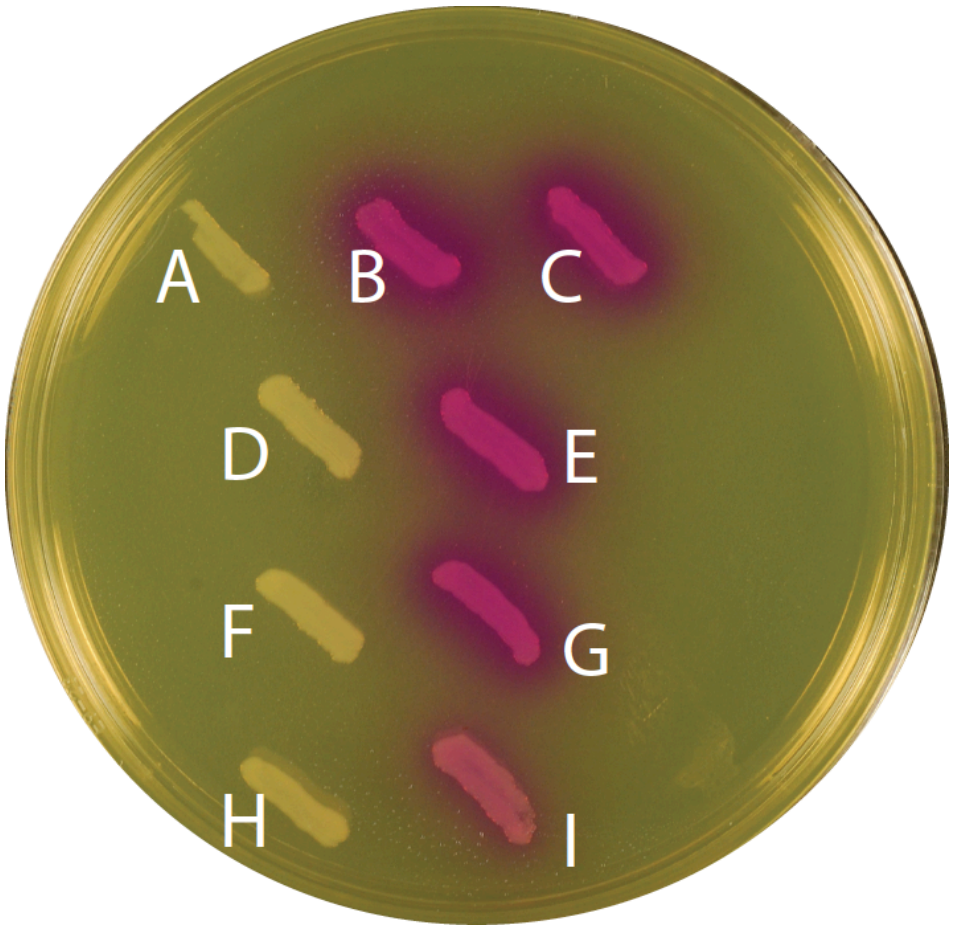

Figure 3.8. The PBP1b* variants are responsive to LpoB *in vivo*. Cells of MG1655 [wild-type] (**A**), CB2 [Δ*ponB*] (**B**), CB7 [Δ*lpoB*] (**C**), MM41 [*ponB(Q411R)*] (**D**), MM47 [*ponB(Q411R)* Δ*lpoB*] (**E**), MM42 [*ponB(I202F)*] (**F**), MM48 [*ponB(I202F)* Δ*lpoB*] (**G**), MM43 [*ponB(E313D)*] (**H**), and MM49 [*ponB(E313D)* Δ*lpoB*] (**I**) were struck out on rich media containing 50 μg/ml of CPRG and 50 μM IPTG and incubated at room temperature for two days.

function in addition to PBP1b activation that helps make PG synthesis more robust thereby reducing the frequency of cell lysis.

Discussion

To better understand how LpoB promotes PBP1b activity and whether or not this activator plays additional roles in PG biogenesis we isolated mutants encoding PBP1b variants that bypass the LpoB-requirement for their function. Five unique PBP1b* variants that result in a LpoB-bypass phenotype were identified. The substitutions cluster in two regions of the PBP1b structure: I202F, Q411R, Q411K and Q447K are located near the UB2H domain and between the PGT and TP domains, and E313D is located in the PGT domain. Interestingly, the strength of the LpoB-bypass phenotype correlates with the location of the substitutions. Changes located near the UB2H domain (I202F and Q411R) result in partial suppression of the LpoB$^-$ phenotype. PBP1b* variants with these substitutions are unable to support the growth of a LpoB$^-$ PBP1a$^-$ strain without basal level production of PBP1a from a P_{ara}::*ponA* expression construct integrated in the chromosome. PBP1b^{E313D}, on the other hand, supported a sufficient level of PG biogenesis for growth without LpoB in the complete absence of the PBP1a system. The observed growth phenotypes correlated with PG synthesis measurements in ether-permeabilized cells. LpoB is normally required for normal levels of PG synthesis in this assay system. Cells producing PBP1b^{E313D} were capable of synthesizing equivalent levels of PG to WT cells with or without LpoB. Conversely, like WT cells, cells producing PBP1b^{I202F} or PBP1b^{Q411R} required LpoB for PG synthetic activity. Since one would expect the partial bypass mutants to display at least some

increased activity in the absence of LpoB, it is currently unclear why they were identified in the selection for bypass mutants. Interestingly, however, the substitutions in the PBP1b* variants with the partial bypass phenotype map near the UB2H domain, the domain implicated in the interaction with LpoB by Typas and co-workers (25). Thus, it is likely that the amino acid substitutions near UB2H influence the conformation of PBP1b in a manner that mimics the interaction with LpoB and that this conformational change may promote PBP1b activity. Further biochemical characterization of the PGT and TP activities of these variants is therefore warranted and may shed light on the LpoB-bypass mechanism of the UB2H-proximal substitutions.

We previously showed that LpoB is able to increase the PGT activity of PBP1b 1.5-fold and that LpoB leads to the production of shorter glycan strands by PBP1b *in vitro* (19). Typas and co-workers also found that LpoB can enhance the ability of PBP1b to form crosslinked PG *in vitro* (25). The relationship between these two observations is currently unclear, but it is possible that they are connected; shorter glycan strands may be better substrates for crosslinking *in vitro*. The location of the E313D substitution in the PGT domain suggests that it may also influence and perhaps enhance the PGT activity of PBP1b in the absence of LpoB, thus resulting in the bypass phenotype. Interestingly, E313 is located towards the end of a cleft in the PGT active site through which the growing glycan chain is thought to pass. An attractive model to explain the activation of PGT activity of PBP1b by LpoB is that the PGT domain exists in two conformations, an inactive “closed” conformation and an active “open” conformation, and that LpoB stimulates the adoption of the open conformation. Thus the E313D substitution could destabilize the closed conformation and thereby

promote PGT activation in the absence of LpoB. Studies of the PGT activity of PBP1b^{E313D} with and without LpoB are underway to test this hypothesis.

We reasoned that the isolation of LpoB-bypass variants of PBP1b would be useful tools to determine if LpoB plays other important roles in the cell in addition to PBP1b activation. The PBP1b^{E313D} variant was illuminating in this respect. It possessed normal levels of PG synthetic activity in ether-permeabilized cells lacking LpoB and it was able to support growth in the absence of LpoB when the PBP1a-LpoA system was inactivated. However, PBP1b^{E313D} failed to fully suppress the elevated lysis frequency observed in LpoB^{-} cells. Since PBP1b activity seems to be fully restored in cells producing the E313D variant, this result suggests that LpoB is indeed important for aspects of cell envelope biogenesis other than PBP activation. Possibilities for this additional activity include: coordinating PG synthesis with OM biogenesis, coordinating PBP activity with PG hydrolase function, and/or supporting OM constriction during cell division as suggested by Typas and co-workers (25). Further work is required to determine which, if any, of these possibilities are correct.

In conclusion, we have isolated PBP1b* variants that bypass the LpoB requirement for PBP1b activity. Future study of these mutants is likely to reveal important insight into PBP1b function and its control by LpoB. An analogous approach for studies of PBP1a and LpoA is also likely to be applicable to studies of PBP1a and its activation by LpoA.

Materials and Methods

Media and bacterial strains. Cells were grown in LB (1% tryptone, 0.5% yeast extract, 0.5% NaCl) or minimal M9 media (17) supplemented with 0.2% casamino acids and 0.2% sugar (glucose or arabinose as indicated). Concentrations of antibiotics used are as indicated.

The bacterial strains used in this study are listed in **Table 3.2**. All strains used for *in vivo* experiments are derivatives of MG1655 (11). Mutants lacking LpoA, LpoB, or PBP1a were constructed by successive rounds of P1 transduction (17) and the curing of the Kan-resistance marker (Kan^r) cassettes flanked by *frt* sites using plasmid pCP20 as described previously (9) (see **Table 3.2** for construction details). The desired chromosomal modification was confirmed by using diagnostic PCR every time Kan^r a cassette was transduced or cured. When a strain contained multiple lesions, diagnostic PCR was used to confirm the status of each lesion. No difference in phenotype was observed when strains containing the Kan^r cassette were compared to the corresponding strains in which the cassette was removed by FLP recombinase. All deletion alleles were constructed to be in-frame deletions as part of the Keio collection (1).

Plasmids. The plasmids used in the present study are listed in **Table 3.3**. Vectors with R6K origins are all derivatives of CRIM plasmids developed by Haldimann and Wanner (12). The vectors were either maintained in the cloning strain DH5α(λ*pir*), where they replicate as plasmids, or they were integrated into phage attachment sites (HK022 or λ) by using the helper vectors pTB102 or pINT-ts, respectively, as previously described (4, 12). Single-copy integrants were identified by using diagnostic PCR (12).

Table 3.2. Strains used in this study.

Strain[a]	Genotype[b]	Source, reference, or construction[c]
MG1655	*rph ilvG rfb-500*	(11)
CAG12025	MG1655 *zad-220::Tn10*	(21)
JW3359	*Δ(araD-araB)567 ΔlacZ4787(::rrnB-3) rph-1 Δ(rhaD-rhaB)568 hsdR514 ponA731::aph*	(1)
JW5157	*Δ(araD-araB)567 ΔlacZ4787(::rrnB-3) rph-1 Δ(rhaD-rhaB)568 hsdR514 ΔycfM767::aph*	(1)
CB2	MG1655 *ponB::aph*	(19)
CB7	MG1655 *lpoB::aph*	(19)
MM41	MG1655 *ponB(Q411R)*	CB2 x P1(MM36(attλTB309))
MM42	MG1655 *ponB(I202F)*	CB2 x P1(MM37(attλTB309))
MM43	MG1655 *ponB(E313D)*	CB2 x P1(MM38(attλTB309))
MM44	MG1655 *ponB(Q411R) lpoB::aph*	MM41 x P1(JW5157)
MM45	MG1655 *ponB(I202F) lpoB::aph*	MM42 x P1(JW5157)
MM46	MG1655 *ponB(E313D) lpoB::aph*	MM43 x P1(JW5157)
MM47	MG1655 *ponB(Q411R) lpoB<>frt*	MM44/pCP20
MM48	MG1655 *ponB(I202F) lpoB<>frt*	MM45/pCP20
MM49	MG1655 *ponB(E313D) lpoB<>frt*	MM46/pCP20
MM66	MG1655 *ponB(E313D) lpoB<>frt ponA::aph*	MM49 x P1(JW3359)
MM67	MG1655 *ponB(E313D) lpoB<>frt lpoA::aph*	MM49 x P1(JW5157)
TB28	MG1655 *ΔlacIZYA<>frt*	(5)
TU121(attλTB309)	TB28 *ponA<>frt* P_{ara}::*ponA*	(19)
CB4(attλTB309)	TB28 *ponA<>frt lpoB::aph* P_{ara}::*ponA*	(19)

Table 3.2. Strains used in this study. (Continued)

Strain[a]	Genotype[b]	Source, reference, or construction[c]
MM33(attλTB309)	TB28 *ponA<>frt lpoB<>frt* P_{ara}::*ponA*	CB4/pCP20
ponBlin39	TB28 *ponA<>frt lpoB<>frt ponB(Q411R)* P_{ara}::*ponA*	From cefsulodin selection
ponBlin65	TB28 *ponA<>frt lpoB<>frt ponB(I202F)* P_{ara}::*ponA*	From cefsulodin selection
ponBlin222	TB28 *ponA<>frt lpoB<>frt ponB(E313D)* P_{ara}::*ponA*	From cefsulodin selection
ponBlin425	TB28 *ponA<>frt lpoB<>frt ponB(Q447K)* P_{ara}::*ponA*	From cefsulodin selection
MM36(attλTB309)	TB28 *ponA<>frt lpoB<>frt ponB(Q411R)* P_{ara}::*ponA*	P1(CAG12025) x ponBlin39
MM37(attλTB309)	TB28 *ponA<>frt lpoB<>frt ponB(I202F)* P_{ara}::*ponA*	P1(CAG12025) x ponBlin65
MM38(attλTB309)	TB28 *ponA<>frt lpoB<>frt ponB(E313D)* P_{ara}::*ponA*	P1(CAG12025) x ponBlin222
MM33(attλTB309) (attHKMM6)	TB28 *ponA<>frt lpoB<>frt* P_{ara}::*ponA* Plac::*gfp-ponBγ*	This study
MM33(attλTB309) (attHKMM79)	TB28 *ponA<>frt lpoB<>frt* P_{ara}::*ponA* Plac::*gfp-ponBγ(Q411R)*	This study
MM33(attλTB309) (attHKMM80)	TB28 *ponA<>frt lpoB<>frt* P_{ara}::*ponA* Plac::*gfp-ponBγ(I202F)*	This study
MM33(attλTB309) (attHKMM81)	TB28 *ponA<>frt lpoB<>frt* P_{ara}::*ponA* Plac::*gfp-ponBγ(E313D)*	This study
MM33(attλTB309) (attHKMM89)	TB28 *ponA<>frt lpoB<>frt* P_{ara}::*ponA* Plac::*gfp-ponBγ(Q447K)*	This study

[a]Strains constructed in this study.
[b]The *aph* (KanR cassette) is flanked by *frt* sites for removal by FLP recombinase. An *frt* scar remains after removal using FLP expressed from pCP20.
[c]Strain constructions by P1 transduction are described using the shorthand: P1(donor) x recipient. In all cases, transductants were selected on LB-Kan plates. Strains resulting from the removal of the *aph* (KanR cassette) using pCP20 are indicated as: parental strain/pCP20.

Table 3.3. Plasmids used in this study.

Plasmid	Genotype	Origin	Source, reference, or construction
pCP20	*bla cat cI857 repA(Ts)* P_R::*flp*	pSC101	(9)
pTB102	*cat cI857 repA(Ts)* P_R::int^{HK022}	pSC101	(4)
pMM6	*att*HK022 *bla* $lacI^q$ P_{lac}::*gfp-ponBγ*	R6K	(19)
pMM79	*att*HK022 *bla* $lacI^q$ P_{lac}::*gfp-ponBγ(Q411R)*	R6K	This study
pMM80	*att*HK022 *bla* $lacI^q$ P_{lac}::*gfp-ponBγ(I202F)*	R6K	This study
pMM81	*att*HK022 *bla* $lacI^q$ P_{lac}::*gfp-ponBγ(E313D)*	R6K	This study
pMM89	*att*HK022 *bla* $lacI^q$ P_{lac}::*gfp-ponBγ(Q447K)*	R6K	This study

Integrated vectors were transferred between strains by P1-mediated transduction. The construction of plasmids in the present study are described below. In all cases, PCR was performed using KOD polymerase (Novagen) according to the manufacturer's instructions. Restriction sites for use in plasmid constructions are underlined in the primer sequences given below. Plasmid DNA was purified using either the Qiagen spin miniprep kit (Qiagen) or the Zippy miniprep kits (Zymo Research) while PCR fragments were purified using a Qiaquick PCR purification kit (Qiagen). The construction for the plasmids used in the present study are described below. For pMM79 [*att*HK022 *bla lacI*^{q} P_{lac}::*gfp-ponB(Q411R)*], pMM80 [*att*HK022 *bla lacI*^{q} P_{lac}::*gfp-ponB(I202F)*], and pMM81 [*att*HK022 *bla lacI*^{q} P_{lac}::*gfp-ponB(E313D)*], the *ponB** genes were amplified from genomic DNA using the primers 5'-GTACGGATCCC CGCGCAAAGGTAAGGG-3' and 5'-GTCACTCGAGATGGGATGTTATTTTACCGGATGG C-3'. The PCR product was then digested with BamHI and XhoI and ligated into the BamHI/SalI digested pTB183 [*att*HK022 *bla* P_{lac}::*gfp-zapA*] (3).

Cefsulodin selection-screen. Cells of MM33(attλTB309) and TU121(attλTB309) were grown overnight in minimal M9 media containing 0.2% arabinose at 30°C. The next morning, the cultures were subcultured 1:100 into 50ml of fresh minimal M9 media containing 0.2% arabinose and grown to fresh saturation (OD_{600} 0.96 to 1.0) at 30°C. Serial dilutions of each strain (10^{-1} to 10^{-7}) were plated onto permissive conditions for colony counts. For MM33(attλTB309), the following volumes of the undiluted culture were centrifuged and plated onto minimal M9 media containing 0.2% arabinose and 0.01 μg/ml: 1 ml, 2 ml, 5 ml and 10 ml. Plates were incubated at 30°C. After three days, 14 suppressors arose on the plate containing 5 ml of culture, while the plate containing

10 ml of culture had 372 suppressors. The efficiency of plating (EOP) for MM33(attλTB309) between the permissive and non-permissive conditions was 1.7 x 10^{-8}. Upon repeating this procedure to potentially independently isolate the same set of mutations, the EOP was 1.4 x 10^{-6}.

Complementation of PBP1a^{-}/LpoB^{-} synthetic lethal phenotype *in trans*. See figure legend for details.

Immunoblotting. Cultures of MG1655, CB2, CB7, MM41, MM42, MM43, MM47, MM48, and MM49 were grown overnight in LB at 30°C. The cultures were diluted 1:100 in 5 ml of LB (with duplicate of each strain) and grown at 30°C to an OD_{600} between 0.52 to 0.66. Cells were harvested by centrifugation at 4°C and resuspended in PBS and 2X Laemmli buffer. Samples were incubated at 100°C for 10 min. Total protein concentrations of the cell extracts were measured using the Non-Interfering™ Protein Assay (G Biosciences). 15 µg of total protein was loaded into each well, cell extracts were separated on a 12% acrylamide gel and transferred to Protran® nitrocellulose membranes (Whatman, 0.22 um). Processing of the immunoblots were performed as previously described (5). PBP1b antisera was used at a dilution of 1:10,000.

Ether-permeabilized cell assay. This assay was performed as described previously in (19) with the following changes. In **Figure 3.6**, ether-treated cells were prepared from cultures grown to an OD_{600} of 0.50 at 37˚C (A) or 30˚C (B).

Acknowledgements

The authors would like to thank Tania Lupoli, David Rudner, Suzanne Walker, Dan Kahne and members of the Bernhardt, Walker and Kahne laboratories for discussion and critical reading of this manuscript. We would also like to thank Morgan Feeney and Jon Beckwith for the generous gift of the CAG12025 strain (21).

References

1. **Baba, T.**, **T. Ara**, **M. Hasegawa**, **Y. Takai**, **Y. Okumura**, **M. Baba**, **K. A. Datsenko**, **M. Tomita**, **B. L. Wanner**, **and H. Mori**. 2006. Construction of Escherichia coli K-12 in-frame, single-gene knockout mutants: the Keio collection. Molecular Systems Biology **2**:1-11.

2. **Barrett, D.**, **T.-S. A. Wang**, **Y. Yuan**, **Y. Zhang**, **D. Kahne**, **and S. Walker**. 2007. Analysis of glycan polymers produced by peptidoglycan glycosyltransferases. J Biol Chem **282**:31964–31971.

3. **Bendezú, F. O.**, **and P. A. J. de Boer**. 2008. Conditional lethality, division defects, membrane involution, and endocytosis in mre and mrd shape mutants of Escherichia coli. J Bacteriol **190**:1792–1811.

4. **Bernhardt, T. G.**, **and P. A. J. de Boer**. 2005. SlmA, a nucleoid-associated, FtsZ binding protein required for blocking septal ring assembly over Chromosomes in E. coli. Molecular Cell **18**:555–564.

5. **Bernhardt, T. G.**, **and P. A. J. de Boer**. 2003. The Escherichia coli amidase AmiC is a periplasmic septal ring component exported via the twin-arginine transport pathway. Mol Microbiol **48**:1171–1182.

6. **Bertsche, U.**, **E. Breukink**, **T. Kast**, **and W. Vollmer**. 2005. In vitro murein peptidoglycan synthesis by dimers of the bifunctional transglycosylase-transpeptidase PBP1B from Escherichia coli. J Biol Chem **280**:38096–38101.

7. **Cabeen, M.**, **and C. Jacobs-Wagner**. 2007. Skin and bones: the bacterial cytoskeleton, cell wall, and cell morphogenesis. The Journal of Cell Biology **175**:381-387.

8. **Cabeen, M. T.**, **and C. Jacobs-Wagner**. 2005. Bacterial cell shape. Nat Rev Micro **3**:601–610.

9. **Datsenko, K. A.**, **and B. L. Wanner**. 2000. One-step inactivation of chromosomal genes in Escherichia coli K-12 using PCR products. Proc Natl Acad Sci USA **97**:6640–6645.

10. **Goffin, C.**, **and J. M. Ghuysen**. 1998. Multimodular penicillin-binding proteins: an enigmatic family of orthologs and paralogs. Microbiol Mol Biol Rev **62**:1079–1093.

11. **Guyer, M. S.**, **R. R. Reed**, **J. A. Steitz**, **and K. B. Low**. 1981. Identification of a sex-factor-affinity site in E. coli as gamma delta. Cold Spring Harb. Symp. Quant. Biol. **45 Pt 1**:135–140.

12. **Haldimann, A.**, **and B. L. Wanner**. 2001. Conditional-replication, integration, excision, and retrieval plasmid-host systems for gene structure-function studies of bacteria. J Bacteriol **183**:6384–6393.

13. **Höltje, J. V.** 1998. Growth of the stress-bearing and shape-maintaining murein sacculus of Escherichia coli. Microbiol Mol Biol Rev **62**:181–203.

14. **Kraus, W.**, **B. Glauner**, **and J. V. Höltje**. 1985. UDP-N-acetylmuramylpentapeptide as acceptor in murein biosynthesis in Escherichia coli membranes and ether-permeabilized cells. J Bacteriol **162**:1000–1004.

15. **Kraus, W.**, **and J. V. Höltje**. 1987. Two distinct transpeptidation reactions during murein synthesis in Escherichia coli. J Bacteriol **169**:3099–3103.

16. **Margolin, W.** 2009. Sculpting the Bacterial Cell. Current Biology **19**:R812–R822.

17. **Miller, J. H.** 1972. Experiments in Molecular Genetics. Cold Spring Harbor Laboratory Pr.

18. **Mirelman, D.**, **Y. Yashouv-Gan**, **and U. Schwarz**. 1976. Peptidoglycan biosynthesis in a thermosensitive division mutant of Escherichia coli. Biochemistry **15**:1781–1790.

19. **Paradis-Bleau, C.**, **M. Markovski**, **T. Uehara**, **T. J. Lupoli**, **S. Walker**, **D. E. Kahne**, **and T. G. Bernhardt**. 2010. Lipoprotein cofactors located in the outer membrane activate bacterial cell wall polymerases. Cell **143**:1110–1120.

20. **Sauvage, E.**, **F. D. R. Kerff**, **M. Terrak**, **J. A. Ayala**, **and P. Charlier**. 2008. The penicillin-binding proteins: structure and role in peptidoglycan biosynthesis. FEMS Microbiol Rev **32**:234–258.

21. **Singer, M.**, **T. A. Baker**, **G. Schnitzler**, **S. M. Deischel**, **M. Goel**, **W. Dove**, **K. J. Jaacks**, **A. D. Grossman**, **J. W. Erickson**, **and C. A. Gross**. 1989. A collection of strains containing genetically linked alternating antibiotic resistance elements for genetic mapping of Escherichia coli. Microbiol Rev **53**:1–24.

22. **Sung, M.-T.**, **Y.-T. Lai**, **C.-Y. Huang**, **L.-Y. Chou**, **H.-W. Shih**, **W.-C. Cheng**, **C.-H. Wong**, **and C. Ma**. 2009. Crystal structure of the membrane-bound bifunctional transglycosylase PBP1b from Escherichia coli. Proceedings of the National Academy of Sciences **106**:8824–8829.

23. **Tamaki, S.**, **S. Nakajima**, **and M. Matsuhashi**. 1977. Thermosensitive mutation in Escherichia coli simultaneously causing defects in penicillin-binding protein-1Bs and in enzyme activity for peptidoglycan synthesis in vitro. Proc Natl Acad Sci USA **74**:5472–5476.

24. **Typas, A.**, **M. Banzhaf**, **C. A. Gross**, **and W. Vollmer**. 2011. From the regulation of peptidoglycan synthesis to bacterial growth and morphology. Nat Rev Micro **10:**123-136.

25. **Typas, A.**, **M. Banzhaf**, **B. van den Berg van Saparoea**, **J. Verheul**, **J. Biboy**, **R. J. Nichols**, **M. Zietek**, **K. Beilharz**, **K. Kannenberg**, **M. von Rechenberg**, **E. Breukink**, **T. den Blaauwen**, **C. A. Gross**, **and W. Vollmer**. 2010. Regulation of peptidoglycan synthesis by outer-membrane proteins. Cell **143**:1097–1109.

26. **van Heijenoort, J.** 2007. Lipid Intermediates in the Biosynthesis of Bacterial Peptidoglycan. Microbiol Mol Biol Rev **71**:620–635.

27. **Vollmer, W.**, **and S. J. Seligman**. 2010. Architecture of peptidoglycan: more data and more models. Trends Microbiol **18**:59–66.

28. **Yousif, S. Y.**, **J. K. Broome-Smith**, **and B. G. Spratt**. 1985. Lysis of Escherichia coli by beta-lactam antibiotics: deletion analysis of the role of penicillin-binding proteins 1A and 1B. J Gen Microbiol **131**:2839–2845.

Chapter 4:

Summary and Future Directions

Summary

The PG layer protects the cytoplasmic membrane from rupture due to high internal turgor pressure (17, 37). Its growth is a complex and dynamic process that requires the interplay of numerous enzymes to build an intact meshwork that encompasses the entire cell. The PG synthases that polymerize and crosslink PG are called the penicillin-binding proteins (PBPs). They have been found to work in the context of large multi-enzyme complexes that are organized by cytoskeletal elements. Two distinct complexes are associated with the different phases of PG growth in rod-shaped cells: elongation and division (6, 7). During elongation, a complex organized by the actin-like MreB directs the insertion of new material into the sidewall of the rod-shaped cell. Following elongation, the mode of PG growth switches to a concentrated zone of synthesis at the division site directed by a complex of proteins called the divisome that is organized by the tubulin-like protein FtsZ (6, 7, 24). The two major PG synthases in *E. coli*, PBP1a and PBP1b, are thought to work in different complexes during these two phases of PG growth. In line with this hypothesis, crosslinking of proteins in *Haemophilus influenzae* cells by Alaedini *et al*. (1) revealed the existence of two different high molecular weight (HMW) complexes containing class A and class B PBPs (see **Introduction** for discussion of the HMW-PBPs). Recent evidence shows that PBP1a may interact with PBP2 and is likely to work with the MreB-directed PG synthetic machine during the elongation phase of PG assembly (33). On the other hand, PBP1b is thought to primarily work during cell division based on observed interactions with the division proteins PBP3 (FtsI) and FtsN (3, 26).

A major outstanding question has been whether or not multi-enzyme complexes contain factors required for PBP function. Using *Escherichia coli* as a model system, we took advantage of the synthetic lethal phenotype resulting from simultaneous inactivation of the two major HMW class A PBPs: PBP1a and PBP1b (19, 39). Using a screen for mutants synthetically lethal with the inactivation of PBP1b, I identified LpoA (YraM) as a factor required for PBP1a function. This is a 678 residue putative outer membrane (OM) lipoprotein with a C-terminal LppC domain of unknown function that is well conserved among γ-proteobacteria (16, 35). A colleague in the lab, Dr. Catherine Paradis-Bleau, performed the analogous screen for mutants synthetically lethal with the loss of PBP1a and identified LpoB (YcfM), a 213 amino acid predicted OM lipoprotein, as a factor necessary for PBP1b function (29).

Based on the sequence of their signal peptides, LpoA and LpoB were predicted to be OM lipoproteins. I confirmed their subcellular localization using a cytological assay for lipoprotein transport where I plasmolysed cells expressing fluorescently-tagged versions of LpoA and LpoB (adapted from (22)). Interestingly, OM localization was required for LpoA but not LpoB. Because our results suggested that the Lpo factors were promoting the *in vivo* activity of the PBPs, we wondered if they did so directly. We used a pull-down assay to show that the purified Lpo factors directly interacted with their cognate purified PBP1 partner. Combined with the knowledge of their subcellular localization, this indicated that they form specific trans-envelope complexes with their cognate PBPs (29). I also showed that loss of both LpoA and LpoB phenocopied the lysis observed in cells lacking PBP1a and PBP1b, indicating that the Lpo factors are critical components of their respective complexes (29).

To assess the effect of the Lpo proteins on PG assembly, we first compared the chemical compositions of PG isolated from wild-type cells to that isolated from PBP1a$^-$ PBP1b$^-$ or LpoA$^-$ LpoB$^-$ cells just before lysis occurred. The absence of either the PBP1s or the Lpo proteins caused a decrease in crosslinking, from 22% in the wild-type down to 18-19% in the case of the mutants (29). Even though this result may seem insignificant, any small decrease in cross-linking can potentially have detrimental effects for the cell *in vivo*, especially if there is a localized drop in crosslinking. We also examined the effect of LpoB on PG synthesis using ether-permeabilized cells and showed LpoB is required for PBP1b activity. The Lpo factors are needed to promote PBP1 activity, however, we did not know which activity they stimulated. To determine which activity they stimulated, we collaborated with the Kahne and Walker groups at Harvard to show that LpoB stimulated the peptidoglycan glycosyltransferase (PGT) activity of PBP1b, leading to the production of shorter glycan strands (29).

To investigate the role of LpoB in the PBP1b PG synthetic complex further, I took a genetic approach to identify PBP1b* variants capable of functioning *in vivo* in the absence of LpoB. To isolate these variants, I took advantage of the cefsulodin hypersensitive phenotype shared amongst *ponB* (encoding PBP1b) and *lpoB* mutants. We reasoned that the cefsulodin hypersensitivity of *lpoB* mutants results from a defect in PBP1b activity and that *ponB** alleles encoding PBP1b* variants might be identified by a selection for increased cefsulodin resistance in a LpoB$^-$ strain background. Using this strategy, I isolated spontaneous suppressors of this phenotype and identified five mutations within the *ponB* gene that arise under these conditions. Preliminary characterization of these variants indicates that only one, PBP1b^{E313D}, is capable of

synthesizing PG in the absence of LpoB. However, while this variant can function without LpoB *in vivo*, PBP1b^{E313D} does not fully suppress a LpoB^{-} defect and exhibits an elevated frequency of lysis similar to a *lpoB* mutant. These results suggest that LpoB might have additional functions within the cell other than PBP activation. Also, the location of this specific mutation provides us with some insight into a possible mechanism by which LpoB activates the PGT of PBP1b.

Taken together, results from my work contribute to our understanding of the functional interplay between the Lpo factors and their PBP1 partner. The unexpected complexity observed in the control of PBP activity was surprising and revealed that these enzymes likely receive regulatory input from both the Lpo factors in the OM and cytoskeletal elements in the cytoplasm. In addition to increasing our knowledge of PG assembly, these studies help to lay the foundation for future investigations into roles the Lpo factors may play *in vivo*.

Future directions

Chapter 2 describes the identification of LpoA and LpoB as the first critical activators for HMW class A PBP function. Chapter 3 goes one step further to identify variants of PBP1b that bypass the need for LpoB *in vivo*. Future study of these mutants is likely to reveal important insight into PBP1b function and its control by LpoB. At this point, however, the physiological significance of the Lpo factors is still unclear. This section includes a discussion of the potential roles the Lpo factors may play in the cell and describes experiments to investigate them in *E. coli*.

The Lpo factors coordinate the rates of PG synthesis and OM biogenesis. The Lpo factors are lipoproteins tethered to the OM and must traverse nearly the entire periplasm to interact with their cognate IM-retained PBP (29). Because these lipoproteins are attached to the OM, one potential role that these factors may play is to help coordinate the rate of PG synthesis with OM biogenesis. Regulation of these two processes would be particularly important during lateral PG synthesis to prevent any breaches in cell envelope integrity. If OM biogenesis were to lag behind PG synthesis the permeability barrier function of the OM may be compromised. Conversely, if OM biogenesis were to outpace PG synthesis, excess membrane would be wasted because it likely has to be shed by vesicle formation.

LpoA is thought to work with the elongation machinery during lateral wall PG synthesis (34), and only OM-tethered LpoA was capable of supporting PBP1a activity (Chapter 2) (29). Taken together, these results suggest a role for LpoA in coordinating PG synthesis and OM biogenesis. If this is true, a *lpoA* mutant may exhibit either increased OM permeability and/or increased OM vesicle formation. With the former

possibility, we would expect a *lpoA* mutant to be more sensitive to detergents and to large antibiotics that normally would not enter Gram-negative cells (like vancomycin or erythromycin). However, if OM biogenesis is increased compared to PG synthesis, then we would expect a *lpoA* mutant to show an elevated frequency of OM vesicles emanating from the cell. To test this, we could integrate a fluorescently-tagged OM marker (e.g. OM-anchored mCherry) and look for increased vesicle formation in a *lpoA* mutant using fluorescent microscopy. Consistent with a role for LpoA in membrane biogenesis, the *lpoA* gene is genetically linked to the *ecfH (yraP)* gene in most γ-proteobacteria. EcfH is predicted to be an OM lipoprotein containing two BON domains thought to bind phospholipids. This observation suggests that LpoA and EcfH may work together to properly control the rates of PG synthesis and OM biogenesis.

LpoB could also play a role in coordinating OM biogenesis with PG synthesis even though IM-anchored LpoB can activate PBP1b (Chapter 2) (29). When tested, the *lpoB* mutant did not exhibit any OM permeability defects. These cells were resistant to sodium dodecyl sulfate (SDS) and to vancomycin and erythromycin (data not shown). However, LpoA is still expressed and may be able to coordinate OM biogenesis and PG synthesis in the absence of LpoB. Since the loss of both LpoA and LpoB results in cell lysis, we cannot test a strain lacking both factors. In Chapter 3, I found that PBP1b^{E313D} can complement this synthetic lethal defect. Thus we can test PBP1b^{E313D} cells without the Lpo factors using the same assays described above for changes in OM integrity.

Control of glycan strand insertion by the Lpo factors. Another potential role that these OM-anchored Lpo factors may fulfill is to help guide where the multi-enzyme PG synthetic complexes insert new material. Adjacent glycan strands in the existing

PG structure would likely prevent lateral diffusion of the trans-envelope complexes containing the Lpo factors in the OM (**Figure 1.1A and Figure 2.14**) to promote the insertion of nascent PG along a directed path. This model is consistent with observed insertion of single strands of new PG between two old strands (9, 10), and previous studies suggesting that the existing PG networks acts as a template (16, 31). According to this model, without the Lpo factors, the PBP complexes would deviate from the template and insert new material in a less orderly manner. Thus, input from the OM and the cytoskeletal elements in the cytoplasm might allow the PG synthetic complexes to better adhere to the existing cell wall template, leading to robust duplication of the PG layer (**Figure 2.14**).

The Lpo factors may coordinate PG synthesis and PG hydrolysis. In order for the PG layer to grow, bonds in the existing PG structure need to be broken to insert new material. Components of the multi-enzyme PG synthetic complexes with PG hydrolase activity are thought to perform this function (17, 34, 36). These potentially dangerous enzymes need to be properly controlled to prevent breaches in the PG layer from forming. Because the Lpo factors are critical for PBP activity, they could potentially couple PBP synthetic activity to hydrolytic activity, thereby restricting PG cleavage to sites of PG growth (17, 33). In fact, PBP1b was shown to be connected to an OM-anchored lytic transglycosylase, MltA, via an adaptor protein MipA (36). Additionally, Typas *et al*. (34) suggest that LpoB may recruit a PG hydrolase to sites of PG synthesis at the septum. In Chapter 3, we showed that both a *lpoB* mutant exhibits an elevated frequency of lysis. Potentially, the rates of PG synthesis and hydrolysis are not coordinated with each other leading to increased lysis and further supporting the

proposed idea. To test this, we plan to use a variant of PBP1b that can function in the absence of LpoB. Using a genetic approach, we could introduce lytic transglycosylase deletions (single or in combination) into a *lpoB* mutant expressing PBP1b^{E313D} and test for suppression of this elevated lysis phenotype using the assays described in Chapter 3.

Homeostatic mechanism for mechanical stress. As mentioned previously, the OM-attached Lpo factors must pass the PG layer to interact with their cognate PBP1s. Vollmer and colleagues provide an intriguing model for the regulation of PG synthesis by the Lpo factors in which they are only able to activate the PBPs when the pore size of the PG layer is large enough for them to pass through. Such a mechanism would make the activation responsive to the state of the PG pores. In growing *E. coli* cells, the PG network has the capacity to stretch up to three-fold in surface area due to turgor pressure (8). Rapid growth in rich media may also stretch the PG layer in a similar way and consequently increase pore size to allow the Lpo factors to interact with and activate their cognate PBP1s. On the other hand, during slow growth conditions (e.g. limited nutrients or during stationary phase) where little new PG material is needed, the pores are predicted to decrease in size, preventing activation of the PBPs by the Lpo factors. This model is attractive because it provides a potential mechanism to coordinate the rate of PG synthesis with environmental conditions and nutritional status. However, the model is unfortunately difficult to test and experimental support for it is limited.

Specific roles of LpoA *in vivo.* In addition to the potential models for Lpo function above, LpoA may perform specific roles in the cell which LpoB cannot. In line with this idea, LpoA and LpoB do not share any sequence homology and are thus likely to have evolved to perform different specific functions *in vivo*. One idea is that LpoA only activates the transpeptidase (TP) activity of PBP1a, as shown by Typas *et al.* (34). Recently Tania Lupoli from the Kahne group developed an *in vitro* PBP TP assay (23) and confirmed that LpoA stimulated the TP activity of PBP1a approximately seven-fold (Tania Lupoli, personal communication). These results suggest that LpoA is stimulating the TP activity of PBP1a *in vivo*. To support this idea, we could identify *lpoA* mutants that no longer stimulate the TP activity of PBP1a.

Furthermore, the *H. influenzae* LpoA homolog was suggested to play a potential role in iron acquisition. During normal *H. influenzae* growth in rich media, LpoA is expressed at low levels. However, it is expressed at high levels when an iron chelator, 2,2-dipyridyl, is added to the medium (35). To support this idea, the *HI1654* gene (*yraL* in *E. coli*) is upstream of the *lpoA* gene. This gene is thought to encode a putative tetrapyrrole methylase that is involved in porphyrin biosynthesis. These observations suggest that LpoA may play a role in acquiring iron. Saper and coworkers believe that this may be important for *H. influenzae* because iron and porphyrin acquisition are required for aerobic growth of this organism; however, all bacteria must use iron for growth and have created many mechanisms to obtain it (e.g. scavenging iron using siderophores). LpoA may be part of another potential route bacteria use to acquire iron. One idea is that PBP1a could require iron to function *in vivo*, and LpoA could provide this cofactor to PBP1a *in vivo*. To test whether LpoA plays a role in iron acquisition, we

could assay for growth of a *lpoA* mutant under no iron conditions or in the presence of 2,2-dipyridyl.

Specific roles of LpoB *in vivo*. An attractive model for LpoB function is one in which LpoB coordinates both the PGT and TP activities of PBP1b. In Chapter 2, we show that LpoB stimulates the PGT activity of PBP1b (29) using the *in vitro* PGT assay system developed by the Walker and Kahne groups (2). Additionally, Vollmer and coworkers showed that LpoB also activates the TP activity of PBP1b (34), and this was recently confirmed by the Kahne group (Tania Lupoli, personal communication). Taken together, these results suggest that LpoB controls both activities of PBP1b. Therefore, binding of LpoB to PBP1b could induce a conformational change that places the TP domain in closer contact with the PGT domain to easily access elongating glycan strands for the crosslinking reaction (**Figure 4.1**). If this model is true, we would predict that a PBP1b* variant that bypasses the need for LpoB would require substitutions in both its PGT and TP domains to activate the enzyme. However, the likelihood of isolating these mutants using the genetic selection in Chapter 3 is very low. Instead, we identified a single substitution in the PGT domain of PBP1b that is LpoB-independent ($PBP1b^{E313D}$) and three substitutions near the LpoB-binding domain that may partially bypass the need for LpoB ($PBP1b^{I202F}$, $PBP1b^{Q411R}$, and $PBP1b^{Q447K}$). Perhaps combining these substitutions with E313D will lead to activation of both PBP1b activities without LpoB.

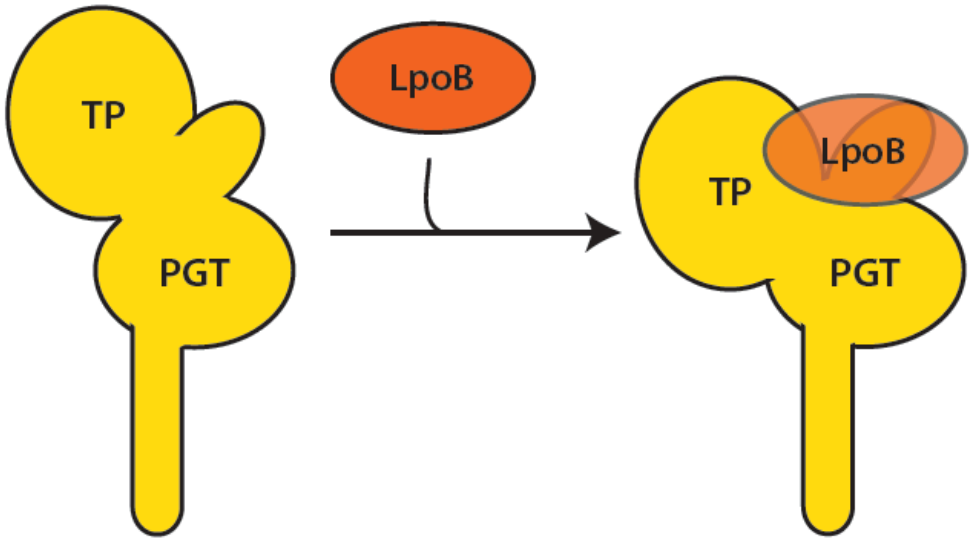

Figure 4.1. LpoB binding induces conformational change in PBP1b. The figure above illustrates a potential conformational change that occurs when LpoB binds to PBP1b. This change may cause the transpeptidase (TP) domain to come into close proximity to the PG glycosyltransferase domain (PGT) of PBP1b.

The Tol-Pal trans-envelope complex is critical for cell envelope integrity and OM invagination during cell division (15). However, these components are not essential, suggesting the existence of redundant systems. Vollmer and colleagues propose that the PBP1b-LpoB complex can perform this role in the absence of Tol-Pal because cells lacking both LpoB and Pal lead to cell lysis in no salt conditions (34). To potentially bypass this phenotype, we can use the LpoB-independent PBP1b^{E313D} variant isolated in Chapter 3. Because it no longer needs LpoB to function *in vivo*, we can test whether PBP1b^{E313D} can complement the synthetic lethal phenotype observed when *lpoB* mutants lack the Tol-Pal pathway. Our preliminary evidence shows that a *lpoB tol* double mutant that expresses PBP1b^{E313D} can survive under no salt conditions (data not shown). However, even though these mutants effectively lack the Tol-Pal pathway, Pal is still expressed and may now work with PBP1b^{E313D} in the absence of LpoB to invaginate the OM. Thus we plan to test a *lpoB pal* double mutant that expresses PBP1b^{E313D} for its ability to complement under no salt conditions.

PBP activators in Gram-positive bacteria. While we identified factors that promote PBP activity in Gram-negative bacteria, one outstanding question is whether they exist in Gram-positive cells that have a thick PG layer. BLAST searches and bioinformatics analysis using the STRING program (25) show that many firmicutes contain weak homologs of either LpoA or LpoB with a maximum sequence identity of 40%. For example, *Staphylococcus aureus* contains a protein with weak homology to *E. coli* LpoA suggesting that these activators do exist in Gram-positive organisms. However, they must be tethered to the IM or soluble within the periplasmic compartment

because these bacteria lack an OM. In line with this idea, our results from Chapter 2 show that both IM-attached and soluble periplasmic LpoB variants are capable of activating PBP1b (29), suggesting that cofactors in these locations can stimulate PBP activity.

However, the physiological significance of these activators is unclear. One potential idea is that to maintain cell wall thickness, these factors coordinate the PGT and TP activities of the PBPs to regulate the length of glycan polymers or the degree of crosslinking. Factors critical for PBP activity could also potentially couple PBP synthetic activity to hydrolytic activity, similar to the model proposed for the Lpo factors (see above) (17, 33). Moreover, the Gram-positive cell wall also contains covalently-attached polymers called lipoteichoic acids (LTAs). LTA biosynthesis is a complex process that requires a substantial energetic and material commitment on part of the cell (30), like PG synthesis. Thus, another attractive model for the function of these PBP cofactors is one where they coordinate PG synthesis with LTA biogenesis.

The growing epidemic of antibiotic-resistant bacteria. Bacterial infections and disease are on the rise due to the growing epidemic of antibiotic-resistant bacteria. Infectious disease is now the second leading cause of death worldwide (27). Since the dawn of the antibiotic age, widespread misuse of antibiotics has led bacteria to evolve various mechanisms of antibiotic resistance, leading to resistance to most commercially available antibiotics (11). The most deadly classes of antibiotic resistant organisms include the ESKAPE pathogens, multi-drug resistant (MDR) and pandrug-

resistant (PDR) Gram-negative bacteria (13), and MDR and extensively drug-resistant strains (XDR) of *Mycobacterium tuberculosis* (12, 14).

The "ESKAPE" pathogens (*Enterococcus faecium*, *Staphylococcus aureus*, *Klebsiella pneumoniae*, *Acinetobacteria baumanii*, *Pseudomonas aeruginosa*, and *Enterobacter* species) currently cause the majority of hospital-acquired infections in the United States and are emerging as significant pathogens worldwide (5). These pathogens obtain their name because they effectively "escape" inhibition by clinically used antibacterials. Data from the Centers for Disease Control and Prevention (CDC) show increasing rates of infection due to methicillin-resistant *S. aureus*, vancomycin-resistant *E. faecium* (VRE), and fluoroquinolone-resistant *P. aeruginosa* (28). About 100,000 patients per year are infected with MRSA, and more people now die of MRSA infections (approximately 19,000 patients per year) in US hospitals than of HIV/AIDS and tuberculosis combined (4, 11, 20, 32). Drastic measures need to be taken to prevent infections caused by these ESKAPE pathogens from becoming a worldwide epidemic.

New arsenal of antibacterials desperately needed. Antibiotics have been crucial in doubling the average life expectancy in the US (21). They are required to treat severe and life-threatening bacterial infections. But the overuse of these antibiotics has given rise to a breed of super bacteria that are resistant to most, if not all, currently used antibiotics (32). However, while antibiotic resistance is on the rise, the discovery of new antibiotics is not (14). Due to economic problems, many large pharmaceutical companies left the field of antibiotic discovery. Thus the number of antibiotics

approved by the US Food and Drug Administration (FDA) has decreased from sixteen in 1983 to only four in 2007 (**Figure 4.2**) (11). To combat infectious disease, efforts must continue to discover and develop new antibiotics.

PBP accessory factors and antibiotic development. The discovery of penicillin ushered in a new era for clinical medicine. Its ability to inhibit the PBPs and induce bacteriolysis opened new avenues for treating bacterial infections, and the PBPs themselves have proven to be very effective drug targets. Regardless of their precise biochemical function, the discovery of LpoA and LpoB as essential for the *in vivo* function of the PBPs suggests new avenues for antibiotic development to help combat drug-resistant bacteria. By investigating how the Lpo factors control PBP function, we may develop a better understanding of the PG synthesis process as a whole.

Furthermore, the observation that LpoA is essential in *H. influenzae* (38) suggests that direct targeting of PBP accessory proteins might be effective in some circumstances. Bioinformatics analysis using the STRING program (25) shows that even the ESKAPE pathogens mentioned above many contain weak homologs of LpoA, LpoB, or both (**Table 4.1**). However, it is not known whether the organisms that contain only a LpoA homolog absolutely require it. Regardless, further study of the mechanisms by which these accessory factors influence PBP activity is likely to reveal novel ways to block PBP function for therapeutic purposes.

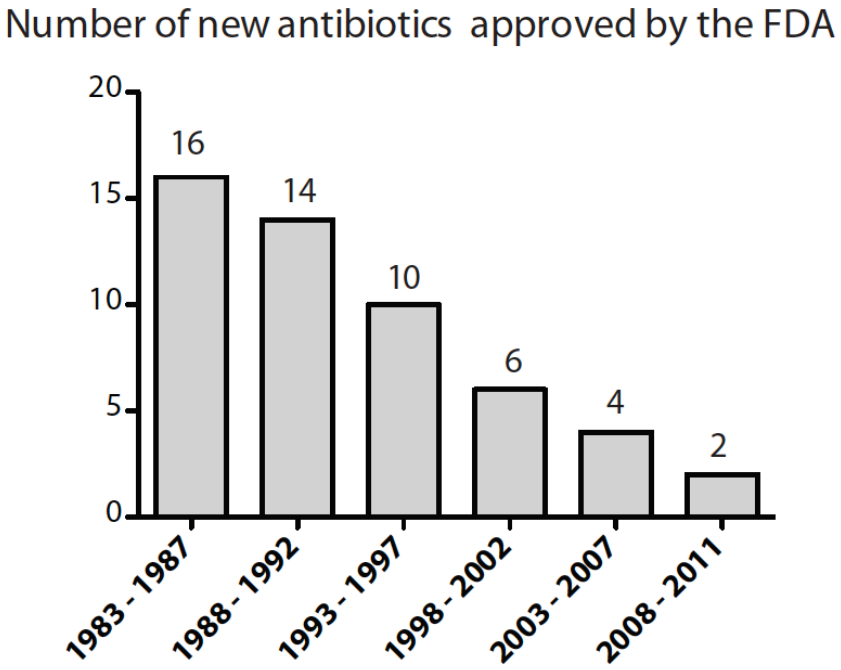

Figure 4.2. Antibiotics approved for clinical use by the US Food and Drug Administration (FDA). This graph shows the steady decline of the number of antibiotics approved by the FDA within the past two decades (11, 18, 32).

Table 4.1. Lpo factor homologs in the ESKAPE pathogens.

	Gram-positive or Gram-negative?	LpoA homolog?	LpoB homolog?
Enterococcus spp.	Gram-positive	-	-
Staphylococcus aureus	Gram-positive	✓[a]	-
Klebsiella pneumoniae	Gram-negative	✓	✓
Acinetobacter spp.	Gram-negative	✓[a]	-
Pseudomonas aeruginosa	Gram-negative	✓	-
Enterobacter sp. 638	Gram-negative	✓	✓

[a]weak homology

References

1. **Alaedini, A.**, **and R. A. Day**. 1999. Identification of two penicillin-binding multienzyme complexes in Haemophilus influenzae. Biochem. Biophys. Res. Commun. **264**:191–195.

2. **Barrett, D.**, **T.-S. A. Wang**, **Y. Yuan**, **Y. Zhang**, **D. Kahne**, **and S. Walker**. 2007. Analysis of glycan polymers produced by peptidoglycan glycosyltransferases. J Biol Chem **282**:31964–31971.

3. **Bertsche, U.**, **T. Kast**, **B. Wolf**, **C. Fraipont**, **M. E. G. Aarsman**, **K. Kannenberg**, **M. von Rechenberg**, **M. Nguyen-Distèche**, **T. den Blaauwen**, **J.-V. Höltje**, **and W. Vollmer**. 2006. Interaction between two murein (peptidoglycan) synthases, PBP3 and PBP1B, in Escherichia coli. Mol Microbiol **61**:675–690.

4. **Boucher, H. W.**, **and G. R. Corey**. 2008. Epidemiology of methicillin-resistant Staphylococcus aureus. Clin. Infect. Dis. **46 Suppl 5**:S344–9.

5. **Boucher, H. W.**, **G. H. Talbot**, **J. S. Bradley**, **J. E. Edwards**, **D. Gilbert**, **L. B. Rice**, **M. Scheld**, **B. Spellberg**, **and J. Bartlett**. 2009. Bad bugs, no drugs: no ESKAPE! An update from the Infectious Diseases Society of America. Clin. Infect. Dis. **48**:1–12.

6. **Cabeen, M.**, **and C. Jacobs-Wagner**. 2007. Skin and bones: the bacterial cytoskeleton, cell wall, and cell morphogenesis. The Journal of Cell Biology **175**:381-387.

7. **Cabeen, M. T.**, **and C. Jacobs-Wagner**. 2005. Bacterial cell shape. Nat Rev Micro **3**:601–610.

8. **Cayley, D. S.**, **H. J. Guttman**, **and M. T. Record**. 2000. Biophysical characterization of changes in amounts and activity of Escherichia coli cell and compartment water and turgor pressure in response to osmotic stress. Biophys J **78**:1748–1764.

9. **Cooper, S.**, **M. L. Hsieh**, **and B. Guenther**. 1988. Mode of peptidoglycan synthesis in Salmonella typhimurium: single-strand insertion. J Bacteriol **170**:3509–3512.

10. **de Jonge, B. L.**, **F. B. Wientjes**, **I. Jurida**, **F. Driehuis**, **J. T. Wouters**, **and N. Nanninga**. 1989. Peptidoglycan synthesis during the cell cycle of Escherichia coli: composition and mode of insertion. J Bacteriol **171**:5783–5794.

11. **Demain, A. L.** 2009. Antibiotics: natural products essential to human health. Med Res Rev **29**:821–842.

12. **Dorman, S. E.**, **and R. E. Chaisson**. 2007. From magic bullets back to the magic mountain: the rise of extensively drug-resistant tuberculosis. Nature Medicine **13**:295–298.

13. **Falagas, M. E.**, **I. A. Bliziotis**, **S. K. Kasiakou**, **G. Samonis**, **P. Athanassopoulou**, **and A. Michalopoulos**. 2005. Outcome of infections due to pandrug-resistant (PDR) Gram-negative bacteria. BMC Infect. Dis. **5**:24.

14. **Fischbach, M. A.**, **and C. T. Walsh**. 2009. Antibiotics for emerging pathogens. Science **325**:1089–1093.

15. **Gerding, M. A.**, **Y. Ogata**, **N. D. Pecora**, **H. Niki**, **and P. A. J. de Boer**. 2007. The trans-envelope Tol-Pal complex is part of the cell division machinery and required for proper outer-membrane invagination during cell constriction in E. coli. Mol Microbiol **63**:1008–1025.

16. **Goodell, E. W.**, **and U. Schwarz**. 1975. Sphere-rod morphogenesis of Escherichia coli. J Gen Microbiol **86**:201–209.

17. **Höltje, J. V.** 1998. Growth of the stress-bearing and shape-maintaining murein sacculus of Escherichia coli. Microbiol Mol Biol Rev **62**:181–203.

18. **Infectious Diseases Society of America (IDSA)**, **B. Spellberg**, **M. Blaser**, **R. J. Guidos**, **H. W. Boucher**, **J. S. Bradley**, **B. I. Eisenstein**, **D. Gerding**, **R. Lynfield**, **L. B. Reller**, **J. Rex**, **D. Schwartz**, **E. Septimus**, **F. C. Tenover**, **and D. N. Gilbert**. 2011. Combating antimicrobial resistance: policy recommendations to save lives. Clin. Infect. Dis. **52 Suppl 5**:S397–428.

19. **Kato, J.**, **H. Suzuki**, **and Y. Hirota**. 1985. Dispensability of either penicillin-binding protein-1a or -1b involved in the essential process for cell elongation in Escherichia coli. Mol. Gen. Genet. **200**:272–277.

20. **Klevens, R. M.**, **J. R. Edwards**, **F. C. Tenover**, **L. C. McDonald**, **T. Horan**, **R. Gaynes**, **National Nosocomial Infections Surveillance System**. 2006. Changes in the epidemiology of methicillin-resistant Staphylococcus aureus in intensive care units in US hospitals, 1992-2003. Clin. Infect. Dis. **42**:389–391.

21. **Lederberg, J.** 2000. Infectious history. Science **288**:287–293.

22. **Lewenza, S.**, **D. Vidal-Ingigliardi**, **and A. P. Pugsley**. 2006. Direct visualization of red fluorescent lipoproteins indicates conservation of the membrane sorting rules in the family Enterobacteriaceae. J Bacteriol **188**:3516–3524.

23. **Lupoli, T. J.**, **H. Tsukamoto**, **E. H. Doud**, **T.-S. A. Wang**, **S. Walker**, **and D. Kahne**. 2011. Transpeptidase-Mediated Incorporation of d-Amino Acids into Bacterial Peptidoglycan. J Am Chem Soc **133**:10748–10751.

24. **Margolin, W.** 2009. Sculpting the Bacterial Cell. Current Biology **19**:R812–R822.

25. **Mering, von, C.**, **L. J. Jensen**, **M. Kuhn**, **S. Chaffron**, **T. Doerks**, **B. Krüger**, **B. Snel**, **and P. Bork**. 2007. STRING 7--recent developments in the integration and prediction of protein interactions. Nucleic Acids Research **35**:D358–62.

26. **Müller, P.**, **C. Ewers**, **U. Bertsche**, **M. Anstett**, **T. Kallis**, **E. Breukink**, **C. Fraipont**, **M. Terrak**, **M. Nguyen-Distèche**, **and W. Vollmer**. 2007. The essential cell division protein FtsN interacts with the murein (peptidoglycan) synthase PBP1B in Escherichia coli. J Biol Chem **282**:36394–36402.

27. **Nathan, C.** 2004. Antibiotics at the crossroads. Nature **431**:899–902.

28. **National Nosocomial Infections Surveillance System**. 2004. National Nosocomial Infections Surveillance (NNIS) System Report, data summary from January 1992 through June 2004, issued October 2004. Am J Infect Control **32**:470–485.

29. **Paradis-Bleau, C.**, **M. Markovski**, **T. Uehara**, **T. J. Lupoli**, **S. Walker**, **D. E. Kahne**, **and T. G. Bernhardt**. 2010. Lipoprotein cofactors located in the outer membrane activate bacterial cell wall polymerases. Cell **143**:1110–1120.

30. **Rahman, O.**, **L. G. Dover**, **and I. C. Sutcliffe**. 2009. Lipoteichoic acid biosynthesis: two steps forwards, one step sideways? Trends Microbiol **17**:219–225.

31. **Schwarz, U.**, **and W. Leutgeb**. 1971. Morphogenetic aspects of murein structure and biosynthesis. J Bacteriol **106**:588–595.

32. **Taubes, G.** 2008. The bacteria fight back. Science **321:**356-361.

33. **Typas, A.**, **M. Banzhaf**, **C. A. Gross**, **and W. Vollmer**. 2011. From the regulation of peptidoglycan synthesis to bacterial growth and morphology. Nat Rev Micro **10:**123-136.

34. **Typas, A.**, **M. Banzhaf**, **B. van den Berg van Saparoea**, **J. Verheul**, **J. Biboy**, **R. J. Nichols**, **M. Zietek**, **K. Beilharz**, **K. Kannenberg**, **M. von Rechenberg**,

E. Breukink, **T. den Blaauwen**, **C. A. Gross**, **and W. Vollmer**. 2010. Regulation of peptidoglycan synthesis by outer-membrane proteins. Cell **143**:1097–1109.

35. **Vijayalakshmi, J.**, **B. J. Akerley**, **and M. A. Saper**. 2008. Structure of YraM, a protein essential for growth of Haemophilus influenzae. Proteins **73**:204–217.

36. **Vollmer, W.**, **M. von Rechenberg**, **and J. V. Höltje**. 1999. Demonstration of molecular interactions between the murein polymerase PBP1B, the lytic transglycosylase MltA, and the scaffolding protein MipA of Escherichia coli. J Biol Chem **274**:6726–6734.

37. **Vollmer, W.**, **D. Blanot**, **and M. A. de Pedro**. 2008. Peptidoglycan structure and architecture. FEMS Microbiol Rev **32**:149–167.

38. **Wong, S. M.**, **and B. J. Akerley**. 2003. Inducible expression system and marker-linked mutagenesis approach for functional genomics of Haemophilus influenzae. Gene **316**:177–186.

39. **Yousif, S. Y.**, **J. K. Broome-Smith**, **and B. G. Spratt**. 1985. Lysis of Escherichia coli by beta-lactam antibiotics: deletion analysis of the role of penicillin-binding proteins 1A and 1B. J Gen Microbiol **131**:2839–2845.

Appendix 1:

Identification of an ABC transporter-like complex that governs cell wall hydrolysis during cell division

Author contributions:

The work presented in this Appendix was a collaborative effort. All authors had a role in conceptualizing experiments, interpreting data, and editing the manuscript while Thomas Bernhardt wrote the manuscript. Much of the work described in this chapter was performed by Desirée C. Yang, a graduate student in our lab, and is a part of her dissertation. She had performed the necessary experiments to show: (i) the subcellular localization of EnvC in wild-type and FtsEX- cells, (ii) that EnvC interacts with loop 1 of FtsX using the bacterial two-hybrid assay and purified protein pulldowns, (iii) that ATPase-defective FtsE results in a cell separation defect, and (iv) that EnvC is no longer recruited to the site of division in FtsX mutants lacking loop 1. My contribution was to help establish a genetic link between FtsEX and EnvC. In the *slb* screen, I identified that transposon insertions in either gene are synthetically lethal with the absence of PBP1b. Nick Peters verified these results by using a PBP1b depletion strain that lacked FtsEX or EnvC. He also performed the localization experiments along with western blots showing that fluorescently-tagged EnvC was stable with and without FtsEX. Katherine Parzych performed experiments showing that Δ*envC* and Δ*ftsEX* mutants phenocopy each other in a Δ*nlpD* strain background. She also showed that EnvC is stable in the absence of FtsEX.

An ABC transporter-like complex governs cell wall hydrolysis at the bacterial cytokinetic ring

Desirée C. Yang, Nick T. Peters†, Katherine R. Parzych†, Tsuyoshi Uehara, Monica Markovski, and Thomas G. Bernhardt

Department of Microbiology and Molecular Genetics

Harvard Medical School

Boston, MA 02115

†These authors contributed equally to this work.

Reprinted with permission from *PNAS*

Summary

ABC transporters are ubiquitous membrane protein complexes that move substrates across membranes. They do so using ATP-induced conformational changes in their nucleotide binding domains (NBDs) to alter the conformation of the transport cavity formed by their transmembrane domains (TMDs). In *Escherichia coli,* an ABC transporter-like complex composed of FtsE (NBD) and FtsX (TMD) has long been known to be important for cytokinesis, but its role in the process has remained mysterious. Here we identify FtsEX as a regulator of cell wall hydrolysis at the division site. Cell wall material synthesized by the division machinery is initially shared by daughter cells and must be split by hydrolytic enzymes called amidases to drive daughter cell separation. We recently showed that the amidases require activation at the cytokinetic ring by proteins with LytM domains, of which EnvC is the most critical. In this report, we demonstrate that the FtsEX directly recruits EnvC to the septum via an interaction between EnvC and a periplasmic loop of FtsX. Importantly, we also show that FtsEX variants predicted to be ATPase defective still recruit EnvC to the septum but fail to promote cell separation. Our results thus suggest the attractive possibility that amidase activation via EnvC in the periplasm is regulated by conformational changes in the FtsEX complex mediated by ATP hydrolysis in the cytoplasm. Since FtsE has been reported to interact with the tubulin-like FtsZ protein, this provides a potential mechanism for coupling amidase activity with the contraction of the FtsZ cytoskeletal ring.

Introduction

Cytokinesis in *Escherichia coli* and other bacteria is mediated by a ring-shaped multi-protein machine called the septal ring or divisome (15). Assembly of this machine begins with the polymerization of the tubulin-like FtsZ protein into a ring-like structure just underneath the cell membrane at the prospective site of division (7). Several FtsZ-binding proteins have been identified in *E. coli* (FtsA, ZipA, ZapA, and ZapC). Along with the ZapA-binding protein ZapB, they appear to play partially redundant roles in the formation and stabilization of the Z-ring structure (11, 17-19, 22, 26, 28, 42). Once formed, the Z-ring promotes septal ring assembly by facilitating the recruitment of the remaining essential and non-essential division proteins to the division site according to a mostly linear dependency pathway (15).

Because the functions of many of its components are ill-defined, the mechanism(s) by which the septal ring promotes cell constriction remain largely mysterious (15). One of the most enigmatic division factors has been the ABC-transporter-like complex formed by FtsE and FtsX (FtsEX) (49). ABC transporters are integral membrane protein complexes that use the energy of ATP hydrolysis to transport substrates across membranes (45). They are typically composed of two polytopic transmembrane domains (TMDs) and a pair of cytosolic nucleotide binding domains (NBDs) often called ATP-binding cassettes (ABCs). Structural studies of complete ABC-transporters indicate that these complexes undergo remarkable conformational changes in response to nucleotide binding and hydrolysis (45). The NBD subunits interconvert between an open and a closed conformation at the membrane surface during an ATP hydrolysis cycle (45). These conformational changes

are, in turn, transmitted to the TMD subunits to promote transitions between outward-facing and inward-facing conformations of the central cavity formed by the TMDs (45). Transport is thus promoted by alternating access of the substrate-binding site to opposing sides of the membrane.

The role of the FtsEX complex in cell division has remained unclear for some time (21, 46). FtsE is the NBD component of the complex and FtsX is the TMD component (16) (**Figure 1.1A-B**). Both factors localize to the septal ring and are conditionally essential for cell division (49). In medium of low osmotic strength, such as LB without added NaCl, cells lacking FtsEX display a lethal division defect (16, 49). They form smooth filaments that assemble Z-rings, but these structures are compromised because they fail to recruit FtsK and other downstream division factors (49). This phenotype along with the observation that FtsE and FtsX interact with several different division proteins (10, 35) has lead to the idea that one important function of FtsEX is to stabilize the septal ring structure (1, 44, 48). Consistent with this idea, the division defect of FtsEX^{-} cells can be partially suppressed by the overproduction of other division proteins (FtsZ, FtsN, or FtsP) (44). Increasing the osmolarity of the medium and lowering the growth temperature also restores division function to FtsEX^{-} mutants (16, 44, 48, 49). The mechanisms by which high osmolarity or division protein overproduction

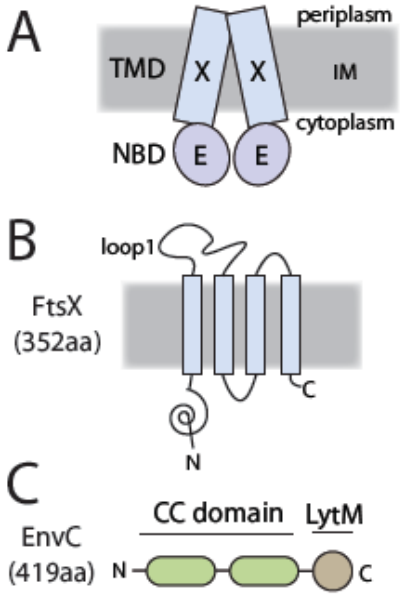

Figure A1.1. Domain structure of FtsEX and EnvC. A. Shown is a diagram of the FtsEX ABC system. FtsX (X) is the transmembrane domain (TMD) component and FtsE (E) is the ATPase component (16). The complex is in the inner membrane (IM) with FtsE located on the cytoplasmic face of the membrane. **B.** Membrane topology of FtsX as determined by Weiss and co-workers (1). The loop1 domain is composed of residues 93-223. Membrane orientation is the same as in (A). **C.** Domain structure of EnvC. EnvC is a periplasmic protein. It possesses an N-terminal signal sequence (residues 1-34), two relatively long segments predicted to form coiled-coils (CC domain, residues 35-277), and a C-terminal LytM domain (residues 278-419) needed for amidase activation.

bypass the FtsEX requirement for cell division are not known. However, these growth conditions presumably allow essential division proteins downstream of FtsEX in the recruitment hierarchy to assemble at the division site in the absence of the complex. Indeed, FtsN has been shown to localize to sites of constriction in FtsEX$^-$ cells grown in LB with 1% NaCl (49). Over the years, many functions for FtsEX have been proposed, most of them assuming that it must transport a substrate (1) (and references therein). In this report, we present evidence that FtsEX may not be a transporter at all but is instead an important regulator of cell wall turnover at the division site.

Most bacteria surround themselves with a polysaccharide cell wall matrix called peptidoglycan (PG) (55). This meshwork is essential for cellular integrity and is composed of glycan strands connected to one another by crosslinks between attached peptide moieties (55) (**Figure A1.2**). During cytokinesis in gram-negative bacteria, septal PG is synthesized by the divisome (15). This material is thought to be initially shared by the developing daughter cells and must be split to facilitate outer membrane constriction and daughter cell separation (15) (**Figure A1.2**). Septal PG splitting is mediated by the periplasmic PG amidases, AmiA, AmiB, and AmiC (30). Amidases are PG hydrolases that break crosslinks in the PG meshwork by cleaving bonds that link stem peptides to the glycan strands. Mutants lacking amidase activity complete inner membrane constriction and fusion. However, they fail to split septal PG and form long chains of cells connected by shared layers of PG and a partially constricted outer membrane layer (30, 43).

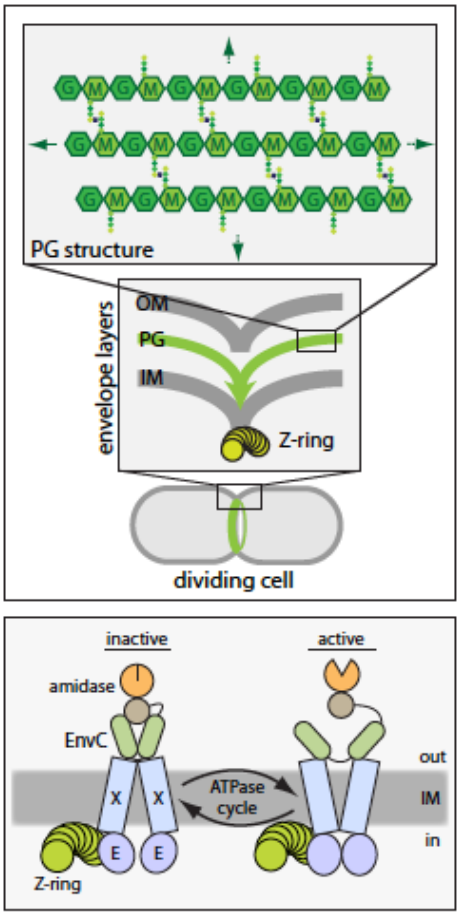

Figure A1.2. Graphical summary of the results described in this paper. See text for details.

The amidases must be tightly controlled to prevent them from creating lesions in the cell wall that can result in cell lysis. Part of this regulation appears to rely on the fact that the PG amidases alone are weakly active enzymes (54). To efficiently hydrolyze PG, they require activation by EnvC and NlpD (54), divisome-associated proteins with LytM domains (Pfam, Peptidase_M23) (4, 53). EnvC specifically activates AmiA and AmiB while NlpD specifically activates AmiC (24). Accordingly, mutants lacking both EnvC and NlpD have a chaining phenotype that resembles a triple amidase mutant (53). A major unresolved question has been understanding how the LytM factors are themselves controlled so that amidase activity at the septum is properly coordinated with other activities of the septal ring, such as membrane invagination and septal PG synthesis.

Using a genetic screen designed to identify factors involved in cell wall assembly (40), we found that mutations in *ftsEX* and *envC* are synthetically lethal with loss-of-function mutations in a common set of genes. This suggested that FtsEX and EnvC might participate in the same biochemical pathway. Indeed, when grown under permissive conditions, FtsEX^{-} cells phenocopy the cell separation defect displayed by EnvC^{-} cells. We further show that EnvC requires FtsEX for its recruitment to the division site and that EnvC interacts directly with the large periplasmic loop domain of FtsX. Importantly, we also show that FtsEX variants predicted to be ATPase defective still recruit EnvC to the septum but fail to promote cell separation. Our results thus suggest the attractive possibility that FtsX regulates amidase activation by EnvC in the periplasm via conformational changes induced by FtsE-mediated ATP hydrolysis on the opposite side of the membrane. Since FtsE has been reported to interact with FtsZ

(10), this provides a potential mechanism for directly coupling septal PG hydrolysis with the contraction of the Z-ring during cell constriction. Interestingly, the accompanying report by Sham and co-workers (50) similarly connects FtsEX with cell separation in the gram-positive pathogen *Streptococcus pneumoniae*, indicating that the regulation of cell wall turnover is likely to be a broadly conserved function for FtsEX.

Results

***ftsEX* and *envC* mutants share common genetic interactions.** To identify factors important for cell wall biogenesis, we recently performed a genetic screen for mutations synthetically lethal with the inactivation of the PG synthase PBP1b (*slb* mutants) (40). In addition to mutants in the *lpoA* gene coding for a lipoprotein cofactor required for the activity of PBP1a (40, 52), we isolated mutants with transposon insertions in *envC* and *ftsEX*. The *ftsEX* mutant was isolated in a screen performed at room temperature, a condition that we find suppresses the lethal effects of FtsEX inactivation. To confirm the synthetic lethality of the mutant combinations, Δ*envC* and Δ*ftsEX* alleles were transduced into strain MM11 [P_{ara}::*ponB*] harboring the low copy plasmid pTB63 [*ftsQAZ*], which expresses the *ftsQAZ* operon from native promoters and suppresses the $FtsEX^{-}$ growth defect. In MM11, the native *ponB* promoter was replaced with P_{ara} such that *ponB* expression is arabinose-dependent (40). Depletion of PBP1b in the absence of FtsEX or EnvC was confirmed to be lethal (**Figure A1.3A**). The terminal phenotype in both cases was cell lysis. Since EnvC is needed to activate the amidases AmiA and AmiB at the developing septum, we tested whether the combined inactivation of AmiA and AmiB was also lethal upon PBP1b depletion. This indeed

proved to be the case (**Figure A1.3A**). We do not currently know why the inactivation of FtsEX, EnvC, or AmiA/AmiB renders PBP1b essential for growth. Nevertheless, the observed phenotypes suggested to us that FtsEX may function in the process of septal PG splitting with EnvC and the amidases.

The loss of FtsEX function was previously shown to be synthetically lethal with the deletion of *ftsP* (*sufI*) (44). We confirmed this and found that the depletion of EnvC was also synthetically lethal with Δ*ftsP* (**Figure A1.3B-C**), thus further connecting the functions of EnvC and FtsEX. As expected for proteins functioning in the same pathway, loss of EnvC function was not lethal upon FtsEX depletion (**Figure A1.3B**).

FtsEX is required for daughter cell separation. While performing the FtsEX depletion experiments in Figure A1.3B, we found that growth on minimal agar at 37ºC partially suppressed the FtsEX$^-$ growth defect. We assume this is due to the higher osmolarity of the medium relative to standard LB (0.5% NaCl) and the slower overall growth rate of the cells. The suppression in liquid minimal medium was even more pronounced, especially when cells were grown at 30ºC. Here, FtsEX$^-$ cells displayed a much more mild division defect resembling that typically observed for EnvC$^-$ cells (53) (see below). A similar division defect was also observed for Δ*envC* and Δ*ftsEX* mutants harboring an *ftsQAZ* overproducing plasmid (pTB63) when we grew them in LB (1% NaCl) (**Figure A1.4A-C**). It thus appeared that under conditions that suppressed the septal ring stability defect of FtsEX$^-$ cells, a potential role for the FtsEX complex in EnvC-mediated cell separation was revealed. Interestingly, we note that, although not as severe

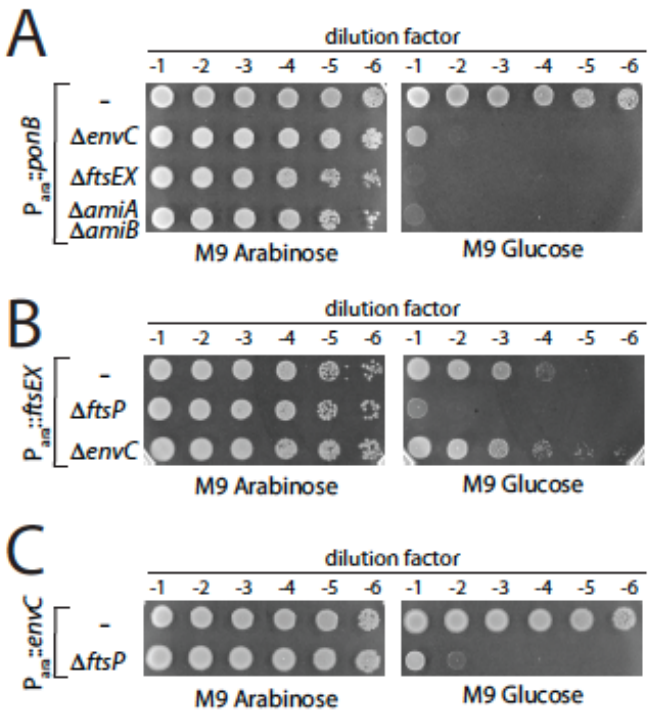

Figure A1.3. Shared synthetic lethal phenotypes of *envC* and *ftsEX* mutants.

A. Cells of MM11/pTB63 [P_{ara}::*ponB*/*ftsQAZ*] and its Δ*envC*, Δ*ftsEX*, or Δ*amiA* Δ*amiB* derivatives were grown overnight in M9 arabinose medium supplemented with 5 μg/ml tetracycline (Tet[5]) at 37°C. Following normalization for cell density (OD_{600} = 2), the resulting cultures were serially diluted (10^{-1}-10^{-6}) and 5 μl of each dilution was spotted on the indicated medium. Plates were incubated overnight at 37°C and photographed. **B.** Cells of TU191(attλTU188) [Δ*ftsEX* (P_{ara}::*ftsEX*)] and its Δ*envC* or Δ*ftsP* derivatives were processed as in (A) except growth was in the absence of tetracycline. **C.** Cells of TB140(attλTD25) [Δ*envC* (P_{ara}::*envC*)] and its Δ*ftsP* derivative were grown and processed as in (**B**).

as the FtsEX$^-$ division defect, EnvC$^-$ cells display a lethal filamentation phenotype when grown in LB without added NaCl at 42^{o}C (29, 33, 47). This suggests that at least part of the constriction defect of FtsEX$^-$ cells may be the result of EnvC inactivation.

We previously showed that cells lacking EnvC become dependent on NlpD for cell separation (53). Cells lacking EnvC and NlpD appear to be completely defective in cell separation and form very long chains that resemble triple amidase mutants (53) (**Figure A1.4D-F**). We reasoned that if FtsEX is truly required for EnvC-mediated cell separation, the simultaneous inactivation of FtsEX and NlpD should also result in a severe chaining phenotype. This indeed proved to be the case (**Figure A1.4D-F**). We therefore conclude that FtsEX is required for EnvC to promote septal PG splitting.

EnvC is stable and released into the periplasm in the absence of FtsEX. A potential reason for the FtsEX-EnvC connection is that EnvC requires FtsEX for its stable accumulation. To investigate this, we compared EnvC levels in total cell extracts prepared from WT versus Δ*ftsEX* cells (**Figure A1.5A**). Immunoblotting with affinity-purified, anti-EnvC polyclonal antibodies revealed that similar amounts of EnvC accumulate whether or not cells produce FtsEX (**Figure A1.5A, compare lanes 1-3 with 7-9**). We did, however, observe low concentrations of smaller immuno-reactive species in the Δ*ftsEX* extract that were not seen in the WT or Δ*envC* extracts, indicating that a small portion of EnvC is probably proteolytically processed in the absence of FtsEX (**Figure A1.5A**). This low level of processing is unlikely to explain the EnvC$^-$ phenotype of Δ*ftsEX* cells.

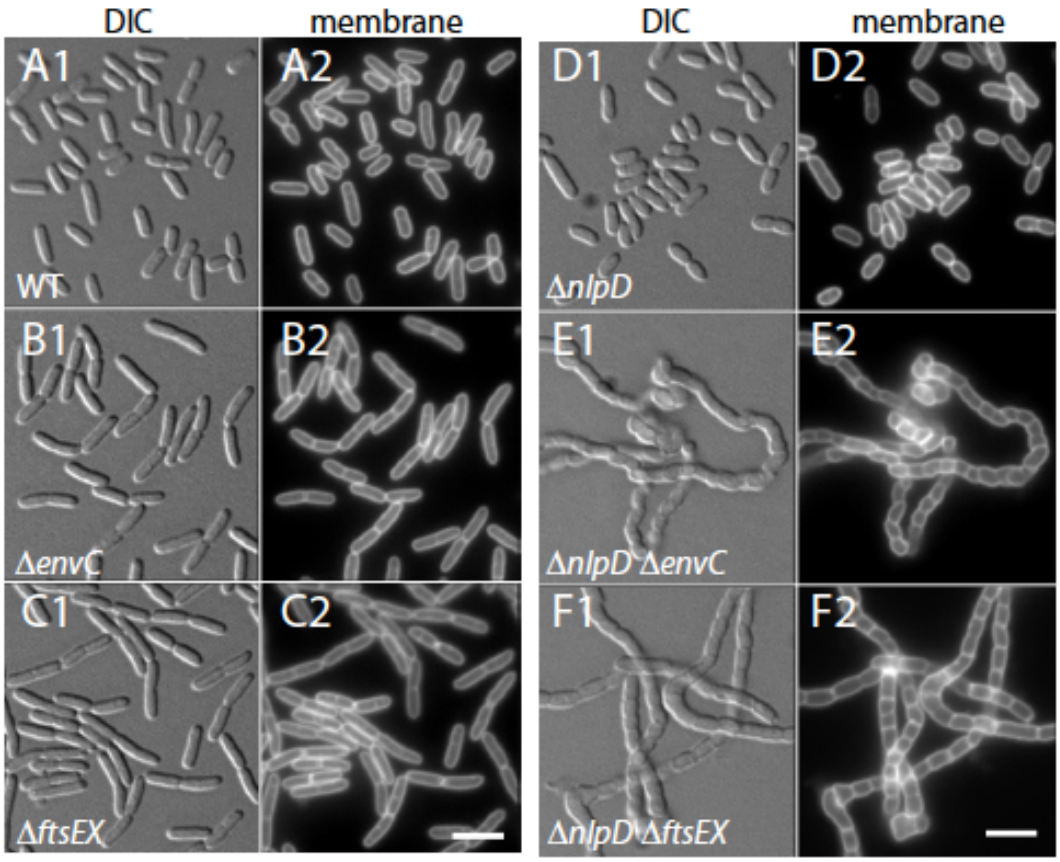

Figure A1.4. FtsEX$^-$ and EnvC$^-$ cells have similar division defects. Cells of TB28 [WT] (**A**), KP4 [Δ*envC*] (**B**), KP5 [Δ*ftsEX*] (**C**), TB145 [Δ*nlpD*] (**D**), KP6 [Δ*nlpD* Δ*envC*] (**E**), and KP7 [Δ*nlpD* Δ*ftsEX*] (**F**) harboring pTB63 [*ftsQAZ*] were grown overnight in LB-Tet[5] [1.0% (**A-C**) or 1.5% (**D-F**) NaCl] at 30°C. Cultures were diluted 1:200 into the same medium and grown at 30°C to an OD_{600} of 0.6-0.8. Cells were then incubated with the fixable membrane stain FM1-43FX (5 μg/ml) for 10 min and fixed. Fixed cells were visualized on 2% agarose pads using DIC (panels **A1-F1**) and GFP (panels **A2-F2**) optics. Bars equal 4 microns.

Since FtsEX is related to ABC transporters, one possible way in which it might promote EnvC function is by facilitating its export to the periplasm. To investigate this, we fractionated cells to determine the subcellular localization of EnvC in the presence or absence of FtsEX. WT and Δ*ftsEX* cells were suspended in buffer containing sucrose and converted to spheroplasts by the addition of EDTA and lysozyme. In WT cells, EnvC pelleted with the spheroplasts rather than remaining in the soluble periplasmic fraction like the MalE control (**Figure A1.5B, lanes 1-3**). In contrast, EnvC was found almost exclusively in the periplasmic fraction from FtsEX- cells. The FtsZ and MalE fractionation controls indicated that this change in EnvC localization was not due to altered fractionation properties of the $FtsEX^-$ cells (**Figure A1.5B, lanes 4-6**). Thus, FtsEX is not required for the export of EnvC to the periplasm. This is consistent with previous reports suggesting that EnvC is a Sec substrate (29) and that its signal sequence can be functionally replaced by alternative signal peptides for Tat- or Sec-mediated transport (4, 54). Furthermore, the fractionation results suggest that EnvC remains associated with the outer face of the inner membrane of WT cells, possibly through an interaction with FtsX, and that it is released into the periplasm in the absence of this interaction (see below).

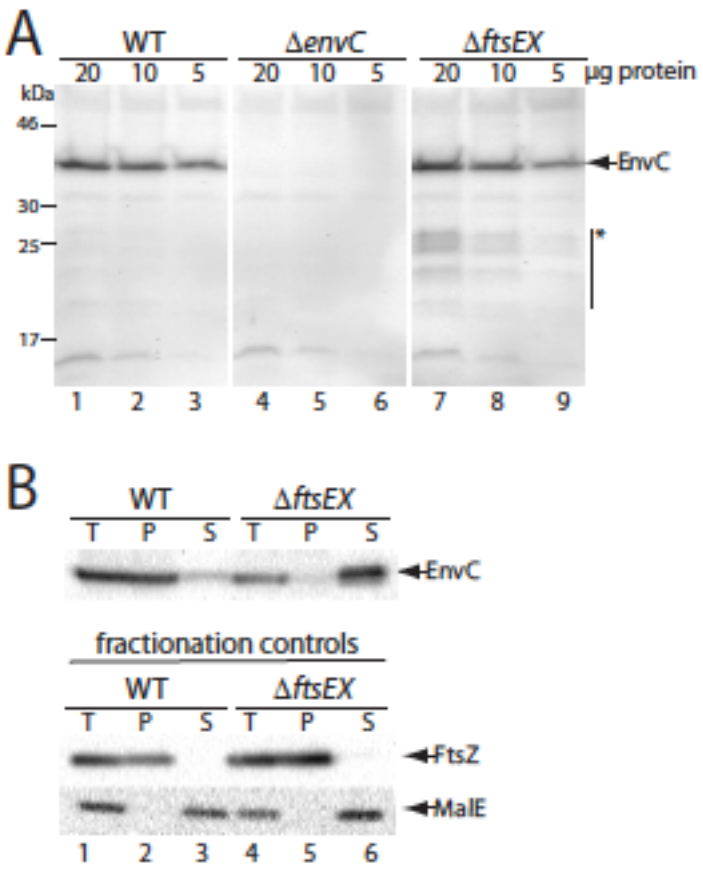

Figure A1.5. Change in EnvC subcellular localization in the absence of FtsEX. A. Cells of TB28 [WT], KP4 [Δ*envC*], or KP5 [Δ*ftsEX*] harboring pTB63 [*ftsQAZ*] were grown overnight in LB (1.0% NaCl)-Tet^{5} at 30^{o}C. Cultures were diluted 1:100 into LB-Tet^{5} and grown at 30^{o}C to an OD_{600} of 0.66-0.72. Cell extracts were then prepared and the indicated total protein amounts (*µ*g) were subjected to immunoblotting using affinity purified EnvC antibodies. Arrow indicates position of ^{FL}EnvC bands, and the bar with the asterisk highlights what appears to be a small amount of EnvC degradation products in extracts from the Δ*ftsEX* mutant. Positions of the molecular weight markers are indicated on the left. **B.** Cultures of the strains in (**A**) were grown as above to an OD_{600} of 0.39-0.46. **(Legend continued on next page.)**

Figure A1.5 (Continued) One aliquot of cells was used to prepare a total cell extract. The remaining cells were converted to spheroplasts and pelleted by centrifugation. The resulting pellet (P) and supernatant (S) fractions along with the total cell extract (T) were analyzed by SDS-PAGE and immunoblotting for EnvC, FtsZ, and MalE as indicated. FtsZ and MalE served as markers for the cytoplasm/spheroplast membranes and periplasm, respectively.

FtsEX is required for the recruitment of EnvC to the septal ring. In addition to subcellular fractionations, we also investigated the role of FtsEX in the recruitment of EnvC to the septal ring. To do so, we constructed an FtsEX depletion strain NP69(*att*λTU188)(*att*HKTB316) [Δ*ftsEX* Δ*envC zapA-gfp* (P_{ara}::*ftsEX*)(P_{lac}::*envC-mCherry*)]. In this strain, the native *ftsEX* locus was deleted and a second copy of *ftsEX* under arabinose promoter (P_{ara}) control was integrated at the λ *att* site. The strain also encodes *zapA-gfp* at the native *zapA* locus and expresses *envC-mCherry* from an expression cassette integrated at the HK022 *att* site. When grown in M9 maltose medium containing a small amount of arabinose (0.01%), cells of NP69(*att*λTU188)(*att*HKTB316) divided normally and displayed bands of both EnvC-mCherry and ZapA-GFP at the division sites of most cells (**Figure A1.6A**). Conversely, when the same cells were grown in M9 maltose medium containing a small amount of glucose (0.01%) to repress P_{ara}::*ftsEX*, they displayed the heterogeneous cell constriction and separation phenotype typical of $FtsEX^-$ and $EnvC^-$ cells (Figure A1.6B). While most cells appeared capable of cell division, many were elongated and appeared to have difficulty completing cell separation. The Z-ring marker, ZapA-GFP, formed rings/bands in these elongated cells at fairly regular intervals, but EnvC-mCherry failed to be recruited to these structures (**Figure A1.6B**). Immunoblot analysis indicated that this localization defect was not due to excessive degradation of the EnvC-mCherry fusion (**Figure A1.7**). We thus conclude that FtsEX is required for the recruitment of EnvC to the septal ring.

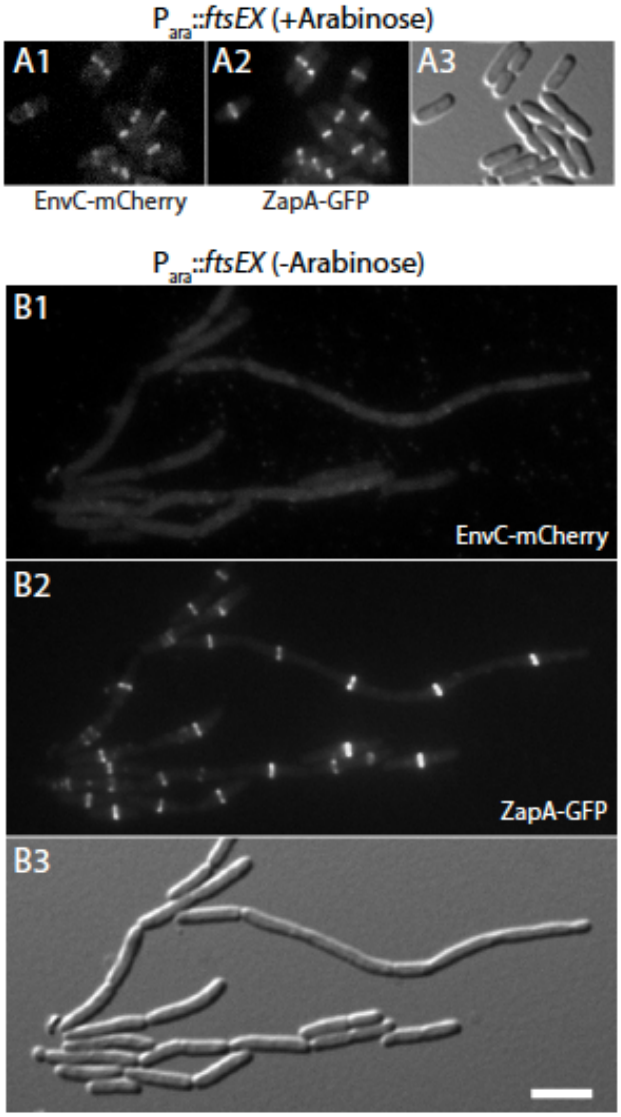

Figure A1.6. FtsEX is required for the recruitment of EnvC to the division site. Cells of NP69(attλTU188)(attHKTB316) [Δ*ftsEX* Δ*envC zapA-gfp* (P_{ara}::*ftsEX*) (P_{lac}::*envC-mCherry*)] were grown overnight in M9 maltose supplemented with 0.01% arabinose. Cells were washed twice with and resuspended in an equal volume of M9 medium without added sugar. They were then diluted 1:100 into M9 maltose and growth was continued at 30°C with the addition of either 0.01% arabinose (**A**) or 0.01% glucose (**B**). **(Legend continued on next page.)**

Figure A1.6 (Continued) When the cultures reached an OD_{600} of 0.4-0.6, cells were visualized on 2% agarose pads using mCherry (panel 1), GFP (panel 2), or DIC (panel 3) optics. Bar equals 4 microns. Note that a peripheral EnvC-mCherry signal was not observed in (**B**) as might be expected for a periplasmic protein. This is likely because too little fusion protein is present to raise the peripheral signal above background.

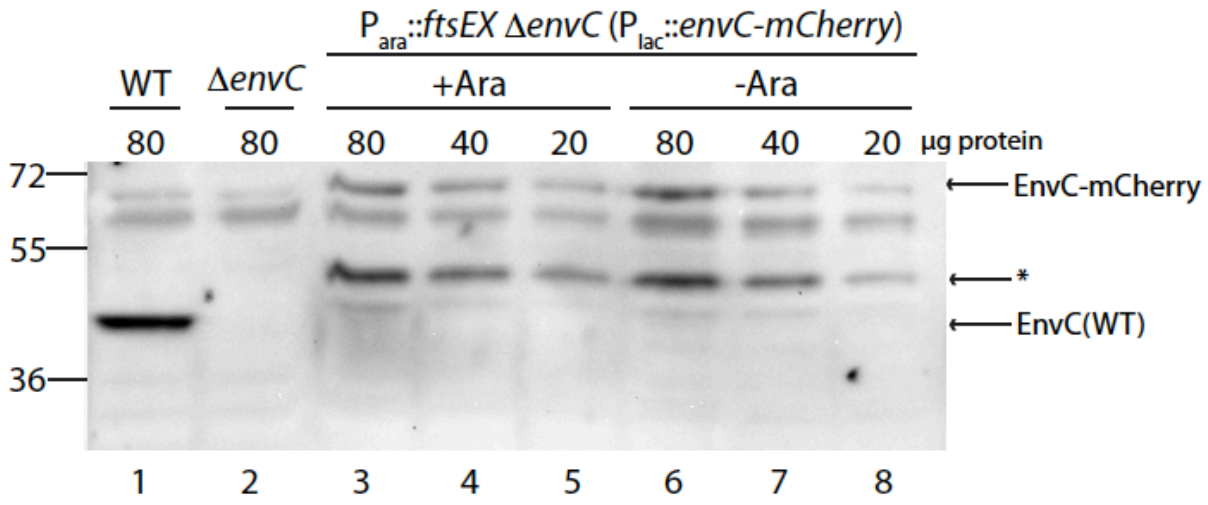

Figure A1.7. EnvC-mCherry accumulation in FtsEX$^+$ and FtsEX$^-$ cells. Cells of TB28 [WT], TB140 [Δ*envC*], and NP69(attλTU188)(attHKTB316) [Δ*ftsEX* Δ*envC zapA-gfp* (P_{ara}::*ftsEX*)(P_{lac}::*envC-mCherry*)] were grown as described in the legend for **Figure A1.6**. When the cultures reached an OD_{600} of 0.4-0.6, cells were harvested for whole-cell extract preparation. Proteins in the resulting extracts were separated by SDS-PAGE, transferred to PVDF, and EnvC was detected with affinity purified anti-EnvC antibodies. Relevant genotypes and growth conditions are indicated above the corresponding lanes as well as the amount of total protein (μg) loaded per lane. Asterisk indicates an EnvC-mCherry breakdown product observed in both FtsEX$^+$ and FtsEX$^-$ cells.

The large periplasmic loop of FtsX interacts directly with EnvC. Our results thus far suggested that FtsEX may directly interact with EnvC to recruit it to the division site. The large periplasmic loop of FtsX (residues 93-223, ^{Loop1}FtsX) (**Figure A1.1B**) seemed a likely candidate for mediating the interaction with EnvC. We therefore tested the potential interaction between full-length, mature EnvC (^{FL}EnvC) and ^{Loop1}FtsX using a bacterial two-hybrid (BACTH) assay based on the reconstitution of adenylate cyclase activity from the fragments T18 and T25 (34). ^{FL}EnvC-T25 showed a strong interaction signal when paired with a ^{Loop1}FtsX-T18 fusion (Figure A1.8A). EnvC contains three identifiable domains: a signal peptide (residues 1-34), a coiled coil (CC) domain (residues 35-271), and a LytM domain (residues 318-413) (4, 29, 33) (**Figure A1.1C**). An interaction signal with ^{Loop1}FtsX-T18 was not detected when an EnvC truncation lacking the CC domain (^{Lyt}EnvC) was fused to T25 in place of ^{FL}EnvC (**Figure A1.8A**). This result suggests that the EnvC-FtsX interaction is mediated by contacts between ^{Loop1}FtsX and the CC domain of EnvC (^{CC}EnvC). However, for reasons that are not clear, T25 fusions to ^{CC}EnvC did not show an interaction signal when co-expressed with ^{Loop1}FtsX-T18.

To further investigate the interaction between FtsX and EnvC, we purified untagged versions of ^{FL}EnvC, ^{Lyt}EnvC, and ^{CC}EnvC as well as a 10xHis (H)-tagged version of ^{Loop1}FtsX (H-^{Loop1}FtsX). We then tested for interactions using “pull-up” assays with magnetic Ni-NTA beads. When ^{FL}EnvC was incubated with H-^{Loop1}FtsX, it was found in the eluate from Ni-NTA beads following two wash steps (**Figure A1.8B**). Consistent with the BACTH results, this was not the case when ^{Lyt}EnvC was incubated

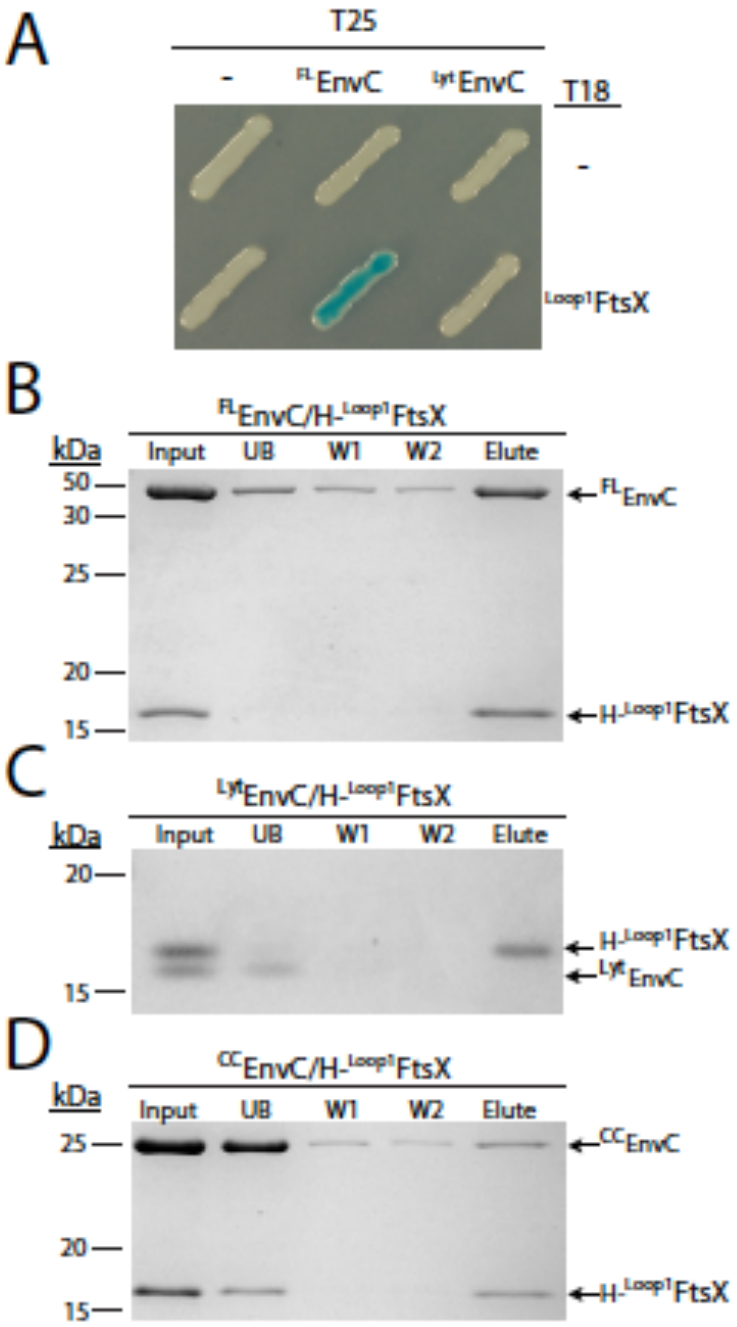

Figure A1.8. EnvC directly interacts with the large periplasmic loop of FtsX. A. Plasmid pairs encoding the indicated ^{FL}EnvC-T25 or ^{Lyt}EnvC-T25 and ^{Loop1}FtsX-T18 fusion proteins were co-transformed into BTH101 [*cya*-99]. Individual colonies were patched on M9-glucose supplemented **(Legend continued on next page.)**

Figure A1.8 (Continued) with Amp, Kan, X-gal, and 1 mM IPTG. Plates were incubated at room temperature and photographed after 72 hours. For this particular BACTH assay, interacting partners bring together T18 and T25 to reconstitute adenylate cyclase activity. This is detected using *lacZ* induction as a reporter. **B-D.** Purified H-^{Loop1}FtsX was incubated with ^{FL}EnvC (**B**), ^{Lyt}EnvC (**C**), or ^{CC}EnvC (**D**) for 100 min at room temperature in binding buffer [20mM Tris-HCl (pH 7.4), 150mM NaCl]. Ni-NTA magnetic agarose beads (Qiagen) were then added to each reaction and they were further incubated for 120 min at 4^{o}C with rotation. The magnetic beads were captured with a magnet, washed twice with binding buffer containing 50mM imadazole, and the proteins retained on the resin were eluted with sample buffer containing EDTA (100 mM). Proteins in the initial reaction (input), initial supernatant (UB), wash supernatants (W1 and W2), and eluate were separated on a 15% Tris-Tricine polyacrylamide gel and stained with Coomassie Brilliant Blue. All proteins were present in the initial binding reaction at a concentration of 4 μM. Positions of molecular weight markers (numbers in kDa) are given to the left of each gel. Control reactions indicated that none of the purified EnvC derivatives could be pulled up with H-GFP.

with H-^{Loop1}FtsX (**Figure A1.8C**). Here, ^{Lyt}EnvC was found primarily in the unbound (UB) fraction. When we incubated ^{CC}EnvC with H-^{Loop1}FtsX, only about half of the H-^{Loop1}FtsX was retained by the beads. It was accompanied in the eluate by a small fraction (about 10%) of the total ^{CC}EnvC, indicating that the two domains weakly interact. The remaining H-^{Loop1}FtsX was found in the unbound fraction with the majority of ^{CC}EnvC. Since H-^{Loop1}FtsX bound efficiently to the beads in the presence of ^{FL}EnvC and ^{Lyt}EnvC, the addition of ^{CC}EnvC appears to adversely affect the accessibility of the H-tag on H-^{Loop1}FtsX. This may be the result of ^{CC}EnvC inducing some sort of conformational change in H-^{Loop1}FtsX, but further investigation is required to test this possibility.

To determine the physiological relevance of the EnvC-^{Loop1}FtsX interaction, we investigated the effect of deleting various portions of the FtsX loop domain on the recruitment of EnvC to the division site. To do so, we a generated a construct expressing the *ftsEX* operon under control of P_{lac} with the *ftsX* reading frame fused to the coding sequence for GFP. The expression construct thus produces untagged FtsE as well as FtsX-GFP. For convenience, we will refer to the fusion as FtsEX-GFP. In addition to the WT fusion, we also generated several variants deleted for various portions of the Loop1 domain of FtsX. When produced as the only source of FtsEX in strain DY18(*att*λTD80)(*att*HKDY156) [Δ*ftsEX* Δ*envC* (P_{lac}::*envC-mCherry*)(P_{lac}::*ftsEX-gfp*)], the FtsEX-GFP fusion corrected the Δ*ftsEX* division phenotype, localized to the division site, and was functional for the recruitment of EnvC-mCherry to the septal ring (**Figure A1.9A**). All of the Loop1 deletion derivatives of FtsX-GFP we tested (Δ152-161, Δ146-165, Δ137-176, and Δ109-213) localized to the division site (**Figure A1.9B and**

Figure A1.10), indicating that the Loop1 domain is not an important localization determinant for FtsX. However, even the derivative with the smallest deletion (Δ152-161) failed to recruit EnvC to the septum, and cells expressing these derivatives displayed an EnvC$^-$ like division defect (**Figure A1.9B and Figure A1.10**). We conclude that the Loop1-EnvC interaction we detected in the BACTH and *in vitro* assays is required for the recruitment of EnvC to the septal ring.

The ATPase activity of FtsE is likely required for amidase activation by EnvC. Weiss and co-workers recently showed that FtsE residues in and around the Walker A (GxxGxGKS/T, where x is any residue) and Walker B (ϕϕϕϕD, where ϕ is a hydrophobic residue) motifs predicted to be important for ATP hydrolysis are required for FtsEX to function in cell division (1). Interestingly, however, these residues were not found to be needed for the stability of FtsE or the recruitment of either FtsE or FtsX to the division site (1). Also, unlike *ftsEX* null mutants, division proteins downstream of FtsEX in the localization hierarchy were recruited to the septal ring in the presence of these predicted ATPase defective variants when mutant cells were grown under non-permissive conditions (1). Thus, by all indications, complete septal rings were forming in the filamentous cells producing the FtsE mutants; they were just unable to promote cell constriction without ATP hydrolysis by FtsEX (1).

Our results thus far indicate that FtsEX directly recruits EnvC to the septal ring. Given the findings of Arends et al. (2009), we also wondered if the ATPase activity of FtsE might be required to stimulate amidase activation by EnvC. We therefore

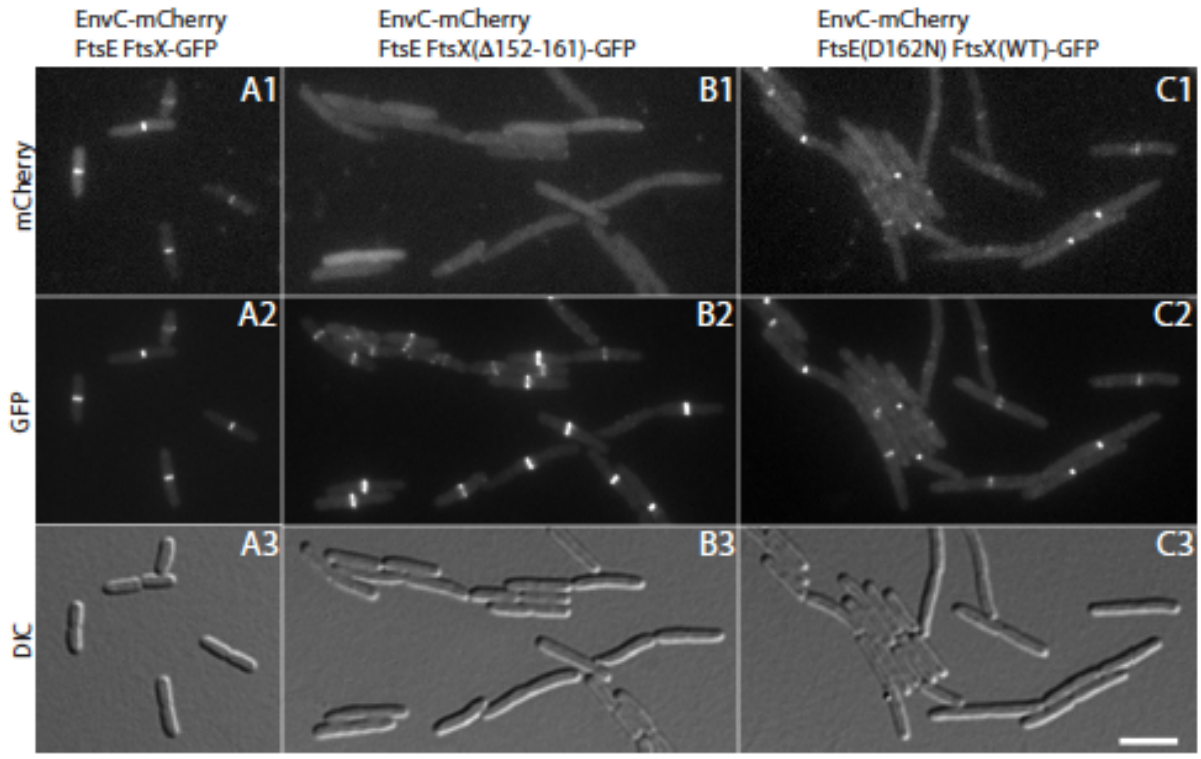

Figure A1.9. EnvC localization in cells producing FtsEX variants. Cells of DY18(*att*λTD80) [Δ*ftsEX* Δ*envC* (P_{lac}::*envC-mCherry*)] harboring the integrated expression constructs (*att*HKDY156) [P_{lac}::*ftsEX-GFP*] (A), (*att*HKDY161) [P_{lac}::*ftsEX*$^{(\Delta 152\text{-}161)}$*-GFP*] (B), or (*att*HKDY167) [P_{lac}::*ftsE(D162N)X-GFP*] (C) were grown overnight at 30°C in LB (1% NaCl). They were then diluted 1:100 into M9 maltose supplemented with 500 μM IPTG. When cells reached an OD_{600} between 0.42-0.54 they were visualized as described in the legend for **Figure A1.6**.

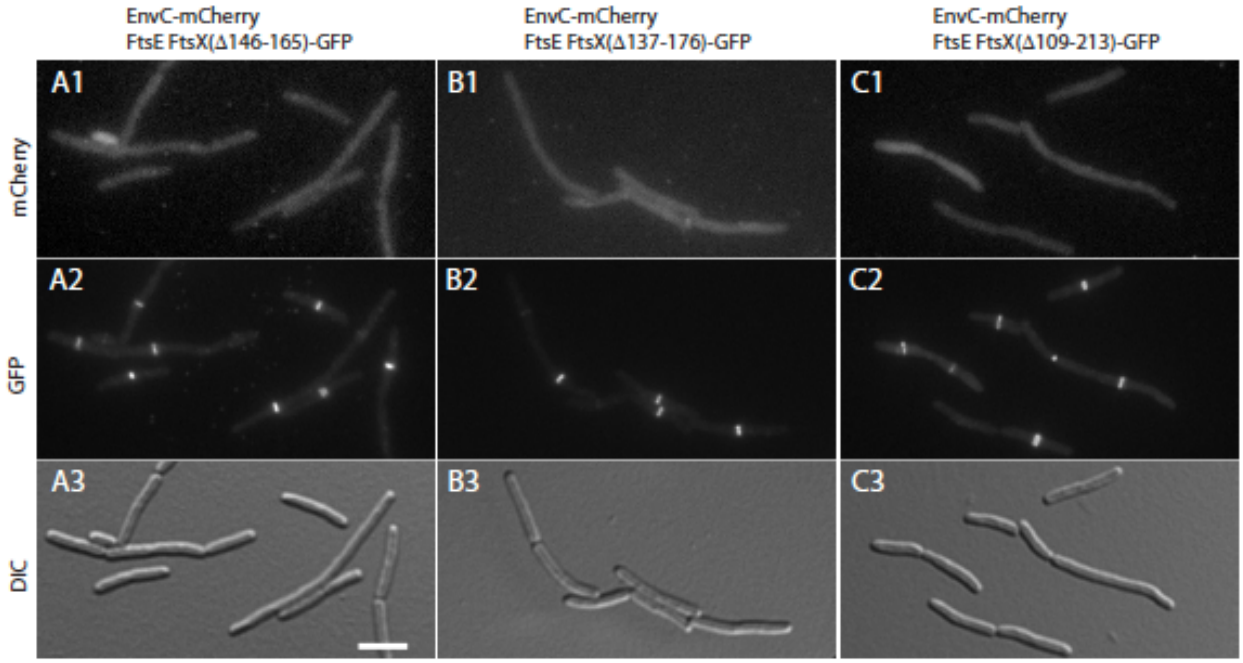

Figure A1.10. EnvC localization in cells producing ^{Loop1}FtsX deletions. Cells of DY18(*att*λTD80) [Δ*ftsEX* Δ*envC* (P_{lac}::*envC-mCherry*)] harboring the integrated expression constructs (*att*HKDY162) [P_{lac}::*ftsEX*$^{(\Delta 146\text{-}165)}$*-GFP*] (**A**), (*att*HKDY163) [P_{lac}::*ftsEX*$^{(\Delta 137\text{-}176)}$*-GFP*] (**B**), or (*att*HKDY165) [P_{lac}::*ftsEX*$^{(\Delta 109\text{-}213)}$*-GFP*] (**C**) were grown and visualized as described in the legend for **Figure A1.9**.

generated *ftsE*(K41M), *ftsE*(D162N), and *ftsE*(E163Q) derivatives of the P_{lac}::*ftsEX-gfp* construct described above. The encoded FtsE variants (FtsE*) in these constructs are similar to those studied previously by Arends et al. (2009), except that more conservative amino acid changes were made. The K41M substitution in the Walker A motif of FtsE is predicted to greatly reduce affinity for ATP (14). The Walker B residue, D162, is predicted to coordinate Mg^{2+} in the active site (14). Substitutions at this residue in other NBDs abrogate ATP binding (14). An acidic residue, E163 in FtsE, typically follows the Walker B motif in ABC transporters. The role of this residue in the ATPase catalytic mechanism is controversial (14). NBDs with Glu to Gln substitutions at this position still bind ATP, but depending on the particular transporter, they may or may not retain residual ATPase activity (14).

The ability of the FtsE* variants to promote cell separation was first assessed by producing them from the P_{lac}::*ftsEX-gfp* construct in Δ*ftsEX* Δ*nlpD* cells. As expected, a construct producing WT FtsE completely reversed the severe chaining phenotype of the $FtsEX^-$ $NlpD^-$ mutants (**Figure A1.11, Table A1.1**). Constructs producing the FtsE* variants, on the other hand, all failed to restore normal cell separation **Figure A1.11, Table A1.1**). However, the mutants did not behave identically. While FtsE(D162N) appeared to be completely defective for cell separation, the FtsE(K41M) and FtsE(E163Q) variants appeared to retain partial function (**Table A1.1**). Based on results from the related LolCDE system, FtsE(K41M) is likely to retain weak affinity for ATP (35). This may allow enough ATPase activity to reduce the length of the chains observed in Δ*ftsEX* Δ*nlpD* cells. For FtsE(E163Q), its ability to shorten Δ*ftsEX* Δ*nlpD* chains may

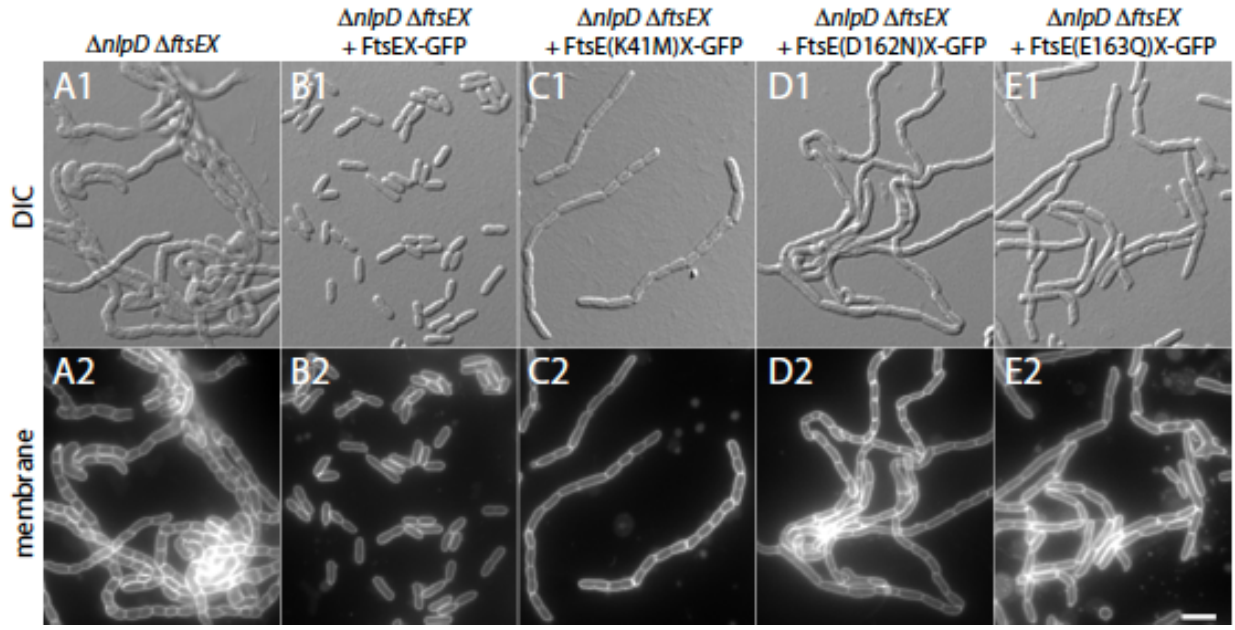

Figure A1.11. FtsE ATP-binding site lesions result in a cell separation defect. Cells of KP7/pTB63 [Δ*ftsEX* Δ*nlpD*/*ftsQAZ*] without an integrated expression cassette (**A**) or harboring (*att*HKDY156) [P_{lac}::*ftsEX-GFP*] (**B**), (*att*HKDY166) [P_{lac}::*ftsE(K41M)X-GFP*] (**C**), (*att*HKDY167) [P_{lac}::*ftsE(D162N)X-GFP*] (**D**), or (*att*HKDY168) [P_{lac}::*ftsE(E163Q)X-GFP*] (**E**)were grown and visualized as described in the legend to **Figure A1.4** except that the medium contained 500 *μ*M IPTG.

Table A1.1. Cell separation phenotypes of FtsE* NlpD$^-$ cells.

strain	genotype	#cells[a]	# cell units[b]	total L (μm)[c]	avg. L (μm)[c]	total septa	L/ septum	septa/ cell
KP7	Δ*ftsEX* Δ*nlpD*	4	225	388	97	218	1.8	55
KP7 (attHKDY156)	Δ*ftsEX* Δ*nlpD* (P_{lac}::*ftsEX-GFP*)	144	200	475	3.3	56	8.5	0.4
KP7 (attHKDY166)	Δ*ftsEX* Δ*nlpD* (P_{lac}::*ftsE(K41M)X-GFP*)	31	202	491	15.8	171	2.9	6
KP7 (attHKDY167)	Δ*ftsEX* Δ*nlpD* (P_{lac}::*ftsE(D162N)X-GFP*)	9	214	434	48.2	208	2.1	23
KP7 (attHKDY168)	Δ*ftsEX* Δ*nlpD* (P_{lac}::*ftsE(E163Q)X-GFP*)	74	200	618	8	127	4.9	2

[a]Cell chains were considered as a single cell regardless of the number of segments they contained.
[b]Indicates the number of cell compartments in chaining cells.
[c]Length measurements represent a minimum because many of the cell chains extended beyond the field of view.

either indicate that ATP-binding alone is sufficient for low-level cell separation activity, or that the E/Q substitution in FtsEX does not completely abolish ATPase activity. Measurement of the ATPase activity of FtsE and the FtsE* variants is required to distinguish between these possibilities, but this has not been possible due to problems with FtsE solubility when it was overproduced. Nevertheless, the (partial) loss-of-function phenotypes displayed by the FtsE* variants clearly highlight a role for key ATP-binding site residues in FtsE for it to promote proper cell separation. Importantly, FtsX-GFP remained capable of recruiting to septal rings in cells producing the FtsE* variants and the efficiency with which EnvC-mCherry was recruited to the FtsX-containing rings was largely unaffected by the FtsE lesions (**Figure A1.9C, Figure A1.12, and Table A1.2**). Furthermore, based on the results of Arends et al. (2009) with similar mutants, we assume that the FtsE* variants described here are also normally recruited to the septal ring. Thus, FtsE*X-EnvC complexes are likely forming at the division site in cells expressing the *ftsE** alleles but they fail to function or function poorly in the septal PG splitting process. We therefore infer that the ATPase activity of the FtsEX complex plays an important role in promoting amidase activation by EnvC at the septum.

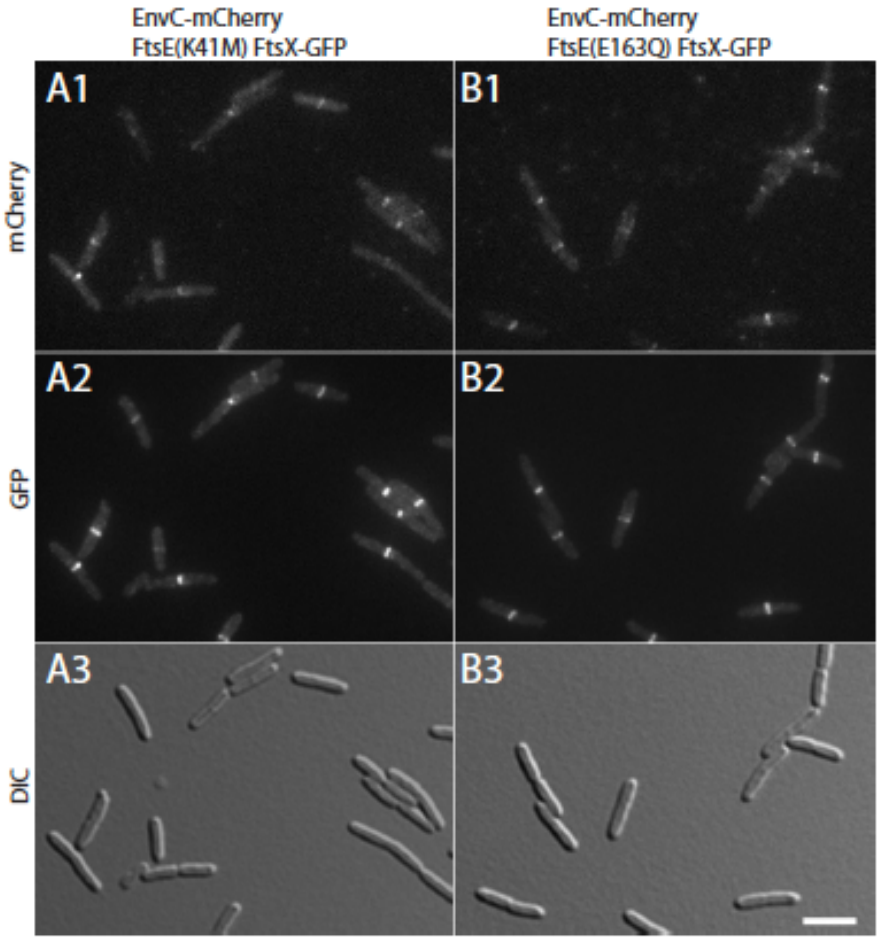

Figure A1.12. EnvC localization in cells producing FtsE* variants. Cells of DY18(*att*λTD80) [Δ*ftsEX* Δ*envC* (P_{lac}::*envC-mCherry*)] harboring the integrated expression constructs (*att*HKDY166) [P_{lac}::*ftsE(K41M)X-GFP*] (**A**) or (*att*HKDY168) [P_{lac}::*ftsE(E163Q)X-GFP*] (**B**) were grown and visualized as described in the legend for **Figure A1.9**.

Table A1.2. Length and localization measurements of FtsE* cells producing FtsX-GFP and EnvC-mCherry.

Strain	genotype	#cells	total L (μm)	avg. L (μm)	# of FtsX-rings	# of EnvC-rings	% co-localization of FtsX and EnvC*	L/FtsX-ring (μm)	L/EnvC-ring (μm)	L/septum (μm)
DY18 (attHKDY156) (attλTD80)	Δ*ftsEX* Δ*envC* (P_{lac}::*ftsEX-GFP*) (P_{lac}::*envC-mCherry*)	125	457	3.7	115	93	81	4.0	4.9	9.3
DY18 (attHKDY166) (attλTD80)	Δ*ftsEX* Δ*envC* (P_{lac}::*ftsE(K41M)X-GFP*) (P_{lac}::*envC-mCherry*)	125	692	5.5	124	95	77	5.5	9.0	13.6
DY18 (attHKDY167) (attλTD80)	Δ*ftsEX* Δ*envC* (P_{lac}::*ftsE(D162N)X-GFP*) (P_{lac}::*envC-mCherry*)	125	1096	8.8	131	109	83	8.4	13.2	12.2
DY18 (attHKDY168) (attλTD80)	Δ*ftsEX* Δ*envC* (P_{lac}::*ftsE(E163Q)X-GFP*) (P_{lac}::*envC-mCherry*)	125	655	5.2	124	91	73	7.2	9.0	12.1

*Reflects the number of FtsX-GFP rings clearly associated with a ring of EnvC-mCherry.

Discussion

The role of the FtsEX ABC system in cytokinesis has long remained mysterious. In this study, we have genetically and physically connected FtsEX with the process of septal PG splitting. Our results indicate that the complex is directly responsible for the recruitment of the amidase activator EnvC to the cytokinetic ring. Importantly, we also showed that variants of the FtsEX complex predicted to have inactive ATPase subunits still recruited EnvC to the septum but failed to induce septal PG splitting. Thus, in addition to connecting EnvC to the septal ring, FtsEX appears to use its ATPase activity to promote amidase activation. An attractive possibility is that it does so using ATPase-induced conformational changes similar to those observed in other ABC systems (45) to allosterically regulate EnvC activity in the periplasm (**Figure A1.13**).

Consistent with this model, sequence analysis groups FtsEX with a sub-class of ABC systems comprised mainly of substrate binding protein (SBP)-dependent importers like the maltose transporter ($MalFGK_2$) (14). The structure of $MalFGK_2$ in complex with maltose binding protein (MalE) indicates that ATP-driven conformational changes in the transporter can alter the conformation of periplasmic MalE (36). In this case, MalE is converted from its closed, maltose-bound conformation to an open conformation that releases maltose into the outward-facing cavity of the transporter for subsequent import (36). We therefore propose that EnvC may be an SBP analog for FtsEX and envision that the conformation of EnvC is similarly modulated by the ABC system so that it interconverts between an “on” and “off” state during an ATPase cycle (**Figure A1.13**). Such a model is appealing for several reasons. Most significantly, it would provide a means for converting septal PG

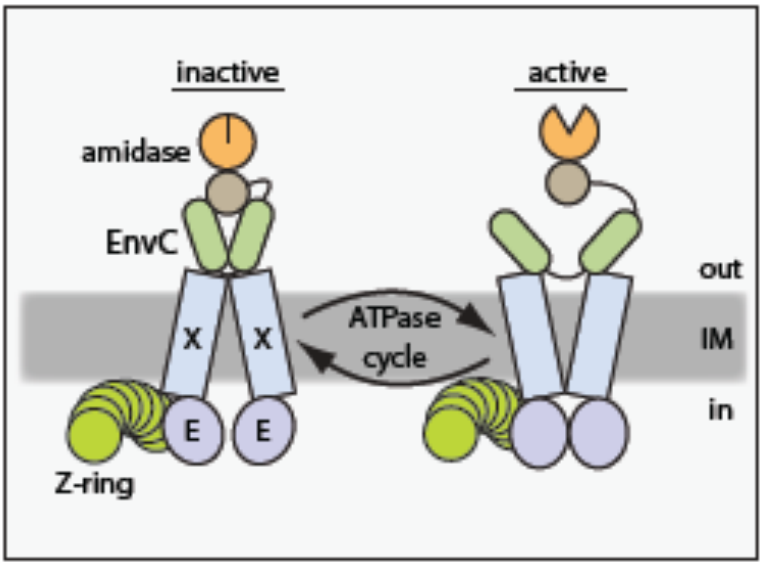

Figure A1.13. Model for FtsEX function in regulating PG hydrolase activity at the division site. Shown is a schematic diagram of a putative FtsEX-EnvC-amidase complex at the Z-ring. We propose that conformational changes in FtsEX induced by FtsE-mediated ATP hydrolysis are transmitted to EnvC to control its ability to activate the amidases so that they can cleave the septal PG (not drawn). The model is not meant to reflect actual interaction stoichiometries as they have yet to be determined. In addition, it is not yet clear if the amidases remain in complex with EnvC as drawn or if this interaction is also regulated. See text for details.

hydrolysis into a discrete process with a fixed number of PG bonds being broken per ATP hydrolyzed. This would afford the septal ring exquisite control over PG hydrolysis, which seems highly desirable given the inherent risks involved in promoting localized PG degradation. Additionally, since FtsE interacts with FtsZ in the cytoplasm, the ATPase activity of FtsE could be directly coupled to Z-ring dynamics. Thus, the FtsEX complex could serve as a molecular governor to properly coordinate the rate of septal PG hydrolysis with the contraction of the Z-ring. Finally, in addition to connecting the Z-ring with septal PG hydrolysis, interactions of FtsX with other transmembrane components of the divisome may help couple the activity of the integral membrane PG synthases with the cell separation amidases. For example, the FtsEX complex may only promote EnvC-activated amidase activity when it is engaged with an active PG synthetic complex.

Control of EnvC activity by FtsEX is likely mediated in part by the observed interaction between the CC domain of EnvC and ^{Loop1}FtsX. Consistent with this possibility, the CC domain of EnvC was previously shown to be important for EnvC regulation (54). An EnvC truncation lacking the CC domain (^{Lyt}EnvC) failed to be recruited to the division site and inappropriately activated AmiA and AmiB to induce cell lysis (54). Since cell lysis is not triggered when ^{FL}EnvC is displaced from the septum by ^{CC}EnvC overproduction (54) or by the deletion of *ftsEX*, proper regulation of amidase activation appears to entail more than just controlling EnvC localization. Because ^{FL}EnvC activates the amidases just as well as ^{Lyt}EnvC *in vitro* (54), we suspect that there is either something about the physiochemical environment of the periplasm that promotes the direct inhibition of ^{FL}EnvC activity by the CC domain itself or that

inhibition is mediated by an additional factor that associates with the CC domain. According to our model for EnvC regulation by FtsEX, it is this auto- or trans-inhibition of EnvC that is cycled on and off in response to the ATPase activity of FtsEX (**Figure A1.13**).

While we favor a model in which FtsEX serves as a transmembrane allosteric regulator of EnvC, scenarios in which FtsEX transports a molecule needed for EnvC activity are difficult to exclude. Arguing against a transport function is the fact that FtsEX is most similar to the LolCDE ABC system. Rather than catalyzing the transport of a substrate across a membrane, LolCDE facilitates the transfer of lipoproteins from the outer leaflet of the inner membrane to the periplasmic LolA carrier protein for their ultimate insertion into the outer membrane (56). The individual TMD components of both FtsEX and LolCDE have only four transmembrane helices, unlike most ABC-transporters, which typically have at least six (1, 12, 14). Moreover, the membrane spanning helices of FtsX do not contain any charged amino acids as might be expected for a factor that transports an electrolyte (1). Based on these observations, Weiss and colleagues have also proposed that FtsEX may not be a transporter (1). Rather, they hypothesized that, as we propose here, FtsE uses ATP hydrolysis to drive a periplasmic activity via conformational changes in FtsX (1). Reconstitution of EnvC regulation by FtsEX is required to definitively demonstrate an allosteric control mechanism. So far, our attempts at reconstitution have been unsuccessful. Addition of purified ^{Loop1}FtsX or full-length FtsX to mixtures of EnvC and AmiB did not affect amidase activation using our standard reaction conditions (54). This suggests that the full FtsEX complex may be needed to observe regulation *in vitro*. Unfortunately, efforts

to purify the complete FtsEX complex have been hampered by the insolubility of FtsE when it is overproduced. This hurdle must be overcome before additional attempts at reconstitution can be pursued.

A role for FtsEX in the process of septal PG splitting appears to be conserved. In an accompanying report (50), Sham et al. directly connect the essential cell separation factor PcsB (39) with FtsEX in *S. pneumoniae*. While their sequences are largely unrelated, the domain structures of PcsB and EnvC are strikingly similar. Like EnvC, PcsB has an N-terminal region predicted to form coiled-coils and a C-terminal PG hydrolase-like CHAP domain (39). However, it is currently not known whether PcsB directly degrades PG or if, analogous to EnvC, it is an activator of other PG hydrolases. Nevertheless, the results of Sham et al. (2011) (50) indicate that PcsB activity is likely governed by FtsEX to properly control the process of septal PG splitting in *S. pneumoniae*. Interestingly, FtsEX does not appear to be involved in cell division in *Bacillus subtilis* (20). We suspect this has to do with the different septal geometries of these organisms. Gram-negative bacteria like *E. coli* and ovococci like *S. pneumoniae* appear to couple septal PG splitting with the invagination of their cytoplasmic membrane to give their pre-divisional cells a constricted appearance (15, 31). This mode of division likely requires regulators of PG hydrolysis like FtsEX to be associated with the septal ring. *B. subtilis* and many other gram-positive bacteria, on the other hand, first construct a flat septum, the splitting of which appears to be uncoupled from membrane constriction and fission (8). Septal PG splitting in these cells is therefore likely to have regulatory requirements that differ from those of constricting cells. It is not clear what the function of FtsEX is in cells with a flat septal morphology, but it may

involve the regulation of PG hydrolysis needed for other aspects of cell wall growth and remodeling.

In conclusion, we have identified a role for the FtsEX ABC system in the regulation of septal PG hydrolysis by the amidases AmiA and AmiB and the LytM factor EnvC. A second pathway for septal PG splitting involving AmiC and the LytM factor NlpD is also operative in *E. coli* (54). How this system is regulated is currently not known. However, since NlpD is an outer membrane lipoprotein (32) rather than a periplasmic protein like EnvC, its activity is likely to be modulated by a distinct mechanism. To our knowledge, this report describes the first example of an ABC system being implicated in the transmembrane regulation of enzymatic activity. Given the diversity and ubiquity of ABC systems in nature (14), it is likely that the ATP-driven conformational changes in these membrane complexes have been adapted to regulate a variety of biological processes.

Materials and Methods

Media, bacterial strains, and plasmids

Cells were grown in LB [1% tryptone, 0.5% yeast extract, (0.5%-1.5% NaCl as indicated)] or minimal M9 medium (37) supplemented with 0.2% casamino acids and 0.2% sugar (glucose, maltose, or arabinose as indicated). Unless otherwise indicated, antibiotics were used at 5, 10, 15, 20, or 50 μg/ml for tetracycline (Tet), chloramphenicol (Cam), ampicillin (Amp), kanamycin (Kan), or spectinomycin (Spec), respectively.

The bacterial strains used in this study are listed in **Table A1.3**. All strains used in the reported experiments are derivatives of MG1655 (23). Plasmids used in this study are listed in **Table A1.4**. Vectors with R6K origins are all derivatives of the CRIM plasmids developed by Wanner and co-workers (25). They were either maintained in the cloning strain DH5α(λ*pir*) where they replicate as plasmids, or they were integrated into phage attachment sites (HK022 or λ) using the helper vectors pTB102 (5) or pInt-ts (25), respectively, as described previously (25). Single copy integrants were identified using diagnostic PCR (25). Integrated vectors were transferred between strains by P1-mediated transduction. In all cases, PCR was performed using KOD polymerase (Novagen) according to the instructions. Unless otherwise indicated, MG1655 chromosomal DNA was used as a template. Restriction sites for use in plasmid constructions are italicized and underlined in the primer sequences given below. Plasmid DNA and PCR fragments were purified using the Qiaprep spin miniprep kit (Qiagen) or the Qiaquick PCR purification kit (Qiagen), respectively.

pTU188

To construct pTU188 [*att*λ *cat* P_{ara}::*ftsE-ftsX*], a fragment containing *ftsE* and *ftsX* was amplified with the primers 5'-GTCA*TCTAGA*TTTGCCCGAGAGGATTAACAATG-3' and 5'-GTCA*AAGCTT*TTATTATTCAGGCGTAAAGTGGCG-3', digested with XbaI and HindIII, and inserted into the corresponding XbaI-HindIII sites of pTB285 (40)}.

Table A1.3. Bacterial strains used in this study.

Strain[a]	Genotype[b]	Source/Reference[c]
DH5α	F⁻ *hsdR*17 *deoR recA*1 *endA*1 *phoA supE*44 *thi*-1 *gyrA*96 *relA*1 Δ(*lacZYA-argF*)U169 ϕ80d*lacZ*ΔM15	Gibco BRL
BL21(λDE3)	*ompT* rB– mB– (P_{lac}UV5::T7*gene1*)	Novagen
BTH101	F⁻, *glnV*44(AS), *recA*1, *endA*1, *gyrA*96, *thi*1, *hsdR*17, *spoT*1, *rfbD*1 *cya*	34
BW25113	Δ(*araD-araB*)567 Δ*lacZ*4787(::*rrnB*-3) *rph*-1 Δ(*rhaD-rhaB*)568 *hsdR*514	2
JW5646	BW25113 Δ*envC*::Kan^R	2
JW2985	BW25113 Δ*ftsP*(*sufI*)::Kan^R	2
MG1655	*rph*1 *ilvG rfb*-50	23
MM9	TB28 (Kan^R *araC* P_{ara})::*ponB*	40
MM11	TB28 (*frt araC* P_{ara})::*ponB*	40
TB10	*rph*1 *ilvG rfb*-50 λΔ*cro-bio nad*::Tn10	4
TB28	MG1655 Δ*lacIZYA*::*frt*	4
TB140	TB28 Δ*envC*::*frt*	53
TB145	TB28 Δ*nlpD*747::*frt*	53
TB172	TB28 Δ*amiA*::*frt* Δ*amiB*::*frt* (Kan^R *araC* P_{ara})::*ponB*	P1(MM9) x TU207
TU122	TB28 Δ*ponB*::frt	40
TU189	TB10 Δ*ftsEX*::Kan^R	λRec
TU190**	TB28 Δ*ftsEX*::Kan^R	P1(TU189) x TB28(*att*λTU188)
TU191	TB28 Δ*ftsEX*::frt	TU190/pCP20
TU195**	TB28 Δ*ftsEX*::frt Δ*envC*::Kan^R	P1(JW5646) x TU191(*att*λTU188)
TU196**	TB28 Δ*ftsEX*::frt Δ*ftsP(sufI)*::Kan^R	P1(JW2985) x TU191(*att*λTU188)
TU205***	TB28 Δ*envC*::frt Δ*ftsP(sufI)*::Kan^R	P1(JW2985) x TB140(*att*λTD25)
TU207	TB28 Δ*amiA*::*frt* Δ*amiB*::*frt*	54
HC260	TB10 *zapA-gfp* Cam^R	λRec
HC261	TB28 *zapA-gfp* Cam^R	P1(HC260) x TB28

Table A1.3. Bacterial strains used in this study. (Continued)

Strain[a]	Genotype[b]	Source/Reference[c]
HC262	TB28 Δ*envC::frt zapA-gfp* Cam^R	P1(HC261) × TB140
NP32	TB28 Δ*envC::frt zapA-gfp frt*	HC262/pCP20
NP65*	TB28 (*frt araC* P_{ara})::*ponB* Δ*envC*::Kan^R	P1(JW5646) x MM11/pTB63
NP66*	TB28 (*frt araC* P_{ara})::*ponB* Δ*ftsEX*::Kan^R	P1(TU190) x MM11/pTB63
NP69	TB28 Δ*envC::frt zapA-gfp frt* Δ*ftsEX*::Kan^R	P1(TU190) x NP32
KP4*	TB28 Δ*envC*::Kan^R	P1(JW5646) x TB28/pTB63
KP5*	TB28 Δ*ftsEX*::Kan^R	P1(TU190) x TB28/pTB63
KP6*	TB28 Δ*nlpD*747::*frt* Δ*envC*::Kan^R	P1(JW5646) x TB145/pTB63
KP7*	TB28 Δ*nlpD*747::*frt* Δ*ftsEX*::Kan^R	P1(TU190) x TB145/pTB63
DY18	TB28 Δ*envC::frt* Δ*ftsEX*::Kan^R	P1(TU190) x TB140

[a] Stains marked with a single asterisk were made by transducing Kan^R cassettes into a recipient harboring plasmid pTB63. Stains marked with a double or triple asterisk were made by transducing Kan^R cassettes into recipients harboring *att*λTU188 or *att*λTD25, respectively.

[b] The Kan^R cassette is flanked by *frt* sites for removal by FLP recombinase. An *frt* scar remains following removal of the cassette using FLP expressed from pCP20.

[c] Strain constructions by P1 transduction are described using the shorthand: P1(donor) x recipient. Transductants were selected on LB Kan or Cam plates where appropriate. Strains resulting from the removal of a Drug^R cassette using pCP20 are indicated as: Parental strain/pCP20. λRec indicates strains were constructed by recombineering (see Experimental Procedures for details).

Table A1.4. Plasmids used in this study[a].

Plasmid	Genotype	Origin	Source or reference
pCP20	*bla cat* cI875 *repA*(Ts) P_R::*flp*	pSC101	13
pInt-ts	*bla* cI875 *repA*(Ts) P_R::int^{λ}	pSC101	25
pKNT25	*aph Plac::T25*	p15A	34
pCH363	*bla* $lacI^q$ P_{lac}::*T18*	pBR/colE1	3
pDY133	*bla* $lacI^q$ P_{T7}::^{10}*H-*^{loop1}*ftsX*	pBR/colE1	This study
pDY138	*bla* $lacI^q$ P_{lac}:: ^{loop1}*ftsX-T18*	pBR/colE1	This study
pDY151	*bla* $lacI^q$ P_{T7}::*H-SUMO-envC(35-276)*	pBR/colE1	This study
pDY156	*att*HK *bla* P_{lac}::*ftsEX-GFP*	R6K	This study
pDY161	*att*HK *bla* P_{lac}::*ftsEX*$^{(\Delta 152-161)}$*-GFP*	R6K	This study
pDY162	*att*HK *bla* P_{lac}::*ftsEX* $^{(\Delta 146-165)}$*-GFP*	R6K	This study
pDY163	*att*HK *bla* P_{lac}::*ftsEX* $^{(\Delta 137-176)}$*-GFP*	R6K	This study
pDY164	*att*HK *bla* P_{lac}::*ftsEX* $^{(\Delta 109-188)}$*-GFP*	R6K	This study
pDY165	*att*HK *bla* P_{lac}::*ftsEX* $^{(\Delta 109-213)}$*-GFP*	R6K	This study
pDY166	*att*HK *bla* P_{lac}::*ftsE(K41M)X-GFP*	R6K	This study
pDY167	*att*HK *bla* P_{lac}::*ftsE(D162N)X-GFP*	R6K	This study
pDY168	*att*HK *bla* P_{lac}::*ftsE(E163Q)X-GFP*	R6K	This study
pTB63	*tetAR ftsQAZ*	pSC101	4
pTB102	*cat* cI875 *repA*(Ts) P_R::int^{HK022}	pSC101	5
pTB316	*attHK022 bla* $lacI^q$ P_{lac}::*envC-mCherry*	R6K	53
pTB332	*aph* P_{lac}*::envC(277-419)-T25*	p15A	This study
pTB333	*aph* P_{lac}*::envC(34-419)-T25*	p15A	This study
pTD25	*att*λ *cat* P_{ara}::*envC*	R6K	53
pTD80	*att*λ *cat* P_{lac}::*envC-mCherry*	R6K	This study
pTU110	*cat* $lacI^q$ P_{lac}::*ponB lacZ*	F	40
pTU188	*att*λ *cat* P_{ara}::*ftsEX*	R6K	This study

[a] P_R, P_{lac}, and P_{ara} indicate the phage λR, lactose, and arabinose promoters, respectively. P_{syn135} is a synthetic *lac* promoter with a consensus -35 element and no operators. Numbers in parenthesis indicate the codons included in the relevant clones. (Legend continued on next page.)

Table A1.4. (legend continued) The GFP allele used in plasmid constructs was superfolder GFP (41) and mCherry was from Shaner and co-workers (51). The linker LEGPAGL was present between the fusion proteins and the protein of interest.

pTB332-333

For pTB332 [*aph Plac::envC(277-419)-T25*], *envC(278-419)* was amplified with the primers 5'- GTAC*AAGCTT*GACCGAAAGCGAAAAATCGCTGATG-3' and 5'-GTCA*GGATCC*TC TCTTCCCAACCACGGCTGTGG-3'. The resulting fragment was digested and ligated with HindIII and BamHI digested pKNT25 (34). pTB333 [*aph* P_{lac}*::envC(34-419)-T25*] was constructed in the same manner except that *envC(34-419)* was amplified with the primers 5'-GTAC*AAGCTT*GGATGAGCGTGACCAACTCAAATCTATTC-3' and 5'-GTCA*GGATCC*TCT CTTCCCAACCACGGCTGTGG-3'. *pTD80*

To construct pTD80 [*att*λ *cat lacI*^{q} P_{lac}::*envC-mCherry*], the P_{lac}::*envC-mCherry* containing EcoRI-HindIII fragment of pTB316 [*att*HK022 *bla lacI*^{q} P_{lac}::*envC-mCherry*] (53) was used to replace the corresponding P_{ara}::*envC* fragment of pTD25 [*att*λ *cat* P_{ara}::*envC*] (53).

pMT1

pMT1 [*cat* P_{ara}::*ftsEX*] was constructed in multiple steps. First, pTU170 [*att*HK022 *bla* P_{syn135}::*gfp-zapA*] was made by ligating the *EcoR*I-*Sal*I digested fragment from pEZ4 (3) into the *EcoR*I-*Sal*I digested backbone of pTB263 [*att*HK022 *bla* P_{lac}::^{ss}*dsbA-sfgfp*] (53). Then pTU176 [*att*HK022 *bla* P_{syn135}::^{ss}*dsbA-sfgfp*] was made by ligating the ^{ss}*dsbA-sfgfp*-containing *Xba*I-*Hind*III fragment from pTB263 (53) with *Xba*I-*Hind*III digested pTU170 to generate pTU176. The ^{ss}*dsbA-sfgfp*-containing *Xba*I-*Hind*III fragment from pTU176 was ligated with *Xba*I-*Hind*III digested pBAD18-cat (24) to generate pTU214 [*cat* P_{ara}::^{ss}*dsbA-sfgfp*]. Using pTU188 [*att*λ *cat* P_{ara}::*ftsEX*] as a

template, *RBSwk2-ftsEX* was amplified with primers 5'-GTCA*TCTAGA*A AAAAGGAAAAATGATTCGCTTTGAACATGTCAGCAAGG-3' and 5'-GTCA*AAGCTT*TTA TTATTCAGGCGTAAAGTGGCG-3'. The resulting fragment was digested with *Hind*III and *Xba*I and ligated with pTU214 digested with the same enzymes to generate pMT1.

pDY133

pDY133 [*bla* P_{lac}::^{loop1}*ftsX-T18*] was constructed in two steps. First, the *amiA* gene was amplified using the primers 5'-GTCA*TCTAGA*AGGATCCGCCAAAGACGAACTTTTAAAA ACCAGC-3' and 5'-GTCA*GAGCTC*GGCTCGAGTCGCTTTTTCGAATGTGCTTTCT GGTTG-3'. The resulting fragment was digested with *Xba*I and *Sac*I and ligated with pCH363 [*bla* P_{lac}::*lacZ-T18*] (3) digested with the same enzymes to generate pTU236 [*bla* P_{lac}::*amiA-T18*]. Second, ^{loop1}*ftsX* was amplified from pMT1 [*cat* P_{ara}::*RBSwk2-ftsEX*] using the primers 5'-GTCATT*GGATCC*GTGTACAAAAACGTTAACCAGGCGGCG-3' and 5'-AGTTAAGCTT ATTA*CTCGAG*GCGCCCGACCAGCCCGGTCAACGCC-3'. The resulting fragment was digested with *BamH*I and *Xho*I and ligated with pTU236 [*bla* P_{lac}::*amiA-T18*] digested with the same enzymes to generate pDY133.

pDY138

pDY138 [*bla* P_{T7}*::His10-ftsXloop1*] was constructed in several steps. pDY42 [*bla* P_{T7}::*His10-mcs*] was made by using the synthetic oligonucleotides 5'-CTAGAAATAATTTTGTTTAACTTTAAGAAGGAGATATACCATGCGTGGTTCTCACCACCAT CACCACCATCACCACCATCATGCTAGCG-3'and 5'-

GATCCGCTAGCATGATGGTGGTGATGG

TGGTGATGGTGGTGAGAACCACGCATGGTATATCTCCTTCTTAAAGTTAAACAAAATTAT

TT-3'. These oligonucleotides were annealed, resulting in the formation of dsDNA with overhangs complementary to *BamH*I and *Xho*I restriction sites. pTD68 [*bla* P_{lac}::^{ss}*dsbA-linker-*^{sf}*gfp*] (38) was digested with *BamH*I and *Xho*I, and the resulting plasmid backbone was ligated with the complementary synthetic dsDNA. Finally, the ^{loop1}*ftsX* was amplified from pMT1 [*cat* P_{ara}::*ftsEX*] using the primers 5'-

GTCATT*GGATCC*GTGTACAAAAACGTTA ACCAGGCGGCG-3' and 5'-

AGTTAAGCTTATTA*CTCGAG*GCGCCCGACCAGCCCG GTCAACGCC-3'. The resulting fragment was digested with *BamH*I and *Xho*I and ligated with pDY42 digested with the same enzymes to generate pDY138.

pDY151

pDY151 [*bla* P_{T7}::*H-SUMO-*^{cc}*envC*] was constructed in several steps. First, pTU138 [*att*HK022 *bla* P_{lac}::^{ss}*dsbA-envC*(35-419)-^{sf}*gfp*] was made by amplifying ^{fl}*envC* using the primers 5'- GTCA*GGATCC*GGTGATGAGCGTGACCAACTCAAATCTATTC-3' and 5'- GTCA*CTCGAG*TCTTCCCAACCACGGCTGTGG-3'. The resulting fragment was digested with *BamH*I and *Xho*I and ligated with pTB282 [*att*HK022 *bla* P_{lac}::^{ss}*dsbA-*^{sf}*gfp*] (9) digested with the same enzymes. Using pTB138 as a template, ^{cc}*envC* was amplified with the primers 5'-

GTCA*GGATCC*GGTGATGAGCGTGACCAACTCAAATCTATTC-3' and 5'-

GTCA*CTCGAG*CGGTTTGTAGGTGGTGCCTTTGC-3'. The resulting fragment was digested with *BamH*I and *Xho*I and ligated with pTB282 (11) digested with the same

enzymes to generate pTU150 [*att*HK022 *bla* P_{lac}::^{ss}*dsbA*-^{cc}*envC*-^{sf}*gfp*]. Finally, the ^{cc}*envC*-containing *BamH*I-*Xho*I fragment from pTU150 was ligated with *BamH*I-*Xho*I digested pTD68 [*bla* P_{T7}::*H-SUMO-mcs*] (54) to generate pDY151.

pDY156

pDY156 [*att*HK022 *bla* P_{lac}::*ftsEX-sfgfp*] was constructed as follows. *ftsEX* was amplified from MG1655 with the primers 5'-GTCA*TCTAGA*TTTGCCCGAGAGGATTAACAATG-3' and 5'-GTCA*CTCGAG*TTCAGGCGTAAAGTGGCGTAAATG-3'. The resulting fragment was digested with *Xba*I and *Xho*I and ligated with pTB311 [*att*HK022 *bla* P_{lac}::^{ss}*dsbA-amiB(23-445)*-^{sf}*gfp*] (54) digested with the same enzymes.

pDY158-160

pDY158 [*att*λ *cat* P_{ara}::*ftsE(K41M)X*] was made by site-directed mutagenesis of pTU188 [*att*λ *cat* P_{ara}::*ftsEX*] using the QuickChange method (Stratagene) and the primer 5'-GATCAGCTTCAGGAGGGTACTCATCCCTGCGCCGGAATGACCGGT-3'.

pDY159 [*att*λ *cat* P_{ara}::*ftsE(D162N)X*] was constructed by site-directed mutagenesis of pTU188 [*att*λ *cat* P_{ara}::*ftsEX*] using the QuickChange method (Stratagene) and the primer 5'-GTCCAGGTTACCAGTCGGTTCGTTCGCCAGCAGTACCGCGGGCTT-3'.

pDY160 [*att*λ *cat* P_{ara}::*ftsE(E163Q)X*] was constructed by site-directed mutagenesis of pTU188 [*att*λ *cat* P_{ara}::*ftsEX*] using the QuickChange method

(Stratagene) and the primer 5'-GTCGTCCAGGTTACCAGTCGGTTGGTCCGCCAGCAGTACCGCGGG-3'.

pDY161-pDY165

pDY161 [*att*HK022 *bla* P_{lac}::*ftsEX(152-161)-sfgfp*] was constructed as follows. To make the 10aa *ftsX* internal deletion *ftsEX(152-161)*, two overlap extension PCR fragments were amplified with the primers 5'-GTCA*TCTAGA*TTTGCCCGAGAGGATTAACAATG-3' and 5'-GTTTTCTTCCAGCATATCCAGCTCACCCAGTGCGTCTTCACG-3' as well as 5'-CGTGAAGACGCACTGGGTGAGCTGGATATGCTGGAAGAAAAC-3' and 5'GTC A*CTCGAG*TTCAGGCGTAAAGTGGCGTAAATG-3' using pDY156 [*att*HK022 *bla* P_{lac}::*ftsEX-sfgfp*] as the DNA template. The resulting PCR fragments were purified and used together as the final DNA template to amplify the *ftsEX(152-161)* fragment using the primers 5'-GTCA*TCTAGA*TTTGCCCGAGAGGATTAACAATG-3' and 5'GTCA*CTCGAG*TTCAG GCGTAAAGTGGCGTAAATG-3'. The resulting fragment was digested with *Xba*I and *Xho*I and ligated with pTB311 [*att*HK022 *bla* P_{lac}::^{ss}*dsbA-amiB(23-445)-sfgfp*] (54) digested with the same enzymes.

pDY162

pDY162 [*att*HK022 *bla* P_{lac}::*ftsEX(146-165)-sfgfp*] was constructed as follows. To make the 20aa *ftsX* internal deletion *ftsEX(146-165)*, two overlap extension PCR fragments were amplified with the primers 5'-GTCA*TCTAGA*TTTGCCCGAGAGGATTAACAATG-3' and 5'-

TGCCGGAAGCGGGTTTTCTTCACGAGAAAGATAGTTCACTTT-3' as well as 5'-AAAGTGAACTATCTTTCTCGTGAAGAAAACCCGCTTCCGGCA-3' and 5'GTCA *CTCGAG*TTCAGGCGTAAAGTGGCGTAAATG-3' using pDY156 [*att*HK022 *bla* P_{lac}::*ftsEX-sfgfp*] as the DNA template. The resulting PCR fragments were purified and used together as the final DNA template to amplify the *ftsEX(146-165)* fragment using the primers 5'-GTCA*TCTAGA*TTTGCCCGAGAGGATTAACAATG-3' and 5'GTCA*CTCGAG*TTCAGGC GTAAAGTGGCGTAAATG-3'. The resulting fragment was digested with *Xba*I and *Xho*I and ligated with pTB311 [*att*HK022 *bla* P_{lac}::^{ss}*dsbA-amiB(23-445)-sfgfp*] (54) digested with the same enzymes.

pDY163

pDY163 [*att*HK022 *bla* P_{lac}::*ftsEX(137-176)-sfgfp*] was constructed as follows. To make the 40aa *ftsX* internal deletion *ftsEX(137-176)*, two overlap extension PCR fragments were amplified with the primers 5'-GTCA*TCTAGA*TTTGCCCGAGAGGATTAACAATG-3' and 5'-CTGGAAATCGAGTTTCGGGATGCCTTGCTCGGCCTGCAACTG-3' as well as 5'-CAGTTGCAGGCCGAGCAAGGCATCCCGAAACTCGATTTCCAG-3' and 5'GTCA*CTCGAG*TTCAGGCGTAAAGTGGCGTAAATG-3' using pDY156 [*att*HK022 *bla* P_{lac}::*ftsEX-sfgfp*] as the DNA template. The resulting PCR fragments were purified and used together as the final DNA template to amplify the *ftsEX(137-176)* fragment using the primers 5'-GTCA*TCTAGA*TTTGCCCGAGAGGATTAACAATG-3' and 5'GTCA*CTCGAG*TTCAGGC GTAAAGTGGCGTAAATG-3'. The resulting fragment was

digested with *Xba*I and *Xho*I and ligated with pTB311 [*att*HK022 *bla* P_{lac}::^{ss}*dsbA-amiB(23-445)-sfgfp*] (54) digested with the same enzymes.

pDY164

pDY164 [*att*HK022 *bla* P_{lac}::*ftsEX(109-188)-sfgfp*] was constructed as follows. To make the 80aa *ftsX* internal deletion *ftsEX(109-188)*, two overlap extension PCR fragments were amplified with the primers 5'-GTCA*TCTAGA*TTTGCCCGAGAGGATTAACAATG-3' and 5'-GATACGATCACGCAGCGTATTTGACGGATAATACTGCGTCGC-3' as well as 5'-GCGACGCAGTATTATCCGTCAAATACGCTGCGTGATCGTATC-3' and 5'GTCA *CTCGAG*TTCAGGCGTAAAGTGGCGTAAATG-3' using pDY156 [*att*HK022 *bla* P_{lac}::*ftsEX-sfgfp*] as the DNA template. The resulting PCR fragments were purified and used together as the final DNA template to amplify the *ftsEX(109-188)* fragment using the primers 5'-GTCA*TCTAGA*TTTGCCCGAGAGGATTAACAATG-3' and 5'GTCA*CTCGAG*TTCA GGCGTAAAGTGGCGTAAATG-3'. The resulting fragment was digested with *Xba*I and *Xho*I and ligated with pTB311 [*att*HK022 *bla* P_{lac}::^{ss}*dsbA-amiB(23-445)-sfgfp*] (54) digested with the same enzymes.

pDY165

pDY165 [*att*HK022 *bla* P_{lac}::*ftsEX(109-213)-sfgfp*] was constructed as follows. To make the 105aa *ftsX* internal deletion *ftsEX(109-213)*, two overlap extension PCR fragments were amplified with the primers 5'-GTCA*TCTAGA*TTTGCCCGAGAGGATTAACAATG-3' and 5'-

CAGCCCGGTCAACGCCGCCAGTGACGGATAATACTGCGTCGC-3' as well as 5'-GCGACGCAGTATTATCCGTCACTGGCGGCGTTGACCGGGCTG-3' and 5'GTCA *CTCGAG*TTCAGGCGTAAAGTGGCGTAAATG-3' using pDY156 [*att*HK022 *bla* P_{lac}::*ftsEX-sfgfp*] as the DNA template. The resulting PCR fragments were purified and used together as the final DNA template to amplify the *ftsEX(109-213)* fragment using the primers 5'-GTCA*TCTAGA*TTTGCCCGAGAGGATTAACAATG-3' and 5'GTCA*CTCGAG*TTCAGGCGTA AAGTGGCGTAAATG-3'. The resulting fragment was digested with *Xba*I and *Xho*I and ligated with pTB311 [*att*HK022 *bla* P_{lac}::^{ss}*dsbA-amiB(23-445)-sfgfp*] (54) digested with the same enzymes.

pDY166-pDY168

pDY166 [*att*HK022 *bla* P_{lac}::*ftsE(K41M)X-sfgfp*] was constructed by amplifying *ftsE(K41M)X* with the primers 5'-GTCA*TCTAGA*TTTGCCCGAGAGGATTAACAATG-3' and 5'-GTCA*CTCGAG*TTCAGGCGTAAAGTGGCGTAAATG-3' using pDY158 [*att*λ *cat* P_{ara}::*ftsE(K41M)X*] as the DNA template. The resulting fragment was digested with *Xba*I and *Xho*I and ligated with pTB311 [*att*HK022 *bla* P_{lac}::^{ss}*dsbA-amiB(23-445)-sfgfp*] (54) digested with the same enzymes.

pDY167

pDY167 [*att*HK022 *bla* P_{lac}::*ftsE(D162N)X-sfgfp*] was constructed by amplifying *ftsE(D162N)X* with the primers 5'-GTCA*TCTAGA*TTTGCCCGAGAGGATTAACAATG-3' and 5'-GTCA*CTCGAG*TTCAGGCGTAAAGTGGCGTAAATG-3' using pDY159 [*att*λ *cat* P_{ara}::*ftsE(D162N)X*] as the DNA template. The resulting fragment was digested with

*Xba*I and *Xho*I and ligated with pTB311 [*att*HK022 *bla* P_{lac}::^{ss}*dsbA-amiB(23-445)-sfgfp*] (54) digested with the same enzymes.

pDY168

pDY168 [*att*HK022 *bla* P_{lac}::*ftsE(E163Q)X-sfgfp*] was constructed by amplifying *ftsE(E163Q)X* with the primers 5'-GTCA*TCTAGA*TTTGCCCGAGAGGATTAACAATG-3' and 5'-GTCA*CTCGAG*TTCAGGCGTAAAGTGGCGTAAATG-3' using pDY160 [*att*λ *cat* P_{ara}::*ftsE(E163Q)X*] as the DNA template. The resulting fragment was digested with *Xba*I and *Xho*I and ligated with pTB311 [*att*HK022 *bla* P_{lac}::^{ss}*dsbA-amiB(23-445)-sfgfp*] (54) digested with the same enzymes.

Recombineering

The Δ*ftsEX*::Kan^R allele was constructed by replacing the region between the 2nd codon of *ftsE* and the 7th codon from the stop codon of *ftsX* with a Kan^R cassette as described previously (2, 57). The Kan^R cassette was amplified from pKD13 (13) using the primers 5'-ACTTTATAGAGGCACT TTTTGCCCGAGAGGAT TAACAATGATTCCGGGGATCCGTCGACC-3' and 5'-AGAGTATAACACGCTTTTATTATT CAGGCGTAAAGTGGCGTGTAGGCTGGAGCTG CTTCG-3'. The resulting product was electroporated into strain TB10 as described previously (4), and the recombinants were selected at 30˚C on an LB plate containing 1% NaCl and 20 μg/ml kanamycin to generate the chromosomal deletion.

To generate a marker for the Z-ring, a *zapA-gfp* fusion was created at its native chromosomal locus by λ recombineering (57). *gfp-mut2* (4) coding sequence and a

linked *cat* cassette flanked by *zapA* 3' end sequence and sequence downstream of *zapA* was amplified using pTB24 (3) as a template and the primers 5'-ACAAGGTCGCATCACCGAAAAAACTAACC AAAACTTTGAAGATCCCCCCG CTGAATTCATG-3' and 5'-TTGTCTTC ACGGTTACTCTACCACAGTAAACCGAAAAGT GGTGTAGGCTGGAGCTGCTTCG-3'. The resulting fragment was used for recombineering in strain TB10 as described previously (4). The *zapA-gfp* fusion linked to the *cat* cassette was transferred between strains by P1-transduction.

Synthetic lethal screen

The screen for mutants with a Slb phenotype was performed as previously described (40). Briefly, TU122/pTU110 [Δ*lacIZYA* Δ*ponB*/P_{lac}::*ponB lacZ*] was mutagenized with the EzTn-Kan2 transposome (Epicenter) as previously described (16). Mutants were selected for Kan resistance at room temperature, yielding a library of 75,000 independent transposon insertions. This mutant library was plated on LB agar supplemented with 50 μM IPTG and X-gal (40 μg/ml) at 30˚C and room temperature to identify mutants with a Slb phenotype. In addition to transposon the insertions in *ponA* and *lpoA* described previously (40), we also isolated mutants with insertions in *envC* (between codon 74 and 75) and *ftsX* (within codon 59).

Fluorescence microscopy

Fluorescence microscopy was performed as described previously (53). See figure legends for specific growth conditions employed for each experiment. Cell fixation and membrane staining was performed as described previously (53).

Protein Purification, pull-up assays, and two-hybrid analysis

^{FL}EnvC and ^{Lyt}EnvC were purified as described previously (54). ^{CC}EnvC was overexpressed and purified with a 6xHis-SUMO (H-SUMO) tag fused to its N-terminus. H-SUMO-^{CC}EnvC was purified from BL21(λDE3)/pDY151 and a 10xHis-tagged version of ^{Loop1}FtsX [H-^{Loop1}FtsX] was purified from BL21(λDE3)/pDY138. Overnight cultures were grown at 37°C in LB supplemented with ampicillin (50 μg/ml) and glucose (0.2%). The cultures were diluted 1:100 into 0.1 L of LB supplemented with ampicillin (50 μg/ml) and glucose (0.04%), and cells were grown at 30°C to an OD_{600} of 0.81 and 0.86 respectively. IPTG was added to 1 mM and the cultures were grown for an additional 3 hrs at 30°C. Cells were harvested by centrifugation and the cell pellets were resuspended in 3 ml of buffer A (50 mM Tris-HCl pH 8.0, 300 mM NaCl, 10% glycerol) with 20 mM imidazole and stored at -80°C. Cells were thawed, disrupted by sonication, and cell debris was pelleted by centrifugation at 20,000 x g for 20 min at 4°C. The supernatants were passed through 0.2 μM syringe filters and loaded onto ProPur IMAC mini spin columns (Nunc) equilibrated in buffer A with 20 mM imidazole. Columns were washed 3x using buffer A with 50 mM imidazole and eluted using buffer A with 300 mM imidazole. For H-SUMO-^{CC}EnvC, the H-SUMO tag was cleaved with 6xHis-tagged SUMO protease (H-SP) as previously described (54). The cleavage reaction was passed through Ni-NTA resin (ProPur IMAC midi spin column) to remove free H-SUMO and H-SP, yielding a pure preparation of untagged ^{CC}EnvC. Amicon Centrifugal Filter Units (MWCO 10 kDa) were used to concentrate both protein preparations and exchange the buffer to buffer A without imidazole. Protein preparations were stored at

-80°C in buffer A. The BACTH assay and Ni-NTA “pull-up” assays are described in the legend to **Figure A1.8**.

EnvC antisera and affinity purification of anti-EnvC antibodies

Polyclonal rabbit antisera was raised agains purified ^{FL}EnvC by Covance according to their standard protocol. The resulting anti-EnvC antibodies were affinity purified using ^{FL}EnvC coupled to AminoLink resin (Pierce) as described previously for SlmA antibody purification (9).

Cell fractionation and immunoblotting

Whole-cell extracts for **Figure A1.5** were prepared as described previously (27). The protein concentration in each extract was determined using the non-interfering protein assay (Genotech) according to the manufacturers instructions. Protein concentrations were normalized between extracts and 20, 10, or 5 µg of total protein from each extract was separated on a 12% SDS-PAGE gel. Proteins were transferred to a PVDF membrane (Whatman) and the membrane was blocked with Rapid-Block (Genotech) for 5 minutes. The membrane was incubated with anti-EnvC antibodies (1:5000 in Rapid-Block) for 1 hour at room temperature. The membrane was washed three times with 25 ml TBST (10 mM Tris-HCl pH7.5, 100 mM NaCl, 0.1% Tween-20) for 10 minutes. Following the wash, the membrane was incubated with goat anti-rabbit antibodies conjugated with HRP (Rockland) (1:20,000 in Rapid-Block) for 1 hour at room temperature. Finally, the membrane was washed an additional four times as above and developed using the Pierce Super-Signal West-Pico reagents.

Chemiluminescence was detected using a BioRad Chemidoc system. Cell fractionations and immunoblotting for **Figure A1.5B** were performed as described previously (6), except that 500 mM NaCl was added to the spheroplasts after they were formed and EnvC was detected as described above. NaCl addition was required to promote the complete release of EnvC to the periplasmic fraction in spheroplasts from FtsEX$^-$ cells.

Acknowledgments

The authors would like to thank members of the laboratory for discussions, support, and critical reading of the manuscript. We would also like to thank Malcolm Winkler and co-workers for communicating their independent discovery that FtsEX in *S. pnuemoniae* interacts with the cell separation factor PcsB prior to publication. This work was supported by the Massachusetts Life Science Center, the Burroughs Wellcome Fund, and the National Institutes of Health (R01 AI083365). T.G.B. holds a Career Award in the Biomedical Sciences from the Burroughs Wellcome Fund.

References

1. **Arends, S. J. R.**, **R. J. Kustusch**, **and D. S. Weiss**. 2009. ATP-Binding Site Lesions in FtsE Impair Cell Division. J Bacteriol **191**:3772–3784.

2. **Baba, T.**, **T. Ara**, **M. Hasegawa**, **Y. Takai**, **Y. Okumura**, **M. Baba**, **K. A. Datsenko**, **M. Tomita**, **B. L. Wanner**, **and H. Mori**. 2006. Construction of Escherichia coli K-12 in-frame, single-gene knockout mutants: the Keio collection. Molecular Systems Biology **2**.

3. **Bendezú, F. O.**, **C. A. Hale**, **T. G. Bernhardt**, **and P. A. J. de Boer**. 2009. RodZ (YfgA) is required for proper assembly of the MreB actin cytoskeleton and cell shape in E. coli. EMBO J **28**:193–204.

4. **Bernhardt, T. G.**, **and P. A. J. de Boer**. 2004. Screening for synthetic lethal mutants in Escherichia coli and identification of EnvC (YibP) as a periplasmic septal ring factor with murein hydrolase activity. Mol Microbiol **52**:1255–1269.

5. **Bernhardt, T. G.**, **and P. A. J. de Boer**. 2005. SlmA, a nucleoid-associated, FtsZ binding protein required for blocking septal ring assembly over Chromosomes in E. coli. Molecular Cell **18**:555–564.

6. **Bernhardt, T. G.**, **and P. A. J. de Boer**. 2003. The Escherichia coli amidase AmiC is a periplasmic septal ring component exported via the twin-arginine transport pathway. Mol Microbiol **48**:1171–1182.

7. **Bi, E. F.**, **and J. Lutkenhaus**. 1991. FtsZ ring structure associated with division in Escherichia coli. Nature **354**:161–164.

8. **Burdett, I. D.** 1979. Electron microscope study of the rod-to-coccus shape change in a temperature-sensitive rod- mutant of Bacillus subtilis. J Bacteriol **137**:1395–1405.

9. **Cho, H.**, **H. R. McManus**, **S. L. Dove**, **and T. G. Bernhardt**. 2011. Nucleoid occlusion factor SlmA is a DNA-activated FtsZ polymerization antagonist. Proceedings of the National Academy of Sciences **108**:3773–3778.

10. **Corbin, B. D.**, **Y. Wang**, **T. K. Beuria**, **and W. Margolin**. 2007. Interaction between Cell Division Proteins FtsE and FtsZ. J Bacteriol **189**:3026–3035.

11. **Dajkovic, A.**, **S. Pichoff**, **J. Lutkenhaus**, **and D. Wirtz**. 2010. Cross-linking FtsZ polymers into coherent Z rings. Mol Microbiol **78**:651–668.

12. **Daley, D. O.** 2005. Global Topology Analysis of the Escherichia coli Inner Membrane Proteome. Science **308**:1321–1323.

13. **Datsenko, K. A.**, **and B. L. Wanner**. 2000. One-step inactivation of chromosomal genes in Escherichia coli K-12 using PCR products. Proc Natl Acad Sci USA **97**:6640–6645.

14. **Davidson, A. L.**, **E. Dassa**, **C. Orelle**, **and J. Chen**. 2008. Structure, Function, and Evolution of Bacterial ATP-Binding Cassette Systems. Microbiol Mol Biol Rev **72**:317–364.

15. **de Boer, P. A.** 2010. Advances in understanding E. coli cell fission. Curr Opin Microbiol. Elsevier Ltd 1–8.

16. **de Leeuw, E.**, **B. Graham**, **G. J. Phillips**, **C. M. ten Hagen-Jongman**, **B. Oudega**, **and J. Luirink**. 1999. Molecular characterization of Escherichia coli FtsE and FtsX. Mol Microbiol **31**:983–993.

17. **Durand-Heredia, J. M.**, **H. H. Yu**, **S. De Carlo**, **C. F. Lesser**, **and A. Janakiraman**. 2011. Identification and Characterization of ZapC, a Stabilizer of the FtsZ Ring in Escherichia coli. J Bacteriol **193**:1405–1413.

18. **Ebersbach, G.**, **E. Galli**, **J. Møller-Jensen**, **J. Löwe**, **and K. Gerdes**. 2008. Novel coiled-coil cell division factor ZapB stimulates Z ring assembly and cell division. Mol Microbiol **68**:720–735.

19. **Galli, E.**, **and K. Gerdes**. 2010. Spatial resolution of two bacterial cell division proteins: ZapA recruits ZapB to the inner face of the Z-ring. Mol Microbiol **76**:1514–1526.

20. **Garti-Levi, S.**, **R. Hazan**, **J. Kain**, **M. Fujita**, **and S. Ben-Yehuda**. 2008. The FtsEX ABC transporter directs cellular differentiation in Bacillus subtilis. Mol Microbiol **69**:1018–1028.

21. **Gill, D. R.**, **G. F. Hatfull**, **and G. P. Salmond**. 1986. A new cell division operon in Escherichia coli. Mol. Gen. Genet. **205**:134–145.

22. **Gueiros-Filho, F. J.** 2002. A widely conserved bacterial cell division protein that promotes assembly of the tubulin-like protein FtsZ. Genes & Development **16**:2544–2556.

23. **Guyer, M. S.**, **R. R. Reed**, **J. A. Steitz**, **and K. B. Low**. 1981. Identification of a sex-factor-affinity site in E. coli as gamma delta. Cold Spring Harb. Symp. Quant. Biol. **45 Pt 1**:135–140.

24. **Guzman, L. M.**, **D. Belin**, **M. J. Carson**, **and J. Beckwith**. 1995. Tight regulation, modulation, and high-level expression by vectors containing the arabinose PBAD promoter. J Bacteriol **177**:4121–4130.

25. **Haldimann, A.**, **and B. L. Wanner**. 2001. Conditional-replication, integration, excision, and retrieval plasmid-host systems for gene structure-function studies of bacteria. J Bacteriol **183**:6384–6393.

26. **Hale, C. A.**, **and P. A. de Boer**. 1997. Direct binding of FtsZ to ZipA, an essential component of the septal ring structure that mediates cell division in E. coli. Cell **88**:175–185.

27. **Hale, C. A.**, **and P. A. de Boer**. 1999. Recruitment of ZipA to the septal ring of Escherichia coli is dependent on FtsZ and independent of FtsA. J Bacteriol **181**:167–176.

28. **Hale, C. A.**, **D. Shiomi**, **B. Liu**, **T. G. Bernhardt**, **W. Margolin**, **H. Niki**, **and P. A. J. de Boer**. 2011. Identification of Escherichia coli ZapC (YcbW) as a Component of the Division Apparatus That Binds and Bundles FtsZ Polymers. J Bacteriol **193**:1393–1404.

29. **Hara, H.**, **S. Narita**, **D. Karibian**, **J. T. Park**, **Y. Yamamoto**, **and Y. Nishimura**. 2002. Identification and characterization of the Escherichia coli envC gene encoding a periplasmic coiled-coil protein with putative peptidase activity. FEMS Microbiol Lett **212**:229–236.

30. **Heidrich, C.**, **M. F. Templin**, **A. Ursinus**, **M. Merdanovic**, **J. Berger**, **H. Schwarz**, **M. A. de Pedro**, **and J. V. Höltje**. 2001. Involvement of N-acetylmuramyl-L-alanine amidases in cell separation and antibiotic-induced autolysis of Escherichia coli. Mol Microbiol **41**:167–178.

31. **Higgins, M. L.**, **and G. D. Shockman**. 1970. Model for cell wall growth of Streptococcus faecalis. J Bacteriol **101**:643–648.

32. **Ichikawa, J. K.**, **C. Li**, **J. Fu**, **and S. Clarke**. 1994. A gene at 59 minutes on the Escherichia coli chromosome encodes a lipoprotein with unusual amino acid repeat sequences. J Bacteriol **176**:1630–1638.

33. **Ichimura, T.**, **M. Yamazoe**, **M. Maeda**, **C. Wada**, **and S. Hiraga**. 2002. Proteolytic activity of YibP protein in Escherichia coli. J Bacteriol **184**:2595–2602.

34. **Karimova, G.**, **J. Pidoux**, **A. Ullmann**, **and D. Ladant**. 1998. A bacterial two-hybrid system based on a reconstituted signal transduction pathway. Proc Natl Acad Sci USA **95**:5752–5756.

35. **Karimova, G.**, **N. Dautin**, **and D. Ladant**. 2005. Interaction network among Escherichia coli membrane proteins involved in cell division as revealed by bacterial two-hybrid analysis. J Bacteriol **187**:2233–2243.

36. **Khare, D.**, **M. L. Oldham**, **C. Orelle**, **A. L. Davidson**, **and J. Chen**. 2009. Alternating Access in Maltose Transporter Mediated by Rigid-Body Rotations. Molecular Cell. Elsevier Ltd **33**:528–536.

37. **Miller, J. H.** 1972. Experiments in Molecular Genetics. Cold Spring Harbor Laboratory Pr.

38. **Morlot, C.**, **T. Uehara**, **K. A. Marquis**, **T. G. Bernhardt**, **and D. Z. Rudner**. 2010. A highly coordinated cell wall degradation machine governs spore morphogenesis in Bacillus subtilis. Genes & Development **24**:411–422.

39. **Ng, W.-L.**, **K. M. Kazmierczak**, **and M. E. Winkler**. 2004. Defective cell wall synthesis in Streptococcus pneumoniae R6 depleted for the essential PcsB putative murein hydrolase or the VicR (YycF) response regulator. Mol Microbiol **53**:1161–1175.

40. **Paradis-Bleau, C.**, **M. Markovski**, **T. Uehara**, **T. J. Lupoli**, **S. Walker**, **D. E. Kahne**, **and T. G. Bernhardt**. 2010. Lipoprotein Cofactors Located in the Outer Membrane Activate Bacterial Cell Wall Polymerases. Cell. Elsevier Inc. **143**:1110–1120.

41. **Pédelacq, J.-D.**, **S. Cabantous**, **T. Tran**, **T. C. Terwilliger**, **and G. S. Waldo**. 2005. Engineering and characterization of a superfolder green fluorescent protein. Nat Biotechnol **24**:79–88.

42. **Pichoff, S.**, **and J. Lutkenhaus**. 2002. Unique and overlapping roles for ZipA and FtsA in septal ring assembly in Escherichia coli. EMBO J **21**:685–693.

43. **Priyadarshini, R.**, **M. A. de Pedro**, **and K. D. Young**. 2007. Role of Peptidoglycan Amidases in the Development and Morphology of the Division Septum in Escherichia coli. J Bacteriol **189**:5334–5347.

44. **Reddy, M.** 2007. Role of FtsEX in cell division of Escherichia coli: viability of ftsEX mutants is dependent on functional SufI or high osmotic strength. J Bacteriol **189**:98–108.

45. **Rees, D. C.**, **E. Johnson**, **and O. Lewinson**. 2009. ABC transporters: the power to change. Nat Rev Mol Cell Biol **10**:218–227.

46. **Ricard, M.**, **and Y. Hirota**. 1973. Process of cellular division in Escherichia coli: physiological study on thermosensitive mutants defective in cell division. J Bacteriol **116**:314–322.

47. **Rodolakis, A.**, **P. Thomas**, **and J. Starka**. 1973. Morphological mutants of Escherichia coli. Isolation and ultrastructure of a chain-forming envC mutant. J Gen Microbiol **75**:409–416.

48. **Samaluru, H.**, **L. SaiSree**, **and M. Reddy**. 2007. Role of SufI (FtsP) in cell division of Escherichia coli: evidence for its involvement in stabilizing the assembly of the divisome. J Bacteriol **189**:8044–8052.

49. **Schmidt, K. L.**, **N. D. Peterson**, **R. J. Kustusch**, **M. C. Wissel**, **B. Graham**, **G. J. Phillips**, **and D. S. Weiss**. 2004. A predicted ABC transporter, FtsEX, is needed for cell division in Escherichia coli. J Bacteriol **186**:785–793.

50. **Sham, L.-T.**, **S. M. Barendt**, **K. E. Kopecky**, **and M. E. Winkler**. 2011. Essential PcsB putative peptidoglycan hydrolase interacts with the essential FtsXSpn cell division protein in Streptococcus pneumoniae D39. Proceedings of the National Academy of Sciences **108**:E1061–9.

51. **Shaner, N. C.**, **R. E. Campbell**, **P. A. Steinbach**, **B. N. G. Giepmans**, **A. E. Palmer**, **and R. Y. Tsien**. 2004. Improved monomeric red, orange and yellow fluorescent proteins derived from Discosoma sp. red fluorescent protein. Nat Biotechnol **22**:1567–1572.

52. **Typas, A.**, **M. Banzhaf**, **B. van den Berg van Saparoea**, **J. Verheul**, **J. Biboy**, **R. J. Nichols**, **M. Zietek**, **K. Beilharz**, **K. Kannenberg**, **M. von Rechenberg**, **E. Breukink**, **T. den Blaauwen**, **C. A. Gross**, **and W. Vollmer**. 2010. Regulation of Peptidoglycan Synthesis by Outer-Membrane Proteins. Cell. Elsevier Inc. **143**:1097–1109.

53. **Uehara, T.**, **T. Dinh**, **and T. G. Bernhardt**. 2009. LytM-Domain Factors Are Required for Daughter Cell Separation and Rapid Ampicillin-Induced Lysis in Escherichia coli. J Bacteriol **191**:5094–5107.

54. **Uehara, T.**, **K. R. Parzych**, **T. Dinh**, **and T. G. Bernhardt**. 2010. Daughter cell separation is controlled by cytokinetic ring-activated cell wall hydrolysis. EMBO J. Nature Publishing Group 1–11.

55. **Vollmer, W.**, **D. Blanot**, **and M. A. de Pedro**. 2008. Peptidoglycan structure and architecture. FEMS Microbiol Rev **32**:149–167.

56. **Yakushi, T.**, **K. Masuda**, **S. Narita**, **S. Matsuyama**, **and H. Tokuda**. 2000. A new ABC transporter mediating the detachment of lipid-modified proteins from membranes. Nat. Cell Biol. **2**:212–218.

57. **Yu, D.**, **H. M. Ellis**, **E. C. Lee**, **N. A. Jenkins**, **N. G. Copeland**, **and D. L. Court**. 2000. An efficient recombination system for chromosome engineering in Escherichia coli. Proc Natl Acad Sci USA **97**:5978–5983.